

Development of an *in vitro* human lung organoid system to study alveolar type 2 stem cell maintenance and dysfunction during disease



Kelly Victoria Evans

Department of Physiology, Development and Neuroscience
Lucy Cavendish College
University of Cambridge

This thesis is submitted for the degree of
Doctor of Philosophy

November 2021

DECLARATION

This thesis is the result of my own work and includes nothing which is the outcome of work done in collaboration except as declared in the Preface and specified in the text. I further state that no substantial part of my thesis has already been submitted, or, is being concurrently submitted for any such degree, diploma or other qualification at the University of Cambridge or any other University or similar institution except as declared in the Preface and specified in the text. It does not exceed the prescribed word limit for the Biology Degree Committee.

Unless otherwise stated, all experiments, analyses and figure preparation in the presented work were performed by me (Kelly Victoria Evans), under the supervision of my primary supervisor Dr Joo-Hyeon Lee. My secondary supervisor Dr Mick Fellows (AstraZeneca) assisted with helpful discussions. Throughout this thesis, I have used the term ‘I’ to denote work which I have performed myself, under the supervision of my supervisors. The term ‘we’ has been used to refer to work that has been performed in my lab (Dr Joo-Hyeon Lee). Any contributions by others have been made clear in the text.

Gene and protein names have been written in accordance with standardised nomenclature, where *Gene*/Protein is denoted for the mouse, and *GENE*/PROTEIN for the human.

Kelly Victoria Evans

This thesis was submitted on 1st November 2021

Development of an *in vitro* human lung organoid system to study alveolar type 2 stem cell maintenance and dysfunction during disease

Kelly Victoria Evans

ABSTRACT

The human adult distal lung parenchyma is maintained by alveolar type 2 (hAT2) cells that have the ability to self-renew and differentiate into alveolar type 1 (hAT1) cells, a critical cell type involved in gas-exchange. Cellular damage within the alveoli can lead to severe lung dysfunction, and major alveolar defects are characteristic of a number of incurable lung diseases, including Idiopathic pulmonary fibrosis (IPF). The appearance of aberrant cell types within disease-associated honeycomb regions of the distal lung are a hallmark of human IPF. However, the role of hAT2 cells in IPF development has not been fully explored, partially due to current *in vitro* human alveolar models failing to maintain hAT2 identity, limiting their study. Therefore, development of alternative platforms are essential for elucidation of hAT2 maintenance during alveolar homeostasis and their potential dysfunction during disease.

Utilising primary adult hAT2 cells isolated from human distal lung samples, I successfully developed and characterised a novel *in vitro* 3D organoid platform that allowed for long-term hAT2 maintenance in chemically-defined conditions. Cultured hAT2-derived organoids underwent clonal expansion, were functionally mature and exhibited maintenance of differentiation capacity. High Wnt signalling and FGF7 presence were found to be essential for primary hAT2 self-renewal, while reduction of Wnt signalling led to hAT1 differentiation. To understand hAT2 dysregulation during disease, hypoxia was

used to mimic an aspect of the IPF lung environment. Culture of healthy hAT2 cells in hypoxic conditions resulted in aberrant differentiation of hAT2 cells to SOX2-expressing airway-like cells. These cells exhibited higher proliferative capacity than normal hAT2 cells, with inhibition of Notch signalling resulting in a reduction in both the number of proliferative cells and SOX2⁺ organoids, indicating that hypoxia-induced induction of SOX2 in hAT2 cells may function through Notch signalling. Similar cells were also identified in honeycomb regions of human IPF patient lungs, implicating the hAT2 cell population as a potential origin for the ‘bronchiolisation’ observed in distal IPF lungs.

My results indicate that functional adult-derived hAT2 cells can be maintained long-term as 3D organoids in chemically-defined conditions. This novel culture system can be utilised to better understand both normal physiological and dysfunctional hAT2 stem cell behaviour. In addition, my data suggest that aberrant activation of signalling pathways implicated in IPF, such as hypoxia and Notch signalling, may function in causing incorrect hAT2 cell differentiation to airway-like cells. This could ultimately lead to a loss of correct alveolar stem cell maintenance, and a decline in lung function, both of which are observed in progressive, chronic lung diseases such as IPF.

*In dedication to my Ampy,
who loved knowledge*

ACKNOWLEDGEMENTS

As with any body of work, there are countless people who have assisted and supported me, both academically and personally, throughout the last four years. Attempting to pursue a PhD during a pandemic definitely had its challenges, but the following people have made the extremely unusual situation much more manageable:

I would like to firstly thank my supervisors Dr Joo-Hyeon Lee and Dr Mick Fellows for allowing me to pursue such an interesting project. You have my deepest gratitude for your support, patience and guidance. Additionally, thank you in advance to my examiners, Professor Gisli Jenkins and Dr Matthias Zilbauer, for accepting the role to examine this work. I already appreciate you both taking the time to read and assess my study. I would also like to thank the University of Cambridge, BBSRC and AstraZeneca for supporting this work, both academically and financially. Sincerest gratitude to all the collaborators I have had the pleasure to work with. These collaborators include multiple members of the Ju lab from KAIST, particularly Taewoo Kim and Jeonghwan Youk, for their excellent work and contribution to our SARS-CoV-2 paper. I am also grateful to the Rawlins lab for helpful discussion and insights in our weekly joint-lab meetings. Finally, thanks to the lab of Professor Sam Janes, particularly Dr Sarah Clarke and Dr Rob Hynds, for hosting me on a few occasions during my first couple of months of the PhD. I had never processed lung tissue before (or travelled to London on my own), so you played a fundamental role in teaching me the technique and making me feel welcome.

For assistance with imaging, histology and all things tissue culture, my thanks go to the core facilities at the Wellcome-MRC Cambridge Stem Cell Institute, particularly Peter Humphries, Darran Clements, Irina Pshenichnaya and Sally Lees.

Of course, particular thanks need to also be given to all members of the Lee lab for providing a supportive and mentally-stimulating environment. I will miss the discussions of experiment outcomes and ideas while working at the bench (and of course lunch will also be greatly missed). Special mentions go to the following people:

Catherine: You were with me throughout this PhD journey from day one, and I could not have asked for a better lab colleague and friend. Thank you so much for proof-reading some of my thesis for me, it's amazing that we were both able to submit at around the same time. Look at us about to enter the working world!

Antranik: You are the best lab manager and one of the nicest people I know. The lab would not have been able to function without your excellent organisational skills. Thank you for tolerating my constant insistence on having lunch at exactly 12pm, although with the amazing lunches you always brought to work, I do not understand how you had the self-control to wait any longer before eating.

Sagar: My fellow nerd. I will always appreciate your love of anime and science-fiction, and will miss discussing Star Wars and Marvel with you. However, a love of all things nerdy is not your only redeeming quality, you are also a fantastic scientist and have been so helpful whenever I had questions or experiment ideas. Thank you for your helpful comments on some of my thesis results chapters (and the compliments on my imaging data were also greatly appreciated).

Frances: Thank you for always being a friendly face in the lab. Your pictures and videos of your adorable kittens really kept my spirits high during the slightly stressful final year of my PhD. I look forward to meeting up with you again when I am back in Cambridge!

While I was extremely fortunate to be surrounded by amazing individuals academically, there are also a number of people outside the lab that helped me so much throughout my four years in Cambridge that I would like to personally thank:

Aleix, thank you for always knowing how to make me laugh, whether it was by pulling ridiculous faces while using a giraffe-face phone filter, or by telling me one of your 'hilarious' jokes. Your support during my PhD has been amazing. I can't wait to go to Barcelona with you! I know that you will most probably walk my little legs off while showing me all the sights, but I wouldn't change it for anything. Here's to many more years of travelling and good food!

Ernie, Shipra and Romana, the best flatmates a girl could ask for. I truly miss coming home from the lab in the evening and seeing the three of you sat in the kitchen. I am so happy that we got to go to a May Ball together in pre-Covid times (remember those?), and I'm so glad that we still keep in touch. I cannot wait to meet up with you all again very soon (graduation, perhaps?).

My college 'Wifey', Emma. You were the first friend I made at Cambridge, and I was so lucky that the college randomly paired us as college spouses. I particularly miss our Saturday morning brunches where we would chat about pretty much everything. Also...first year BOPs were an experience. I miss you! I will see you in London soon (hopefully for another brunch)!

James, Jess and my assortment of furry nieces and nephews. The pictures of Percy, Bertie, Marcie and Benji really put a smile on my face. A special thank you also to Sasha for being the best cat in the world and keeping me company during thesis writing (but not for stealing my chair as soon as I left the room).

Thank you to all my family, particularly my amazing parents for your continued love and support throughout my entire educational journey, and all the bits either side. Our weekends exploring Cambridgeshire were the best! Mam, I loved all the little food-related gifts that you would send to Cambridge, I was so excited unboxing those parcels whenever they arrived. Dad, thank you for being my personal taxi service all these years. Hopefully I can repay the favour soon if I get my own car...

And last, but most certainly not least, a sincere thank you to the tissue donors and their families, without whom this work could not exist.

Kelly Victoria Evans

PUBLICATIONS and CONTRIBUTIONS

Work from this thesis has directly contributed to the following published paper:

Youk, J.*, Kim, T.*, **Evans, K.V.***, Jeong, Y.I.*, Hur, Y.*, Hong, S.P.*, Kim, J.H., et al. (2020). Three-dimensional human alveolar stem cell culture models reveal infection response to SARS-CoV-2. *Cell Stem Cell* 27 (6), 905-919. *Denotes equal contribution

Additional published works that I have been involved with:

Choi, J., Jang, Y.J., Dabrowska, C., Lich, E., **Evans, K.V.**, Simons, B., Koo, B.K., et al. (2021). Release of Notch activity coordinated by IL-1 β signalling confers differentiation plasticity of airway progenitors via Fosl2 during alveolar regeneration. *Nat. Cell Biol.* 23.

Marjanovic, N.D., Hofree, M., Chan, J.E., Canner, D., Wu, K., Trakala, M., Hartmann, G.G., Smith, O.C., Kim, J.Y., **Evans, K.V.**, et al. (2020). Emergence of a High-Plasticity Cell State during Lung Cancer Evolution. *Cancer Cell* 38, 229-246.e13.

Evans, K. V., & Lee, J. (2020). Alveolar wars: The rise of in vitro models to understand human lung alveolar maintenance, regeneration, and disease. *Stem cells translational medicine* 9 (8), 867-881.

I would like to thank the following for their contributions to some of the featured experimental work:

- Taewoo Kim; 2D differentiation of human AT2 cells, TEM analysis, polarity assessment.
- Ho Min Kim; TEM analysis.
- Yongsuk Her; TEM analysis.
- Seon Young Kim; Karyotyping of human AT2 cells in 6-month-old organoids.

TABLE OF CONTENTS

DECLARATION	2
ABSTRACT	3
ACKNOWLEDGEMENTS	6
PUBLICATIONS AND CONTRIBUTIONS	9
LIST OF FIGURES AND TABLES	17
LIST OF ABBREVIATIONS	20
CHAPTER 1	22
INTRODUCTION	22
1.1. Physiology, structure and function of the human lung	23
1.2. The lung during homeostasis.....	23
1.2.1. <i>Major cell types of the human airway epithelium</i>	27
1.2.1.1. Basal cells	27
1.2.1.2. Secretory cells.....	28
1.2.1.3. Ciliated cells, neuroendocrine cells and minor cell types	28
1.2.2. <i>Major cell types of the human alveolar epithelium</i>	29
1.2.2.1. Alveolar type 2 cells	29
1.2.2.2. Alveolar type 1 cells	30
1.2.3. <i>Fibroblast and immune cell populations of the human alveoli</i>	31
1.3. Lung development	32
1.3.1. <i>Mouse lung development</i>	33
1.3.2. <i>Human lung development</i>	34
1.3.3. <i>Alveolar lineage differentiation from bipotent progenitors during development</i>	35
1.3.4. <i>Major signalling pathways involved in alveolar and airway lineage differentiation in the mouse and human lungs</i>	36
1.3.4.1. Wnt signalling	36
1.3.4.2. Fibroblast growth factor (Fgf) signalling	38

1.3.4.3. Epidermal growth factor (EGF) signalling	40
1.4. Lung regeneration and injury	41
1.4.1. <i>Regeneration and injury in the mouse lung</i>	43
1.4.2. <i>Regeneration in the small airways and alveoli of the human lung</i>	45
1.5. In vitro 3D-lung organoid models.....	47
1.5.1. <i>Airway organoids and the need for improved in vitro alveolar models</i>	48
1.5.2. <i>Alveolar organoids from mouse adult stem cells</i>	49
1.5.3. <i>Alveolar organoids from human adult stem cells</i>	50
1.5.4. <i>Alveolar organoids from human pluripotent and induced pluripotent stem cells</i>	51
1.5.5. <i>Alveolar organoids from human embryonic lungs</i>	53
1.5.6. <i>Current drawbacks of human alveolar organoids</i>	54
1.6. Idiopathic pulmonary fibrosis	58
1.6.1. <i>Epidemiology, disease pathology and bronchiolisation</i>	58
1.6.2. <i>Potential IPF disease mechanisms</i>	61
1.6.2.1. Alveolar cell dysfunction	61
1.6.2.2. TGFβ signalling.....	63
1.6.2.3. Wnt signalling.....	64
1.6.2.4. Notch signalling.....	64
1.6.2.5. Hypoxia	66
1.6.2.6. The inflammatory niche.....	67
1.6.3. <i>Current models of lung fibrosis</i>	69
1.6.3.1. Bleomycin and transgenic mouse models	69
1.6.3.2. Precision-cut lung slices	71
1.6.3.3. In vitro cultures.....	71
1.7. Outstanding questions and project aims	72
CHAPTER 2.....	74
MATERIALS AND METHODS	74
2.1. Human lung tissue.....	74
2.1.1. <i>Tissue acquirement, ethics and HTA guidance</i>	74
2.1.2. <i>Fixation and preparation for paraffin embedding/cryo-protection</i>	74
2.1.3. <i>Tissue processing for cell dissociation from normal background lung</i>	75
2.1.4. <i>Tissue processing for cell dissociation from IPF patient lungs</i>	76
2.1.5. <i>Cryopreservation of human lung tissue for long-term storage</i>	76

2.2. Generation and culture of human 3D adult alveolar organoids.....	80
2.2.1. <i>Antibody preparation for flow cytometry</i>	80
2.2.2. <i>Antibody preparation for Magnetic-activated cell sorting (MACS)</i>	80
2.2.3. <i>Establishment of 3D human alveolar organoids</i>	81
2.2.4. <i>Organoid culture conditions</i>	81
2.2.5. <i>2D-differentiation of organoid-derived hAT2 cells to alveolar type 1 cells</i>	82
2.2.6. <i>3D-differentiation of organoid-derived hAT2 cells to hAT1 cells</i>	82
2.2.7. <i>Chemical induction of hypoxia in hAT2-derived organoid cultures</i>	82
2.3. Maintenance of adult alveolar and airway organoids.....	89
2.3.1. <i>Enzymatic passaging of organoids</i>	89
2.3.2. <i>Mechanical passaging of organoids</i>	89
2.3.3. <i>Karyotyping of late passage alveolar organoids</i>	89
2.3.4. <i>Transmission electron microscopy</i>	90
2.3.5. <i>Cryopreservation of alveolar organoids for long-term storage</i>	90
2.4. Organoid preparation for immunofluorescence analysis.....	90
2.4.1. <i>Histogel/ paraffin embedding of organoids</i>	90
2.4.2. <i>Wholemout staining of organoids in situ</i>	91
2.4.3. <i>Immunofluorescence staining of paraffin-embedded organoids and tissue</i>	92
2.5. Immunofluorescence staining of cryo-protected tissue	92
2.6. RNA extraction and qRT-PCR	93
2.6.1. <i>TRIZOL RNA extraction from organoids</i>	93
2.6.2. <i>DNase treatment</i>	93
2.6.3. <i>cDNA synthesis</i>	93
2.7. SFTPC-eGFP lentiviral production.....	96
2.7.1. <i>Bacterial transformation</i>	96
2.7.2. <i>Bacterial midi-prep of plasmid DNA</i>	96
2.7.3. <i>Culture and maintenance of HEK293T cells</i>	96
2.7.4. <i>Lentiviral packaging by lipofectamine</i>	98
2.7.5. <i>Lentiviral packaging by calcium phosphatase transfection of HEK293T cells</i>	98
2.7.6. <i>Lentiviral concentration by Lenti-X concentrator</i>	99
2.7.7. <i>Lentiviral transduction of human alveolar organoids</i>	99
2.8. Data analysis	100
2.8.1. <i>Cell counting and organoid forming efficiencies</i>	100
2.8.2. <i>Image acquisition and analysis</i>	100
2.8.3. <i>Flow cytometry data analysis</i>	100

2.8.4. <i>Statistics and reproducibility</i>	100
CHAPTER 3	101
RESULTS I: IDENTIFICATION AND CHARACTERISATION OF EPITHELIAL PROGENITOR CELLS IN THE ADULT HUMAN LUNG PARENCHYMA	101
3.1. Introduction.....	101
3.2. Aims.....	103
3.3. Results.....	103
3.3.1. <i>Characterisation of the healthy human adult lung parenchyma</i>	103
3.3.2. <i>Establishment of in vitro human lung organoids</i>	106
3.3.3. <i>Characterisation of EpCAM⁺-derived human parenchymal lung organoids</i>	110
3.3.4. <i>Establishment and characterisation of airway organoids from human EpCAM⁺ HTII-280 cells</i>	114
3.4. Conclusions.....	122
CHAPTER 4	123
RESULTS II: ESTABLISHMENT AND CHARACTERISATION OF A CHEMICALLY-DEFINED <i>IN VITRO</i> HUMAN ALVEOLAR ORGANOID SYSTEM FROM ADULT LUNG STEM CELLS	123
4.1. Introduction.....	123
4.2. Aims.....	124
4.3. Results.....	124
4.3.1. <i>Establishment of alveolar organoids from primary hAT2 cells</i>	124
4.3.2. <i>Investigation of molecular pathways involved in hAT2-to-hAT1 differentiation</i>	132
4.3.3. <i>Investigation of purification strategies to specifically isolate hAT2 cells following sub-culture</i>	136
4.3.4. <i>Downstream applications of hAOs</i>	143
4.4. Conclusions.....	147
CHAPTER 5A	148

RESULTS IIIA: ESTABLISHMENT AND CHARACTERISATION OF EPITHELIAL LUNG ORGANIDS FROM PATIENTS WITH IDIOPATHIC PULMONARY FIBROSIS (IPF) 148

5A.1. Introduction 148

5A.2. Aims 149

5A.3. Results 149

 5A.3.1. *Characterisation of the distal lung of adult IPF patients* 149

 5A.3.2. *Characterisation of isolated EpCAM⁺ IPF-derived lung cells* 152

 5A.3.3. *Establishment and characterisation of epithelial organoids derived from human IPF lungs* 155

5A.4. Conclusions 160

CHAPTER 5B 162

RESULTS IIIB: INVESTIGATING THE ROLE OF HYPOXIA IN THE APPEARANCE OF ABERRANT EPITHELIAL CELLS IN HUMAN IDIOPATHIC PULMONARY FIBROSIS (IPF) 162

5B.1. Introduction 162

5B.2. Aims 163

5B.3. Results 163

 5B.3.1. *Up-regulation of hypoxia-related genes in human IPF lungs* 163

 5B.3.2. *Chemical induction of HIF1 α -mediated hypoxia results in SOX2 expression in hAT2-derived organoids* 164

 5B.3.3. *Aberrant SOX2⁺ epithelial cells localise to IPF honeycomb cysts and exhibit increased Notch signalling* 166

 5B.3.4. *ITGB4 as a potential marker for aberrant SOX2⁺ IPF cells* 172

 5B.3.5. *SOX2⁺ cells in both hAOs and IPF lung tissue display increased levels of proliferation* 177

5B.4. Conclusions 180

CHAPTER 5C 182

RESULTS IIIC: INVESTIGATING THE EFFECT OF INFLAMMATORY CYTOKINES ON HAT2 CELL IDENTITY	182
5C.1. Introduction	182
5C.2. Aims	183
5C.3. Results	183
5C.3.1. <i>Increased inflammatory cytokine presence in human IPF lungs</i>	183
5C.4. Conclusions	186
 CHAPTER 6.....	 188
 DISCUSSION.....	 188
6.1. Alveolar and airway organoids from normal background human adult lungs	189
6.1.1. <i>Fgf and Wnt signalling are essential for in vitro self-renewal of distal EpCAM⁺ and hAT2 primary human lung cells</i>	189
6.1.2. <i>p38 MAP-Kinase inhibition and its potential role in lumen establishment in primary airway organoids</i>	192
6.1.3. <i>Modulation of Wnt signalling allows hAT2-hAT1 differentiation in vitro</i>	192
6.1.4. <i>Culture of adult-derived hAOs versus recently published systems</i>	194
6.1.5. <i>Loss of pro-SFTPC expression in hAOs following 6 months of culture</i>	197
6.2. Aberrant epithelial cell types co-expressing alveolar and airway transcripts are present within human IPF lungs	199
6.2.1. <i>Origin of aberrant epithelial cell types in human IPF lungs</i>	200
6.2.2. <i>Hypoxia-induced Notch signalling and SOX2 expression in hAT2 cells</i>	202
6.2.3. <i>IL-1β and TNF-α-mediated induction of airway cell fate in hAT2-derived hAOs</i>	205
6.2.4. <i>Lack of hAT2 cells and abundance of airway cell types in IPF-derived patient organoids</i>	207
6.3. Limitations and Future work	208
6.3.1. <i>Lack of sequencing for IPF-derived tissue and organoids</i>	208
6.3.2. <i>Use of DFO as a hypoxia mimetic</i>	209
6.3.3. <i>Current drawbacks to adult hAT2-derived hAO system</i>	210
 CONCLUSIONS	 212

REFERENCES..... 213

LIST OF FIGURES AND TABLES

Figure	Title	Page
Fig. 1.1.	<i>Structure and cellular composition of the human lung.</i>	24
Fig. 1.2.	<i>Cell lineage relationships during homeostasis for the mouse and human lung.</i>	26
Fig. 1.3.	<i>Mouse-human differences in cellular composition of the lung alveoli.</i>	32
Fig. 1.4.	<i>Comparison of developmental stages in the human and mouse lung.</i>	34
Fig. 1.5.	<i>Canonical Wnt signalling pathway.</i>	37
Fig. 1.6.	<i>Cell lineage relationships during injury and regeneration in the mouse lung.</i>	42
Fig. 1.7.	<i>Human organoids established from adult stem cells.</i>	47
Fig 1.8.	<i>Canonical Notch signalling pathway.</i>	65
Fig. 2.1.	<i>Plasmid map for SFTPC-eGFP vector.</i>	97
Fig. 3.1.	<i>Characterisation of the human adult lung parenchyma from normal background lungs.</i>	105
Fig. 3.2.	<i>Tissue dissociation method for deriving cells from human lung parenchyma samples.</i>	107
Fig. 3.3.	<i>FGF7 and Wnt are required for the growth of human lung primary epithelial cells.</i>	108
Fig. 3.4.	<i>Human EpCAM⁺ epithelial lung parenchymal cells can be passaged repeatedly for up to 11 months.</i>	112
Fig. 3.5.	<i>Characterisation of EpCAM⁺ organoids retaining alveolar and airway organoids.</i>	113
Fig. 3.6.	<i>The strategy of FACS based cell isolation for hAT2 cells and non-hAT2 cells from human lung parenchymal tissues.</i>	115
Fig. 3.7.	<i>HTII-280⁻ cells form airway organoids in low WNT conditions.</i>	117
Fig. 3.8.	<i>Passage of HTII-280⁻ cell-derived organoids.</i>	118
Fig. 3.9.	<i>Culture of primary HTII-280⁻ in Sachs et al. 2019 human airway organoid conditions.</i>	121
Fig. 3.10.	<i>Switching airway organoids to media containing SB2 leads to lumen formation.</i>	122
Fig. 4.1.	<i>Primary HTII-280⁺ cells cultured in high Wnt conditions form hAOs comprising hAT2 cells.</i>	127
Fig. 4.2.	<i>Cultured hAT2 cells from alveolar organoids are functionally mature and display correct polarity.</i>	128
Fig. 4.3.	<i>Human alveolar organoids can be stably maintained for up to 11 months in culture and exhibit no chromosomal aberrations.</i>	129

Fig. 4.4.	<i>Organoid-derived hAT2 cells maintain their ability to differentiate into hAT1 cells following long-term culture.</i>	133
Fig. 4.5.	<i>WNT3A-conditioned medium results in hAT1 marker induction in hAOs.</i>	137
Fig. 4.6.	<i>HTII-280 does not reliably correspond with hAT2 identity during continuous in vitro culture.</i>	138
Fig. 4.7.	<i>Investigation of the use of Lysotracker for improved sub-culturing of organoid-derived hAT2 cells.</i>	140
Fig. 4.8.	<i>HLA-DR as a novel marker to isolate adult hAT2 cells from primary human lungs and cultured hAOs.</i>	142
Fig. 4.9.	<i>hAT2-derived alveolar organoids can undergo successful lentiviral transduction but exhibit limited expansion.</i>	144
Fig. 4.10.	<i>Alveolar organoids can be freeze-thawed for long-term storage and culture.</i>	145
Fig. 5.1.	<i>Human IPF lungs are characterised by honeycomb structures containing abnormal airway-like cells in the distal region of the lung.</i>	151
Fig. 5.2.	<i>Tissue dissociation method for deriving cells from human IPF distal lung samples.</i>	154
Fig. 5.3.	<i>The number of HTII-280⁺ cells is dramatically reduced in IPF lungs.</i>	155
Fig. 5.4.	<i>IPF-derived epithelial cells exhibit growth in low WNT conditions and form organoids with unusual morphologies.</i>	157
Fig. 5.5.	<i>IPF-derived HTII-280⁺ and HTII-280⁻ cells form organoids comprising airway cell types which persist upon passage.</i>	159
Fig. 5.6.	<i>Lentiviral transduction of IPF-derived HTII-280⁺ cells with SFTPC-GFP reporter highlights low number of SFTPC-expressing hAT2 cells in culture.</i>	161
Fig. 5.7.	<i>Levels of hypoxia are increased in IPF epithelial cells versus healthy controls.</i>	164
Fig. 5.8.	<i>Culture of airway organoids in 5% oxygen did not lead to upregulation of the downstream hypoxia-related gene SLC2A1.</i>	165
Fig. 5.9.	<i>DFO treatment leads to SOX2 induction in SFTPC⁺ hAT2 cells.</i>	168
Fig. 5.10.	<i>Notch signalling is increased in IPF honeycomb lesions and may function downstream of hypoxia.</i>	170
Fig. 5.11.	<i>ITGB4 is expressed in epithelial cells of IPF honeycomb cysts.</i>	173
Fig. 5.12.	<i>The number of ITGB4⁺ cells is drastically increased in IPF distal lungs.</i>	175
Fig. 5.13.	<i>Treatment of hAT2 organoids with DFO leads to an increase in ITGB4⁺ cells.</i>	176
Fig. 5.14.	<i>hAT2-derived SOX2⁺ cells display increased proliferation versus SOX2⁻ hAT2 cells.</i>	179
Fig. 5.15.	<i>IL-1β and TNF-α receptors are up-regulated in hAT2 cells.</i>	183
Fig. 5.16.	<i>IL-1β and TNF-α treatment induce airway-like phenotypes in hAT2 cell-derived hAOs.</i>	185

Table 1.1.	<i>Human lineage markers for lung epithelial cells.</i>	25
Table 1.2.	<i>Current strategies for the in vitro culture of hAT2 cells.</i>	56/57
Table 2.1.	<i>List of reagents and commercial kits.</i>	77/78
Table 2.2.	<i>Patient information.</i>	79
Table 2.3.	<i>Conjugated antibodies for FACS analysis.</i>	83
Table 2.4.	<i>Primary antibodies for immunofluorescence staining.</i>	84/85
Table 2.5.	<i>Secondary antibodies for immunofluorescence staining.</i>	86
Table 2.6.	<i>Chemical compounds for culture of 3D human-derived alveolar organoids.</i>	87
Table 2.7.	<i>Additional organoid culture reagents.</i>	88
Table 2.8.	<i>Recipes for antigen retrieval.</i>	92
Table 2.9.	<i>TaqMan probes.</i>	94
Table 2.10.	<i>Primer sequences for SYBR Green qPCR.</i>	95
Table 2.11.	<i>Recipe for 2X HBS used in calcium phosphatase transfection.</i>	99
Table 3.1.	<i>Featured media conditions.</i>	110
Table 3.2.	<i>Antibody panel for IF staining of alveolar and airway EpCAM⁺-derived organoids.</i>	112
Table 4.1.	<i>Comparison of hAOs in chemically-defined conditions versus co-culture.</i>	131
Table 5.1.	<i>Patient samples utilised for characterisation of IPF tissue and organoids.</i>	152
Table 6.1.	<i>Comparison of culture methods for adult hAO production in chemically-defined conditions.</i>	196

LIST OF ABBREVIATIONS

Abbreviation	Full name
2D	Two-dimensional
3D	Three-dimensional
AEP	Alveolar epithelial progenitor
AHLM	Adult human lung mesenchyme
ALI	Air-liquid interface
AM	Alveolar macrophage
AT1	Alveolar type 1 cell (mouse or rat)
AT2	Alveolar type 2 cell (mouse or rat)
BADJ	Bronchoalveolar duct junction
BALF	Bronchoalveolar lavage fluid
BASC	Bronchoalveolar stem cell
BPD	Bronchopulmonary dysplasia
CAV1	Caveolin-1
CHIR	CHIR99021
CoCl ₂	Cobalt chloride
DATP	Damage associated transient progenitor
DFO	Deferoxamine
DKK1	Dickkopf WNT Signaling Pathway Inhibitor 1
E	Embryonic day (mouse)
ECM	Extracellular matrix
EGF	Epidermal growth factor
EGFR	Epidermal growth factor receptor
EMT	Epithelial-mesenchymal transition
ER	Endoplasmic reticulum
FACS	Fluorescence-activated cell sorting
FBS	Foetal bovine serum
FGF	Fibroblast growth factor
FGFR	Fibroblast growth factor receptor
GSK3 β	Glycogen synthase kinase beta
hAO	Human alveolar organoid
hAT1	Human alveolar type 1 cell
hAT2	Human alveolar type 2 cell
HES1	Hes family bHLH transcription factor 1
HIF	Hypoxia-inducible factor
HPS	Hermansky-Pudlak syndrome

hPSC	Human pluripotent stem cell
HTA	Human tissue act
IBMX	3-isobutyl-1-methylxanthine
IF	Immunofluorescence
IL1	Interleukin-1
ILD	Interstitial lung disease
IPF	Idiopathic pulmonary fibrosis
iPSC	Induced pluripotent stem cell
KRT5	Cytokeratin-5
LNEP	Lineage negative epithelial progenitor
MACS	Magnetic-activated cell sorting
MAPK	Mitogen-activated protein kinase
NEB	Neuroendocrine body
NICD	Notch intracellular domain
PATS	Pre-alveolar type 1 transitional cell state
PCW	Post-conception weeks
PDPN	Podoplanin
PHd	Prolyl-hydroxylase
SAGM	Small airway epithelial growth medium
SB2	SB202190
SB4	SB431542
scRNA-seq	Single-cell RNA sequencing
SFTPb	Surfactant protein B
SFTPc	Surfactant protein C
Shh	Sonic hedgehog
TEM	Transmission electron microscopy
TNF	Tumour necrosis factor
TSP1	Thrombospondin 1
UIP	Usual interstitial pneumonia
VAFE	Ventralised anterior foregut endoderm

CHAPTER 1

Introduction

The lungs are a complex and beautiful system of branching tubes that lead down to around 400 million alveoli whose primary function is gas-exchange (Ochs et al., 2004). The delicate structure of the alveoli has made them prone to damage, and as such they are considered as the main site for a host of lung diseases including developmental bronchopulmonary dysplasia (BPD) and Idiopathic pulmonary fibrosis (IPF; Barratt et al., 2018; Bourbon et al., 2005; Davidson and Berkelhamer, 2017; Jobe and Ikegami, 1998; Jobe et al., 2008; Parimon et al., 2020; Wu et al., 2018). Despite this, little is known about the maintenance of the human alveolar epithelium, in part due to a lack of relevant *in vitro* models. The development of such models would not only improve our understanding of the mechanisms governing alveolar maintenance during both regeneration and disease, but could also aid in the discovery of improved therapeutics for the treatment of chronic lung diseases.

In this chapter, I will outline the structure, function and cellular composition of the human lungs. I will then go on to describe what is currently known about the signalling pathways and mechanisms involved in mouse lung development and how similar developmental programmes are activated upon injury. Specifically, I will be focussing on describing the development and composition of the alveoli, part of the functional unit of the lungs that facilitates gas exchange, and describe how this relates to the limited knowledge we have for human development and lung maintenance. Finally, I will address what is currently known about the incurable disease IPF in terms of pathogenesis and clinical presentations,

and will discuss current *in vivo* and *in vitro* models that have been utilised to better understand alveolar maintenance. To avoid confusion, the following work will mainly focus on aspects of the human lung. For cases in which the majority of our knowledge comes from mouse models, appropriate comparisons between the human and mouse system will be made. There have been tremendous efforts made in elucidating stem cell identity, regulation and developmental processes in both the mouse and human lung. Although I will provide a thorough overview of the relevant studies, I apologise to all the authors of the excellent works I could unfortunately not include in this discussion.

1.1. Physiology, structure and function of the human lung

The human respiratory system consists of a complex, 3-dimensional tree-like structure that begins with a single proximal trachea that branches out into two mainstem bronchi, followed by further branching into respiratory bronchioles that eventually terminate in millions of delicate, gas-exchanging alveolar sacs at the distal end (Figure 1.1; Hogan et al., 2014). The lungs are located either side of the thorax and in humans are divided into five lobes by fissures; two lobes on the left to accommodate space for the heart and three on the right. The primary function of the lungs is gas exchange between the air and the blood, and this is mediated by the alveoli which are arranged by acini and located within the distal parenchyma (Knudsen and Ochs, 2018). The alveoli, along with the bronchi, bronchioles, alveolar ducts and alveolar sacs make up the functional unit of the lungs. While the trachea and mainstem bronchi are anchored by cartilage, the alveoli are surrounded by the interstitium that contains blood vessels and cells of the extracellular matrix (ECM) that supports alveolar structural integrity and function (Knudsen and Ochs, 2018). The structure of each compartment of the lung differs, with the trachea and bronchi being lined with a pseudostratified columnar ciliated epithelium, while the bronchioles are lined by simple columnar cuboidal epithelium. On the other hand, the alveoli possess a lining of mainly thin squamous epithelium (Hogan et al., 2014).

1.2. The lung during homeostasis

The lungs are made up of a plethora of cell types that differ along the proximo-distal axis, with each having its own specific function in the maintenance of proper lung homeostasis

(Figure 1.1). The lack of specific human cell surface markers and incomplete characterisation of the human lung has made it difficult to identify and fully characterise specific cell types and stem/progenitor populations. However, comparison with mouse lungs and the recent advent of single-cell RNA sequencing (scRNA-seq) analyses has improved our knowledge of cellular identities and cell-specific proteins and markers (Table 1.1). Furthermore, optimisation of *in vitro* cultures of human cells have permitted the study of putative stem cell populations in the human lung, allowing for comparison with findings from *in vivo* mouse models (Figure 1.2). These cell types include basal, secretory cells, (including secretory club cells) and ciliated cells in the epithelium of the trachea and bronchiolar regions, while alveolar type 1 (hAT1; AT1 for mouse and rat) and alveolar type 2 cells (hAT2; AT2 for mouse and rat) exist in the alveoli.

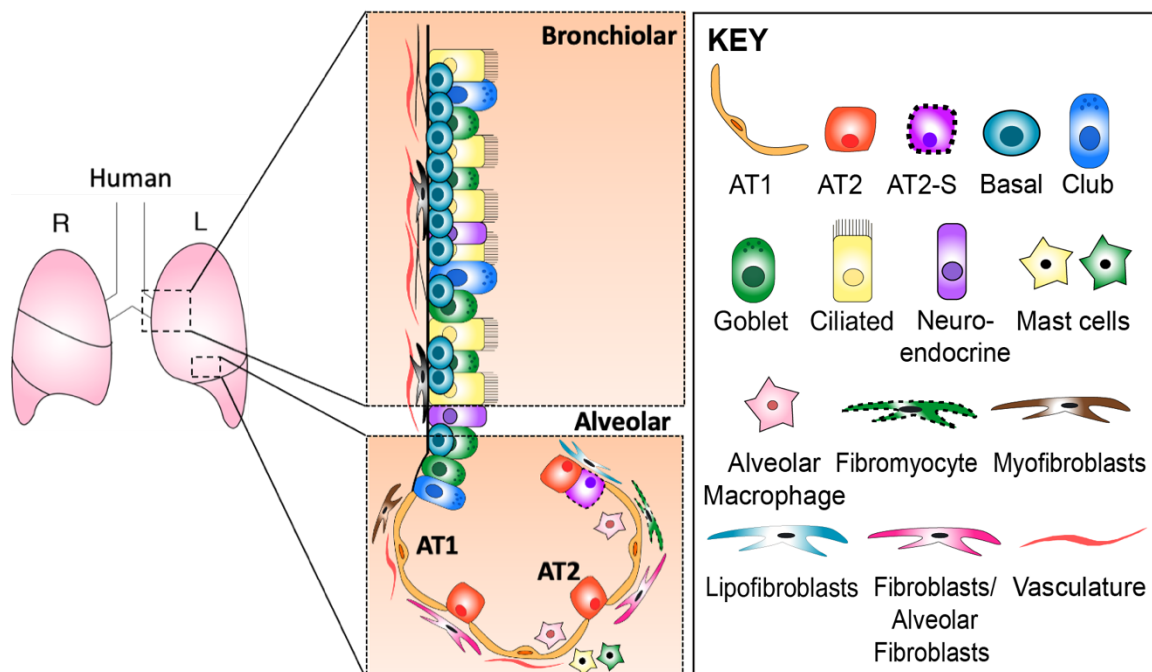


Figure 1.1. Structure and cellular composition of the human lung.

Schematic illustrating the structure and cellular composition of the human lung along the proximo-distal axis (bronchiolar-alveolar). Featured cell types have been described in a number of major studies involving both histological analysis, comparison with mouse lungs and single-cell RNA sequencing (scRNA-seq; Hogan et al., 2014; Travaglini et al., 2020). Cells marked with a dotted line highlight putative populations that have been identified through scRNA-seq, but require further characterisation and phenotypic analysis. AT2-S (AT2-signalling) are a putative cell population that were identified on the basis of their expression of Wnt-related transcripts in scRNA-seq studies (Travaglini et al., 2020). Adapted from Evans and Lee, 2020.

Table 1.1. Human lineage markers for lung epithelial cells.

Human epithelial cell type	Established lineage markers	Suggested lineage markers	References
Alveolar Type II (hAT2)	ABCA3, HTII-280, LAMP3, LPCAT1, SFTPC, SFTPA, SFTPB, SFTPD	*TM4SF1, MUC1	Barkauskas et al., 2013; Chen et al., 2017; Gonzalez et al., 2010; Jacob et al., 2017; Jacob et al., 2019; Nikolić et al., 2017; Travaglini et al., 2020; Yamamoto et al., 2017; Zacharias et al., 2018
Alveolar Type I (hAT1)	AGER, AQP5, CAV-1, HOPX, HTI-56, PDPN	IGFBP2, CLIC5	Nikolić et al., 2017; Travaglini et al., 2020; Wang et al., 2018
Basal	KRT5, *KRT14, *NGFR, TP63, PDPN	KRT15, KRT17, DAPL1	Rock et al., 2009; Teixeira et al., 2013; Travaglini et al., 2020
Secretory club	*PLUNC, SCGB1A1, *SCGB3A1, *SCGB3A2	CCKAR, CYP2F2	Dye et al., 2016; Travaglini et al., 2020
Ciliated	Acetylated tubulin, β 3-tubulin, FOXJ1	TUBB1	Dye et al., 2016; Travaglini et al., 2020
Goblet	MUC5AC, MUC5B, SPDEF		Travaglini et al., 2020

*Expressed in a subset of cells. Suggested lineage markers have not yet been fully validated. Adapted from Evans and Lee, 2020.

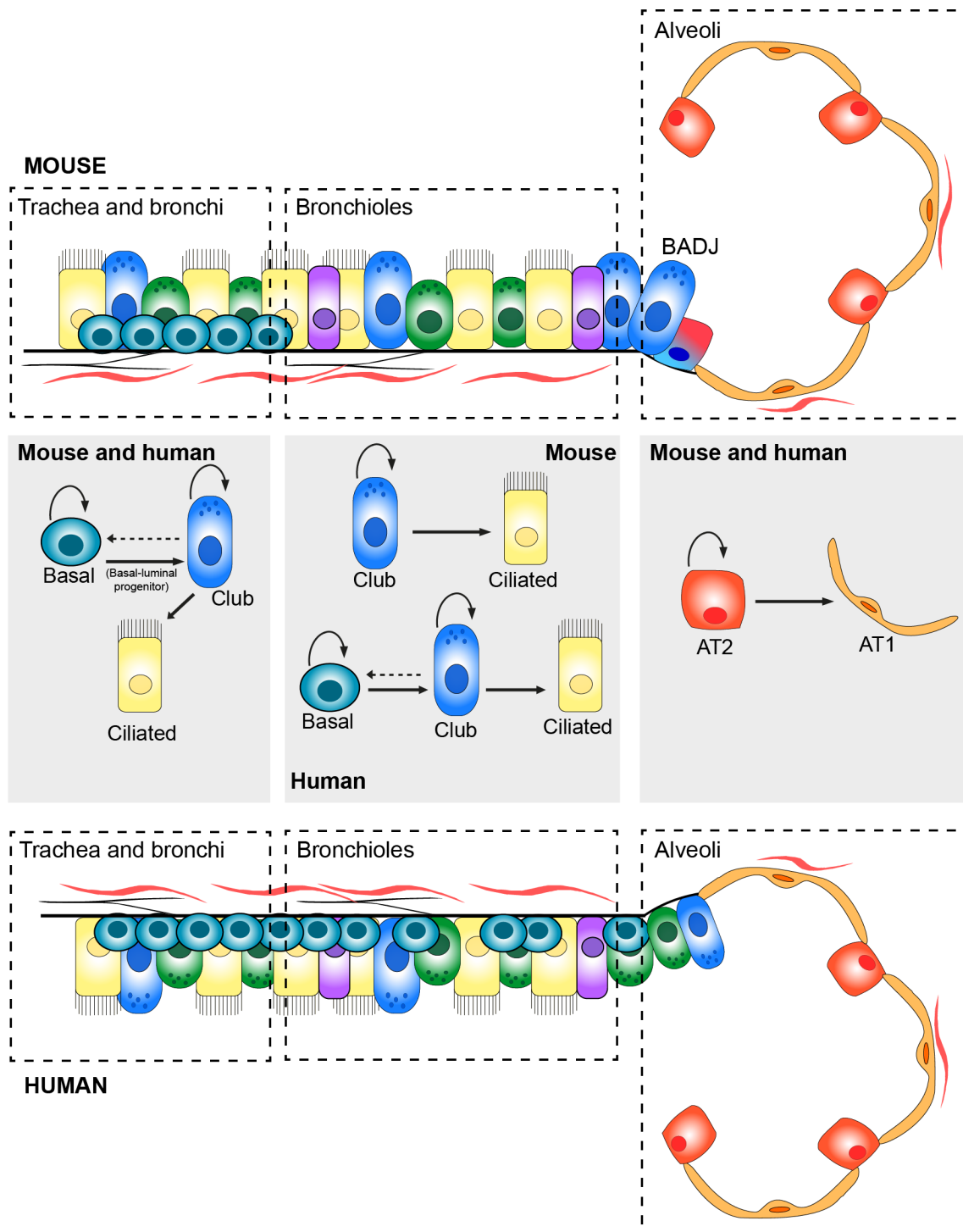


Figure 1.2. Cell lineage relationships during homeostasis for the mouse and human lung.

Simplified schematic outlining major proposed cell lineage relationships for the mouse and human lung during homeostasis. Lineage-tracing studies in the mouse have identified putative stem/progenitor populations, while *in vitro* studies utilising human epithelial cells have suggested human lineages. Many other epithelial cell types are present within the lungs, but have been omitted for clarity. Dotted arrow represents possible lineage elucidated from *in vitro* findings. Many works have contributed to the discovery of these lineage relationships, including Barkauskas et al., 2013; Choi et al., 2021; Hogan et al., 2014; Rawlins et al., 2009a; Rock et al., 2009; Watson et al., 2015.

1.2.1. Major cell types of the human airway epithelium

1.2.1.1. Basal cells

Cuboidal basal cells are present throughout the trachea, bronchi and bronchioles, where they reside at the base of the epithelium, attached to the basement membrane but not extending into the luminal space (Figure 1.1.; Hogan et al., 2014). Unlike in the mouse, where basal cells are confined to the trachea and mainstem bronchi, basal cells in the human lung extend more distally, reaching as far as the respiratory bronchioles, although their numbers decrease with increasing distance (Rock et al., 2009). The presence of basal cells in the human respiratory bronchioles suggests that these cells may have a human-specific function, although this has not yet been identified. Basal cells are defined by their expression of markers including *Tp63/TP63* and cytokeratin 5 (*Krt5/KRT5*). Lineage-tracing studies in the mouse under homeostatic conditions have revealed that basal cells act as a stem cell population by self-renewing and differentiating into secretory cells (Rock et al., 2009). Utilizing a *Krt5-Cre^{ER}* transgenic mouse line, basal cells were genetically labelled and traced during normal homeostasis, where they were shown to give rise to ciliated and secretory club cells in both the adult lung and during postnatal development (Rock et al., 2009). More recently, adult mouse basal cells have also been shown to produce neuroendocrine cells *in vivo* (Watson et al., 2015). It has also been suggested that mouse basal cells consist of two populations; classical basal cells which possess the capacity for self-renewal, and basal-luminal progenitors that have lost their self-renewal capacity and are committed to a luminal fate (Watson et al., 2015). Similarly, basal cells from the human lung have also been defined as stem cells, owing to their ability to self-renew and differentiate *in vitro* (Hynds et al., 2016; Rock et al., 2009). FACS-enrichment of TP63⁺ human basal cells using the markers NGFR and ITGA6 and subsequent 3D culture resulted in the formation of bronchospheres, containing basal, luminal and ciliated cells, demonstrating that human basal cells function as stem cells *in vitro* (Rock et al., 2009). More recent studies have also demonstrated that human basal cells can self-renew and differentiate in culture (Hynds et al., 2016; Sachs et al., 2019). The observation of the same somatic mitochondrial mutations in clones of epithelial human airway cells has also suggested that human basal cells may be multipotent *in vivo* (Teixeira et al., 2013). Furthermore, basal cell heterogeneity has been identified in human lungs, with only a subset of KRT5⁺ basal cells expressing the nuclear transcription factor TP63. These cells are suggested to be parabasal ‘intermediate’ cells that express markers of basal and luminal

cells (KRT5⁺ TP63⁻ KRT8⁺) and are found in both human and mouse lungs (Hynds and Janes, 2017).

1.2.1.2. Secretory cells

Two major secretory cell types exist within the pulmonary epithelium, the aforementioned secretory club cells (formerly known as Clara cells) and goblet cells (Wansleben et al., 2013). Secretory club cells are non-ciliated cells that secrete several distinctive proteins, including the surfactant proteins A, B and D, and SCGB1A1, which is alternatively referred to as ‘club cell secretory protein’ or ‘uteroglobin’ (Singh and Katyal, 2006). In the mouse, club cells are more common, whereas goblet cells are enriched in human airways (Mercer et al., 1994, as cited by Nikolić et al., 2018). While basal cells have been defined as stem cells of the proximal airways at homeostasis, their absence from mouse bronchioles indicates an alternative cell source for airway maintenance. This led to the discovery that *Scgbl1*⁺ secretory club cells act as a stem cell population in the proximal and distal bronchioles, due to their ability to self-renew and differentiate into ciliated cells (Rawlins et al., 2009a). Meanwhile, genetic lineage tracing studies in the mouse have highlighted that *Scgbl1*⁺ secretory club cells in the trachea mainly act as a transit-amplifying population during homeostasis, dividing only for a limited time, with basal cells existing as the primary stem cell as previously described (Rawlins et al., 2009a; Rock et al., 2009; Watson et al., 2015). It is currently unknown whether human club cells differ between the trachea and more distal bronchioles. Secretory club stem cell capacity has also been observed *in vitro* upon culturing human or mouse secretory club cells in chemically-defined conditions (Choi et al., 2021). In contrast, goblet cells are responsible for the production of mucus, which lines the airways and traps pathogens and particulates, and are not thought to possess stem cell capacity.

1.2.1.3. Ciliated cells, neuroendocrine cells and minor cell types

Ciliated cells are the most abundant cell type of the human pulmonary epithelium and comprise a columnar shape (Davis and Wypych, 2021). Transcriptional analysis of healthy human lungs using scRNA-seq has identified at least two subtypes of ciliated cells based on their molecular profiles (Travaglini et al., 2020). They function in moving mucus, microbes and debris out of the airways towards the nasal passage. In addition, ciliated cells are considered to be terminally-differentiated in the mouse, with the same likely applying

to the human (Rawlins and Hogan, 2008). On the other hand, rare cell types also exist, including pulmonary neuroendocrine cells, which are present at higher frequencies in mouse lungs versus human lungs, tuft cells and CFTR-expressing pulmonary ionocytes (Montoro et al., 2018; Plasschaert et al., 2018).

1.2.2. Major cell types of the human alveolar epithelium

1.2.2.1. Alveolar type 2 cells

hAT2 cells are the major epithelial cell type of the distal alveoli, although due to their cuboidal nature they only comprise approximately 5-10% of the alveolar epithelial surface area (Crapo et al., 1982 and Haies et al., 1981, as cited by Penkala et al., 2021). hAT2 cells are located within the alveolar corner and are responsible for the biosynthesis and secretion of pulmonary surfactant, a complex mixture of phospholipids and proteins which is vital for the maintenance of low alveolar surface tension (Crapo et al., 1982, as cited by Nikolić and Rawlins, 2017). A low surface tension is required to prevent the thin and delicate alveoli from collapsing upon themselves during exhalation. Surfactant is synthesised in the endoplasmic reticulum (ER) and stored within lamellar bodies, acidic secretory organelles that exist within hAT2 cytoplasm (Beers and Moodley, 2017). hAT2 cells are considered to act as defenders of the alveoli, with additional functions including a role in the innate immune response and secretion of antimicrobial and anti-inflammatory substances (Wright, 2005). Furthermore, multiple studies have highlighted that at least a proportion of hAT2 cells act as a stem cell population, having the ability to both self-renew and differentiate into hAT1 cells (Barkauskas et al., 2013; Desai et al., 2014; Evans et al., 1973; Frank et al., 2016; Nabhan et al., 2018; Travaglini et al., 2020; Zacharias et al., 2018). Isolation of AT2 cells from the mouse has involved the use of cell surface marker combinations, such as Epcam⁺ Sca1⁻ or fluorescent reporters including Sftpc-tdTomato (Barkauskas et al., 2013; Lee et al., 2014). Meanwhile, hAT2 cells have been more difficult to specifically isolate from human lungs, although recent efforts have included use of the surface marker HTII-280 (Gonzalez et al., 2010).

Under normal homeostasis, AT2 cells have been shown to be relatively quiescent, with turnover in a Wnt-responsive *Axin2*⁺ subset approximately once every four months in the mouse (Nabhan et al., 2018). However, it is not clear whether AT2 cell heterogeneity arises as a result of intrinsic potential or microenvironmental regulation. The localisation of many

Axin2⁺ AT2 cells next to single fibroblasts expressing *Wnt* genes suggests that it could be an environmental effect (Nabhan et al., 2018). However, a Wnt-responsive HTII-280⁺ TM4SF1⁺ sub-population of hAT2 cells representing 29% of total hAT2 cells from primary human lungs demonstrated increased responsiveness to Wnt modulation when compared to bulk HTII-280⁺ hAT2 cells *in vitro* (Zacharias et al., 2018). Additionally, depletion of the TM4SF1⁺ subset from hAT2 cells severely diminished *in vitro* organoid formation. This work suggested that hAT2 cells within adult human lungs exhibit transcriptional and functional heterogeneity. However, while the *Axin2*⁺ subset of AT2 cells in adult mouse lungs is well described, there are conflicting reports as to how much heterogeneity exists in the hAT2 population of the adult human lung. Reyfman et al. proposed that adult hAT2 cells are a relatively homogenous population, as scRNA-seq failed to identify a subset of hAT2 cells enriched for *AXIN2* or *TM4SF1* (Reyfman et al., 2019). However, the same study also failed to identify AT2 heterogeneity in the normal mouse lung, which may be due to sample preparation or sequencing depth. In contrast, a separate scRNA-seq study of healthy adult human lungs revealed heterogeneity in the hAT2 population, with the identification of a distinct cluster of hAT2 cells, termed hAT2-signalling, that selectively expressed Wnt-related genes (Travaglini et al., 2020). Furthermore, a number of studies utilising induced pluripotent stem cell (iPSC)-derived hAT2 cells have observed TM4SF1 in their cultures, although one study identified increased expression upon induction of a *KRAS* mutation, suggesting potential regenerative capacity upon damage (Dost et al., 2020; Schruf et al., 2020). Full validation and phenotypic analysis of these populations is required in order to understand their exact role in lung maintenance. The composition of the mouse and human alveoli is outlined in Figure 1.3.

1.2.2.2. Alveolar type 1 cells

While hAT2 cells are considered to make up the highest proportion of total epithelial cells in the human alveoli, it is the hAT1 cell population that comprises ~96% of the alveolar epithelial surface area due to their thin, squamous structure (Crapo et al., 1982 and Haies et al., 1981, as cited by Penkala et al., 2021). Their thin cytoplasmic extensions allow for easier gas permeability with the underlying capillaries, and thus hAT1 cells are vital for proper gas-exchange. Under normal homeostasis in the mouse, it is not thought that AT1 cells possess the ability to self-renew *in vivo*, and it is likely that the same applies to the human (Hogan et al., 2014). Instead, they are replaced via differentiation of hAT2/AT2

cells (Barkauskas et al., 2013). However, limited studies in the rat have indicated that AT1 cells have proliferative capacity and exhibit cellular plasticity *in vitro* (Gonzalez et al., 2009). The same finding has yet to be observed in the human.

1.2.3. Fibroblast and immune cell populations of the human alveoli

In addition to cells of the epithelium, multiple other cell types including fibroblasts, immune cells and cells of the vasculature are present throughout the lungs. The lung mesenchyme is an important source of specification signals. A lack of defined markers has made it difficult to prise apart the cellular diversity of the lung mesenchyme in both the human and the mouse. However, recent advances in scRNA-seq technology have begun to elucidate specific mesenchymal populations. In the proximal lung, myofibroblasts and previously undescribed fibromyocytes, a population of fibroblasts that exhibit high expression of contractile genes have been identified through scRNA-seq analyses of human donor lungs (Travaglini et al., 2020). Meanwhile, in the alveoli at least two main types of fibroblast have been found to exist; alveolar fibroblasts and lipofibroblasts. However, it has been debated whether lipofibroblasts truly exist within human lungs, and the exact role of both cell types remains to be defined (Rehan et al., 2006; Tahedl et al., 2014). Recent studies employing scRNA-seq analyses have identified additional populations of fibroblasts based on their transcriptional signatures (Travaglini et al., 2020). These include two subpopulations of *COL1A1*⁺ fibroblasts; alveolar fibroblasts and adventitial fibroblasts which are found localised to vascular adventitia. However, these cell types, along with other components of the human lung mesenchyme await detailed characterisation and phenotypic analysis. Components of the immune system also make up the human lung parenchyma. Alveolar macrophages (AMs) comprise more than 95% of phagocytes in the alveoli during steady state and are located on the luminal surface of the alveolar epithelium (Balhara and Gounni, 2012; Evans and Lee, 2020; Guilliams et al., 2013; Sibille and Reynolds, 1990). They are responsible for clearing surfactant and protecting against pathogens, acting as the first line of defence. In healthy human lungs, scRNA-seq has revealed heterogeneity in the AM population, with at least two types present in the normal adult lung based on their proliferation status (Travaglini et al., 2020).

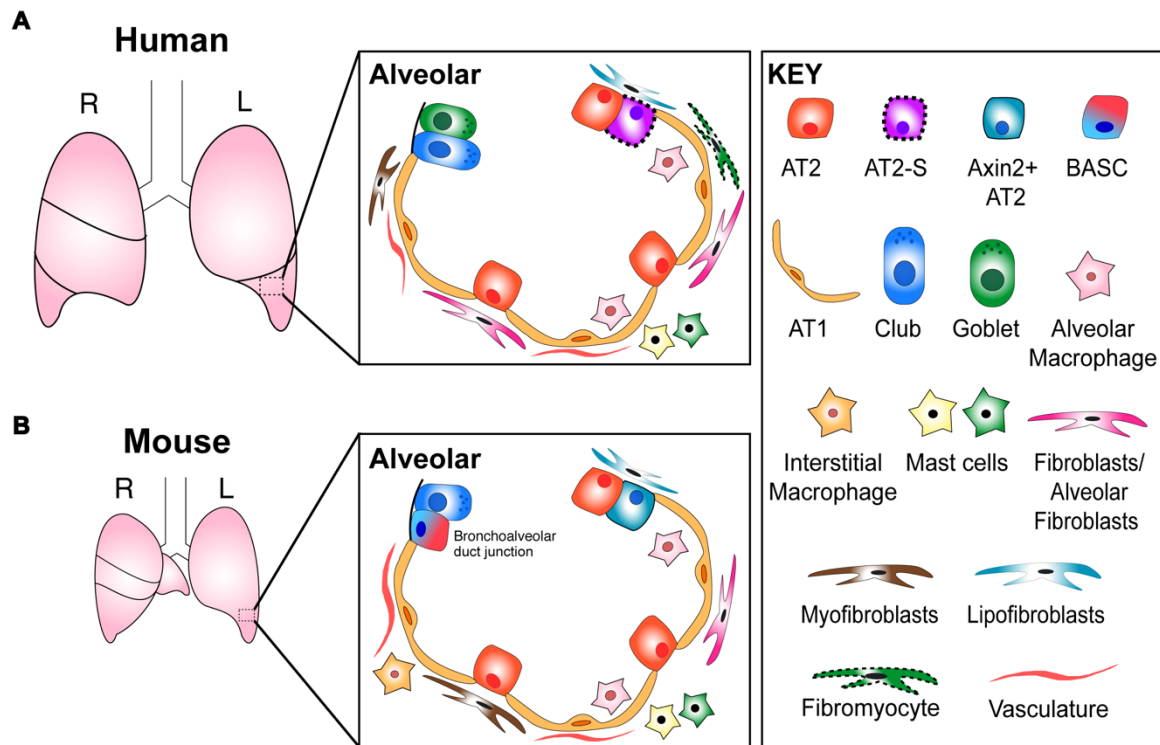


Figure 1.3. Mouse-human differences in cellular composition of the lung alveoli.

Schematic illustrating the differences in structure and cellular composition of the human and mouse distal lung alveoli. Human and mouse lung diagrams are not to scale. Cells types outlined with a dashed line have been identified based on their transcriptional signature obtained from scRNA-seq studies, but await phenotypic analysis (Travaglini et al., 2020). Image was created by me and has been previously published (Evans and Lee, 2020).

1.3. Lung development

The majority of our current knowledge in regard to lung development has come from in-depth studies of the mouse lung *in vivo*, particularly late stage alveologenesis, due to the inability to study human-derived tissue from late-stage embryonic lungs. Therefore, this section will focus on the information we have garnered from mouse lung development, and how this relates to what we know of human-specific development. In particular, recent advances in *in vitro* culture of embryonic lungs has improved our understanding of various aspects of human lung development.

1.3.1. *Mouse lung development*

In order to better understand lung stem cell maintenance and disease mechanisms, knowledge of lung development is required, and this information is often used in generating or improving *in vitro* lung models. Similar to the human, the mouse lung is made up of five individual lobes. However, their arrangement differs to that of the human, with four lobes on the right and one on the left. These lobes initially arise as two lung buds from *Nkx2.1*⁺ ventral anterior foregut endoderm during development, a process that is orchestrated by a number of signalling cues (Morrissey and Hogan, 2010). For example, Wnt and Bmp signalling have been shown to be required for specifying the *Nkx2.1*⁺ respiratory endoderm progenitors required for lung fate. *Wnt2/2b* combined null mutants fail to form the trachea or branching lung due to loss of *Nkx2.1*⁺ endoderm, while *Bmp4* is required to repress the transcription factor *Sox2*, allowing further expression of *Nkx2.1* in the presumptive lung endoderm (Goss et al., 2009). Lung development occurs in stages that most likely overlap to some extent (Nikolić et al., 2018; Figure 1.4). Lung specification begins at around embryonic day (E) 9.0 in the mouse (post-conception week [pcw] 4-7 in the human), leading to the formation of the trachea and two lung buds by E9.5, and complete separation of the trachea from the oesophagus by E12 (embryonic stage; Figure 1.4). During the pseudoglandular stage (E12 – E15) branching morphogenesis occurs, resulting in the formation of thousands of terminal airway branches from the two lung buds, which eventually narrow to form epithelial alveolar sacs at the canalicular (E15-E17) and saccular (E17 to birth) stages. Alveologenesis (birth to post-natal day [P] 20) follows, which allows full maturation of the alveolus and efficient gas-exchange. Throughout all stages, the lung mesenchyme develops alongside the endoderm, and provides the signalling cues and regulatory mechanisms required to promote branching and differentiation, highlighting the important crosstalk that occurs between the different cell types (Nikolić et al., 2018). *Fgf10* signalling in the mesoderm to *Fgfr2* in the endoderm is essential for branching morphogenesis. *Fgf10* is thought to be regulated by additional signalling pathways including Sonic hedgehog (*Shh*) and *Bmp4* at specific regions of the distal lung mesenchyme. The *Nkx2.1*⁺ endoderm gives rise to both *Sox2*⁺ proximal progenitors and *Sox9*⁺/*Id2*⁺ distal progenitors, which eventually form the airways and distal alveoli respectively (Rawlins et al., 2009b). At E10-E15, cells exiting the distal tip turn off *Sox9* and upregulate *Sox2*, allowing cells to differentiate along bronchiolar lineages, while cells exiting the tip at E16-E18 turn off *Sox9* and co-express markers of epithelial alveolar cells

(Nikolić et al., 2018). The development of the alveoli is critical, with lack of mature alveoli in premature human babies leading to the neonatal disease BPD (Davidson and Berkelhamer, 2017; Toti et al., 1997). Furthermore, even in adulthood, destruction of the alveoli due to a number of various diseases or environmental insults can have severe clinical implications, highlighting the importance in understanding alveolar development, maintenance and repair.

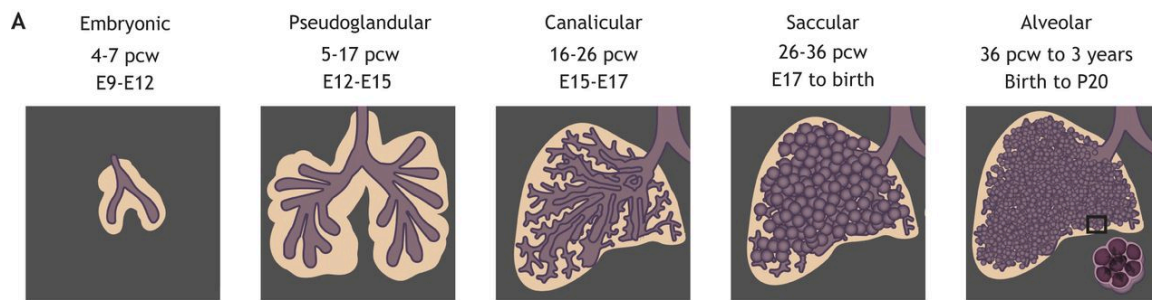


Figure 1.4. Comparison of developmental stages in the human and mouse lung.

Schematic outlining the approximate time frames for lung development stages in the human (post-conception weeks, pcw) and the mouse (embryonic day, E). Image obtained from Nikolić et al., 2018.

1.3.2. Human lung development

The difficulty in obtaining human lung tissue at particular developmental stages has made it challenging to understand human lung developmental processes, with many cellular and molecular findings still relying on mouse models. Although possessing the same general structure and function as the mouse lung, aspects of the human lung, including developmental processes, cell types and cellular arrangements display many clear distinctions. Like the mouse lung, the human lung arises from anterior foregut endoderm during development, although the timings of developmental stages differ, including the observation that alveologenesis continues well into early adulthood (Herring et al., 2014; Narayanan et al., 2012). As with the mouse, human lung specification begins during the embryonic stage of lung development (4-7 post conception weeks, pcw; Figure 1.4) with the appearance of two primary lung buds. These lung buds are derived from NKX2.1⁺ ventral anterior foregut endoderm at around 4 pcw, adjacent to a ventral trachea that connects the lung buds. The pseudoglandular stage, which involves branching morphogenesis into the surrounding mesenchyme occurs from 5-17 pcw. It is also during this stage that foetal breathing begins (~10 pcw), highlighting the importance of mechanical

stimuli for lung development. This is then followed by epithelial differentiation at the canalicular stage (16-26 pcw) and alveolar sac formation at 26-36 pcw (saccular stage). Alveologenesis was initially thought to occur from birth up until 3 years of age, although more recent evidence using advanced imaging has suggested that alveolar formation can continue into early adulthood (~ 21 years; Herring et al., 2014).

Recently, a study described a number of clear differences in terms of marker expression within cells of pseudoglandular human lungs when compared with mouse equivalents (Nikolić et al., 2017). For example, while distal epithelial tip cells of the embryonic lung during the pseudoglandular stage is Sox2⁻/Sox9⁺ in the mouse, they are SOX2⁺/SOX9⁺ in the human (Danopoulos et al., 2018; Miller et al., 2018; Nikolić et al., 2017). The functional significance of SOX2 presence in the human lung tip epithelium is currently unknown. In addition, the timing of marker gene onset for a number of lineage-specific genes differs between the mouse and human. Moreover, the terminal bronchioles during human development are SOX2⁺, but co-express alveolar markers, which has yet to be described in the mouse (Laresgoiti et al., 2016; Nikolić et al., 2017). Such findings highlight the need to study human-specific lung development and differentiation.

1.3.3. Alveolar lineage differentiation from bipotent progenitors during development

The classic model of alveolar lineage differentiation during development suggests that a pre-AT2 cell differentiated into a mature AT2 cell, followed by formation of an intermediate cell type that eventually gave rise to an AT1 cell (Adamson and Bowden, 1975, as cited by Desai et al., 2014). However, the observation of AT1 marker expression up to 5 days prior to the appearance of mature AT2 cells, along with the lack of evidence for a partially flattened cell with lamellar bodies (the expected AT2-AT1 intermediate cells) contradicted this model (Desai et al., 2014). Furthermore, lineage tracing of *Axin2*⁺ AT2 cells demonstrated that this population gave rise to mainly AT2 cells during sacculation, with only rare AT1 progeny observed (Frank et al., 2016). An alternative hypothesis, and one that has now garnered continued support through increasing experimental evidence, suggests that AT1 and AT2 cells both arise from a common multipotent progenitor during development (Desai et al., 2014; Frank et al., 2016; Jain et al., 2015). Initially, these cells were identified through analysis of AT1 and AT2 markers in the embryonic lungs of mice,

where they were found to express markers of both cell types, including *Sftpc* and *Pdpr*, during pre-sacculation but not late sacculation (Desai et al., 2014). Clonal analysis utilizing an inducible *Shh-cre* to label individual epithelial tip cells at E15 confirmed the presence of localised alveolar lineage clusters with marked AT1 and AT2 cells, providing additional evidence for individual bipotent cells. Furthermore, ultrastructural analysis revealed the presence of three classes of distal epithelial cell based on their morphology. For example, cuboidal cells with lamellar bodies were considered to be early AT2 cells, while partially flattened cells with vacuoles but no lamellar bodies were thought to be early AT1 cells (Desai et al., 2014). More recent studies utilising genetic lineage tracing techniques to label AT1 (*Hopx-Cre*) and AT2 (*Sftpc-Cre*) have also confirmed the presence of bipotent alveolar cells (Frank et al., 2019; Jain et al., 2015). Despite the observation of bipotent alveolar progenitors during lung development, there is currently no evidence to suggest that such a cell exists in the mature lung (Desai et al., 2014; Nikolić et al., 2017). Bipotent alveolar progenitors may also exist during human lung development (Nikolić et al., 2017)

1.3.4. Major signalling pathways involved in alveolar and airway lineage differentiation in the mouse and human lungs

Many signalling pathways contribute to lung developmental processes, with much crosstalk occurring between the endodermal and mesodermal compartments, in addition to epithelial-epithelial and epithelial-mesenchymal crosstalk later in development. The recent increase in directed differentiation protocols of human pluripotent stem cells to various lung cell lineages has improved our knowledge of some of the signalling pathways responsible for human lung developmental processes.

1.3.4.1. Wnt signalling

The Wnt signalling pathway is a major pathway involved in the development of multiple tissues and plays a critical role in the self-renewal and specification of multiple stem cells (Barker et al., 2007; Clevers et al., 2014b). In the lung, Wnt signalling plays an essential role in the specification of lung endoderm and early development (Frank et al., 2016; Goss et al., 2009). Canonical Wnt (Wnt/ β -catenin) signalling involves the binding of WNT1 class ligands (WNT2, WNT3, WNT3A and WNT8A) to a member of the Frizzled trans-membrane receptor family (MacDonald et al., 2009; Raslan and Yoon, 2020; Figure 1.5).

Binding can also occur with a co-receptor such as Lipoprotein Receptor-related Protein (LRP)-5 or LRP-6. Binding of Wnt ligands to a receptor culminates in the accumulation of β -catenin protein within the cytoplasm through inhibition of glycogen synthase kinase 3 beta (GSK-3 β). This subsequently results in the translocation of β -catenin to the nucleus, where it can activate target gene transcription. Secretory agonists such as R-spondin (RSPO) ligands also act alongside Wnt ligands to positively regulate Wnt signalling, while antagonists such as dickkopf-1 (DKK1) achieve the reverse (MacDonald et al., 2009). For modulation of Wnt signalling, a number of chemical Wnt activators exist, including the small molecule CHIR99021 (CHIR) which acts to enhance Wnt signalling through the inhibition of GSK-3 β .

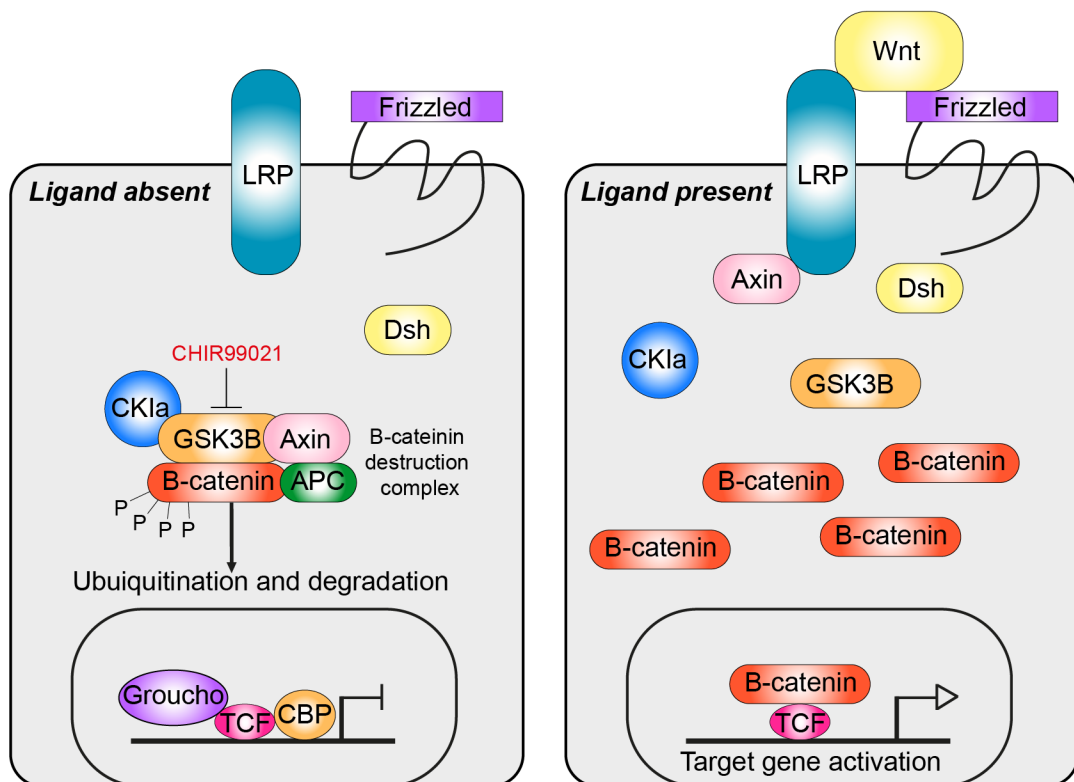


Figure 1.5. Canonical Wnt signalling pathway.

Simplified schematic of the canonical Wnt signalling pathway in mammals. β -catenin is usually marked for ubiquitination and degradation by the destruction complex, a component of which is GSK-3 β . Upon binding of a Wnt ligand to a member of the Frizzled family of receptors (along with occasional co-binding with a co-receptor such as LRP; lipoprotein receptor-related protein) GSK-3 β is inhibited, leading to an accumulation of β -catenin in the cytoplasm. β -catenin is then free to move to the nucleus and activate target gene transcription. CHIR99021 is small molecule that can be used to activate canonical Wnt signalling through the inhibition of GSK-3 β .

As previously stated, the transcription factor Nkx2.1 is expressed throughout lung development and is regulated by a number of signalling pathways. Wnt7b is expressed in the developing lung epithelium, with promoter activity shown to be regulated by Nkx2.1, which is essential for differentiation of the lung epithelium, particularly AT2 cells, with *Nkx2.1*^{-/-} mice failing to produce functional alveoli (Minoo et al., 1995; Weidenfeld et al., 2002). Wnt signalling is further implicated in proper alveolar formation later in development by the observation of a Wnt-responsive AT2 subset defined by *Axin2* expression (AT2^{Axin2}) that arises during alveologenesi s (Frank et al., 2016). Labelling of these cells using a Wnt-signalling *Axin2*^{CreERT2-TdTom} reporter mouse line revealed that they emerge at the onset of alveologenesi s, suggesting that a wave of Wnt signalling regulates alveolar self-renewal and differentiation. It was also shown using *in vitro* organoid models of mouse AT2 cells that activation of Wnt signalling resulted in proliferation of AT2 cells, while Wnt inhibition led to an AT1 fate (Frank et al., 2016). This *Axin2*⁺ subset were later shown to represent approximately 20% of AT2 cells in the adult mouse lung (Zacharias et al., 2018). A similar Wnt-responsive population has also been reported in human lungs and is marked by the surface marker TM4SF1 (Zacharias et al., 2018).

While it has been difficult to elucidate the precise signalling pathways involved in human lung development and alveolar lineage specification *in vivo*, advances in *in vitro* culture systems utilising either human embryonic cells or pluripotent stem cells (hPSCs)/ iPSCs have begun to further our understanding. For example, Wnt activation (CHIR), BMP4 and retinoic acid were sufficient for the specification of NKX2.1⁺ lung progenitors from hPSCs (Gotoh et al., 2014; Jacob et al., 2017; Rankin et al., 2016). Meanwhile, 3D-culture of hPSC-derived ventral anterior foregut endoderm (VAFE) in high Wnt conditions promoted alveolar differentiation, while low Wnt signalling encouraged differentiation to airway fates (McCauley et al., 2017). Furthermore, culture of hPSCs as 3D-lung alveolar organoids require Wnt activation in the form of CHIR (Jacob et al., 2017; Jacob et al., 2019; Yamamoto et al., 2017).

1.3.4.2. Fibroblast growth factor (Fgf) signalling

The FGF family of growth factors are involved in a range of biological processes in both the human and mouse, including organogenesis, homeostasis and repair (Danopoulos et al., 2019a). The canonical FGFs, including FGF7 (also known as keratinocyte growth factor;

KGF) and FGF10, are classed as paracrine/autocrine factors and bind to one of the four known FGF receptors (FGFR1, FGFR2, FGFR3 and FGFR4). Binding to one of the FGFRs activates phosphorylation of a specific tyrosine residue on the receptor, which in turn initiates downstream intracellular signalling; RAS-MAPK, PI3K-AKT, PLC γ , or STAT (Danopoulos et al., 2019a). FGFR2B is a reporter receptor for both FGF7 and FGF10.

During mouse lung development, several Fgf ligands are expressed, including Fgf7 and Fgf10 (Volckaert and De Langhe, 2015). Fgf10 signalling has been found to be vital for lung branching morphogenesis in the mouse, with *Fgf10*-deficient mutants failing to form appropriate branching structures *in vivo* (Volckaert and De Langhe, 2015). As a result, *Fgf10*-deficient mice exhibit peri-natal lethality. Additionally, deletion of *Fgfr2b* also results in complete failure of proper lung formation, resulting in viable mice with severe lung defects (Arman et al., 1999; De Moerlooze et al., 2000; Sekine et al., 1999). Despite utilising the same cell surface receptor, Fgf7 was found to not be vital for lung branching morphogenesis, with *Fgf7*-deficient mutant mice displaying correct lung branching and no obvious lung phenotype (Guo et al., 1996). Fgf signalling is critical during mouse alveologenesis and Fgf receptors 1 to 4 are all expressed (Li et al., 2017; Powell et al., 1998). Alveolar formation coincides with upregulation of *Fgfr2* and *Fgfr4*, with mice lacking both receptors failing to form secondary alveolar septae (Li et al., 2017). A mouse alveolar mesenchyme lineage expressing *Axin2* and *Pdgfra* was found to promote AT2 self-renewal via IL6 and Fgf7 signalling (Zepp et al., 2017). Furthermore, Fgf7 can stimulate rat AT2 cells to proliferate *in vitro* and have a stimulatory effect on AT2 maturation during development (Portnoy et al., 2004; Zhang et al., 2004).

In the human, *FGF10* is expressed throughout lung development from 10-21 gestational weeks, with expression increasing in the canalicular stage, unlike the pseudoglandular increase in expression observed in mouse lungs (Al Alam et al., 2015; Danopoulos et al., 2019b). However, it is not known whether *FGF10* expression plays the same role in the human lung as it does in the mouse. Activation of Fgf signalling, in addition to EGF and Wnt and inhibition of BMP was sufficient to grow human epithelial tip cells from pseudoglandular lungs as self-renewing organoids (Nikolić et al., 2017). Removal of individual factors, including FGF7 and FGF10 still resulted in the formation of organoids, but their size was considerably smaller and further culture could not be attempted. Furthermore, removal of FGF7 and FGF10 together resulted in a significant decrease in

SOX9 expression and an increase in *SOX2*, suggesting that both were required to promote tip cell self-renewal. Removal of FGF7 or FGF10 alone had no effect (Nikolic et al., 2017). Furthermore, FGF7 was required for initial *in vitro* cell expansion of epithelial human tip progenitor cells in a separate study (Miller et al., 2018). Treatment of hPSC-derived foregut spheroids with high levels of FGF10 in 1% serum was sufficient to drive the generation of lung organoids containing airway-like structures, mesenchymal cells and cells expressing markers of both hAT1 and hAT2 lineage (Miller et al., 2019). This work, combined with previous studies, suggests the FGF10 alone may not be important in the initial establishment of lung tip progenitors in human development, but may instead play a role in establishing distal fate, as well as differentiation of airway epithelial cells.

1.3.4.3. Epidermal growth factor (EGF) signalling

EGF plays an important role in the regulation of growth, survival, proliferation and differentiation of mammalian cells, in addition to providing resistance to apoptosis (Wee and Wang, 2017). EGF acts as one of the many ligands that can bind the EGF receptor (EGFR) in order to elicit downstream signalling pathways, including MAPK, PI3K-AKT, SRC, PLC- γ 1-PKC, JNK and JAK-STAT pathways. Upon EGF binding to EGFR, the receptor undergoes dimerization and trans-autophosphorylation for full activation, followed by recruitment of signalling proteins or adaptors. A role for EGF has previously been established in mouse lung development and epithelial maturation (Miettinen et al., 1995). *Egfr*^{-/-} mice exhibit respiratory failure, with a 50% reduction in branching, and die shortly after birth (Miettinen et al., 1995; Miettinen et al., 1997). Furthermore, a correlation was observed between low *SFTPC* expression and deficient alveolisation in these mice (Miettinen et al., 1997). *In vitro* culture of AT2 cells demonstrated that EGFR activity was essential for their self-renewal capacity, with dying AT1 cells being the most likely source of such signalling *in vivo* (Desai et al., 2014). *In vitro*, EGF addition has also been found to promote epithelial cell proliferation at the expense of differentiation (Barkauskas et al., 2017).

In addition to the signalling pathways described previously, a host of additional pathways play roles in the proper development of the lungs. For example, in the developing mouse lung, *Bmp4* is expressed predominantly in the epithelium, with increased expression at the branch tips, and is thought to be a potent stimulator of lung branching, in addition to other

roles. Meanwhile, *BMP2* and *BMP7* are expressed at high levels in human tip cells, highlighting subtle differences between lung development in the human and the mouse (Bellusci et al., 1996, as cited by Nikolić et al., 2018). Meanwhile, *Bmp4* has been found to inhibit AT2 proliferation in mouse AT2-derived organoids co-cultured with lung stromal cells *in vitro* (Chung et al., 2018). In contrast, antagonists of *Bmp4* such as *noggin* promote AT2 self-renewal at the expense of differentiation to AT1 cells. Furthermore, Sonic hedgehog signalling is important in driving early embryonic distal lung branching, while the VEGF pathway has displayed a critical role in early lung morphogenesis (Cardoso and Lü, 2006).

1.4. Lung regeneration and injury

Tissue regeneration processes following injury often employ similar signalling pathways to those occurring during development. During homeostasis, the lung is suspected to be a relatively quiescent tissue, with genetic lineage-tracing studies in the mouse suggesting that a rare *Axin2*⁺ AT2 population exhibit cellular turnover once every 4 months (Nabhan et al., 2018). Similarly, mouse tracheal basal cells exhibit turnover once every 11 days, while secretory club cells self-renew or differentiate to ciliated cells once every 25 days (Watson et al., 2015). This is in stark contrast to fast-cycling tissues such as the intestines, which are expected to turnover once every 3 to 5 days under normal conditions (Zhu et al., 2021). Despite slow cell turnover during steady state, the mouse lung is thought to possess remarkable regenerative capacity upon injury. *In vivo* ablation of specific cell populations has demonstrated that during injury settings, cells become activated and act to repair the damaged epithelium, with the observation of injury-induced cellular plasticity (Figure 1.6). However, due to the plethora of chronic lung diseases that can arise in human lungs, and the inability to assess regeneration *in vivo*, it has been debated as to what extent the human lung is able to regenerate, if at all. Nevertheless, recent studies involving the culture of isolated human lung cell lineages have begun to identify that multiple cell types have the ability to rapidly expand *in vitro*, suggesting at least some regenerative capacity.

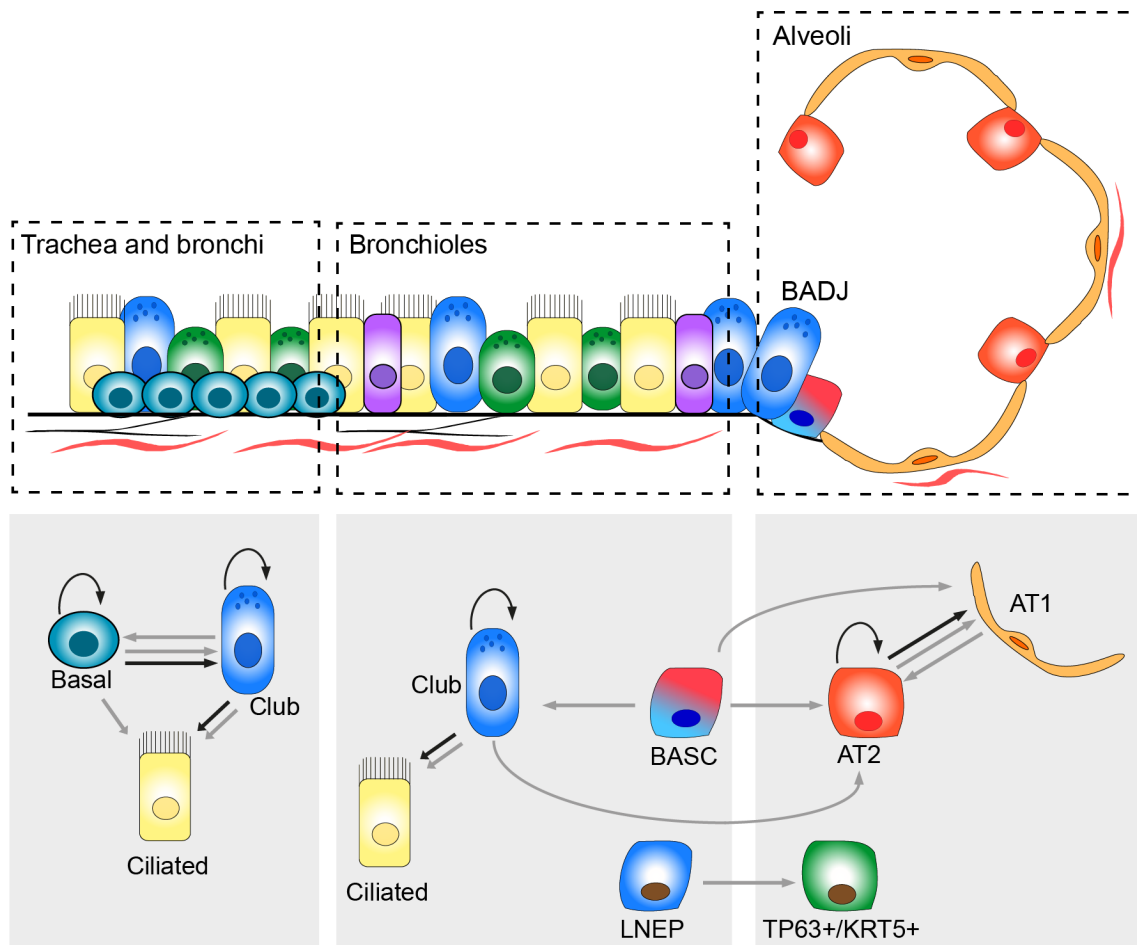


Figure 1.6. Cell lineage relationships during injury and regeneration in the mouse lung.

Simplified schematic outlining major proposed cell lineage relationships for the mouse lung during injury repair. Lineage-tracing studies in the mouse have identified epithelial cell lineage relationships upon injury. Many other epithelial cell types are present within the lungs, but have been omitted for clarity. A grey arrow represents differentiation capability upon injury, while a black arrow indicates lineage during homeostasis. Lineage negative epithelial progenitors (LNEPs) will be discussed in section 1.6. BASC; bronchoalveolar stem cell. Many works have contributed to the discovery of these lineage relationships, including (Barkauskas et al., 2013; Choi et al., 2021; Hogan et al., 2014; Kim et al., 2005; Lee et al., 2014; Rawlins et al., 2009a; Rock et al., 2009; Watson et al., 2015).

1.4.1. *Regeneration and injury in the mouse lung*

Epithelial lung cell-lineage relationships during homeostatic maintenance of the mouse lung, and their possible similarities to human, have been described in Section 1.2. Upon injury, the mouse lung exhibits increased levels of cellular plasticity, with multiple cell-lineage relationships arising that are not known to occur during homeostasis. An overview of these injury-induced lineage relationships can be found in Figure 1.6.

Tracheal secretory club cells have been shown to de-differentiate to basal cells following ablation of resident *Krt5*⁺ basal cells (Tata et al., 2013). Early xenograft studies suggested that basal cells displayed stem cell properties, while genetic lineage tracing of *Krt14*⁺ basal cells highlighted their remarkable capacity to self-renew and differentiate *in vivo* into multiple airway cell types following Naphthalene injury (Hong et al., 2004). In the small airways, secretory club cell heterogeneity has been suggested, with at least two subsets present based on their ability to repopulate the epithelium following injury. Ablation of club cells using naphthalene revealed a minor population of naphthalene-resistant club cells within the conducting airways, later referred to as variant club cells, that reside close to clusters of neuroendocrine cells termed neuroendocrine bodies (NEBs) (Hong et al., 2001). These variant club cells successfully repopulated the severely damaged lung airway epithelium. Furthermore, in the distal lung, resident *Scgbla1*⁺ secretory club cells exhibit differentiation capacity to AT2 cells during alveolar regeneration upon bleomycin injury (Choi et al., 2021). Secretory club-to-AT2 differentiation occurred through an Il1 β -Notch-Fosl2 axis, with Il-1 β signalling responsible for modulating expression of the Notch ligands *Jag1* and *Jag2* in ciliated cells. This in turn resulted in Notch inhibition within the neighbouring secretory club cells and subsequent lineage plasticity. In contrast to airway basal and secretory club cells, ciliated cells in the mouse have been shown to be terminally-differentiated, and do not proliferate even after injury (Rawlins and Hogan, 2008).

The transitional zone between the conducting airways and the alveoli in the mouse is referred to as the Bronchoalveolar Duct Junction (BADJ). In this region exists a rare population of cells that co-express the club cell secretory protein *Scgbla1*, in addition to the normally AT2-restricted protein *Sftpc* (Kim et al., 2005; Lee et al., 2014). Initially found as small clusters of cells present in *Lox-k-ras* tumours, these cells were also observed within wild type adult murine lungs, and were later named bronchoalveolar stem cells

(BASCs; Jackson, 2001; Kim et al., 2005). Upon *in vivo* bronchiolar injury with naphthalene or alveolar injury with bleomycin, BASCs were found to proliferate, and displayed self-renewal and multi-lineage differentiation *in vitro* by differentiating to alveolar or club cells (Kim et al., 2005). *In vitro* 3D organoid cultures utilizing single FACS-isolated BASCs also demonstrated that BASCs produced alveolar, bronchiolar and mixed bronchioalveolar organoids containing club and AT2 cells (Lee et al., 2014). Alveolar identity could be encouraged by the modulation of a Bmp4-controlled NFATc1-TSP1 signalling axis in supporting endothelial cells (Lee et al., 2014). Although these properties indicated stem cell function, evidence that such cells actually contributed to lung epithelial repair *in vivo* following injury was lacking. Lineage-tracing analysis using an *Scgbl1-CreER* mouse did not find evidence that BASCs contribute to adult homeostasis or repair (Rawlins et al., 2009a). However, later use of both a dual genetic lineage tracing system utilizing cre- and dre-recombinase and a split-effector based targeting system specifically labelled and traced BASCs *in vivo* (Liu et al., 2019; Salwig et al., 2019). During homeostasis, the number of BASCs remained stable, indicating that they do not contribute significantly to cellular turnover under homeostatic conditions. However, following bronchiolar injury, BASCs gave rise to club and ciliated cells, while alveolar injury with bleomycin resulted in differentiation to AT1 and AT2 cells, highlighting that different modes of injury could lead to different differentiation outcomes. Clonal analysis demonstrated that single BASCs substantially expanded after bronchiolar or alveolar injury, although were not the only population that were responsible for repopulating the lung epithelium (Liu et al., 2019). Furthermore, DTA-mediated ablation of BASCs was shown to compromise appropriate regeneration of distal airways, suggesting their contribution to repair is essential (Salwig et al., 2019). However, further investigations are needed to assess the highlighted discrepancies between different systems and studies in regard to BASC contribution to injury, and to establish whether an equivalent population of cells exists within human lungs.

It has been shown that following infection with *Pseudomonas aeruginosa*, Notch signalling is activated and results in differentiation of AT2 cells to AT1 (Finn et al., 2019). Alternatively, clonal lineage analysis of surviving AT2 cells following targeted AT2 ablation using diphtheria toxin demonstrated enhanced clonal growth and differentiation during the regeneration phase, albeit at lower levels than those observed following

bleomycin injury, highlighting that different injuries elicit diverse responses (Barkauskas et al., 2013). Such findings suggest either the presence of a dedicated subset of AT2 cells that have an increased capacity for regeneration, or the ability of all AT2 cells to become “activated” following injury. As previously addressed, lineage tracing studies and *in vitro* organoid assays in the mouse have revealed that a subset of Wnt-responsive AT2 cells expressing *Axin2* have an increased capacity to regenerate the alveolar epithelium following injury (Frank et al., 2016; Nabhan et al., 2018; Zacharias et al., 2018). Following pneumonectomy, a subset of AT1 cells expressing the immature AT1 marker *Hopx*, but not *Igfbp2*, were found to be able to transdifferentiate to AT2 cells in order to aid in repairing the injury, demonstrating that even cells that were previously considered to be terminally differentiated can gain phenotypic plasticity within injury settings (Jain et al., 2015; Wang et al., 2018). Furthermore, AT1 differentiation to AT2 cells has also been observed upon hyperoxic injury in both neonatal and adult mouse lungs (Penkala et al., 2021). Additional lineage negative epithelial progenitors (LNEPs) have been observed to form TP63⁺/KRT5⁺ ‘pods’ in the alveoli following injury such as influenza infection, which will be discussed in greater detail in Section 1.6 (Vaughan et al., 2015).

1.4.2. Regeneration in the small airways and alveoli of the human lung

It has been challenging to determine whether the human lung possesses equivalent regenerative capacity and cellular plasticity as that observed in the mouse. Unlike the BADJ of the mouse, the human distal lung does not consist of a transitional zone of epithelium between the airways and the alveoli. Instead, there is an abrupt transition between airway and alveolar epithelium in this region. As mentioned previously, the human lungs comprise basal cells as distally as the respiratory bronchioles. It is not yet known whether basal cells in the human distal lung are functionally distinct from those of the upper respiratory tract. However, basal cells from both the proximal airways and the distal lung parenchyma of human lungs have been shown to form organoids *in vitro*, having the ability to self-renew and differentiate into multiple airway cell types (Rock et al., 2009; Sachs et al., 2019; Salahudeen et al., 2020). It has been reported that a rare population of human SOX9⁺ basal cells were able to give rise to alveolar and bronchiolar epithelium when transplanted into injured mouse lungs (Ma et al., 2018). Transplantation of these SOX9⁺ basal cells was also performed in two human patients suffering with Bronchiectasis. This resulted in the observation of thinner bronchial walls and improved pulmonary function. However, the

direct contribution of delivered cells and the long-term effects of this procedure are currently unknown. Furthermore, the differentiation capacity and identity of these cells upon transplantation in the human remains unknown, and reproducibility needs to be proven. Alternatively, evidence in the mouse has suggested that upon injury, “pods” of KRT5⁺ basal arise within the alveoli (Kumar et al., 2011). Interestingly, the alveolar epithelium of human idiopathic pulmonary fibrosis (IPF) patients often consists of airway-like cells, although their origin remains to be elucidated (Adams et al., 2020; Habermann et al., 2020; Xu et al., 2016). The significance of distal basal cells in the human lung and their role during homeostasis and disease needs to be confirmed.

Human AT2-derived alveolar culture systems have demonstrated that hAT2 cells can self-renew and differentiate into hAT1 cells (Barkauskas et al., 2013; Fuchs et al., 2003; Mason and Williams, 1977; Uhal, 1997; Zacharias et al., 2018). As I have discussed previously, a subpopulation of TM4SF1⁺ hAT2 cells were shown to have increased capacity for proliferation and differentiation to hAT1 cells, displaying increased Wnt-responsiveness in 3D-organoid culture (Zacharias et al., 2018). These ‘alveolar epithelial progenitor’ (AEP) cells behave in a similar way to the *Axin2*⁺ AT2 cells of the mouse lung, and were found to exhibit increased clonogenic capacity upon Wnt activation. It remains to be elucidated whether subpopulations of hAT2 cells are functionally distinct *in vivo*, and what their relevance, if any, is during lung homeostasis, repair, and disease. However, it is clear that recent utilisation of *in vitro* systems, such as organoid production from human stem cells, has been fundamental in increasing our understanding of human epithelial stem/progenitor populations in the lung.

1.5. In vitro 3D-lung organoid models

Organoids are multicellular 3-dimensional (3D) structures made from stem cells that can self-organise and give rise to some or all epithelial cell types of a particular tissue. Recent years have experienced a vast increase in the production of human organoid models, for tissues including but not limited to the intestines, lung, pancreas, liver and endometrium (Broutier et al., 2017; Huch et al., 2015; Sachs et al., 2018; Sachs et al., 2019; Seino et al., 2018; Figure 1.7). They have a number of advantages over traditional 2D cell cultures, such as increased physiological relevance and 3D arrangement, and allow for the study of cell-to-cell interactions. Initially established from adult mouse and rat cells, the platform has now expanded to the human, allowing for improved understanding of human stem cell maintenance and dysregulation during disease. The human-specific nature of the system has also allowed for some level of investigation into disease modelling and patient-targeted therapies (Broutier et al., 2017; Dutta et al., 2017; Sachs et al., 2019; Youk et al., 2020).

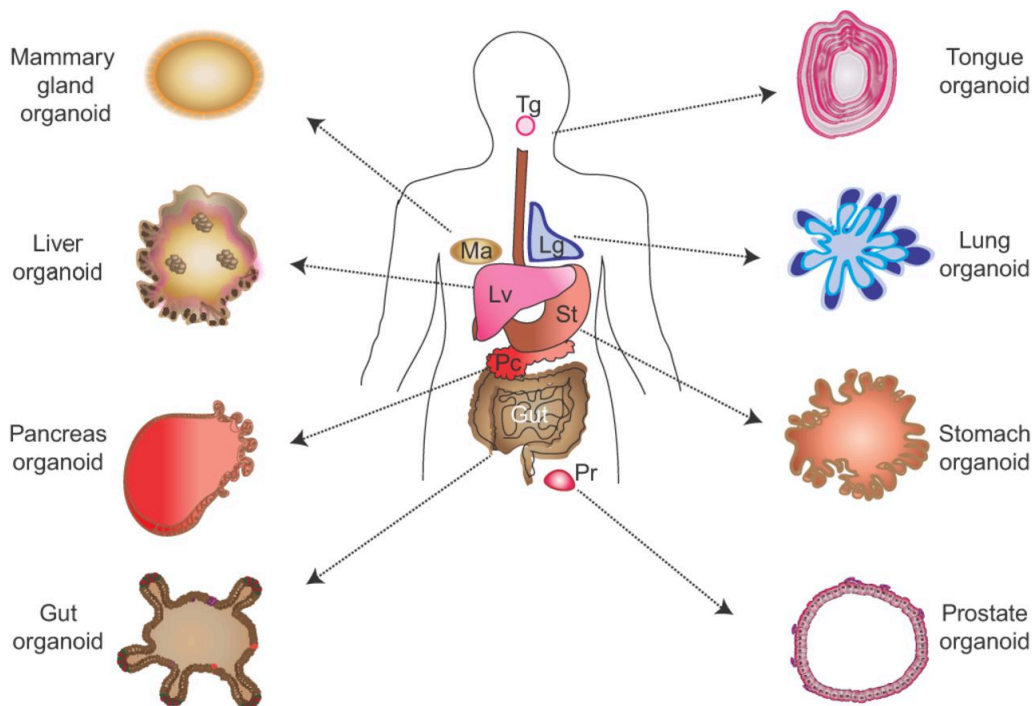


Figure 1.7. Human organoids established from adult stem cells.

Schematic overview of various organoids derived from adult human stem cells. Lg, Lung; Lv, Liver; Ma, mammary gland; Pc, Pancreas; Pr, Prostate; St, Stomach; Tg, Tongue. Image obtained from Huch and Koo, 2015.

1.5.1. Airway organoids and the need for improved *in vitro* alveolar models

A number of studies have successfully established airway organoids from human basal cells or bulk epithelial populations from human airways upon *in vitro* culture with supporting mesenchyme populations (Hynds et al., 2016; Rock et al., 2009). More recent bodies of work have successfully reported the molecular requirements for the *in vitro* culture and differentiation of airway cell types from human adult basal and secretory club cells, embryonic lung tip progenitors and hPSCs/iPSCs (Chen et al., 2017; Choi et al., 2021; McCauley et al., 2017; Nikolić et al., 2017; Sachs et al., 2019). For example, Sachs et al., reported the first chemically-defined culture condition for the “long-term” maintenance and differentiation of airway organoids derived from adult lungs (Sachs et al., 2019; Zhou et al., 2018). Upon culture of EpCAM⁺ lung cells derived from proximal airway brushings in conditions including FGF activation, BMP inhibition and TGFβ inhibition, the study reported the formation of organoids that contained basal, secretory and ciliated cells. Despite utilising whole epithelial cell fractions, no alveolar cell types were observed, likely due to the utilisation of proximal airway samples. A host of additional studies have since reported similar findings (Salahudeen et al., 2020; Zhou et al., 2018).

Despite knowledge that many lung diseases, including IPF, cause massive damage and destruction to the alveolar unit, the challenge of culturing alveolar epithelial cell types has hindered our understanding of how such diseases specifically affect these cells. Traditionally, research into human alveolar maintenance has primarily utilised the *in vitro* study of human airway cell types, either from normal tissue or cancer cell lines, generally due to their ease of culturing or increased availability of material (Foster et al., 1998; Ren et al., 2016; Rucka et al., 2013; Salomon et al., 2014). Therefore, in contrast to airway cell types, study of both human and mouse alveolar epithelial cells have lagged behind their airway counterparts, due to incomplete understanding of the mechanisms governing hAT2 maintenance. The majority of current culture conditions have utilised feeder cells, which do not fully support hAT2 maintenance or differentiation, leading to suboptimal conditions (Barkauskas et al., 2013; Glisinski et al., 2020; Zacharias et al., 2018). Therefore, long-term culture of functionally mature hAT2 cells has remained challenging. However, recent advances in cell isolation strategies and directed differentiation of hPSCs/iPSCs to alveolar lineages have slowly begun to fill this research gap.

1.5.2. Alveolar organoids from mouse adult stem cells

Traditional *in vitro* systems for the study of primary adult AT2 cells from mice, rats and humans have involved the culture of cells in two-dimension (2D) on tissue culture plastic with serum (Dobbs et al., 1988). However, such culture systems failed to maintain AT2 identity, with cells instead terminally differentiating into AT1 cells within 3-5 days, limiting their study. The need to establish *in vitro* systems that allowed for the maintenance of AT2 cell identity has therefore been a topic of great interest. Many strategies exist that have been utilized to isolate AT2 cells from mouse lungs, including the use of antibodies bound to cell surface markers or lineage-traced fluorescent reporters coupled with FACS. A genetic mouse model combining the *Sftpc-CreER* knock-in and *Rosa26-lox-stop-lox-tdTomato* alleles was utilized to isolate *Sftpc*-expressing AT2 cells, which were subsequently co-cultured in matrigel with *Pdgfra*⁺ mesenchymal cells to produce 3D-alveolospheres (Barkauskas et al., 2013). These structures consisted of *Sftpc*⁺ AT2 cells on the periphery and AT1 cells internally. Alternatively, antibody strategies for AT2 cell isolation have included the selection of *Epcam*⁺ *Sca1*⁻ or *Epcam*⁺ *Sca1*⁻ *Cd24*⁻ *Sftpc*-GFP^{high} cells, leading to the formation of alveolar organoids again consisting of *Sftpc*⁺ AT2 cells on the periphery and *Hopx*⁺/*Pdpn*⁺/*Ager*⁺ AT1 cells internally (Lee et al., 2013; Lee et al., 2014). Both of these studies relied on co-culture with mesenchymal populations in undefined culture conditions, making it difficult to identify specific regulatory mechanisms for AT2 maintenance or differentiation. However, more recently a number of studies have successfully established feeder-free alveolar organoids from mouse AT2 cells (Choi et al., 2021; Katsura et al., 2020; Shiraishi et al., 2019b). scRNA-seq analysis of adult AT2 cells cultured in MTEC media with fibroblasts revealed a number of differentially-expressed ligand-receptor pairs in epithelial AT2 cells (Katsura et al., 2020). This subsequently resulted in the identification of factors that were sufficient to promote proliferation and maintenance of AT2 cells as 3D-organoids *in vitro* without the need of supporting stromal cells. Resulting conditions promoted Wnt, *Fgf10* and *Egf* signalling and inhibited Bmp and p38 Map kinase. AT1 differentiation was achieved upon culture with 10% foetal bovine serum (FBS). In a separate study, AT2 cells derived from *SFTPC-CreER*^{T2/+}; *R26R*^{tdTomato/+} adult reporter mice were cultured under similar conditions (Choi et al., 2021). These organoids comprised *Sftpc*⁺ AT2 cells that could be maintained long-term, although differentiation to AT1 cells was not assessed.

In addition to alveolar organoid derivation from adult AT2 cells, lung cell lineage plasticity has led to the production of organoids containing alveolar lineages derived from cells besides AT2 cells. BASCs have been shown to possess the ability to differentiate into secretory club or AT2 cells both *in vitro* and *in vivo*, with the endothelial protein thrombospondin-1 (Tsp1) being suggested to induce alveolar lineage differentiation following bleomycin-induced lung injury (Lee et al., 2014). Similarly, *in vitro* 3D-organoid culture of mouse club cells demonstrated multi-lineage differentiation capabilities depending on the identity of the supporting mesenchymal cells, with Lgr5⁺ lung mesenchymal cells leading to alveolar fate (Lee et al., 2017). Similarly, culture of *Scgb1a1*⁺ club cells from distal lungs of fluorescent reporter mice and culture in Wnt and Fgf7/Fgf10-enriched, feeder-free conditions resulted in the formation of airway organoids and alveolar organoids containing Sftpc⁺ AT2 cells and some AT1 markers (Choi et al., 2021). A proportion of organoids were described as mixed and contained both secretory club and AT2 cells, with these organoids eventually comprising 100% of cultures by passage 5. Interestingly, inhibition of Notch signalling increased differentiation of secretory club to AT2 cells (Choi et al., 2021). This study indicated that *Scgb1a1*⁺ secretory club cells have the ability to differentiate to alveolar lineages under certain conditions, a finding that was also confirmed *in vivo*. Isolation of human secretory club cells with the cell surface marker KDR demonstrated similar results (Choi et al., 2021). Finally, 3D co-culture of Epcam⁺ Sca1⁺ distal lung epithelial progenitors with mesenchymal stem cells increased alveolar differentiation, resulting in filled spheres of SFTPC⁺ AT2 cells (Leeman et al., 2019).

1.5.3. Alveolar organoids from human adult stem cells

The relative difficulty in obtaining distal human lung parenchyma samples and the resulting lack of knowledge regarding requirements for human alveolar cell maintenance has hindered the *in vitro* culture of human alveolar cell types. Suboptimal culture conditions coupled with poor *in vitro* growth and lack of appropriate cell surface markers for hAT2 isolation have presented major problems. However, in 2010 a monoclonal antibody was developed which marked the apical surface of hAT2 cells (Gonzalez et al., 2010). This antibody was found to recognise a 280- to 300-kDa protein, later called HTII-280, which has the biochemical properties and characteristics of an integral membrane protein. This was the first instance that a surface marker was identified that could be used to specifically isolate hAT2 cells from adult donor lungs, leading to the production of human alveolar

organoids from adult tissue (Barkauskas et al., 2013). However, the precise role of HTII-280 remains unknown. Following co-culture of HTII-280⁺ hAT2 cells with MRC5 fibroblasts, spheres of cells formed, some of which expressed SFTPC, although no cells resembling hAT1 cells were present, suggesting that MRC5 fibroblasts may not be sufficient to fully support hAT2 cell differentiation. However, cells could be passaged at least once, highlighting the self-renewal capacity of adult hAT2 cells. Prior to sorting and subsequent culture, cells were grown overnight in commercial media, possibly leading to preferential selection of specific cell populations. Building upon this, EpCAM⁺HTII-280⁺TM4SF1⁺ hAT2 cells were isolated and cultured, with these organoids possessing higher organoid forming efficiency than EpCAM⁺HTII-280⁺TM4SF1⁻ or bulk EpCAM⁺HTII-280⁺ cells (Zacharias et al., 2018). However, in this case long-term culture was not supported, and morphology and cellular structure differed to the previous study, with organoids often forming as a sphere of cells mainly expressing SFTPC, although the presence of the hAT1 marker AQP5 was also observed in some cells. This difference in cellular composition may be due to differences in cell isolation strategies and culture conditions. Modulation of Wnt signalling with the Wnt-inhibitor XAV-939 resulted in an increased number of AQP5⁺ cells and reduced SFTPC, implicating Wnt signalling in the maintenance of hAT2 cells, as previously reported for the mouse (Frank et al., 2016; Zacharias et al., 2018). Furthermore, hAT2 cells derived from adult lungs failed to form organoids when cultured in commercialised small airway growth medium (SAGM) without the addition of mesenchymal (MRC5) feeder cells (Jacob et al., 2017; Jacob et al., 2019)

During late 2020 and early 2021, a number of studies were published that successfully established alveolar organoids from adult hAT2 cells in chemically-defined conditions (Ebisudani et al., 2021; Katsura et al., 2020; Salahudeen et al., 2020; Youk et al., 2020 [current study]). These will be described and discussed in greater detail in Chapter 6 (*Discussion*).

1.5.4. Alveolar organoids from human pluripotent and induced pluripotent stem cells

In addition to the establishment of alveolar organoids from isolated adult hAT2 stem cells, a number of studies have utilised hPSCs and iPSCs as an alternative culture method. Increased understanding of human lung development has allowed for improved directed

differentiation protocols to alveolar lineages. For example, alveolar spheroids were established through directed differentiation of hPSCs to foregut endoderm, followed by induction of an NKX2.1⁺ lung progenitor phase and eventual initiation of an SFTPC⁺ cell subset (Dye et al., 2015; Gotoh et al., 2014). Additionally, two separate studies successfully established alveolar organoids from hPSCs by generating improved protocols for hAT2 induction (Jacob et al., 2017; Jacob et al., 2019; Yamamoto et al., 2017). Utilising SFTPC-reporter lines of iPSCs, Jacob et al., demonstrated that hAT2 transcriptional signatures could be activated upon treatment of NKX2.1⁺ lung progenitor cells with CHIR, FGF7 and three further maturation factors, some of which are known to increase surfactant production in hAT2 cells of premature babies (Dexamethasone, IBMX and 8-bromo cyclic AMP; Jacob et al., 2017). Resulting ‘alveolospheres’ comprised SFTPC⁺ hAT2 cells with functional lamellar bodies, and exhibited *in vitro* self-renewal capacity. Little evidence of hAT1 cell presence was observed, although hAT1 marker expression greatly increased upon 2D-culture of alveolospheres in 10% serum. In a separate study, pre-conditioning of NKX2.1-enriched CPM⁺ VAFE cells from human iPSCs with CHIR, FGF7, FGF10 and the Notch inhibitor DAPT was found to be optimal for the induction of SFTPC (Yamamoto et al., 2017). 3D co-culture of these cells with human foetal lung fibroblasts resulted in the formation of alveolar organoids. Both of these highlighted studies also achieved induction of SFTPC⁺ hAT2 cells without the presence of mesenchymal support cells, although long-term culture of hAT2 cells in these conditions was only reported in one study, possibly due to differences in cell derivation. These organoids again lacked fully-differentiated hAT1 cells, although some hAT1 marker expression was observed, including AQP5 and podoplanin (PDPN; Yamamoto et al., 2017). Temporal activation of Wnt signalling has been suggested to promote hAT2 cell maturation (Jacob et al., 2017). However, culture of hPSCs in Collagen I gels, rather than the Matrigel that was used for previous studies, indicated that CHIR withdrawal induced multilineage maturation of proximal and distal fates (de Carvalho et al., 2019). This work contradicts previous studies in which exogenous Wnt (CHIR) was required for hAT2 cell fate, but may be due to differences in experimental design (Jacob et al., 2017; McCauley et al., 2017).

1.5.5. Alveolar organoids from human embryonic lungs

As briefly described in Section 1.3, the use of human embryonic lungs is an alternative approach to establishing organoids of human lung lineages, and is an excellent way to study human-specific developmental processes. Culture of pseudoglandular (5-9 pcw) epithelial tips from human embryonic lungs formed organoids in 3D culture when supplemented with activators of Wnt and Fgf signalling (Nikolić et al., 2017). These could be propagated as self-renewing organoids of SOX2⁺SOX9⁺ tip epithelial cells, with limited stromal cell contamination. Upon transplantation of cultured tip cells into the lungs of immunocompromised *NOD-scid-IL2rg^{-/-}* (NSG) mice, human cells were observed in the bronchioles and alveoli, and exhibited early signs of airway differentiation, but not alveolar. Attempts to differentiate tip cells to alveolar lineages *in vitro* in chemically-defined conditions (CHIR, FGF7, FGF10, Dexamethasone, cAMP, IBMX, T3 and DAPT) led to improper differentiation to hAT2 cells. Resulting cells were SOX2⁻SOX9⁻ and exhibited low levels of pro-SFTPC, but their columnar morphology suggested alveolar fate as opposed to full differentiation. More robust hAT2 differentiation was achieved upon co-culture with PDGFRβ⁺ mesenchymal support cells (Nikolić et al., 2017). Similarly, Miller et al., successfully propagated human embryonic (12-week gestation) epithelial bud tip progenitor cells *in vitro* in the presence of CHIR, FGF7 and retinoic acid (Miller et al., 2018). SOX2⁺SOX9⁺ tip cells expressed low levels of SFTPC, but differentiation to alveolar lineages was not investigated. In contrast, Shiraishi et al., successfully established feeder free alveolar spheroids from embryonic (20 week and 18 week) lungs in fibroblast-free culture (Shiraishi et al., 2019a). These cultures utilised GSK3β, TGFβ and BMP4 inhibitors, along with Notch and Fgf ligands to form spheres of SFTPC⁺ hAT2 cells that could be passaged at least four times. However, it is important to note that this study utilised hAT2 cells from a commercial source, therefore the precise isolation strategy and pre-culture environment are unknown and could influence downstream analyses. An alternative approach for differentiation from 3D-cultured human lung tip cells involved transferral of cells to 2D-culture, resulting in the formation of a “bronchioalveolar” model (Lamers et al., 2021).

1.5.6. Current drawbacks of human alveolar organoids

Despite recent advances in the *in vitro* culture of human alveolar cell types, particularly in regard to the culture of hAT2 cells derived from multiple sources, there are still a number of caveats that need to be overcome. One of the main issues is the lack of defined culture media for hAT2 cell growth and maintenance. The majority of studies to date that have utilised adult hAT2 cells have relied on co-culture with supporting stromal or mesenchymal cells, often with commercial media that include serum and unspecified components. The stromal/mesenchymal cells may not fully support hAT2 stem cell activities due to possible differences to the *in vivo* microenvironment, potentially resulting in incorrect signalling cues. Similarly, the presence of unspecified factors in the culture medium makes it difficult to identify key regulators of cell maintenance and differentiation. This has impeded studies to analyze precise regulatory mechanisms and cellular requirements for supporting alveolar stem/progenitor cells and maintaining their differentiated lineages. Long-term expansion of adult lung alveolar organoids with sustained functional lineages, as well as efficient isolation and expansion of cells from limited material have also been challenging.

Another major drawback of current human alveolar organoid models from multiple sources is the lack of hAT1 cells, suggesting that there are still gaps in our knowledge in regard to hAT2-to-hAT1 cell differentiation. Furthermore, the low number of hAT2-specific cell surface markers and isolation strategies makes it difficult to isolate hAT2 cells under certain conditions. For example, the most commonly used marker for hAT2 cell isolation from adult lung tissue, HTII-280, is not expressed on all hAT2 cells, with HTII-280⁻SFTPC⁺ hAT2 cells occasionally observed *in vitro* (Shiraishi et al., 2019a). Furthermore, differential expression is observed in certain disease settings, and HTII-280 is a less useful marker for subculture of hAT2 cells *in vitro*, as expression can be lost during culture (Gonzalez et al., 2010; Korogi et al., 2019). Alternative hAT2 isolation strategies, such as the use of fluorescent LysoTracker dye to mark lamellar bodies, have recently been utilised (Korogi et al., 2019).

Due to the sometimes-limited access to adult lung tissue, the use of hPSCs and iPSCs is an attractive alternative to adult stem cell cultures. However, while a number of studies have begun to investigate specific mechanisms and growth factors in the directed-differentiation of hPSCs/iPSCs to hAT2 cells, it has become apparent that full differentiation to mature

cell types remains incomplete. Multiple groups have reported the establishment of alveolar organoids or “alveospheres” from hPSCs and iPSCs, but the hAT2 cells within these structures share transcriptional similarities with embryonic lungs as opposed to adult hAT2 cells (Jacob et al., 2017; Yamamoto et al., 2017). Additionally, epigenetic, age-related signatures can potentially be captured through culture of adult-derived hAT2 cells, while patient-derived adult cells could help elucidate disease mechanisms or potential intrinsic dysfunction. Therefore, the need to establish adult-derived cultures is still of particular interest.

Table 1.2. Current strategies for the *in vitro* culture of hAT2 cells.

Isolation strategy	Culture method	Cell types present (primary)	Culture capacity/ primary forming efficiency	Reference
<i>Adult cells</i>				
FACS enrichment of adherent overnight culture cells derived from primary distal lung tissue (EpCAM ⁺ HTII-280 ⁺)	Co-culture with MRC5 fibroblasts and ALI-medium (Randell et al., 2011)	Some SFTPC ⁺ hAT2 cells	~ 3 passages 4.2% ± 0.8%	(Barkauskas et al., 2013)
MACS enrichment from primary distal lung tissue (EpCAM ⁺ HTII-280 ⁺ TM4SF1 ⁺)	Co-culture with MRC5 fibroblasts and SAGM medium (Lonza)	SFTPC ⁺ hAT2 cells and AQP5 ⁺ cells	Not disclosed (analysed after 14-21 days) ~4-5%	(Zacharias et al., 2018)
<i>Embryonic lungs</i>				
Enzymatic dissociation of 5-20 pcw lungs and culture of dissected epithelial tips and stalks in matrigel.	Self-renewal medium, chemically-defined (EGF, NOGGIN, FGF7, FGF10, CHIR, SB4).	SOX2 ⁺ /SOX9 ⁺ cells. Airway-like cells formed upon transplantation into mouse lungs. Also formed alveolar cells when transplanted under mouse kidney capsule.	Long-term culture. 100% efficiency from dissociated tips.	(Nikolić et al., 2017)

Mechanical and enzymatic dissociation of 12-week lungs. Lung buds placed into matrigel.	Bovine serum albumin (BSA), FGF7, FGF10, BMP4, retinoic acid (RA).	SOX9 ⁺ and SOX2 ⁺ cells. Weak SFTPC staining, no TP63 or HOPX.	Not reported.	(Chen et al., 2017)
<i>hPSCs/iPSCs</i>				
hPSCs differentiated into lung epithelial cells via an NKX2.1 ⁺ VAFE stage.	Co-culture with human foetal lung fibroblasts and RA, CHIR and BMP4	SFTPC ⁺ , SFTPB ⁺ , AQP5 ⁺ , NKX2.1 ⁺ .	Not reported.	(Gotoh et al., 2014)
FACS isolation of CPM ^{hi} cells from NKX2.1 ⁺ VAFE cells.	Cultured with FGF7, FGF10, dexamethasone, 8-Br-cAMP, IBMX, CHIR and SB4.	hAT2 cells and hAT1 marker expression.	Fibroblast co-culture for over 200 days.	(Yamamoto et al., 2017)
Reporter lines of VAFE cells sorted for NKX2.1 GFP ⁺ /SFTPC tdTomato ⁺ cells.	Cultured with FGF7, FGF10, dexamethasone, 8-Br-cAMP, IBMX, CHIR and SB4.	hAT2 cells	Serial passage with and without mesenchymal co-culture.	(Jacob et al., 2017)
hPSCs were used to form NKX2.1 ⁺ VAFE spheroids, and plated in matrigel.	Media including BSA, FGF7, RA and CHIR.	NKX2.1 and SOX2. Removal of CHIR and RA increased hAT2 and hAT1 marker expression.	Over 16 weeks in culture.	(Miller et al., 2018)

1.6. Idiopathic pulmonary fibrosis

1.6.1. *Epidemiology, disease pathology and bronchiolisation*

End-stage respiratory failure is the third most common mortality due to non-infectious disease. Interstitial lung diseases (ILD) are a host of pathologies that affect the parenchymal region of the lung, and are characterised by varying levels of inflammation and fibrosis. While some have known causes, including drug or toxin exposure, others are idiopathic, with Idiopathic Pulmonary Fibrosis (IPF) existing as the most common ILD with no identifiable cause (Barratt et al., 2018). Primarily observed in adults, IPF is increasing in prevalence globally, with an incidence of 32,500 people in the UK alone in 2012 (British Lung Foundation, 2012). Patients usually present with dyspnea, persistent cough and a general decline in lung function, while acute exacerbations of the disease are observed in some patients, although the reason for such exacerbations is not yet known. Prognosis is poor and treatments are limited, with only two anti-fibrotic drugs; Pirfenidone and Nintedanib currently available in the clinic (Lancaster et al., 2019; Margaritopoulos et al., 2016; Margaritopoulos et al., 2018; Ryerson et al., 2019). Despite providing a survival advantage to some patients, prevention or reversal of fibrosis has not been achieved, and disease progression is inevitable. The only option for end-stage disease to-date is lung transplantation, although access to suitable donor lungs is limited, and survival rates remain low, with a median survival of 2-3 years post diagnosis (Barratt et al., 2018). Additionally, IPF is a heterogeneous disease, further complicating treatment.

The most characteristic histopathological hallmark of IPF is the presence of usual interstitial pneumonia (UIP). This includes aberrant deposition of collagen ECM, architectural remodelling, hyperplastic hAT2 cells and clusters of fibroblasts and myofibroblasts arranged into structures termed fibroblastic foci, considered to be the “active” regions of lung remodelling. Epithelial micro-“honeycombing” is also observed in the distal lung parenchyma of IPF patients. Traditionally thought to be caused by inflammation, treatment options involving immunosuppressive drugs displayed little effect, suggesting an alternative disease mechanism (King et al., 2009; Raghu et al., 2008; The Idiopathic Pulmonary Fibrosis Clinical Research Network, 2012). Many hypotheses exist as to how the disease arises. A key feature of IPF is bronchiolisation of the distal lung parenchyma, where cell types that normally reside in the airways are present within the

alveoli of remodelled IPF lungs. The recent advances in scRNA-seq analyses of whole patient lungs have begun to prise apart cellular diversity that arises during disease, with the description of aberrant cell types that arise in the distal lung parenchyma of IPF patients (Adams et al., 2020; Habermann et al., 2020; Xu et al., 2016). In 2016, one study utilised Illumina technology and reported the presence of “indeterminate” cell types within the EpCAM⁺ population of human IPF lungs, a population that was not observed in healthy background lungs (Xu et al., 2016). This unusual cell population was characterised based on its mixed alveolar (hAT2 and hAT1) and airway transcriptional signature. *SOX2* expression was observed in some cells expressing RNAs normally restricted to hAT2 cells, and was frequently co-expressed with *SOX9*, highlighting potential disruption in proximal-distal patterning. Furthermore, two additional cell clusters were also identified in distal IPF lungs; secretory club/goblet cells and basal cells. Together with the observation that the majority of cells from healthy background lungs were hAT2 cells, this study indicated an enrichment of airway cell types in the lung parenchyma of IPF patients. A more recent study by Adams et al. has since described a unique population of “aberrant basaloid cells” characterised by their *SOX9*⁺ *TP63*⁺ *KRT5*⁻ *KRT17*⁺ profile, while a separate study discovered a *KRT5*⁻ *KRT17*⁺ population in peripheral human IPF lung tissue, likely representing the same cell population (Adams et al., 2020; Habermann et al., 2020). Such cells may be implicated in IPF pathogenesis due to their observed proximity to fibroblastic foci and their expression of genes related to pathological ECM and epithelial-to-mesenchymal transition (EMT). Characterization and phenotypic analysis of these populations need to be performed to determine their role, if any, in IPF initiation and progression, as well as to validate their cellular identity. Aberrant basaloid cells have also been identified in the lungs of patients with chronic obstructive pulmonary disease (COPD), although their numbers were significantly lower than those of IPF lungs (3.3% of total epithelial cells in IPF versus 1.1% in COPD; Adams et al., 2020). However, this suggests the possibility for at least some overlapping disease mechanisms between IPF and other lung diseases.

With the presence of aberrant epithelial cell types in the distal lung parenchyma of IPF patients, the question arises as to where these cells originate from. It is also not known how such cells contribute to disease and whether they are a driver or consequence of disease-related processes. Studies in the mouse have observed migration of epithelial Sox2-derived *Krt5*⁺ cells to distal lung regions following influenza injury (Kumar et al., 2011; Ray et al.,

2016; Vaughan et al., 2015; Xi et al., 2017; Zuo et al., 2015). Genetic lineage tracing of *Axin2*⁺ AT2 cells following influenza infection demonstrated that no *Krt5*⁺ cells arose from this AT2 population (Zacharias et al., 2018). Furthermore, levels of *Sox2* and *Krt5* were low in *Axin2*⁺ AT2 cells, indicating that they were derived from a separate lineage to distal *Krt5*⁺ cells. *Krt5*⁺ epithelium has been exclusively observed within areas of severe alveolar injury following influenza infection, although the number of *Sftpc*⁺ or *Sftpc*⁺ *Krt5*⁺ cells were rare, suggesting that *Krt5*⁺ cells do not efficiently regenerate *Sftpc*⁺ cells (Vaughan et al., 2015; Xi et al., 2017; Zacharias et al., 2018). In the context of human disease, such a finding could have severe implications in proper functioning of the alveolar unit. It is therefore possible that aberrant basaloid cells or indeterminate cells in IPF lungs arise from epithelial cells of the airway, where they migrate to the alveoli upon repeated alveolar insult to assist in re-creating an epithelial barrier. However, recent studies have suggested the hAT2 population as a potential alternative source for aberrant epithelial remodelling in IPF. Upon damage with bleomycin, AT2 cells have been found to transition through an intermediate cell state during the differentiation process to AT1 cells (Choi et al., 2020; Kobayashi et al., 2020; Strunz et al., 2020). These cells, termed damage-associated transient progenitors (DATPs; Choi et al., 2020) or pre-alveolar type-1 transitional cell state (PATS; Kobayashi et al., 2020) expressed the luminal cell marker *Krt8*, and were found to persist in response to chronic *Il-1β*-mediated inflammation (Choi et al., 2020). Interestingly, cells expressing similar transcriptional signatures have been found to persist in fibrotic lungs of human IPF patients (Choi et al., 2020; Kobayashi et al., 2020). Therefore, it is possible that in IPF, chronic inflammation and damage to the hAT2 population results in a stall in differentiation between hAT2-DATP-hAT1 cells, leading to accumulation of DATPs, loss of hAT1 cells and inefficient repair of the alveolar epithelium. It remains to be confirmed whether aberrant epithelial cell types in IPF, such as basaloid cells, are the same population as DATPs/PATS, or whether they represent a different population. However, due to the heterogenous nature of the disease, coupled with a host of complex disease processes that act across cellular compartments, it is possible that the aberrant epithelial cell types observed in the IPF lung epithelium arise from multiple sources and could be considered as separate populations. Future work involving detailed phenotypic characterisation and comparison of molecular signatures will increase our understanding of these cells and how they contribute to disease.

1.6.2. Potential IPF disease mechanisms

1.6.2.1. Alveolar cell dysfunction

While traditionally considered to be an inflammatory-driven disease, with chronic inflammation thought to lead to repetitive damage to the alveolar epithelium, the lack of ongoing inflammation and failure of immunosuppressant treatments in alleviating IPF-related symptoms suggested an alternative source (King et al., 2009; Raghu et al., 2008; The Idiopathic Pulmonary Fibrosis Clinical Research Network, 2012). Due to the observation of epithelial remodelling and “hyperplastic” hAT2 cells in IPF-derived lung parenchyma, the contribution of the alveolar epithelium to IPF-related fibrogenesis and scar formation was alternatively considered. Specifically, chronic injury to resident hAT2 stem cells has more recently been proposed as a potential source of dysregulated repair and pathogenic activation of fibroblasts in IPF. There are number of studies that appear to support this hypothesis.

Firstly, as discussed in the previous section, scRNA-seq analysis of human IPF lung parenchyma has indicated a reduction in the total number of hAT2 cells versus healthy control lungs, suggesting potential stem cell exhaustion (Xu et al., 2016). A number of additional studies involving analysis of human IPF lungs have also revealed increased levels of apoptotic cells, a finding that is not recapitulated in healthy lungs, again suggesting potential hAT2 exhaustion. Furthermore, Transforming Growth Factor- β 1 (TGF β 1), a potent pro-fibrotic cytokine that is present at high levels in human IPF lungs, has been shown to mediate fibroproliferative effects through induction of AT2 apoptosis (Lee et al., 2004). This study utilised a triple transgenic mouse system to target biologically active TGF β 1 to the lung using a CC10 (Scgb1a1) protein promoter, and achieved epithelial apoptosis followed by inflammation, fibrosis and alveolar remodelling. TGF β 1 and its role in IPF will be discussed in greater detail in section 1.6.2.2.

In some cases of familial or sporadic human IPF, around 60 separate mutations have been discovered within the *SFTPC* gene, a key gene expressed in hAT2 cells (Katzen et al., 2019). Of these mutations, two have been identified as the most prevalent and well-studied; I73T and L188Q. I73T, the most common SFTPC-related mutation observed in IPF, is a missense mutations that has been shown to cause mis-trafficking of SFTPC to the cell surface rather than to multivesicular bodies in both mouse and human AT2 cells

(Alysandratos et al., 2021; Dickens et al., 2021). Meanwhile L188Q is a T→A transversion in exon 5, causing the SFTPC precursor protein to not fold correctly in the ER, leading to ER stress and activation of the unfolded protein response. ER stress can also initiate hAT2 apoptosis (Kropski and Blackwell, 2018). Both of these mutations suggest a role for dysregulated hAT2 cells in the pathogenesis of IPF. As a proof-of-concept, an inducible knock-in mouse model was created that allowed for regulated expression of *Sftpc*^{L73T} (Nureki et al., 2018). Upon tamoxifen treatment and induction of *Sftpc*^{L73T}, levels of misprocessed pro-Sftpc^{L73T} rapidly increased, in addition to mortality rates. This early stage was accompanied by diffuse parenchymal lung injury, inflammation and poly-cellular alveolitis, while later stages (2-4 weeks) displayed aberrant remodelling, collagen deposition and AT2 dysplasia. Interestingly, multiple human-related IPF biomarkers were also observed. This study indicated that induction of an IPF-related mutation into the *Sftpc* gene of AT2 cells was sufficient to drive spontaneous lung fibrosis, further strengthening the role of AT2 cells in IPF pathogenesis. Similar findings have also been observed upon induction of *SFTPC*^{L73T} in hAT2 cells *in vitro*. For example, establishment of iPSC-derived hAT2 cells from the fibroblasts or peripheral blood mononuclear cells of patients with heterozygous *SFTPC*^{L73T/WT} mutation successfully modelled aspects of pulmonary fibrosis (Alysandratos et al., 2021). Mutant iPSC-derived hAT2 cells exhibited reduced progenitor capacity, metabolic reprogramming and acted as a pro-inflammatory hub through activation of the NFκB pathway. As with previous studies, SFTPC was found to be misprocessed and mis-trafficked within hAT2 cells when compared with gene corrected iPSC-derived hAT2 cells.

While the *SFTPC*^{L73T} mutation represents the most common clinical *SFTPC*-related mutation involved in pulmonary fibrosis, the majority of the 60 described human-related mutations in the *SFTPC* gene occur in the distal C-terminal (residues 94–197) BRICHOS domain of the SFTPC pro-protein (pro-SFTPC; Katzen et al., 2019; Maguire et al., 2011). Such mutations lead to aggregation of pro-proteins and ER stress. A mouse model generated containing a *Sftpc*^{C121G} mutation confirmed retention of pro-Sftpc in the ER which led to substantial epithelial ER stress both *in vitro* and *in vivo* (Katzen et al., 2019). Furthermore, fibrotic remodelling of the lung was also observed and cytokine expression was similar to that observed in BALF of paediatric ILD patients. As with previously described studies, this work again implicated the role of dysregulated hAT2 cells in the aberrant induction of sporadic pulmonary fibrosis. Finally, besides mutations within the

SFTPC gene, 20-25% of sporadic and familial forms of IPF also exhibit shorter telomeres, particularly within hAT2 cells, leading to increased cellular stress (Alder et al., 2008; Courtwright and El-Chemaly, 2019; Victorelli and Passos, 2017). Furthermore, approximately 15% of patients with familial IPF have TERT/TERC mutations. A number of telomere-related mutations have been reported, including missense, frameshift, and splice site mutations. Together, these studies implicate the hAT2 population as a key cell involved in IPF-initiation and progression. However, much work still remains to determine the precise mechanisms for hAT2 dysregulation or depletion in IPF, particularly in the context of early stages of the disease.

1.6.2.2. TGF β signalling

Of all the signalling pathways and signalling molecules that have been implemented in playing a role in IPF initiation or progression, one of the major contenders is TGF β . TGF β is one of the most well-studied pro-fibrotic cytokines and has a role in several different processes, including cellular differentiation, proliferation, wound healing and apoptosis (Meng et al., 2016). In the lung, it is produced by a wide variety of cell types, including alveolar macrophages and activated alveolar epithelial cells (Fernandez and Eickelberg, 2012). While usually secreted as an inactive form, activation of TGF β under various conditions, including but not limited to presence of reactive oxygen species (ROS) or tissue stiffness, results in its cleavage and release from the latency-associated peptide/latent TGF β -binding protein complex. Such activation of extracellular TGF β stores is considered a fundamental process in fibrogenesis and fibrotic diseases, including IPF (Meng et al., 2016). Although TGF β has three major isoforms in mammals, it is TGF β 1 that has been implicated as having a substantial role in IPF (Ask et al., 2008; Khalil et al., 1996). TGF β 1 can induce differentiation of pulmonary fibroblasts to myofibroblasts, which in turn produce high levels of collagen and ECM deposition, resulting in a loss of lung elasticity and function (Yue et al., 2010). Additionally, activation of TGF β 1 via cell surface integrin receptors, in particular α β 6 integrins, has been shown to be a central process in disease pathogenesis in animal models of fibrosis (Tatler et al., 2016). Furthermore, the α β 6 integrin is up-regulated in patients with IPF (John et al., 2020). Together, these findings highlight the potential role of TGF β in fibrotic diseases such as IPF.

1.6.2.3. Wnt signalling

As discussed previously, Wnt signalling plays a vital role in tissue development, as well as in the self-renewal and specification of multiple stem cells (Barker et al., 2007; Clevers et al., 2014a). Aberrant reactivation of developmental signalling pathways has been suggested to play a role in IPF pathogenesis (Königshoff et al., 2008). Increased nuclear β -catenin has been reported in IPF tissue sections, suggesting an increase in Wnt signalling (Chilosi et al., 2003). Furthermore, matrix metalloproteinase (Mmp) 7, a Wnt target gene, is also increased in IPF along with numerous components of the Wnt signalling pathway, including multiple Wnt receptors and the intracellular signal transducer GSK3 β (Königshoff et al., 2008). Therefore, Wnt signalling is considered to be another major player in the pathogenesis of IPF.

1.6.2.4. Notch signalling

Reactivation of a series of developmental programmes, including Wnt, Hippo and Notch, has been observed in IPF tissues. The Notch signalling pathway is a highly conserved cell-cell signalling pathway that functions through short-range cellular communication in a juxtacrine manner (Bray, 2006; Bray, 2016; Figure 1.8). In both humans and mice, the pathway initiates with four receptors and five canonical ligands. Upon binding of one of the ligands to the Notch receptor, the Notch intracellular domain (NICD) undergoes three cleavages, the third of which is performed by γ -secretase. This leads to the NICD being cleaved from the receptor and its translocation to the nucleus, where it acts as a co-receptor for the induction of Notch target genes such as Hes family bHLH transcription factor 1 (HES1; Bray, 2016). A number of studies, including scRNA-seq analysis, have reported that Notch signalling becomes re-activated in hAT2 cells of IPF lungs (Reyfman et al., 2019; Wasnick et al., 2019). Inhibition of Notch signalling in IPF-derived *ex vivo* precision-cut lung slices resulted in an increase in mature surfactant protein B (SFTPB) and a reduction of ECM staining versus PCLS from healthy lungs (Wasnick et al., 2019). This study indicated that Notch signalling induced a fibrotic phenotype, whereas Notch inhibition attenuated lung fibrosis. Nuclear HES1 expression has also been observed within hAT2 cells of human IPF lung tissue (Wasnick et al., 2019). In the mouse, it has been shown that following acute lung injury with *Pseudomonas aeruginosa*, Notch signalling is activated in AT2 cells for alveolar repair (Finn et al., 2019). However, deletion of Dlk1 (a non-canonical Notch ligand that can inhibit Notch signalling) in an inducible AT2-specific

conditional knock-out mouse line (*Dlk1^{ΔAT2}*), followed by genetic lineage tracing, demonstrated impaired AT2-to-AT1 differentiation (Finn et al., 2019). This work suggested that inhibition of Notch by the non-canonical Notch ligand *Dlk1* is required for complete AT2-AT1 differentiation, implicating persistent Notch signalling in the impairment of AT2-to-AT1 differentiation. Furthermore, persistent Notch activation has been found to activate a Δ Np63/Krt5 program in LNEPs of influenza or bleomycin damaged mouse lungs (Vaughan et al., 2015). Activation of this programme resulted in a failure to properly regenerate the damaged alveolus. Interestingly, the development of epithelial honeycomb cysts similar to those found in IPF were also observed during persistent activation of Notch post-injury. In contrast, blocking Notch promoted an alveolar cell fate (Vaughan et al., 2015). Inhibition of Notch signalling has also been implicated in driving secretory club cell plasticity to AT2 cells in both the human and mouse, again suggesting that repression of Notch can promote alveolar differentiation programmes (Choi et al., 2021).

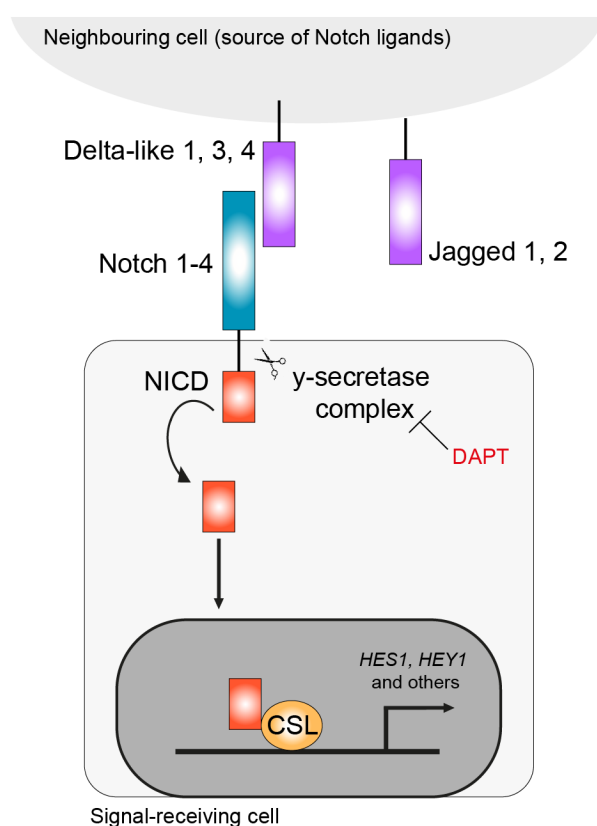


Figure 1.8. Canonical Notch signalling pathway.

Simplified schematic of the Notch signalling pathway. CSL, CBF1/suppressor-of-hairless/Lag-1; NICD, Notch intracellular domain. DAPT is a molecule that can be used to inhibit notch signalling through the inhibition of γ -secretase.

1.6.2.5. Hypoxia

Due to the excess accumulation of fibroblasts, myofibroblasts and ECM components that occurs in IPF lungs, a lack of tissue oxygenation leads to the creation of a hypoxic environment, with hypoxia considered to be one of the prominent features of late-stage IPF (Aquino-Gálvez et al., 2019). Thus, hypoxia has been found to contribute to the pathogenesis of fibrotic diseases and is also observed in cancers (Lee et al., 2019; Senavirathna et al., 2018; Zhang et al., 2013). Hypoxia mediates the expression of many downstream genes through hypoxia-inducible factors (HIFs), of which there are three isoforms; HIF1, HIF2 and HIF3 (Lee et al., 2019). Each isoform is further composed into two subunits; alpha (α) and beta (β). While the HIF- β subunit is constitutively expressed, the HIF α subunit is sensitive to oxygen levels, and contains amino- and carboxyl-terminal oxygen-dependent degradation domains (termed NODDD and CODDD, respectively). When oxygen concentration within tissue is low, proline residues within the HIF α degradation domains are not hydroxylated, preventing HIF α from undergoing proteasomal degradation. This in turn allows HIF α to translocate to the nucleus, where it subsequently binds to the HIF β subunit to initiate target gene transcription. Hypoxia mimetics such as cobalt chloride and deferoxamine allow for stabilisation of HIF1 α under normal physiological oxygen levels through inhibition of prolyl-hydroxylase-mediated HIF1 α degradation (Guo et al., 2006; Triantafyllou et al., 2006).

While the majority of studies have concentrated on the effect of hypoxia on fibroblast populations and myofibroblast activation, a number of more recent studies have indicated a role for hypoxia in the regulation of epithelial cells during pulmonary fibrosis. As previously discussed, following influenza infection, LNEPs within mouse lungs exhibit induction of a Δ Np63/Krt5 program in a Notch-dependent manner, while blockade of Notch signalling resulted in differentiation to AT2 cells (Vaughan et al., 2015). Interestingly, further studies have identified that local lung hypoxia, mediated by HIF1 α , drives Notch signalling and Krt5⁺ basal-like cell expansion in mouse lungs following H1N1 (P8) influenza infection (Xi et al., 2017). In contrast, deletion of *HIF1 α* within Sox2⁺ LNEPs blocked Notch and Krt5 activation and instead promoted differentiation to AT2 cells, allowing for improved alveolar repair (Xi et al., 2017). Furthermore, transcriptional profiling of single hAT2 cells from fibrotic human lungs revealed the presence of a hypoxic subpopulation that displayed activated Notch levels, reduced SFTPC expression and

aberrant trans-differentiation to a KRT5⁺ basal-like cell state (Xi et al., 2017). In an alternative study, IL-1 β -driven inflammation and HIF1 α regulation has also been implicated as an essential regulator of AT2-to-AT1 differentiation in the mouse lung (Choi et al., 2020). Analysis of scRNA-seq data derived from lineage-traced AT2 cells from *SFTPC-Cre^{ERT2};R26^{RtdTomato}* mice following bleomycin lung injury revealed the presence of the AT2-AT1 intermediate cell state, DATPs. A unique metabolic signature was identified in DATPs that featured higher expression of glycolysis-related genes and enrichment of *HIF1 α* expression. Interestingly, deletion of *HIF1 α* specifically within the AT2 cell population inhibited generation of AT1 cells, both *in vitro* and *in vivo* (Choi et al., 2020). DATPs share similar transcriptional signatures to the aberrant “basaloid” populations of KRT5⁻ KRT17⁺ cells in the lungs of IPF patients (Adams et al., 2020; Choi et al., 2020; Habermann et al., 2020; Kobayashi et al., 2020). Therefore, it is possible that incorrect maintenance of HIF1 α -mediated glycolysis in hAT2 cells leads to inefficient differentiation to hAT1 cells and accumulation of DATPs. As local lung hypoxia has been reported to be increased in IPF lungs, particularly in regions of active remodelling, additional work needs to be performed to better understand the effects of hypoxia on epithelial cells of the human lung during IPF progression.

1.6.2.6. The inflammatory niche

While no longer considered to be the main driving force of IPF pathogenesis, the contribution of the inflammatory system to complex IPF-related disease processes cannot be overlooked, particularly as a number of inflammatory cytokines are found to be increased in IPF patient lungs (Schruf et al., 2020). Various studies have highlighted that rather than being initiated by an inflammatory mechanism, innate and adaptive immune processes could instead orchestrate existing fibrotic responses (Desai et al., 2018). For example, early work demonstrated that alveolar macrophages from IPF patients stimulated fibroblast accumulation in a paracrine manner, while more recent studies confirmed the fibroblast-stimulating properties of lung-derived macrophages (Bitterman et al., 1986; Zhou et al., 2014). In addition to fibroblast stimulation and accumulation, release of inflammatory cytokines from macrophage populations may also have an effect on epithelial cell populations. IL-1 β is a cytokine protein that in humans is encoded by the *IL1 β* gene. Upon IL-1 β binding to its receptor (IL1R1) a structural change occurs in the receptor that allows binding of the co-receptor IL1R3, eventually triggering a cascade of kinases that

produce a pro-inflammatory signal and activation of NF κ B (Dinarello, 2018). A subset of AT2 cells have been found to express the IL1 receptor IL1R1 in both the mouse and human, with levels increased in hAT2 cells from fibrotic lungs (Choi et al., 2020; Reyfman et al., 2019). In the mouse, IL-1 β secreted by interstitial macrophages upon injury has been found to prime IL1R1⁺ AT2 cells prior to their differentiation to DATPs and AT1 cells (Choi et al., 2020). However, mimicking chronic injury and inflammation through sustained IL-1 β treatment of adult mouse AT2-derived organoids resulted in an accumulation of DATPs and stalled AT1 differentiation. This stall in AT1 differentiation could be rescued upon 7-day withdrawal of IL-1 β from the culture system. As mentioned previously, DATPs expressing markers such as *Krt8* and *Cldn4* display similar transcriptional signatures to the KRT5⁻ KRT17⁺ basaloid cells observed in human IPF (Adams et al., 2020; Choi et al., 2020; Habermann et al., 2020; Kobayashi et al., 2020). It is therefore possible that such cells can arise in the lungs of IPF patients through persistent inflammation and injury to the hAT2 population. However, a similar study utilising adult mouse AT2 cells did not find the presence of DATPs in their culture system, and instead suggested that IL-1 β (and TNF- α) treatment promoted increased AT2 proliferation (Katsura et al., 2019). Nevertheless, this could be due to the use of a lower concentration of recombinant cytokine versus the study by Choi et al. Furthermore, presence of DATP-related markers was not specifically assessed.

In addition to IL-1 β , TNF- α is another inflammatory cytokine that is present at high levels in the BALF of IPF patients and is thought to play an important role in the development of pulmonary fibrosis (Fujita et al., 2003; Schruf et al., 2020). TNF receptor 1 (TNFSFR1) is expressed across many cell types in the human lung. However, there is increased expression in some fibrosis-derived AT2 cells (Reyfman et al., 2019). The effects of cytokines on hAT2 cells have also been assessed *in vitro*. IL-13 was found to reduce SFTPC expression in both mouse and human organoids established from adult AT2 cells (Glisinski et al., 2020). Interestingly, IL-13-treated mouse AT2 cells exhibited aberrant expression of KRT5, a phenomenon that is observed in fibrotic or injured lungs of both mouse and humans (Adams et al., 2020; Habermann et al., 2020). The same was not observed for hAT2 cells, but may be due to the presence of MRC5 fibroblasts in the culture system. A separate study utilising iPSC-derived hAT2 cells in an air-liquid interface (ALI) culture discovered a similar loss of SFTPC and gain of KRT5 and airway-related transcripts upon culture with a ‘cytokine cocktail’ (Schruf et al., 2020). This cytokine cocktail contained

nine individual cytokines found to be upregulated in IPF-derived BALF or sputum; TGF- β 1, IL-1 β , TNF- α , IL-8, MCP-1, IL-33, TSLP, IL-13 and IL-4. IL-13 in particular was postulated to be a driver of proximalisation in the culture system, as removal of IL-13 from the cytokine cocktail impaired the induction of airway-associated markers. However, IL-13 failed to fully recapitulate all findings associated with the full cytokine cocktail, making it likely that a single cytokine may not be sufficient to drive all aspects of IPF disease. Furthermore, during the differentiation process to AT2 cells, rare KRT5⁺ basal cells were already present prior to cytokine treatment (Schruf et al., 2020). Therefore, the potential contribution of these cells to the observed increase in airway cells upon cytokine treatment needs to be assessed to rule out the possibility of basal cell expansion rather than KRT5 induction in hAT2 cells. It is important to note that due to the complex nature of IPF disease processes, coupled with various interactions between cells across multiple compartments, the likelihood of one specific mechanism being involved in the initiation of IPF is unlikely.

1.6.3. Current models of lung fibrosis

In an attempt to better understand the initiation and progression of IPF and pulmonary fibrosis, a host of *in vivo* and *in vitro* models have been employed. These have included *in vivo* mouse models in addition to various *in vitro* and *ex vivo* studies involving the use of human primary cells and lung tissue. However, no IPF models thus far have been able to fully-recapitulate all aspects of disease.

1.6.3.1. Bleomycin and transgenic mouse models

The majority of IPF disease models to date have involved the use of various animal models (Tashiro et al., 2017). A number of models exist that have involved the use of various chemicals, such as silica and asbestos (Tashiro et al., 2017). However, the most traditional model for studying IPF initiation and disease processes *in vivo* has been the bleomycin experimental mouse model. This system involves instillation (usually through the trachea) of a single-dose of bleomycin, a chemotherapeutic drug known to cause pulmonary interstitial fibrosis, into the lungs of mice. Although such models result in an increase in collagen deposition within the lung parenchyma, as is observed in patients with IPF, the development of patchy fibrosis and rapid immune infiltration are unlike human disease. Furthermore, resolution of fibrosis approximately 21 days after bleomycin injury is unlike

the progressive fibrosis that is observed in human IPF lungs. From the observation of rapid immune infiltration and assessment of early molecular signatures, it has been shown that bleomycin injury results in injury more similar to the accelerated acute phase of IPF in humans rather than long-term, progressive fibrosis (Peng et al., 2013). Despite these findings, the bleomycin mouse model remains the most well-characterised *in vivo* model of IPF, and has been used for preclinical studies into the two approved IPF drugs; Pirfenidone and Nintedanib. A more human-relevant bleomycin mouse model was later achieved through repetitive intratracheal instillation of bleomycin in order to more accurately model the recurrent alveolar injury thought to occur in human IPF (Degryse et al., 2010). Similar to human UIP, harvested lungs following multi-dose bleomycin treatment exhibited AT2 hyperplasia and marked fibrosis. When compared to single-dosed mice, multi-dose bleomycin injury (twice a week for 8 weeks) resulted in significantly higher overall levels of lung fibrosis. Furthermore, fibrotic remodelling persisted for 10 weeks, longer than the ~21 days observed in single-dose models (Degryse et al., 2010). However, unlike in human IPF lungs, observations of fibroblastic foci were rare and epithelial honeycombing was not observed, although this could be due to the relatively short experimental time-frame. Despite this, bleomycin mouse models of IPF have been fundamental in advancing our knowledge of various disease processes, such as defining the role of fibroblasts and myofibroblasts in pulmonary fibrosis and identifying cytokines involved in fibrotic development. The majority of bleomycin lung injury studies have involved the use of young male mice, therefore it will be important in future to assess the effects of bleomycin injury on aged mice, as IPF is generally considered to be an age-related disease (Redente et al., 2011; Sueblinvong et al., 2012).

In addition to bleomycin injury, more recent animal models have involved transgenic approaches to introduce IPF-related mutations into the cells of mouse lungs. As previously discussed, development of an inducible knock-in mouse model that allowed for regulated expression of *Sftpc*^{L73T}, a human IPF-associated mutation, resulted in diffuse parenchymal lung injury, inflammation and poly-cellular alveolitis (Nureki et al., 2018). This was then followed by aberrant lung remodelling, collagen deposition and AT2 dysplasia, similar to observations made in human IPF lungs. In addition, introduction of an alternative mutation into the *Sftpc* gene (*Sftpc*^{C121G}) led to fibrotic remodelling of the lung and similar cytokine expression patterns to those observed in BALF of paediatric ILD patients, again highlighting the utility of animal models (Katzen et al., 2019). However, although animal

models have proved useful in modelling aspects of lung fibrosis, they fail to fully recapitulate the complexity of human disease initiation and progression. Therefore, more human-specific models are required to better understand IPF.

1.6.3.2. Precision-cut lung slices

The need to find a suitable human-specific model that could complement animal studies has led to the development of *ex vivo* and *in vitro* systems that allow the culture and propagation of tissue and cells derived from human IPF lungs, or the study of IPF-related mutations and processes (Evans and Lee, 2020). PCLS involve the isolation and *ex vivo* culture of tissue from healthy or diseased lungs, and recapitulate tissue-specific features such as cellular architecture. One of the benefits of this system has been maintenance of alveolar structure, a component that is lacking from *in vitro* systems (see also Section 1.6.6.3; Parrish et al., 1995; Placke and Fisher, 1987). A recent pre-print demonstrated the utility of PCLS in modelling IPF-associated disease related to a specific cell type, in this case hAT2 cells (Wasnick et al., 2019). PCLS derived from IPF patients exhibited an increase in mature SFTPb upon inhibition of Notch signalling with the γ -secretase inhibitor DAPT (Wasnick et al., 2019). Meanwhile, a separate study assessed the effects of a ‘fibrosis cocktail’ on PCLS derived from excess tissue of healthy donor lungs (Stegmayr et al., 2021). Following 48-hours of treatment, bulk RNA-sequencing analysis demonstrated that PCLS exhibited increased gene expression levels of fibrotic-related transcripts and decreased alveolar markers such as *SFTPC* and *HOPX*, indicating a fibrotic response. Resulting fibrotic PCLS were also treated with two novel drugs, both of which demonstrated a reduction in fibrotic gene expression *ex vivo*. Together, these studies highlight the utility in using human PCLS to assess aspects of IPF-related processes. However, their limited long-term culture ability coupled with the inability to study *in vivo* processes such as immune cell recruitment indicate that improvements need to be made to increase their usefulness in studying complex diseases such as IPF (Evans and Lee, 2020; Neuhaus et al., 2017)

1.6.3.3. *In vitro* cultures

Advances in *in vitro* culture of human epithelial cells, particularly as 3D-organoids, have allowed for investigations into IPF- and fibrotic-related processes. CRISPR/Cas9 editing of hPSC-derived lung organoids was used to model Hermansky-Pudlak syndrome (HPS),

a rare disorder in which specific mutations within protein complexes leads to the development of pulmonary fibrosis. The resulting organoids demonstrated a fibrotic phenotype, with the presence of increased numbers of mesenchymal cells, and enhanced levels of fibronectin and collagen deposition compared with non-mutated organoids (Chen et al., 2017; Strikoudis et al., 2019). Patient-derived HPS organoids containing a mutation in the HPS2 gene were gene-corrected using CRISPR/Cas9, with restoration of the protein trafficking gene *APB31* achieved at the transcriptional level (Korogi et al., 2019). Subsequently, the inflammatory cytokine IL-11 was found to be upregulated in both fibrotic organoids and IPF patients, and treatment of HPS-mutated organoids with IL-11 was essential for fibrosis induction (Strikoudis et al., 2019). Similarly, IL-13 is upregulated in the broncho-alveolar lavage fluid (BALF) of IPF patients, and may be implicated in IPF pathogenesis. Interestingly, IL13 was found to reduce the number of SFTPC⁺ hAT2 cells in adult hAT2 cell-derived organoid culture (Glisinski et al., 2020). As the organoids were co-cultured with supporting stromal cells, it is not yet known whether the effects of IL-13 were acting directly on the hAT2 population or indirectly through interaction with the supporting mesenchyme. In contrast to assessing the effect of inflammatory cytokines, a separate study assessed the effect of the IPF-associated mutation *SFTPC*^{I73T} in iPSC-derived hAT2 cells (Alysandratos et al., 2021). Resulting hAT2 cells exhibited reduced progenitor capacity, improper SFTPC trafficking and metabolic reprogramming similar to IPF patients. Despite the increase in human-relevant models of IPF, the precise mechanisms of disease initiation and progression remain to be discovered.

1.7. Outstanding questions and project aims

It is evident that there is much knowledge still to be gained in regard to hAT2 cell maintenance mechanisms, and how these mechanisms may become dysregulated in IPF. The lack of appropriate, human-specific *in vitro* hAT2 models has made it difficult to understand hAT2 cell maintenance and their potential role in disease. Furthermore, although mouse alveolar and IPF models are currently more numerous and advanced than their human counterparts, the clear differences between the mouse and human lung need to be considered. Therefore, establishment of a human-relevant hAT2 cell model is required. In particular, defining conditions that do not rely on supporting mesenchymal cells is of particular interest. Optimising conditions for *in vitro* culture of adult hAT2 cells will not

only increase our understanding of their cellular requirements for growth, cell maintenance and differentiation, but will also allow for investigations into how their dysregulation can lead to disease.

Therefore, during my project I aimed to establish an *in vitro* human alveolar organoid system from adult hAT2 stem cells in chemically-defined conditions. I investigated multiple growth factors to assess the essential requirements for hAT2 self-renewal, maintenance and differentiation. Finally, I utilised my alveolar organoid system in order to assess the effect of HIF1 α -mediated hypoxia and cytokine presence on hAT2 cell maintenance. Both hypoxia and chronic inflammation have been previously found to result in an accumulation of DATPs and a stall in proper AT2 differentiation to AT1 cells in injured mouse alveoli (Choi et al., 2020), and have also been implicated in IPF. Application of my organoid system allowed for the study of these aberrant disease-processes, implicating hAT2 cells as a potential contender in the initiation or progression of IPF.

CHAPTER 2

Materials and Methods

A list of reagents and commercial kits used in this study can be found in Table 2.1.

2.1. Human lung tissue

2.1.1. *Tissue acquirement, ethics and HTA guidance*

Distal parenchymal tissues from deidentified lungs not required for transplantation were obtained from adult donors with no background lung pathologies from Addenbrookes Hospital (Cambridge University NHS foundations trust; Krishnaa T. Mahbubani, Kourosh Saeb-Parsy) under appropriate Human Tissue Act (HTA) guidance. Additional control lung tissue was obtained from UCL Hospital (NHS University College London Hospitals; Sam Janes and Sarah Clarke) and Papworth Hospital NHS research tissue bank (Research Tissue Bank Generic REC approval, Tissue Bank Project number T02233) and derived from regions distant from tumours of patients undergoing lobectomy for lung cancer. Normal lung architecture and absence of tumour tissue was confirmed by a pathologist. IPF lung tissue was obtained from patients upon lung transplantation and provided by Papworth Hospital NHS research tissue bank (T02233). Informed consent was obtained from all subjects. Tissue information can be found in Table 2.2.

2.1.2. *Fixation and preparation for paraffin embedding/cryo-protection*

Fresh tissue was transported in alphaMEM (STEMCELL Technologies) or Hibernate media (Gibco) supplemented with 1 U/mL Penicillin/Streptomycin (Pen/Strep), 50 µg/mL Gentamicin, 250 ng/mL Amphotericin B and either processed immediately, or stored overnight at 4 °C. For fixation, spare tissue was cut using a scalpel into 1 cm x 1 cm cubes

and immersed into 4% formaldehyde for 12 hours at 4 °C with rotation. Following fixation, tissue was washed three times with PBS for 5 min each wash, followed by a 1 hr wash in PBS at 4 °C with rotation. Tissue was transferred to plastic histology cassettes and stored in 70% ethanol (EtOH) prior to paraffin embedding. Dehydrated samples were cleared in xylene, and paraffin infiltration was performed overnight using a TP1020 Leica Tissue Processor. The following day, tissue was paraffin embedded using EG1160 Leica Embedding Station, and 4.5 µm paraffin sections were prepared using a microtome (RM2255: Leica). Sections were flattened using a 45 °C water bath, and collected on Superfrost Plus slides. Paraffin embedding, section cutting and mounting was performed by Irina Pshenichnaya (Wellcome-MRC Cambridge Stem Cell Institute histology core facility). H&E staining was performed using Harris Haematoxylin and 0.5% Eosin. For cryoprotection, fixed tissues were incubated in increasing concentrations of sucrose solution (15%, 20%, 30%; diluted in PBS) for 1 hr each at room temperature (RT) with agitation. Tissue was then transferred to a cryoblock containing 100% optimal cutting temperature (OCT) compound, and allowed to freeze on dry ice. Sections were cut to a thickness of 5-7 µm using a cryostat (Leica).

2.1.3. Tissue processing for cell dissociation from normal background lung

Tissue was processed as soon as possible in order to minimise cell yield loss and maintain cell viability. Tissue was washed with PBS to remove excess blood and transferred to a 10 cm petri dish, where it was minced into small (1 mm) pieces using a scalpel. Once minced, tissue pieces were transferred into fresh, pre-warmed digestion buffer containing 2U/ mL Dispase II (Sigma), 1 mg/mL Collagenase/dispase (Sigma) and 0.1 mg/mL DNase I (Sigma) in PBS. Tubes were sealed with parafilm, and placed on a rotor at 37 °C for 1 hr with agitation. Time in digestion buffer was limited to maintain cell viability. Tissue cell suspensions were filtered through a 100 µm cell strainer into a 50 mL falcon tube to remove cell debris, and washed with 10 mL of DMEM (Gibco). Remaining tissue in the cell strainer was ground using a syringe plunger to increase cell yield, and washed with a further 10 mL of DMEM. Cells were centrifuged at 350 x g for 10 min, supernatant was carefully aspirated, and cell pellet resuspended in 5 mL red cell lysis buffer (150 mM NH₄Cl, 10 mM KHCO₃ in distilled H₂O) for 5 min at RT. The reaction was quenched using 5 mL of DMEM, and the entire 10 mL of cell suspension was transferred to a 15 mL falcon tube, followed by 10 min centrifugation at 350 x g. Supernatant was removed, and cell pellet

resuspended in DMEM for counting. On average (depending on tissue quality and digestion efficiency) a sample of normal background lung of 2 cm x 2 cm in size was expected to yield in the region of 30 million total cells. These cells could then be used for either fluorescence activated cell sorting (FACS) or magnetic-activated cell sorting (MACS).

2.1.4. Tissue processing for cell dissociation from IPF patient lungs

IPF tissue consists of increased amounts of ECM components and fibrosis in comparison with healthy background lung tissue, which makes the tissue stiffer and more difficult to digest. To combat this, tissue was digested for a longer period of time (2-3 hr), with digested tissue suspension harvested following 1 hr, and undigested tissue fragments incubated in fresh digestion buffer at 37 °C for a further 1 to 2 hr.

2.1.5. Cryopreservation of human lung tissue for long-term storage

When clinical specimens were not immediately required, they were prepared for cryopreservation and long-term storage. Upon receipt of donor or IPF lung specimens, tissue was washed with PBS, followed by transferral to a petri dish. Tissue was chopped into 1 cm³ pieces using a scalpel, and each piece was placed onto the inner surface of a 50 mL conical tube on ice. Using a pair of scissors, tissue pieces were minced into a thick paste. Freezing medium (FBS/10% DMSO) was prepared fresh, and added to the tissue using a 5 mL Strippette. Tissue pieces were pipetted up and down in the freezing solution a couple of times, and then 1 mL of tissue solution was transferred to a cryopreservation tube. Tubes were transferred to a Mr Frosty and stored at -80 °C overnight, after which they were stored in liquid nitrogen for long-term storage. When tissue was required, tubes were thawed quickly for 1 min in a water bath at 37 °C, and tissue solution transferred to 9 mL of pre-warmed DMEM, followed by 5 min centrifugation at 400 x g. Supernatant was then removed, and the tissue pellet was transferred to digestion solution and processed as in 2.1.3 and 2.1.4.

Table 2.1. List of reagents and commercial kits.

Name	Company	Cat. no.
4% Paraformaldehyde	Biosesang	PC2031-050-00
Accutase	STEMCELL Technologies	07920
Alpha Modified Eagle Medium	Merck Sigma-Aldrich	M4526-500ML
Ammonium chloride	Merck Sigma-Aldrich	213330
Amphotericin B	Merck Sigma-Aldrich	A2942
Ampicillin	Merck Sigma-Aldrich	A0166-5G
Anti-mouse IgM human MicroBeads	Miltenyi	130-047-301
Bambanker solution	Alpha Labs	302-14681
Bovine Serum Albumin	Merck Sigma-Aldrich	AB412-100ML
Calcium chloride (CaCl ₂)	Merck Sigma-Aldrich	C1016
CD31 MicroBead kit, human	Miltenyi	130-091-935
CD326 Microbeads, human	Miltenyi	130-061-101
CD45 MicroBead kit, human	Miltenyi	130-045-801
Chloroform	Sigma-Aldrich	C2432
Click-iT EdU kit	Vector Laboratories	C10640
Collagenase/Dispase	Sigma-Aldrich	10269638001
D-glucose	Sigma-Aldrich	G8270
ddH ₂ O	CSCI Core Facilities	N/A
Dispase (Corning)	Fisher Scientific	11553550
Dispase II	Sigma-Aldrich	4942078001
DMSO	Sigma-Aldrich	D2650
DNase I	Sigma-Aldrich	D4527-10KU
EDTA	Sigma-Aldrich	E9884
Ethanol	CSCI Core Facilities	N/A
FBS	Gibco	16000-044
Gentamicin	Sigma-Aldrich	G1397
GFR-Matrigel	CORNING	356231
HEPES	Invitrogen	15630-080
Histogel	Fisher Scientific	HG-4000
Human Serum	Sigma-Aldrich	H4522
Hydrochloric acid (concentrated)	Sigma-Aldrich	320331

Isopropanol	Sigma-Aldrich	I9516
KaryoMAX™ Colcemid™ Solution	Gibco	15212012
KCl	Sigma-Aldrich	P3911
Lenti-X concentrator	Takara Bio Europe	631231
Matrigel growth factor reduced basement membrane matrix	SLS (Corning)	356231
Na ₂ HPO ₄	Sigma-Aldrich	S9763
NaCl	Sigma-Aldrich	S9888
NaOH (5N)	Sigma-Aldrich	S5881
Normal donkey serum	Jackson immuno	NC9624464
OCT compound	VWR International	361603E
PBS	Sigma-Aldrich	D8537-6X500ML
Potassium bicarbonate	Merck Sigma-Aldrich	237205
Power SYBR Green PCR Master Mix	Thermo Fisher Scientific	4367659
PureLink™ HiPure Plasmid Midiprep Kit	Thermo Fisher Scientific	K210005
Rapiclear®	SUNJin Lab	RC152001
Serum-free DMEM	Gibco	41966-029
Sodium citrate tribasic dihydrate	Sigma-Aldrich	6858-44-2
Sucrose	Sigma-Aldrich	S0389-500G
SuperScript IV	Thermo Fisher Scientific	18091050
Tris-base	Merck Sigma-Aldrich	TRIS-RO
Triton X-100	Sigma-Aldrich	T9284-100ML
TRIzol	Thermo Fisher Scientific	15596026
TrypLE Select	Gibco	12563-029
Trypsin/EDTA	CSCI Core Facilities	N/A

Table 2.2. Patient information.

Patient number	Patient ID	Age	Sex	Procedure and diagnosis	Background lung disease (excluding cancer)	Smoking history	Cells isolated
Donor 1	P306	68	F	Right upper lobectomy for LUAC	Mild emphysema	Yes (current)	EpCAM+
Donor 2	P312	57	M	Squamous cell carcinoma	None	Yes (current)	EpCAM+
Donor 3	TB18.0130	57	M	Right upper lobectomy for LUAC	None	Yes (current)	EpCAM+
Donor 4	P329	56	F	Right lower lobectomy for lesion	None	No	HTII-280 (+ and -)
Donor 5	P367	74	F	Lobectomy for LUAC	None	No	HTII-280 (+ and -)
Donor 6	502B	61	F	Donation after brainstem death	None	No	HTII-280 (+ and -)
Donor 7	538C	52	M	Donation after circulatory death	None	Yes (current)	HTII-280 (+ and -)
Donor 8	ASC-017X	57	F	Lobectomy for LUAC	None	No	HTII-280 (+ and -)
Donor 9	640C	74	F	Donation after circulatory death	None	No	HTII-280 (+ and -)
IPF 1	TB18.0763	68	M	Single right lung transplant	IPF	No	HTII-280 (+ and -)
IPF 2	TB18.0893	57	M	Single left lung transplant	IPF	Yes (past)	HTII-280 (+ and -)
IPF 3	TB19.0018	67	M	Lung transplant	IPF and emphysema	Yes (past)	HTII-280 (+ and -)
IPF 4	TB19.0379	66	M	Single left lung transplant	IPF	Yes (past)	HTII-280 (+ and -)
IPF 5	TB20.0031	56	M	Single left lung transplant	IPF	No	HTII-280 (+ and -)
IPF 6	TB21.0215	64	M	Lung transplant	IPF and asbestos exposure	Yes (past)	HTII-280 + ITGB4

2.2. Generation and culture of human 3D adult alveolar organoids

2.2.1. Antibody preparation for flow cytometry

For isolation of LysoTracker^{high} cells, cells were incubated prior to primary antibody addition with 50 ng/ μ L of LysoTrackerTM (Invitrogen, L12492), diluted in pre-warmed expansion medium, for 30 min at 37 °C and protected from light. Cells were pelleted by centrifugation at 350 x g for 5 min, and washed twice in PF10 buffer (10% FBS in PBS). Supernatant was removed, and cells were resuspended in PF10 buffer at a ratio of 4 million cells/ 100 μ L of buffer. A small volume of cell suspension was removed and placed into separate Eppendorf tubes for non-stained and single stained FACS controls. Cells were stained with primary antibodies (Table 2.3 and 2.4) at a dilution of 1:40 per 4 million cells for 30 min on ice, unless otherwise stated. Non-stained and single-stained samples were prepared as compensation controls. Cells were washed twice with excess cold PF10 buffer, and incubated with fluorescence-conjugated secondary antibodies, where required (Table 2.3) at 1:100 for 30 min on ice. Cells were washed with PF10 buffer, and counted using a haemocytometer to assess dilution required for final volume. Cells were diluted at a concentration of 30 million cells/ mL and filtered through a 35 μ m cell strainer into polypropylene FACS tubes. Samples were sorted on an Aria III fusion using a 100 μ m nozzle into polypropylene collection tubes containing 1 mL of PF10 buffer.

2.2.2. Antibody preparation for Magnetic-activated cell sorting (MACS)

Cells were centrifuged at 350 x g for 5 min, supernatant was removed, and cells resuspended in fresh cold MACS buffer (2 mM EDTA, 0.5% BSA in PBS) at a dilution of 50 million cells per 500 μ L of buffer. For negative antibody selection, cells were stained with CD31 and CD45 beads (Miltenyi) at a ratio of 1:50 each, and incubated for 30 min on ice. LD-columns (Miltenyi) were placed into a MACS separator stand (Miltenyi) above 15 mL falcon tubes, and equilibrated with 3 mL of cold MACS buffer. Cells were washed with MACS buffer, applied directly to the columns and allowed to filter through. Columns were washed twice with 3 mL of MACS buffer each wash, and the resulting cell suspension was centrifuged at 350 x g for 5 min. For positive antibody selection of human alveolar type 2 (hAT2) cells, cells were incubated with HTII-280

(IgM) for 30 min on ice, followed by two washes with cold MACS buffer. The staining process was repeated with MACS IgM beads (Miltenyi). LS-columns (Miltenyi) were placed into a MACS separator stand above 15 mL falcon tubes, and equilibrated with 3 mL of cold MACS buffer. Cell suspensions were applied directly to the column, and allowed to filter through, followed by three column washes with 1 mL of MACS buffer each wash. Columns containing the cells of interest were removed from the MACS separator stand and placed above a 15 mL falcon tube containing 1 mL of MACS buffer, followed by application of 5 mL of MACS buffer to the column. A plunger was used immediately to flush the labelled cells through the beads and into the collection tube. Cells were then ready for culture. For further isolation of epithelial HTII-280⁺ cells, HTII-280-depleted cells were incubated with EpCAM beads for 30 min on ice, followed by selection with LS columns as described above.

2.2.3. Establishment of 3D human alveolar organoids

Sorted hAT2 cells (EpCAM⁺ HTII-280⁺; EpCAM⁺ LysoTracker^{hi}, EpCAM⁺ HLA-DR⁺) were cultured in Matrigel growth factor reduced basement membrane matrix (henceforth referred to as Matrigel; Corning) at a ratio of 5000-10,000 cells/ 20 μ L Matrigel in 48-well culture plates or 8-well chamber slides. Matrigel was allowed to solidify for 20 min at 37 °C. For culture in 0.4 μ m pore transwell inserts (Corning), 50 μ L of Matrigel/cell suspension was diluted 1:1 with DMEM at a concentration of 10,000 -20,000 cells per 100 μ L of total volume. 100 μ L of cell suspension was applied to each transwell insert within a 24-well plate, and allowed to solidify at 37 °C for 1 hr. The protein concentration of Matrigel used for this study ranged between 8.7-8.9 mg/mL.

2.2.4. Organoid culture conditions

Culture reagents for alveolar maintenance medium can be found in Table 2.6. To 48-well plates and 8-well chamber slides, 250 μ L of pre-warmed medium was added carefully to each well so that the Matrigel/cell domes were completely submerged. For transwell inserts, 500 μ L of pre-warmed medium was added to each lower chamber. Cultures were maintained under standard conditions (37 °C, 5% CO₂), with medium changes every 2-3 days. ROCK inhibitor was added to cultures for the first 24-48 hr. Additionally-tested components can be found in Table 2.7, further information for which is outlined in the

results. Human airway organoids were cultured under published conditions, unless otherwise stated (Sachs et al., 2019).

2.2.5. 2D-differentiation of organoid-derived hAT2 cells to alveolar type 1 cells

2D-differentiation was performed in collaboration with Taewoo Kim (Ju lab, KAIST). Alveolar organoids were dissociated into single cells using Accutase (STEMCELL Technologies) for 5 min at 37 °C. Following a 5 min wash with PBS, dissociated cells were resuspended in differentiation medium containing DMEM, 10% human serum (Sigma) and 1% Pen/Strep, and seeded at a ratio of 25,000 cells per well either in a LabTek 8-well glass-bottomed slide (ThermoFisher), or in Collagen I coated 8-well glass slide (SPL). Following 4 days of culture, cell attachment was observed, after which cells were fixed and stained with a number of hAT2 and alveolar type 1 (hAT1) markers *in situ* in order to assess differentiation ability (Tables 2.4 and 2.5).

2.2.6. 3D-differentiation of organoid-derived hAT2 cells to hAT1 cells

For 3D-differentiation of organoid-derived hAT2 cells in serum, passage (P)3 or P6 hAT2 cells were cultured in complete medium (Table 2.6) for 10 days, followed by a switch to basic medium containing 10% human serum for a further 11 days of culture. For chemically-defined 3D-differentiation, primary or P6 hAT2 cells were cultured for 14 days in complete medium, followed by removal of CHIR99021 for a further 7 days.

2.2.7. Chemical induction of hypoxia in hAT2-derived organoid cultures

To assess the effect of chemical inducers of hypoxia on hAT2 cell behaviour and identity, primary or P6 hAT2 cells were cultured in complete medium for 14 days, followed by addition of either Cobalt Chloride (CoCl₂) or deferoxamine (DFO) to the complete medium at a concentration of 50 µM or 100 µM for an additional 7 days. For assessment of Notch signalling on hypoxia cultured hAT2 cells, 20 µM of the γ -secretase inhibitor DAPT was added to DFO-treated cultures for the final 4 days of culture.

Table 2.3. Conjugated antibodies for FACS analysis.

Antibody	Conjugation	Dilution	Company	Cat no.	Research Resource Identifier (RRID)
Anti-human CD31	APC	1:40	BioLegend	303116	AB_1877151
Anti-human CD45	APC	1:40	BioLegend	368512	AB_2566372
Anti-human EpCAM	FITC	1:40	BioLegend	324204	AB_756078
Anti-human EpCAM	bv-421	1:40	BioLegend	324220	AB_2563847
Anti-human HLA-DR	FITC	1:50	eBioscience	11-9956-42	AB_2572544
Anti-human ITGB4	Biotin	1:50	Thermo Fisher	13-1049-82	AB_1210583
Anti-mouse IgM	PE	1:100	eBioscience	12-5790-81	AB_465939
Lysotracker TM	Deep Red	50 ng/ μ L	Invitrogen	L12492	N/A
Streptavidin	APC-Cy7	1:100	eBioscience	47-317-82	N/A

Table 2.4. Primary antibodies for immunofluorescence staining (continued on next page).

Antibody	Dilution	Antigen retrieval (paraffin)	Antigen retrieval (cryo)	Whole-mount	Company	Cat no.	Research Resource Identifier (RRID)
Goat anti-RAGE/AGER	1:200	Tris-EDTA	Tris-EDTA	Yes	R&D Systems	AF1145	AB_354628
Mouse anti-ABCA3	1:300	Citrate	N/A	No	Seven Hills Bioreagents	WRAB-ABCA3	AB_577286
Mouse anti-ACT	1:3000	No	N/A	No	Sigma	T7451	AB_609894
Mouse anti-HTI-56 IgG	1:100	N/A	Tris-EDTA	No	Terrace Biotech	TB-29AHT1-56	AB_2847898
Mouse anti-HTII-280 IgM	1:500	Citrate	Citrate	Yes	Terrace Biotech	TB-27AHT2-280	AB_2832931
Mouse anti-KI67	1:200	Citrate	Citrate	Yes	BD Pharmigen	550609	AB_393778
Mouse anti-MUC5AC	1:100	N/A	No	No	Thermo Fisher	MS-145-P0	AB_2314822
Mouse anti-TP63	1:500	Citrate	Citrate	Yes	Abcam	ab735	AB_305870
Rabbit anti-AQP5	1:200	N/A	N/A	Yes	Abcam	ab92320	AB_2049171
Rabbit anti-CAV1	1:200	Citrate	N/A	N/A	Cell Signaling Tech	3267S	AB_2275453
Rabbit anti-CRB3	1:400	N/A	N/A	Yes	Novus Biologicals	NBP1-81185	AB_11038157

Rabbit anti-HOPX	1:200	Citrate	Citrate	Yes	Santa Cruz	sc-30216	AB_2120833
Rabbit anti-ITGB4	1:200	Citrate	Citrate	Yes	Sigma	HPA036349	AB_2675078
Rabbit anti-KI67	1:200	N/A	N/A	Yes	MenaPath	MP-325-CRM01	N/A
Rabbit anti-KRT5	1:500	Citrate	No	Yes	Biologend	905501	AB_2565050
Rabbit anti-KRT8	1:200	Citrate	N/A	N/A	DSHB	TROMA-I	AB_531826
Rabbit anti-KRT17	1:200	Citrate	N/A	N/A	Abcam	ab53707	AB_869865
Rabbit anti-LPCAT1	1:100	Citrate	Tris-EDTA	No	Proteintech	16112-1-AP	AB_2135554
Rabbit anti-SCRIB	1:100	Citrate	N/A	N/A	GeneTex	GTX107692	AB_1241297
Rabbit anti-SFTPB	1:200	Citrate	N/A	N/A	Seven Hills Bioreagents	WRAB-48604	N/A
Rabbit pro-SFTPC	1:500	Citrate	N/A	Yes	Merck Millipore	AB3786	AB_91588
Rat anti-SCGB1A1	1:200	Citrate	N/A	Yes	R&D Systems	MAB4218	AB_2183286
Rat anti-SOX2	1:200	Citrate	N/A	Yes	Thermo Fisher	53-9811-82	AB_2574479
Sheep anti-PDPN	1:200	Citrate	N/A	N/A	R&D Systems	AF3670	AB_2162070

Table 2.5. Secondary antibodies for immunofluorescence staining.

Antibody	Dilution	Company	Cat no.	Research Resource Identifier (RRID)
Donkey anti-goat IgG (H+L), Alexa Fluor 555	1:1000	Thermo Fisher Scientific	A-21432	AB_141788
Donkey anti-Mouse IgG (H+L), Alexa Fluor 488	1:1000	Thermo Fisher Scientific	A-21202	AB_141607
Donkey anti-Mouse IgG (H+L), Alexa Fluor 555	1:1000	Thermo Fisher Scientific	A-31570	AB_2536180
Donkey anti-Mouse IgG (H+L) Alexa Fluor 647	1:1000	Thermo Fisher Scientific	A-31571	AB_162542
Donkey anti-Rabbit IgG (H+L) Alexa Fluor 488	1:1000	Thermo Fisher Scientific	A-21206	AB_2535792
Donkey anti-Rabbit IgG (H+L), Alexa Fluor 555	1:1000	Thermo Fisher Scientific	A-31572	AB_162543
Donkey anti-Rabbit IgG (H+L), Alexa Fluor 647	1:1000	Thermo Fisher Scientific	A-31573	AB_2536183
Donkey anti-Rat IgG (H+L), Alexa Fluor 488	1:1000	Thermo Fisher Scientific	A-21208	AB_2535794
Donkey anti-Sheep IgG (H+L), Alexa Fluor 488	1:1000	Abcam	ab150177	AB_2801320
Goat anti-Mouse IgM (heavy chain), Alexa Fluor 555	1:1000	Thermo Fisher Scientific	A-21426	AB_2535847
Streptavidin-APC	1:1000	eBioscience	17-4317-82	N/A

Table 2.6. Chemical compounds for culture of 3D human-derived alveolar organoids.

Media component	Signalling pathway		Supplier and catalogue number	Stock Concentration	Final Concentration
	activation	block			
Advanced DMEM	Base medium		Fisher Scientific 11510436	N/A	N/A
Hepes	Buffer		Invitrogen 15630-080	1M	10mM
Penicillin / Streptomycin	Antibiotics		CSCI core facility	100U/ml	1U/ml
L/glutamine	Amino acid		CSCI core facility	200mM	2mM
R-Spondin 1 conditioned medium	Wnt/b-catenin signalling		CSCI core facility	N/A	10%
B27 supplement	a.o. insulin signalling		Thermofisher 17504044	50x	1x
FGF 7	FGFR2b signalling		Peptotech 100-19	100µg/ml	100 ng/ml
FGF 10	FGFR2b signalling		Peptotech 100-26	100µg/ml	100ng/ml
Noggin	TGFβ signalling		Peptotech 250-38	100µg/ml	100ng/ml
EGF	Promotes proliferation, differentiation, and survival		Life Technologies PMG8043	2000x	50ng/ml
N-Acetylcysteine	Antioxidant		Sigma A9165	500mM	1mM
Nicotinamide	Co-enzyme precursor		Sigma N0636	2M	10mM
SB431542	TGFβ signalling		Tocris 1614/10	10mM	10uM
*CHIR99021	Wnt/b-catenin signalling		Tocris 4423/10	10mM	3uM
Y-27632 (for first 48 hr)	ROCK signalling		Cambridge Bioscience SM02-100	10mM	10µM

* CHIR99021 not required for culture of airway organoids from EpCAM⁺ HTII-280⁻ cells.

Table 2.7. Additional organoid culture reagents.

Media component	Signalling pathway		Supplier and catalogue number	Stock Concentration	Final Concentration
	activation	block			
Cobalt Chloride (COCl ₂)	HIF1 α -dependent hypoxia		Sigma C8661-25G	100 mM	50 or 100 μ M
DAPT	Notch signalling		Sigma D5942-25MG	20 mM	20 μ M
Deferoxamine (DFO)	HIF1 α -dependent hypoxia		Sigma D9533-1G	100 mM	50 or 100 μ M
Human serum	N/A		Sigma H4522	100%	10%
Recombinant IL-1 β	Inflammatory cytokine		Peptotech 200-01B-2	100 μ g/mL	50 or 100 ng/mL
Recombinant human RSPO-1	Wnt/b-catenin signalling		Peptotech 120-38	500 μ g/mL	500 ng/mL
SB202190	p38 MAPK signalling		Sigma S7067	500 μ M	500 nM
Recombinant TNF- α	Inflammatory cytokine		Peptotech 300-01A-10	100 μ g/mL	50 or 100 ng/mL
WNT3A conditioned medium	Wnt/b-catenin signalling		CSCI core facility	100%	50%

2.3. Maintenance of adult alveolar and airway organoids

2.3.1. *Enzymatic passaging of organoids*

Organoid lines were passaged at different days depending on organoid size, with culture days varying from 21-35 days. Culture medium was removed from wells, 250 μ L of dispase (Fisher Scientific) was added on top of each Matrigel dome, and allowed to incubate at 37 °C for 30 min to allow Matrigel to dissolve. For transwell inserts, media was removed from the bottom chamber, and 100 μ L dispase was added directly to the Matrigel plug. Following incubation, the bottom of the wells were scraped with a P1000 pipette, and the solution gently pipetted up and down and transferred to a 15 mL falcon tube, where the contents of 3 wells were pooled. Wells were washed with 250 μ L DMEM-F12 to harvest as many organoids as possible. Organoids were centrifuged at 350 x g for 10 min. For production of single cells, the pellet was resuspended in 200 μ L of TrypLE (ThermoFisher), and incubated at 37°C for 5-10 min, with pipetting every 1-2 min to gently break up organoids. Success of single cell dissociation was checked under a microscope. TrypLE was quenched by addition of 800 μ L DMEM-F12, cells were centrifuged at 350 x g, and washed once with DMEM-F12. Following counting with a haemocytometer, cells were resuspended in Matrigel at a dilution of 5,000 cells/ 20 μ L and cultured as before. For transwell inserts, 50 μ L of Matrigel/cell suspension was combined with 50 μ L DMEM-F12 per insert at a concentration of 10,000 cells per 100 μ L total volume and cultured as above.

2.3.2. *Mechanical passaging of organoids*

When single cells were not required, organoids could be broken into fragments by removing the media and adding 300 μ L of cold PBS, and incubating at RT for 5 min, or on ice if the entire plate was to be passaged. The well was gently scraped with a pipette tip, and the organoids harvested, followed by further pipetting to break into fragments. This method did not require the use of dispase.

2.3.3. *Karyotyping of late passage alveolar organoids*

Organoid karyotyping was performed by Seon Young Kim (Chungnam National University College of Medicine). Briefly, organoids from 6-month-old cultures were

harvested from Matrigel using Cell Recovery Solution (Corning), and dissociated into single cells using Accutase (STEMCELL technologies) at 37 °C for 5 min. Following a short wash with PBS, cells were incubated with colcemide (Gibco) for 45 min at 37 °C, then rinsed with PBS and incubated with KCl in order to allow for cell enlargement. Cells were fixed with acetone, stained with Giemsa, and karyotypes were observed using Cytovision (Leica).

2.3.4. Transmission electron microscopy

Transmission electron microscopy (TEM) was performed by Yongsuk Her (Biomedical Research Centre, KAIST), Taewoo Kim (KAIST), and Ho Min Kim (KAIST). TEM was performed according to Youk et al., 2020.

2.3.5. Cryopreservation of alveolar organoids for long-term storage

For long-term storage of hAOs, organoids were enzymatically passaged to single cells as described above (section 2.3.1). Single cells were re-suspended in freezing medium (FBS/10% DMSO or serum-free Bambanker [Thermo Fisher]) at a ratio of at least 100,000 cells per mL, and 1 mL was transferred to a cryotube. Tubes were transferred to a Mr Frosty and stored at -80 °C overnight, after which they were stored in liquid nitrogen for long-term storage. When cells were required, tubes were thawed quickly for 1 min in a water bath at 37 °C and cell solution transferred to 9 mL of pre-warmed DMEM, followed by 5 min centrifugation at 400 x g. Cells were then counted and plated at a ratio of 5,000-10,000 cells per 20 µL of Matrigel in a 48-well plate, and cultured as described above.

2.4. Organoid preparation for immunofluorescence analysis

2.4.1. Histogel/ paraffin embedding of organoids

Organoids grown in transwell inserts were used for paraffin embedding and histology at day 21 of culture. Cell medium was removed from the lower chamber of transwell inserts, and pre warmed 4% formaldehyde was added; 500 µL to the lower chamber and 100 µL to the top. Plates were sealed and incubated in the dark at RT for 1-2 hr. Formaldehyde was carefully removed by turning each insert on its side onto a roll of tissue and gently

shaking. Inserts were washed three times with PBS for 5 min each wash. Histogel (ThermoFisher) was warmed, and small 50 μ L flat disks were pipetted onto a cell culture plate lid placed on ice. Transwell inserts were dried using tissue, turned upside down, and the membrane was carefully cut using a razor blade. Once the membrane was detached, the entire matrigel plug was removed with tweezers and placed face up directly on top of a Histogel disk. An additional 50-100 μ L of Histogel was layered over the Matrigel, and allowed to solidify for 5 min. Histogel-embedded organoids were transferred to plastic histology cassettes, and stored in 70% EtOH until processing and paraffin embedding (as described in Section 2.1.2).

2.4.2. Wholemout staining of organoids *in situ*

Prior to staining, organoids were cultured in 8-well chamber slides (LabTek) under standard culture conditions. At day 21 of culture, media was removed from each well, being careful to avoid the matrigel dome, and a 5 min wash was performed with PBS at RT. PBS was removed, and organoids were fixed by adding 200 μ L of prewarmed 4% formaldehyde to each well and incubating at RT for 30 min. Formaldehyde was removed, and the wells were washed gently three times with PBS for 5 min each wash. For quenching of auto-fluorescence, 50 mM NH_4Cl was added for 30 min at RT. Two PBS washes were performed for 5 min each wash, organoids were permeabilized with 0.2% Triton-X in PBS for 30 min, and washed a further two times with PBS. Non-specific antigen sites were blocked with 5% normal donkey serum (NDS) in PBS for 1 hr, followed by overnight incubation with primary antibodies (Table 2.4) at 4 °C. Antibodies were removed, wells were washed three times in PBS for 5 min, organoids were incubated with secondary antibodies (Table 2.5) for 1 hr at RT, washed twice with PBS, and incubated with 0.5 μ g/mL DAPI for 5 min to stain nuclei. Following two further PBS washes (5 min) chamber sides were removed according to the manufacturer's instructions. Slides were mounted with RapiClear (Sun Jin Lab) and sealed with clear nail polish. Samples were imaged on a Leica SP5 confocal microscope. For LysoTracker™ staining of lysosomes, live organoids were incubated *in situ* with 50 ng/ μ L of LysoTracker™ (Invitrogen, L12492), diluted in pre-warmed complete medium, for 1 hr at 37 °C. LysoTracker was removed, and organoid/matrigel suspension was carefully washed for 5 min in PBS, followed by addition of fresh, pre-warmed complete medium.

Cells were protected from light and imaged immediately using an EVOS cell imaging system.

2.4.3. Immunofluorescence staining of paraffin-embedded organoids and tissue

Pre-cut paraffin sections were de-waxed and rehydrated using a Leica AutoStainer (ST5010; sequential immersion in xylene, 100% EtOH, 90% EtOH, 75% EtOH, distilled water). Where antigen retrieval was required, slides were submerged into pre-heated antigen retrieval buffer (Citrate buffer or Tris-EDTA buffer, depending on antibodies; Table 2.4, 2.5 and 2.8) and allowed to boil in a rice cooker for 15 min. Slides were cooled in buffer for 20 min, washed in running water for 3 min, and permeabilised with 0.3% Triton-X in PBS for 15 min. Following permeabilization, tissue/organoid sections were circled with a hydrophobic PAP pen, blocked for 1 hr in 5% NDS serum in PBS at RT, and incubated with primary antibody mix (Table 2.4) overnight at 4 °C. Antibodies were removed with three PBS washes, and samples were incubated with secondary antibodies (Table 2.5) for 1 hr at RT. Following PBS washes, nuclei were stained with 0.5 µg/mL DAPI for 5 min, slides were mounted with RapiClear and sealed with clear nail polish.

Table 2.8. Recipes for antigen retrieval.

	Reagent	Amount for 500 mL
Citrate buffer (pH 6)	Sodium citrate tribasic dihydrate	1.47 g
	DI water	Up to 500 mL
	Hydrochloric acid (concentrated)	~ 200 µL
TE Buffer (pH 8)	Tris-base	0.606 g
	EDTA	0.185 g
	DI water	Up to 500 mL

2.5. Immunofluorescence staining of cryo-protected tissue

Fixed lung tissue samples were cryo-protected, and 5-7 µM sections were cut on a cryostat (Leica) and fixed to glass slides (Superfrost plus). Slides were stored at -80 °C prior to use. Slides were allowed to thaw at RT for 5 min, before either immersing in

antigen-retrieval buffer (if antigen retrieval was required) or permeabilizing immediately with 0.3% Triton-X in PBS for 15 min. Antibody staining was performed as for paraffin sections (Table 2.4 and 2.5; Section 2.4.3).

2.6. RNA extraction and qRT-PCR

2.6.1. *TRIZOL RNA extraction from organoids*

Organoids were harvested with dispase as stated above, and either frozen as a pellet on dry ice and stored at -80 °C for later extraction, or lysed immediately by addition of 1 mL of TRIZOL for 5 min at RT. Phase separation was performed by addition of 200 µL of chloroform and vortexing for 15 sec, followed by incubation at RT for 5 min. Samples were centrifuged at 12,000 x g for 15 min at 4 °C, and the upper aqueous phase was carefully transferred to a new Eppendorf tube. RNA was precipitated by addition of 500 µL isopropanol for 10 min at RT, and centrifugation at 12,000 x g for 10 min at 4 °C. Supernatant was removed, and RNA washed once with 75% EtOH in DiEthylPyroCarbonate (DEPC)-treated water. Following centrifugation at 7,500 x g for 5 min at 4 °C, supernatant was removed and the pellet was air-dried. RNA was dissolved in 15 µL DEPC-treated water and concentration analyzed using 1 µL of sample on a NanoDrop One Microvolume UV-Vis Spectrophotometer (ThermoFisher). RNA was stored at -80 °C, or DNase-treated immediately.

2.6.2. *DNase treatment*

For DNase treatment of RNA, up to 500 ng of RNA was combined with 1 µL 10X DNase reaction buffer, 1 µL DNase I and an appropriate amount of DEPC-treated water to a final volume of 10 µL. Samples were incubated for 15 min at RT, and the reaction inactivated by 1µL 25 mM EDTA at 65 °C for 10 min. DNase-treated RNA was then used for cDNA synthesis.

2.6.3. *cDNA synthesis*

cDNA was synthesized using the Superscript IV cDNA kit. DNase-treated RNA (up to 11 µL) was combined with 50 µM random hexamers (1 µL), 10 nM dNTP mix (1 µL) and nuclease-free water to a final volume of 13 µL, and heated at 65 °C for 5 min.

Samples were then combined with 5X SSIV buffer (4 μ L), 100 mM DTT (1 μ L), RNaseOUT inhibitor (1 μ L), and 200 U/ μ L SuperScript IV reverse transcriptase (1 μ L), and incubated in a thermocycler (23 $^{\circ}$ C for 10 min, 55 $^{\circ}$ C for 10 min, 80 $^{\circ}$ C for 10 min). cDNA synthesized from 500 ng RNA was diluted in 40 μ L nuclease free water, and either used immediately for qPCR analysis, or stored at -80 $^{\circ}$ C.

2.6.4. qRT-PCR

Taqman 96 well plates were set-up with 7.7 μ L DNase-free water, 10 μ L taqman 2X Master Mix, 1 μ L target probe (Table 2.9), 0.3 μ L of housekeeping probe (β -Actin, VIC reporter dye), and 1 μ L cDNA. Samples were run in duplicate in a StepOne real-time PCR machine and comparative cycle threshold (CT) values measured. For SYBR Green probes (Table 2.10), 1 μ L cDNA was combined with 1 μ L of forward primer, 1 μ L of reverse primer, 10 μ L Fast SYBR Green master mix and 7 μ L DNase-free water in a 96 well qPCR plate. All reactions were performed in duplicate as for Taqman probes.

Table 2.9. TaqMan probes.

Gene	Company	Name	Cat no.	Dye
ACTB	Thermofisher	Hs01060665_g1	4448491	VIC - MGB
AGER	Thermofisher	Hs00542584_g1	4331182	FAM - MGB
FOXJ1	Thermofisher	Hs00230964_m1	4331182	FAM - MGB
TP63	Thermofisher	Hs01114115_m1	4453320	FAM - MGB
SCGB1A1	Thermofisher	Hs00171092_m1	4331182	FAM - MGB
SFTPC	Thermofisher	Hs00951326_g1	4448892	FAM - MGB

Table 2.10. Primer sequences for SYBR Green qPCR.

Gene	Forward sequence	Reverse sequence	Reference
ABCA3	TCTCCTTCAGCTTCATGGTCAG	TGGCTCAGAGTCATCCAGTTG	Korogi et al. 2019
AGER	GCCACTGGTGCTGAAGTGTA	TGGTCTCCTTTCCATTCCCTG	Korogi et al. 2019
GAPDH	AATGAAGGGGTCATTGATGG	AAGGTGAAGGTCGGAGTCAA	Miller et al. 2018
HES1	AGTGAAGCACCTCCGGAAC	TCACCTCGTTCATGCACTC	PrimerBank
HOPX	GCCTTTCCGAGGAGGAGAC	TCTGTGACGGATCTGCACTC	Miller et al. 2018
IL17RA	TTCATTCCCTATGCCTGAGTC	TACAGTAAGTGGCTCGACCT	PrimerBank
IL1R1	AGAGGAAAACAAACCCACAAGG	CTGGCCGGTGACATTACAGAT	PrimerBank
NOTCH1	GAGGCGTGGCAGACTATGC	CTTGTACTCCGTCAGCGTGA	PrimerBank
RPL13A	CAGGTCCTGGTGCTTGATG	GGCCCAGCAGTACCTGTTTA	PrimerBank
SFTPC	AGCAAAGAGGTCCTGATGGA	CGATAAGAAGGCGTTTCAGG	Miller et al. 2018
SLC2A1	GGCCAAGAGTGTGCTAAAGAA	ACAGCGTTGATGCCAGACAG	PrimerBank
SOX2	GCTTAGCCTCGTCGATGAAC	AACCCCAAGATGCACAACCTC	Miller et al. 2018
TNFR1	ACCAAGTGCCACAAAGGAAC	CTGCAATTGAAGCACTGGAA	PrimerBank
TNFR2	TTCGCTCTTCCAGTTGGACT	CACCAGGGGAAGAATCTGAG	PrimerBank
TP63	CCACAGTACACGAACCTGGG	CCGTTCTGAATCTGCTGGTCC	Miller et al. 2018

2.7. SFTPC-eGFP lentiviral production

2.7.1. Bacterial transformation

Lenti-EF1a-tagRFP-SFTPC-eGFP (hereafter SFTPC-eGFP) plasmid DNA was kindly provided by Dr Emma Rawlins and Dr Kyungtae Lim (Figure 2.1; Lim et al., 2020). Approximately 15 µg (5 µL) of SFTPC-eGFP plasmid DNA was combined with 100 µL of competent cells in an Eppendorf tube, and mixed gently by flicking the bottom of the tube. The competent cell/DNA mixture was allowed to incubate for 30 min on ice. Cells were heat shocked by incubation in a 42°C water bath for 45 sec, after which tubes were incubated on ice for a further 2 min. Cell/DNA mix (50 µL) was plated onto a 10 cm LB-agar plate containing ampicillin, and grown in an incubator overnight at 37°C. As a negative control, plates containing non-transformed cells were also prepared. The following day, single bacterial colonies were picked using a pipette tip, and incubated overnight in 15 mL tubes containing 2 mL LB medium with ampicillin in a shaker at 37 °C, 220 rpm.

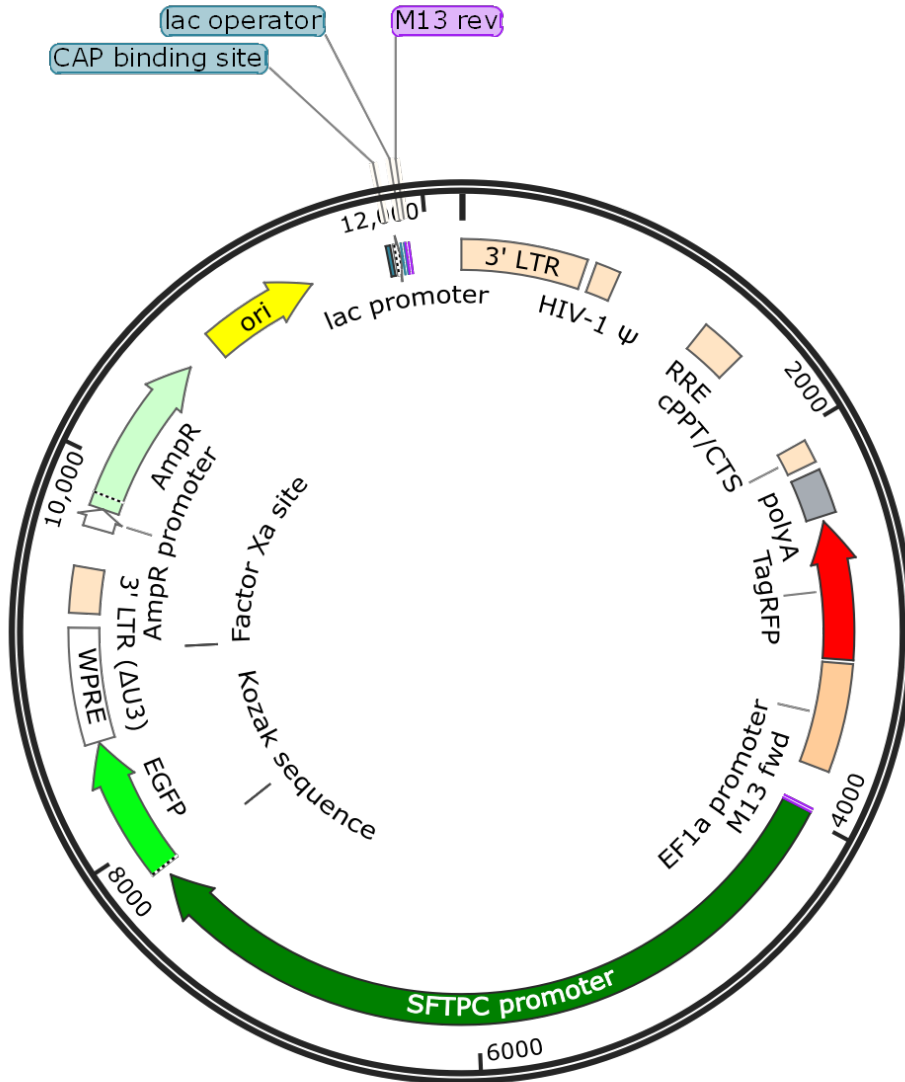
2.7.2. Bacterial midi-prep of plasmid DNA

Overnight bacterial cultures of expanded bacteria in Ampicillin-LB medium were prepared, and plasmid DNA isolation was performed using the PureLink™ HiPure Plasmid Midiprep Kit (Invitrogen) according to the manufacturer's instructions.

2.7.3. Culture and maintenance of HEK293T cells

Frozen stocks of P4, mycoplasma-free HEK293T cells were thawed for 2 min in a 37°C water bath, and added slowly to 9 mL of pre-warmed HEK293T culture medium (DMEM, 1% Pen/Strep, 10% FBS). Cells were centrifuged for 5 min at 350 x g, supernatant was removed, and cell pellet was resuspended in 1 mL of culture medium. Cells were seeded in 15 cm plates at a density of 5 x 10⁵ per dish in 20 mL of culture medium. Cultures were maintained under standard conditions (37 °C, 5% CO₂), with media changes every 2 days, and passaging twice a week for general maintenance. For passaging, medium was removed and plates were washed gently with PBS at RT, followed by trypsination by adding 2 mL of trypsin/EDTA for 2-5 min at 37 °C. Following cell detachment, trypsin was quenched with 8 mL of culture medium, cells were centrifuged for 5 min at 350 x g, and re-seeded into fresh culture plates. Cells were

passed at least twice prior to performing lentiviral packaging, to allow any possible adverse growth effects from freezing to be minimised.



Lenti-EF1a-tagRFP-SPC-EGFP
12,171 bp

Figure 2.1. Plasmid map for SFTPC-eGFP vector.

Plasmid map created in SnapGene.

2.7.4. Lentiviral packaging by lipofectamine

For lentiviral packaging, 7×10^6 HEK293T cells were seeded per 10-cm plate in DMEM/10% FBS (without antibiotics) and cultured overnight at 37 °C. Fresh pre-warmed medium was added to plates and allowed to rest at 37 °C while packaging reagents were prepared. For the DNA plasmid mix, 3 µg pMD2.G, 6 µg psPAX2, 3 µg pAdvantage, and 10 µg of p-lentiviral vector of interest (SFTPC-eGFP; Figure 2.1) was added to 750 µL of Opti-MEM in a tube, mixed gently, and allowed to incubate at RT for 5 min. Following incubation, 800 µL Opti-MEM/Lipofectamine mix (750 µL Opti-MEM, 50 µL lipofectamine) was added to the DNA plasmids, mixed gently, and incubated at RT for 20 min. The mixture was carefully added dropwise to a pre-prepared plate of HEK293T cells, and incubated at 37 °C for 6-8 hr. Medium was replaced with fresh DMEM/ 10% FBS, and incubated at 37 °C for 24 hr. Supernatant containing the viral particles was removed and stored at 4 °C in a 50 mL conical tube. Fresh DMEM/ 10% FBS was added to cells and plates were incubated for a further 24 hr at 37 °C. New viral supernatant was harvested and transferred to the pre-collected supernatant.

2.7.5. Lentiviral packaging by calcium phosphatase transfection of HEK293T cells

Prior to transfection, plates of HEK293T cells at 70-90% confluency were split at a ratio of 1:10 into 10 cm plates, and allowed to grow overnight so that plates were approximately 70% confluent by the following morning. For each plate, the following reagents were added to an Eppendorf tube to make the DNA solution: 315 µL DI water, 10 µg SFTPC-GFP vector DNA, 3 µg pMD2.G, 6 µg psPAX2, 3 µg pAdvantage, and 2.5 M CaCl₂. A second Eppendorf containing 2X HBS was prepared, and the DNA mixture was added dropwise to the tube while vortexing in order to properly aerate the system and achieve appropriate formation of calcium-DNA precipitates (Table 2.11). The solution was allowed to stand at RT for 20 min, during which time fresh DMEM/10% FBS medium was added to HEK293T cells. Calcium phosphatase DNA solution was added dropwise to the cells, and the plates moved gently in order to ensure homogenous distribution of the solution. Plates were incubated for 8-12 hr at 37 °C, after which plates were washed with PBS, medium was changed, and plates incubated for a further 48 hr to allow collection of properly packaged lentivirus, with supernatant collected and pooled at both 24 hr and 48 hr.

Table 2.11. Recipe for 2X HBS used in calcium phosphatase transfection

	Reagent	Amount for 500 mL
2X HBS	D-glucose	1 g
	HEPES	5 g
	KCl	0.36 g
	NaCl	8 g
	Na ₂ HPO ₄	0.1 g
	ddH ₂ O	Up to 500 mL
	NaOH (5N)	Adjust to pH 7.05

2.7.6. Lentiviral concentration by Lenti-X concentrator

Lentiviral-containing supernatant was centrifuged at 300 x g for 5 min at 4 °C to remove debris, the supernatant was filtered through a 0.45 µm filter and the virus was concentrated using Lenti-X™ concentrator (Takara). Briefly, a third volume of concentrator was added to viral supernatant and incubated overnight at 4 °C on a tube rotator. Tubes were centrifuged at 1,500 x g at 4 °C for 45 min, the pellet resuspended in 500 µL PBS per starting plate, and stored as a single-use aliquot at -80 °C.

2.7.7. Lentiviral transduction of human alveolar organoids

Organoids cultured in 48-well plates for at least 14 days (between P0 and P2) were dissociated to single cells using dispase and TrypLE according to section 2.3.1. For lentiviral transduction, 100,000 – 300,000 single cells in PBS were re-suspended 1:1 with the lentivirus of interest, transferred to a single well of a 48-well plate, and sealed with parafilm. Plate was spinoculated at 1,500 x g at 32 °C for 90 min. Plates were then allowed to rest at 37 °C for 1-4 hr. Following incubation, virus/cell mix was harvested, washed with PBS, and plated in an appropriate volume of matrigel as previously described (section 2.3.1). Plates were incubated at 37 °C, 5% oxygen, and analysed at 72 hr post-plating to visualise GFP and RFP expression.

2.8. Data analysis

2.8.1. Cell counting and organoid forming efficiencies

Total number of organoids per well were counted for each sample/treatment at day 14 of culture using the Fiji cell counter plugin. Each sample was counted in triplicate for N=3 individual patients, unless otherwise stated. Organoid forming efficiencies were expressed as a percentage of total organoids formed per well (number of organoids formed/number of cells seeded x100), and are expressed as the mean \pm SEM of 3 individual donors/patients, unless otherwise stated. For each donor/patient sample, a minimum of 3 wells were assessed as technical replicates, with the mean value then used, unless otherwise stated. For hAOs, a structure was counted as an organoid if it possessed a 2D-surface area of more than 1600 μM^2 . Organoid sizes were assessed using the 'analyse particles' function in Fiji. Quantification of organoid doubling time was performed according to Huch et al., 2015.

2.8.2. Image acquisition and analysis

Brightfield images were captured using an EVOS FL cell imaging system (ThermoFisher) with a X2, X4 or X10 objective. Immunofluorescence images were captured using a Leica SP5 confocal microscope with a X20 or X40 objective. Images were analysed using Fiji imaging software. All images included in the study are representative of at least 3 individual experiments, unless otherwise stated. For assessment of cell staining percentages for specific proteins (e.g., pro-SFTPC) within an organoid, the total number of pro-SFTPC⁺ cells were assessed and expressed as a percentage of the total number of DAPI⁺ cell nuclei. Cells within organoids were counted on a single imaging plane, unless otherwise stated.

2.8.3. Flow cytometry data analysis

FACS plots were analysed and presented using FlowJo analysis software.

2.8.4. Statistics and reproducibility

All graphs and statistical analyses were performed using Prism 8 GraphPad software. All individual data points are the mean of 3 technical replicates (e.g., wells) per biological sample, unless otherwise stated. Statistical significance across biological replicates (where relevant) was assessed using the non-parametric Mann-Whitney U test.

CHAPTER 3

Results I: Identification and characterisation of epithelial progenitor cells in the adult human lung parenchyma

3.1. Introduction

The human adult lung parenchyma consists of the gas-exchanging unit of the lung and is made up of delicate, thin-walled alveoli and respiratory bronchioles. This region comprises a plethora of cell types, ranging from mesenchymal, endothelial and immune cells to epithelial cells of both alveolar and airway lineages (Evans and Lee, 2020; Hogan et al., 2014). The vast array of cell types present, coupled with poor characterisation, has made it difficult to isolate and culture individual cell types and lineages from the human lung. The need to understand the regulation of epithelial progenitor cell populations, including the alveolar type 2 (hAT2) population of the human lung parenchyma has clinical relevance, owing to the number of respiratory diseases that affect this region, including Idiopathic pulmonary fibrosis (IPF; Barratt et al., 2018; Lawson et al., 2004; Wu et al., 2018). Within the lung parenchyma, a number of epithelial stem/progenitor populations have been proposed from both mouse studies and *in vitro* human systems. While basal cells are confined to the trachea and mainstem bronchi of the mouse, they extend distally in the human. *In vivo*, use of a *Krt5-Cre^{ER}* transgenic mouse line identified that basal cells self-renew and differentiate to secretory club and ciliated cells under normal homeostasis, while a separate study suggested that there are two populations of mouse basal cells; classical

basal cells which possess the capacity for self-renewal, and basal-luminal progenitors that have lost their self-renewal capacity and are committed to a luminal fate (Rock et al., 2009; Watson et al., 2015). Genetic lineage tracing studies have highlighted that *Scgbl1*⁺ secretory club cells maintain the small airways, differentiating to ciliated and additional secretory club cells, due to the absence of basal cells from mouse lung bronchioles (Rawlins et al., 2009a). Meanwhile, AT2 cells were identified as a stem cell population of the alveoli, demonstrating the ability to both self-renew and differentiate to alveolar type 1 (AT1) cells *in vivo* using an *SFTPC-Cre* lineage traced mouse line (Barkauskas et al., 2013). Similar findings have also been suggested in the human upon *in vitro* culture of isolated cells (Barkauskas et al., 2013; Choi et al., 2021; Rock et al., 2009). While mouse models have proved useful in elucidating cellular identities and some of the regulatory mechanisms associated with human lung epithelial maintenance during homeostasis and disease, the presence of mouse-human differences and failure of mouse models to fully recapitulate human disease indicates the need for understanding human-specific processes (Nikolić et al., 2017; Tashiro et al., 2017).

Prior to the start of my PhD, the molecular requirements for the *in vitro* growth, maintenance and differentiation of primary epithelial cells from the adult human lung parenchyma were unknown. Traditionally, research into the maintenance of epithelial cells of the human parenchyma has primarily utilised the *in vitro* study of human airway cell types, either from normal tissue or cancer cell lines generally due to their ease of culturing or increased availability of material (Foster et al., 1998; Ren et al., 2016; Rucka et al., 2013; Salomon et al., 2014). More recently, cells derived from primary human lung tissue, such as basal cells and hAT2 cells, were either co-cultured with stromal cells or cultured in poorly-defined conditions. Such culture conditions often exhibited suboptimal cell growth or maintenance capacity, and it was difficult to assess the effect of individual exogenous growth factors on specific epithelial cell types. For example, primary hAT2 cells were co-cultured with MRC5 foetal fibroblasts, but exhibited poor passage ability and loss of hAT2 identity and surfactant production (Barkauskas et al., 2013; Zacharias et al., 2018). Similarly, a separate study confirmed human airway basal cells as a stem cell population of the lung using an *in vitro* 3D-culture system, but utilised a commercial medium for which the components were not well-defined (Rock et al., 2009). Later, a study was published from the Clevers' group that successfully established airway organoids from proximal lung samples and bronchoalveolar lavage fluid in chemically-defined conditions (Sachs et al.,

2019). Airway organoids comprised basal, secretory and ciliated cells, and displayed long-term self-renewal capacity and disease-modelling capabilities. Despite this finding, a chemically-defined culture system for the study of hAT2-derived alveolar organoids remained elusive, owing to the molecular requirements for their self-renewal and maintenance being unknown. Therefore, this chapter will explore the *in vitro* characteristics of epithelial progenitor cell populations of the human adult lung parenchyma and aim to elucidate the molecular requirements for *in vitro* growth, differentiation and maintenance of these cell lineages.

3.2. Aims

- Assess the expression of canonical lung epithelial markers in distal parenchymal regions of human donor lungs.
- Establish a chemically-defined *in vitro* culture system to support and expand primary human lung epithelial cells from multiple cell lineages of the lung parenchyma in order to understand the molecular requirements for their self-renewal and differentiation.
- Characterise organoids derived from epithelial HTII-280⁻ (non-alveolar type 2) cell cultures.

3.3. Results

3.3.1. *Characterisation of the healthy human adult lung parenchyma*

The human adult lung consists of a number of different epithelial cell types, with single-cell RNA sequencing (scRNA-seq) analyses identifying between 11 and 15 individual populations in normal background lungs (Adams et al., 2020; Habermann et al., 2020; Travaglini et al., 2020). Of these, at least 9 are present within the distal lung parenchyma (Travaglini et al., 2020). As outlined in Section 1.1, the parenchymal region of the lung comprises the gas-exchanging unit and is made up of the alveoli and respiratory bronchioles. In order to establish a 3D-organoid model utilising cells of the lung parenchyma, it was important to first gain an understanding of these cell types and the markers that could be used for their visualisation and characterisation. Healthy human parenchymal lung tissue was obtained from either patients undergoing lobectomies for lung cancer, with tissue distant from the tumour being confirmed as macroscopically

inconspicuous by a pathologist prior to use, or from donors with no background lung disease. Tissue from both types of donor were utilised and characterised in the study. By conducting haematoxylin and eosin (H&E) staining of paraffin-embedded parenchymal lung tissue, I confirmed the presence of squamous hAT1 and cuboidal hAT2 epithelial cells forming individual alveolar subunits (Figure 3.1A). For all tissue samples analysed, the alveoli represented the major structure present, with only few airways identified, as expected due to the distal location of obtained samples.

In order to better characterise these cells, I performed immunofluorescence (IF) staining for a number of previously described lung lineage markers, as outlined in Section 1.2 (Table 1.1.). As previously reported, hAT2 cells expressed a number of markers, including pro-SFTPC, SFTPB, ABCA3, LPCAT1 and the cell surface marker HTII-280 (Barkauskas et al., 2013; Gonzalez et al., 2010; Figure 3.1B). However, I observed that heterogeneity existed within the hAT2 population in regard to marker expression. Although the expression of HTII-280, a monoclonal antibody that marks the apical membrane of adult hAT2 cells (Gonzalez et al., 2010) was found abundantly on hAT2 cells expressing SFTPB, a minority of SFTPB⁺HTII-280⁻ cells were also observed (Figure 3.1B, arrowhead). Furthermore, a number of HTII-280⁺ hAT2 cells were also positive for nuclear HOPX, a transcription factor that is normally present in hAT1 cells, although its presence in hAT2 cells at low transcriptional levels has been recently reported (Travaglini et al., 2020). This is unlike reports involving AT2 cells from the mouse, which do not express Hopx in the adult lung, highlighting a clear difference in canonical marker expression between the mouse and the human (Jain et al., 2015). hAT1 cells were marked by membrane expression of a number of markers, including HTI-56, AGER, podoplanin (PDPN) and caveolin-1 (CAV1) (Figure 3.1B).

In addition to alveoli, a small number of bronchioles were also observed in the lung parenchyma, with the number and size varying from sample-to-sample, likely due to slight differences in tissue biopsy location (Figure 3.1C). As previously reported (Table 1.1), bronchioles consisted of a number of airway cell types, including KRT5⁺ and TP63⁺ basal cells, KRT8⁺ luminal cells, SCGB1A1⁺ secretory club cells, MUC5AC⁺ goblet cells and acetylated tubulin (ACT)⁺ ciliated cells. The cytokeratin KRT17 was also found to mark basal cells, while the hAT2 cell markers HTII-280 and pro-SFTPC were not observed in small airways (Figure 3.1D).

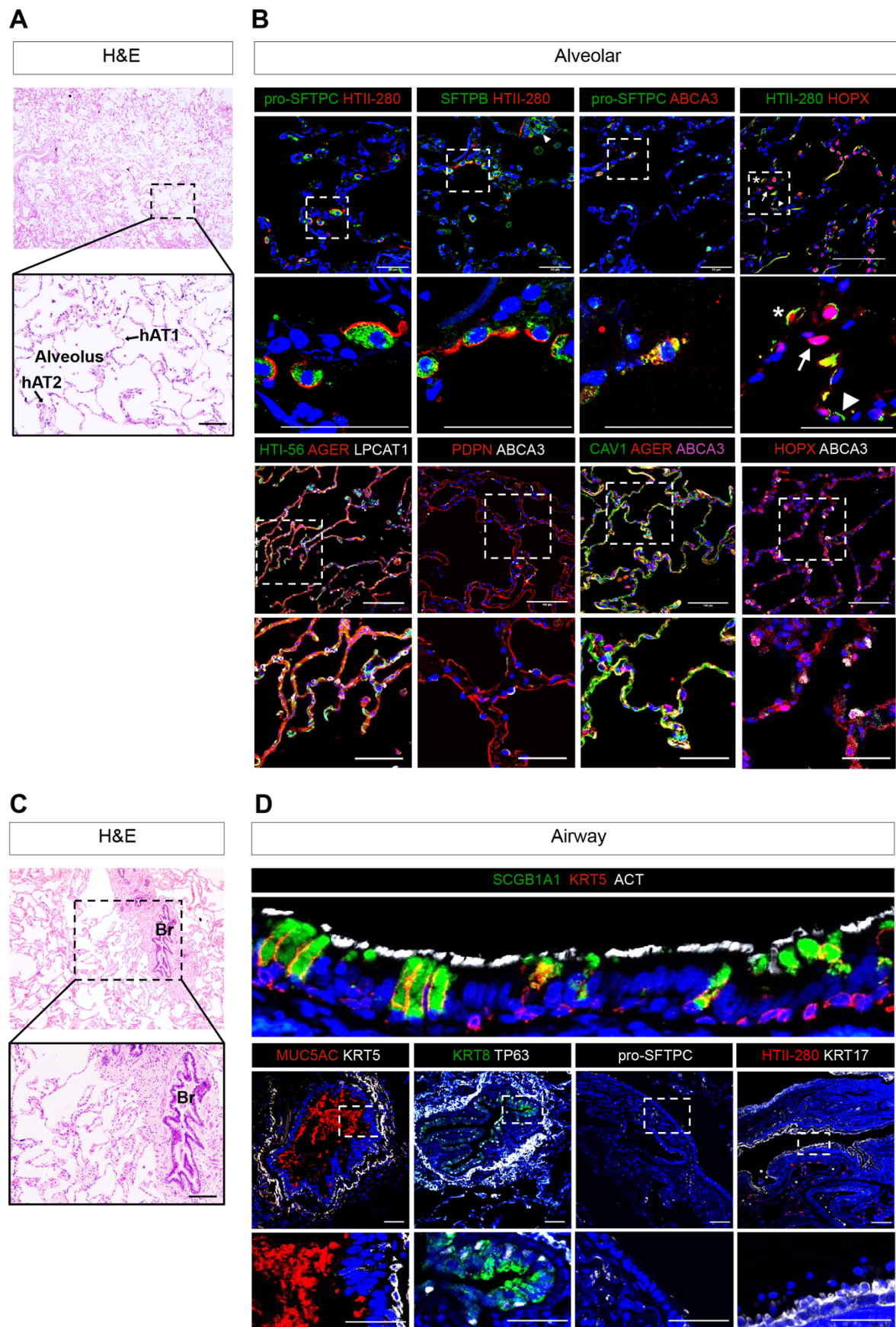


Figure 3.1. Characterisation of the human adult lung parenchyma from normal background lungs (figure legend on next page).

Figure 3.1. Characterisation of the human adult lung parenchyma from normal background lungs.

A. Representative H&E image of the healthy human adult lung parenchyma showing the presence of epithelial alveolar type 1 (hAT1) and alveolar type 2 (hAT2) cells arranged into individual alveoli. Scale bar, 50 μm . **B.** hAT2 cells express a number of canonical markers, including (from left to right) pro-SFTPC (green), HTII-280 (red, green), SFTPB (green), ABCA3 (red, white, pink) and LPCAT1 (white). Although expressed in the majority of hAT2 cells, rare HTII-280⁺ cells exist (SFTPB/HTII-280 arrowhead). hAT1 cells express markers including HOPX (red), HTI-56 (green), AGER (red), PDPN (red), and CAV1 (green). An orange colour shows co-localisation of the studied markers. For HTII-280/HOPX, asterisk denotes co-expression of both markers, arrow denotes HOPX-only cell, arrowhead denotes HTII-280-only cell. Scale bars (from left to right); 50 μm (top row, panels 1-3 and their magnifications), all other panels, 100 μm . **C.** Representative H&E image of a respiratory bronchiole (Br) in the human lung parenchyma. Scale bar, 100 μm . **D.** IF images of respiratory bronchioles; basal cells, TP63 (white), KRT5 (red, white) and KRT17 (white); luminal cells, KRT8 (green) and SCGB1A1 (green); goblet cells, MUC5AC (red); ciliated cells, acetylated tubulin (ACT, white). No hAT2 markers are present within respiratory bronchioles (pro-SFTPC, white; HTII-280, red). Scale bars, 100 μm . For A to D, boxed regions are magnified below the relevant panels.

3.3.2. Establishment of *in vitro* human lung organoids

To better understand the functional role of human lung epithelial progenitor cells in tissue maintenance, I sought to establish physiologically relevant *in vitro* culture models by determining the molecular requirements for their growth. Utilising healthy background tissue derived from the distal lung parenchyma of patients undergoing lobectomy for lung cancer, I mechanically and enzymatically dissociated the tissue to produce single cell suspensions (Figure 3.2A to E). To achieve this, I used a scalpel to cut the tissue into small (1 mm³) pieces and transferred the pieces into an enzymatic digestion solution containing collagenase/dispase, dispase II and DNase. Following a one-hour incubation in the digestion solution at 37 °C, digested cellular suspension was filtered to remove remaining debris and processed for magnetic-activated cell sorting (MACS). More detailed discussion of the tissue processing method can be found in Section 2.1.3. Using MACS beads, EpCAM⁺ epithelial cells were isolated and seeded at a ratio of 5,000 or 10,000 cells in 20 μL Matrigel per well of a 48-well plate, and cultured under a number of various growth factor conditions (Figure 3.3A to G). Ratio for initial cell seeding was determined from existing literature, which I then optimised for my own culture system by plating cells at different densities and assessing cell growth (Barkauskas et al., 2013; Broutier et al., 2017; Huch et al., 2015; Rock et al., 2009; Sato et al., 2011). Factors were chosen and tested

based on the culture conditions for mouse lung epithelial progenitor cells in my lab, which were in accordance with previous literature regarding mouse and human lung development, current knowledge of mouse lung organoid culture conditions and recent efforts in deriving organoids from multiple human epithelial tissues (Barker et al., 2007; Broutier et al., 2017; Choi et al., 2021; Huch et al., 2015; Nikolić et al., 2017).

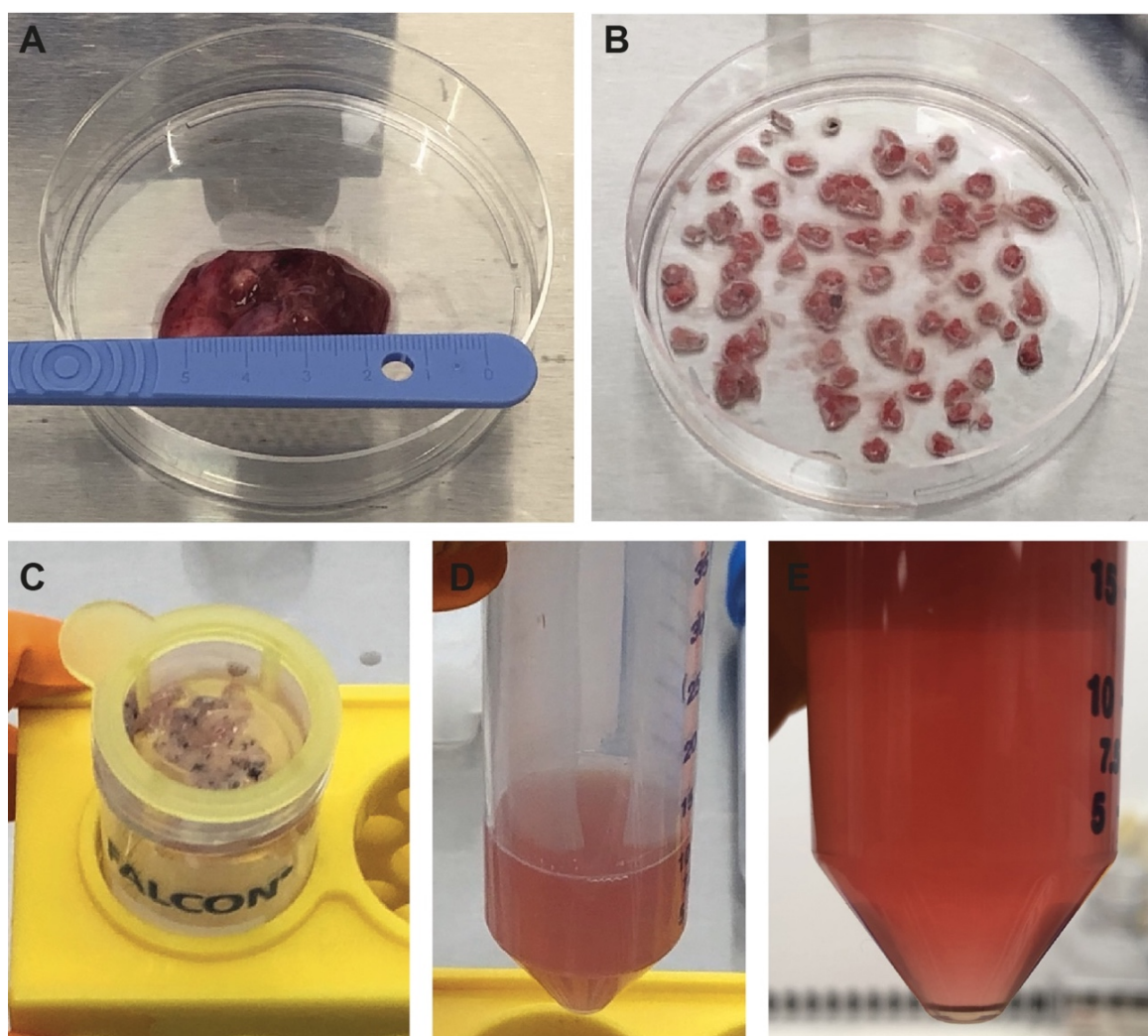


Figure 3.2. Tissue dissociation method for deriving cells from human lung parenchyma samples.

A. Representative image of clinical lung parenchyma specimen derived from a human normal background lung. **B.** Representative image of tissue pieces following mechanical dissociation with a scalpel. **C.** Remaining tissue debris following 1-hour enzymatic digestion with collagenase/dispase, dispase II and DNase. **D.** Digested cellular supernatant achieved after filtering digested lung solution through a 100 μm mesh cell strainer. **E.** Cell pellet following centrifugation of digested lung supernatant. More detailed discussion of tissue-processing method can be found in Section 2.1.3.

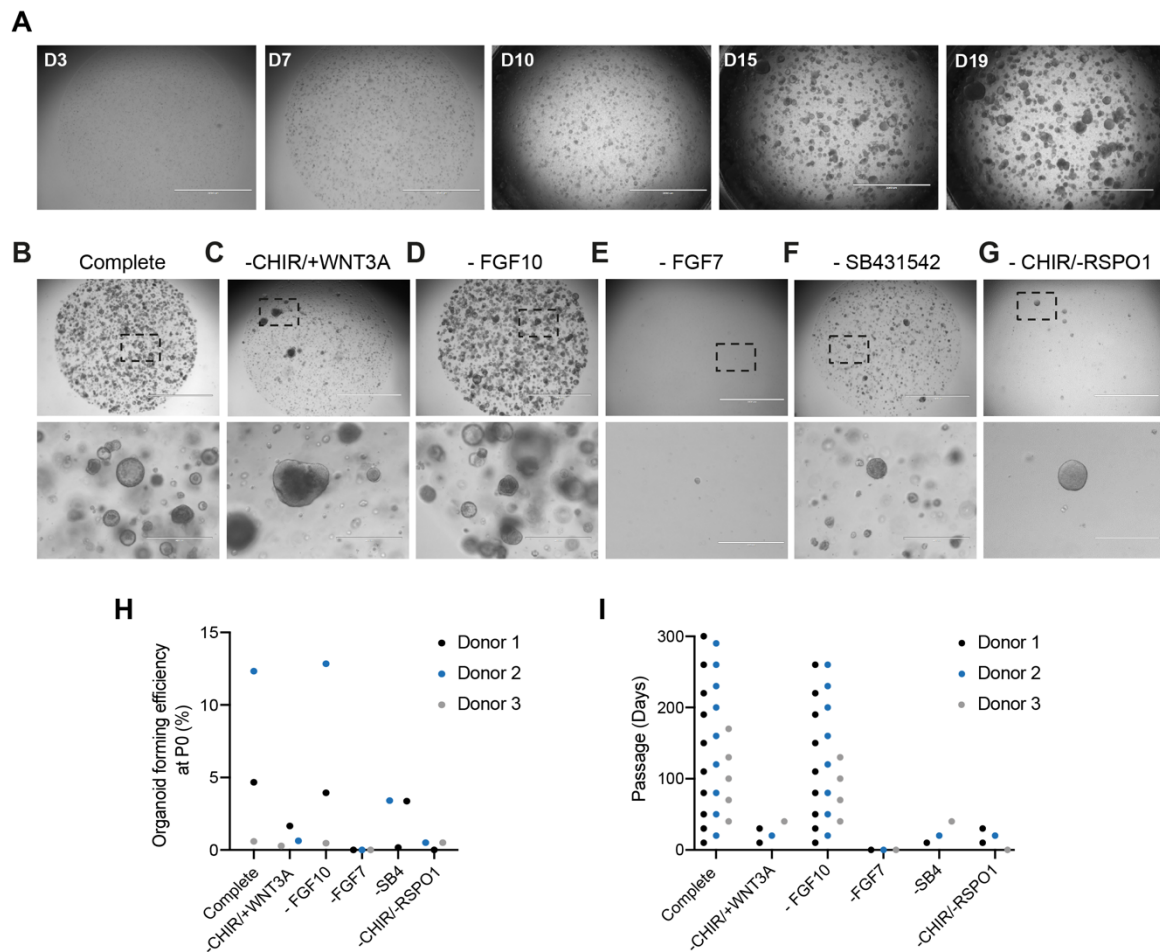


Figure 3.3. FGF7 and Wnt are required for the growth of human lung primary epithelial cells.

A. MACS-derived EpCAM⁺ cells cultured in complete medium consisting of factors including FGF7, FGF10, NOGGIN, RSPO-1 (R-spondin 1)- conditioned medium, CHIR99021 (CHIR) and SB431542 (SB4). Images were taken at day (D) 3, D7, D10, D15 and D19. Scale bars, 2000 μm. **B to G.** Culture of primary EpCAM⁺ cells for 14 days (D0-D14) in various conditions. **B.** Complete medium. **C.** Replacement of CHIR99021 with WNT3A-conditioned medium. **D.** Removal of FGF10. **E.** Removal of FGF7. **F.** Removal of the TGFβ inhibitor SB431542. **G.** Removal of exogenous Wnt (CHIR99021) and RSPO-1-conditioned medium. Scale bars for images B-G; top panels, 2000 μm, bottom panels, 400 μm (10x magnifications of boxed regions). Representative brightfield images were taken at D14 of culture at P0. **H.** Organoid forming efficiency of EpCAM⁺ cells at passage 0 (P0) following 14 days of culture. Each individual dot represents the mean of 3 technical replicates (separate wells) for 3 independent biological samples. **I.** Passage ability of organoids grown under tested conditions for 3 individual donor lung samples, with each dot representing an individual passage (passage 10 equivalent to more than 300 days in culture).

EpCAM⁺ cells cultured in complete medium (EGF, Noggin, R-spondin 1-conditioned medium, FGF7, FGF10, CHIR99021, and SB431542) began to form small spherical structures by day 3 of culture, becoming visible organoids by day 7-10 of culture, and

increased in size for up to 3 weeks (Figure 3.3A and 3.3B; Table 3.1). Due to the inclusion of EpCAM⁺ cells that comprised multiple epithelial cell populations, organoid morphologies and sizes were heterogeneous (Figure 3.3B). Organoid passage ability and forming efficiency varied between individual patients, with primary cultures in complete medium forming organoids at an average efficiency of 4.7% ± 3.83% (Figure 3.3H and 3.3I). In order to assess which growth factors were essential for organoid establishment and maintenance, I withdrew individual factors at day 0 (D0) of primary culture, and maintained cells in these conditions for 3 weeks. Culturing EpCAM⁺ cells in the absence of FGF10 had no major effect on organoid size or organoid forming efficiency, although long-term passage ability was reduced by a single passage for each of the three donor samples analysed (Figure 3.3B, 3D, 3.3H and 3.3I). However, the absence of FGF7 resulted in failure of cells to form organoids, indicating the importance of FGF7 in human lung epithelial cell maintenance and organoid formation (Figure 3.3E, 3.3H and 3.3I). Although resulting in the formation of a limited number of spherical organoids, a similar effect was also observed in conditions lacking the Wnt-activator CHIR99021 (CHIR). This finding implicated Wnt-signalling as another important factor in the maintenance and growth of isolated human lung epithelial cells (Figure 3.3G). Additionally, I compared CHIR-containing cultures with cultures containing WNT3A-conditioned medium as the source of Wnt-signalling, but found that WNT3A led to decreased or variable organoid forming efficiency, possibly due to batch effects of the in-house made conditioned medium (Figure 3.3C and 3.3H). I therefore chose CHIR as the Wnt-activator for subsequent cultures. Finally, although successfully forming organoids, albeit at a lower efficiency than complete medium (2.02% ± 0.96%), cultures lacking the TGFβ inhibitor SB431542 (SB4) failed to re-form organoids following enzymatic dissociation and re-seeding upon passage (Figure 3.3F, 3.3H and 3.3I). This finding has been observed in multiple human epithelial organoid cultures, where TGFβ inhibition was required for long-term maintenance of stem cell self-renewal capacity *in vitro* (Huch and Koo, 2015; Huch et al., 2015; Sato et al., 2011). The same was not true for mouse organoid cultures, suggesting an important difference between mouse and human epithelial cell requirements. For further analysis and characterisation, I utilised organoids cultured in complete medium containing FGF7 and FGF10. Although I have shown that FGF10 had no discernible advantages during early culture in terms of organoid establishment and forming efficiency compared with medium containing FGF7 alone, my observation that FGF10 addition led to a slight increase in long-term passage ability encouraged me to include it in subsequent culture conditions (Figure 3.3H and 3.3I).

Table 3.1. Featured media conditions.

Media condition	Media composition (main factors)
Complete (+ CHIR)	*CHIR99021, *FGF7, *FGF10, NOGGIN, EGF, *Rspo-1 conditioned medium, *SB431542
- CHIR	FGF7, FGF10, NOGGIN, EGF, Rspo-1 conditioned medium, SB431542
- CHIR + SB2	FGF7, FGF10, NOGGIN, EGF, Rspo-1 conditioned medium, SB431542, SB202190

*Denotes compound for which its removal was singly-tested in growth of primary EpCAM⁺ human lung cells.

3.3.3. Characterisation of EpCAM⁺-derived human parenchymal lung organoids

Culture of EpCAM⁺ cells in complete medium resulted in the formation of organoids of multiple morphologies (Figure 3.4A). It is important to note that all organoids, regardless of their identity, formed initially as a small, filled sphere of cells, with clear morphological differences not arising until day 5 to 7 of culture. Cultures could be passaged by enzymatic dissociation to single cells and were successfully maintained for up to 11-months, although I observed a trend for decreased organoid forming efficiency during later culture (Figure 3.4A, 3.4B and 3.4C). Heterogeneity existed between individual tissue samples, with some organoid cultures growing slower or smaller than others, occasionally with more limited expansion capacity (Figure 3.4B and 3.4C). Therefore, I passaged individual organoid lines at different timepoints depending on their growth, with each donor-derived line possessing varying organoid forming efficiencies over passage (Figure 3.4B and 3.4C). However, I generally observed with all samples that organoid forming efficiency would peak around passage 2 to 5, followed by a gradual decline until organoids could not be cultured further (Figure 3.4C).

I next sought to investigate the cell types present within the organoids. IF analysis of primary cultures revealed the presence of at least two types of organoids retaining alveolar lineages (hereafter alveolar organoids) and airway lineages (hereafter airway organoids). They displayed clear morphological differences (Figure 3.5A; Table 3.2). Alveolar

organoids of varying sizes tended to consist of a folded structure, often with an inner lumen, although more spherical structures were also present at lower frequency. All primary alveolar organoids were characterised by expression of pro-SFTPC and the hAT2 cell surface marker HTII-280 (Figure 3.5A). Alveolar organoids represented around 60% of organoids in primary EpCAM⁺-derived cultures (Figure 3.5B). In contrast, airway organoids made up approximately 25% of primary EpCAM⁺-derived cultures, were generally much larger and stained negative for pro-SFTPC and HTII-280, instead consisting of cells expressing the basal cell markers TP63 and KRT5 (Figure 3.5A and 3.5B). SCGB1A1⁺ secretory club cells were also present within the majority of these organoids, often residing in the centre of the sphere. Basal cell-only organoids were also observed at a lower frequency and were usually smaller in size, potentially suggesting that differentiation to secretory club cells had not yet occurred, or that a rare subpopulation of human basal cells are slow-cycling and only self-renew without undergoing differentiation *in vitro*. Furthermore, rare SCGB1A1⁺/KRT5⁻ organoids were occasionally observed, which likely arose from secretory club cells, as has been previously reported for both mouse and human (Choi et al., 2021; data not shown). No ACT⁺ ciliated cells were identified in airway organoids, potentially indicating that differentiation of ciliated cells was not supported.

The majority of airway organoids cultured under these conditions had large spherical morphologies with no lumen, although some lumen-containing airway organoids were present. Occasional organoids existed that did not express any of the tested markers, and I have described these as ‘undetermined’ cell types, due to their lineage identity not being clear. Undetermined organoids made up the remaining 15% of organoids (Figure 3.5B). At later passages, following enzymatic dissociation to single cells, pro-SFTPC-expressing alveolar organoids still existed, although their number was reduced compared to primary culture (Figure 3.5A and 3.5B). Analysis of *SFTPC* mRNA levels in EpCAM⁺-derived cultures confirmed the reduction in *SFTPC* expression over time, whereas *TP63* expression levels remained stable (Figure 3.5C).

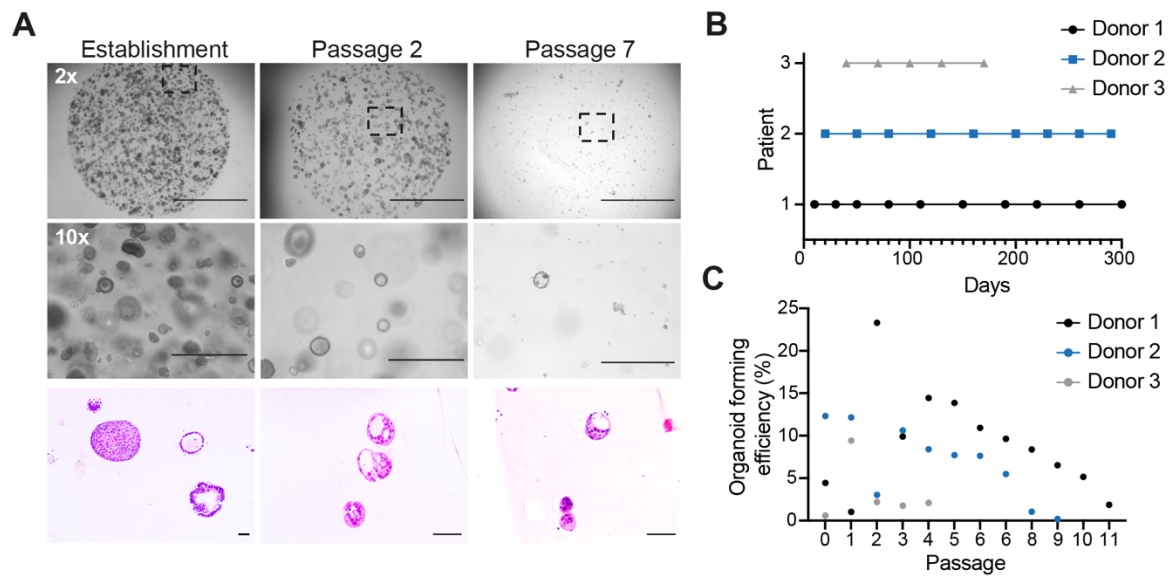


Figure 3.4. Human EpCAM⁺ epithelial lung parenchymal cells can be passaged repeatedly for up to 11 months.

A. Representative brightfield and H&E images of EpCAM⁺ organoids following 2 weeks of culture in complete medium at multiple passages. Scale bars (brightfield); 2000 μm (top), 400 μm (bottom); H&E, 50 μm. **B.** Organoid cultures from different patients were passaged at different timepoints depending on growth. Each point represents a single passage. N= 3 donor lungs. **C.** Organoid forming efficiencies over multiple passages for EpCAM⁺ cells grown in complete medium for 3 individual donors. A single point represents the mean of 3 technical replicates (separate wells) for each individual donor. P0 to P4, 3 biological replicates; P5 to P9, 2 biological replicates; P10 to P11, 1 biological replicate.

Table 3.2. Antibody panel for IF staining of alveolar and airway EpCAM⁺-derived organoids.

Organoid identity	Antibody staining panel
Alveolar	HTII-280/pro-SFTPC
Airway (secretory and basal/parabasal)	SCGB1A1/KRT5
Airway (ciliated and basal/parabasal)	ACT/KRT5
Alveolar and airway (secretory, hAT2 and basal/parabasal)	SCGB1A1/pro-SFTPC/KRT5
Alveolar and airway (secretory, hAT2 and basal/parabasal)	SCGB1A1/HTII-280*/KRT5
Alveolar and airway (hAT2 and basal)	pro-SFTPC/TP63

*HTII-280 expression only used to determine hAT2 cell fate when expressed with another hAT2 marker.

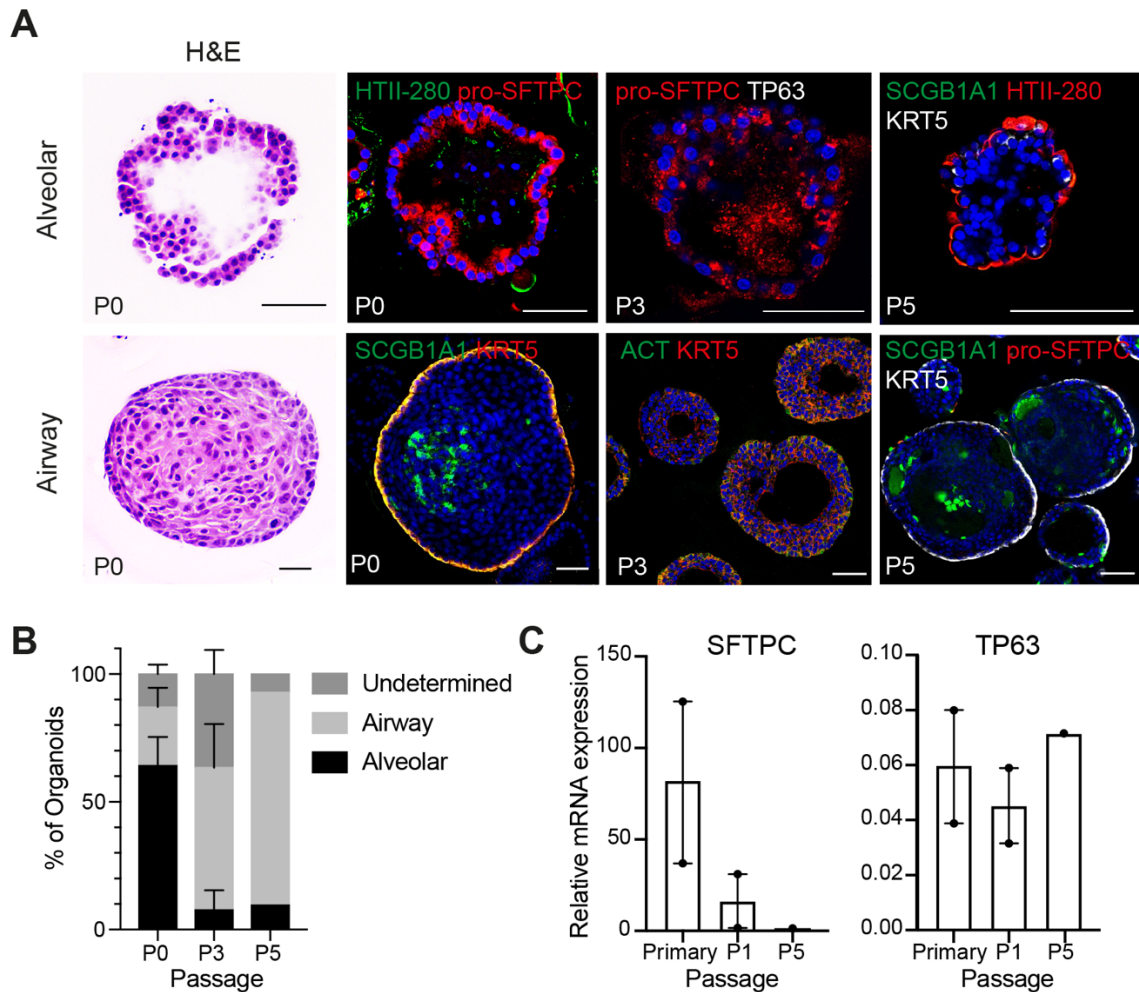


Figure 3.5. Characterisation of *EpCAM*⁺ organoids retaining alveolar and airway organoids.

A. Representative H&E and IF images of alveolar (top) and airway (bottom) organoids presented in *EpCAM*⁺ primary culture. IF images show various epithelial lineages within organoids at P0, P3 and P5. hAT2 cells, pro-SFTPC (red) and HTII-280 (green, red); basal cells, KRT5 (red, white); secretory cells, SCGB1A1 (green). ACT⁺ ciliated cells were not observed (green). DAPI (cell nuclei, blue). Scale bars, 50 μ m. Images were obtained at D (day) 21 of primary culture. H&E images are increased magnification of organoids found in Figure 3.4A. **B.** Quantification of organoid identity from IF analysis in A. Data are mean \pm SEM of 2 biological replicates (P0 and P3) and 1 biological replicate (P5). Total number of organoids (n) assessed for each passage; P0 (n= 204), P3 (n= 38) and P5 (n= 43). **C.** Relative mRNA expression of lung lineage genes over passage. Data are mean \pm SEM for 2 biological samples (primary and P1) and 1 biological sample (P5). Data are expressed as relative to the housekeeping gene *GAPDH*.

Interestingly, a number of organoids began to arise which no longer expressed the alveolar marker pro-SFTPC, but still retained HTII-280 staining on the surface (Figure 3.5A). By P3, alveolar organoids were dramatically reduced, while airway and ‘undetermined’ organoids increased, and this trend continued during P5 (Figure 3.5B). This suggested that either my culture conditions for EpCAM⁺ cells were preferentially allowing outgrowth of airway cell types and undetermined cells over their alveolar counterparts, or that airway cells expand at a faster rate (Figure 3.5B). While undetermined cells still maintained NKX2.1 expression (data not shown), indicating their maintenance of lung lineage, no other tested lung-lineage markers were expressed. Therefore, it was not known what these cell types were. However, they still maintained self-renewal capacity. Although a limited number of organoids still expressed HTII-280, the lack of all other hAT2 cell markers led me to no longer refer to these organoids as alveolar (Figure 3.5A and 3.5B). Throughout all passages, no organoids containing both alveolar and airway cells were observed in any cultures (Figure 3.5A and 3.5B). Collectively, these data showed that FGF7 and Wnt signalling were required for organoid establishment, while TGFβ inhibition in the form of the small molecule SB4 was required for long-term self-renewal and culture maintenance. Such conditions resulted in a heterogenous mix of alveolar and airway organoids, arranged in multiple organoid morphologies. However, the number of alveolar organoids decreased over time. This possibly indicated that either the conditions were not fully optimal for long-term maintenance of alveolar cell types, or that the conditions allowed preferential outgrowth of airway cell types and later undetermined cell types.

3.3.4. Establishment and characterisation of airway organoids from human EpCAM⁺ HTII-280⁻ cells

In Section 3.3.2. and 3.3.3., the observation that alveolar organoids decreased over time in culture led me to next investigate whether I could separate hAT2 cells from non-hAT2 cells and culture them separately in complete medium. To do this, I mechanically and enzymatically dissociated fresh human lung parenchymal samples derived from healthy background lung donors as before, and employed fluorescence-activated cell sorting (FACS). I gated the cells based on their CD31⁻CD45⁻EpCAM⁺ profile to remove endothelial and immune cells and select epithelial cells, and subsequently isolated hAT2 cells based on HTII-280 expression (Figure 3.6A). HTII-280⁺ hAT2 cells represented approximately 75% of total EpCAM⁺ cells, as has been shown previously, while HTII-280⁻

cells should have included other epithelial cell types, including basal cells and secretory club cells, according to tissue staining data (Figure 3.1D; Barkauskas et al., 2013; Zacharias et al., 2018). This was also confirmed by qPCR analysis, where HTII-280⁻ cells displayed higher levels of airway marker genes such as *TP63*, *SCGB1A1* and *FOXJ1* than HTII-280⁺ cells (Figure 3.6B). In contrast, HTII-280⁺ cells expressed significantly higher levels of hAT2 marker genes such as *SFTPC* (Figure 3.6B).

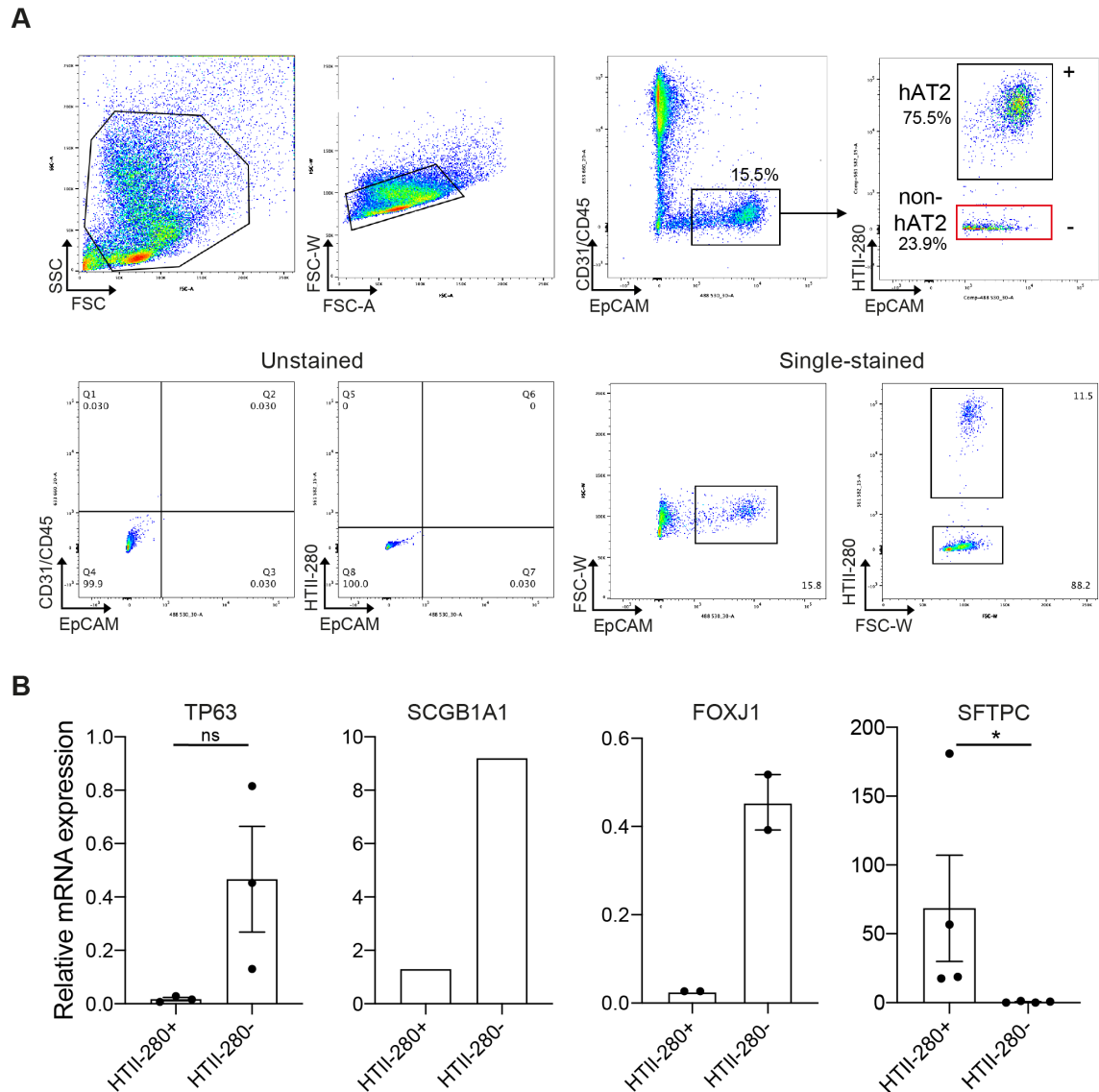


Figure 3.6. The strategy of FACS based cell isolation for hAT2 cells and non-hAT2 cells from human lung parenchymal tissues (figure legend continued on next page).

A. Primary human lung cells from healthy background lung specimens were sorted with FACS based on their CD31⁻ CD45⁻ EpCAM⁺ profile in order to isolate epithelial cells, and further gated on the basis of their HTII-280 expression in order to specifically isolate hAT2 cells (HTII-280⁺) from other epithelial cell types (non-hAT2, HTII-280⁻). Unstained and single-stained controls are also provided. FACS plots representative of 3

individual samples. **B.** Relative mRNA expression of lung lineage markers in isolated primary human epithelial lung cells (HTII-280⁺ and HTII-280⁻). Data are the mean \pm SEM of 3 biological replicates (*TP63*), 1 biological replicate (*SCGB1A1*), 2 biological replicates (*FOXJ1*) and 4 biological replicates (*SFTPC*), and are expressed as relative mRNA expression versus the housekeeping gene *GAPDH*. Each individual dot represents the mean of 1 biological replicate (2 technical replicates each). For TP63 and SFTPC, statistical significance was tested using the non-parametric Mann-Whitney U test; ns = non-significant, * = $p < 0.05$.

In order to establish alveolar organoids derived from HTII-280⁺ hAT2 cells to better understand the functional behaviours of hAT2 cells, I decided to use HTII-280⁻ cells as a control to compare *in vitro* growth capacity. Therefore, before setting up culture conditions for hAT2 cells, I wanted to test and characterise the growth of non-hAT2 epithelial cells isolated from the HTII-280⁻ cell fraction which includes basal and secretory club cells. I isolated HTII-280⁻ cells with FACS as described above and plated single cells in Matrigel at a ratio of 5000 cells per well and cultured in complete medium. As low Wnt conditions had been previously demonstrated to promote airway cell development (McCauley et al., 2017), I also cultured HTII-280⁻ cells in complete medium without CHIR (-CHIR medium; Table 3.1). I found that upon culturing HTII-280⁻ cells in -CHIR medium, filled, spherical organoids could be observed by day 14 of culture, and these continued to grow for up to 28 days, forming large structures (Figure 3.7A). This was consistent with the airway organoids that were observed in EpCAM⁺-derived cultures (section 3.3.2. and 3.3.3.). In contrast, culture of HTII-280⁻ cells in complete medium resulted in failure of cells to form organoids, an observation that was consistent for all tested donor samples. This suggested that when hAT2 cells were absent from the culture system, remaining epithelial cells were sensitive to exogenous Wnt addition, at least during primary culture (Figure 3.7B). This may be due to the possibility that the presence of hAT2 cells allowed for the growth of airway cell types in high Wnt conditions, either through physical cell-to-cell contact or secretion of ligands and signalling molecules. Such cell-to-cell interactions have been suggested previously, such as the inhibition of secretory cell de-differentiation to basal cells when mouse basal and secretory cells are cultured together *in vitro*, but not when secretory cells are cultured alone (Tata et al., 2013). However, the precise effect of hAT2 cells on airway organoid growth warrants further study. Although HTII-280⁻ cells cultured in -CHIR medium could be passaged multiple times depending on donor sample, the number of passages achievable was reduced in comparison with organoids derived from EpCAM⁺ cells (Figure 3.7C and 3.7D; Figure 3.4B and 3.4C). Upon passaging and re-plating as single cells, organoids were

re-established and again formed large, spherical structures lacking a lumen, although rare lumen-containing organoids were also present, which became more prevalent during later passages (Figure 3.8A). IF of primary cells cultured in -CHIR medium confirmed that organoids formed large spherical structures with occasional small lumen, resembling the airway organoids generated from EpCAM⁺ cells (Figure 3.5A). HTII-280⁻ organoids cultured in -CHIR medium were characterised as possessing extensive KRT5 staining throughout the entire organoid structure, and also possessed some TP63⁺ and SOX2⁺ cells, identifying these cells as airway basal cells (Figure 3.8B). Occasional organoids also expressed the secretory club cell marker SCGB1A1 (data not shown), but no other cell lineage was observed (Figure 3.8B). At later passages, the number of cells expressing TP63 decreased, although cells still retained KRT5 expression, indicating that these cells could have been parabasal cells, a basal-secretory intermediate cell type (Figure 3.8B; Hynds and Janes, 2017). However, KRT8 expression was not assessed, so it is difficult to determine the exact identity of these cells. However, these data confirmed that HTII-280⁻ cells mainly retain basal cells in culture, which can preferentially grow and differentiate in low, but not high, Wnt conditions.

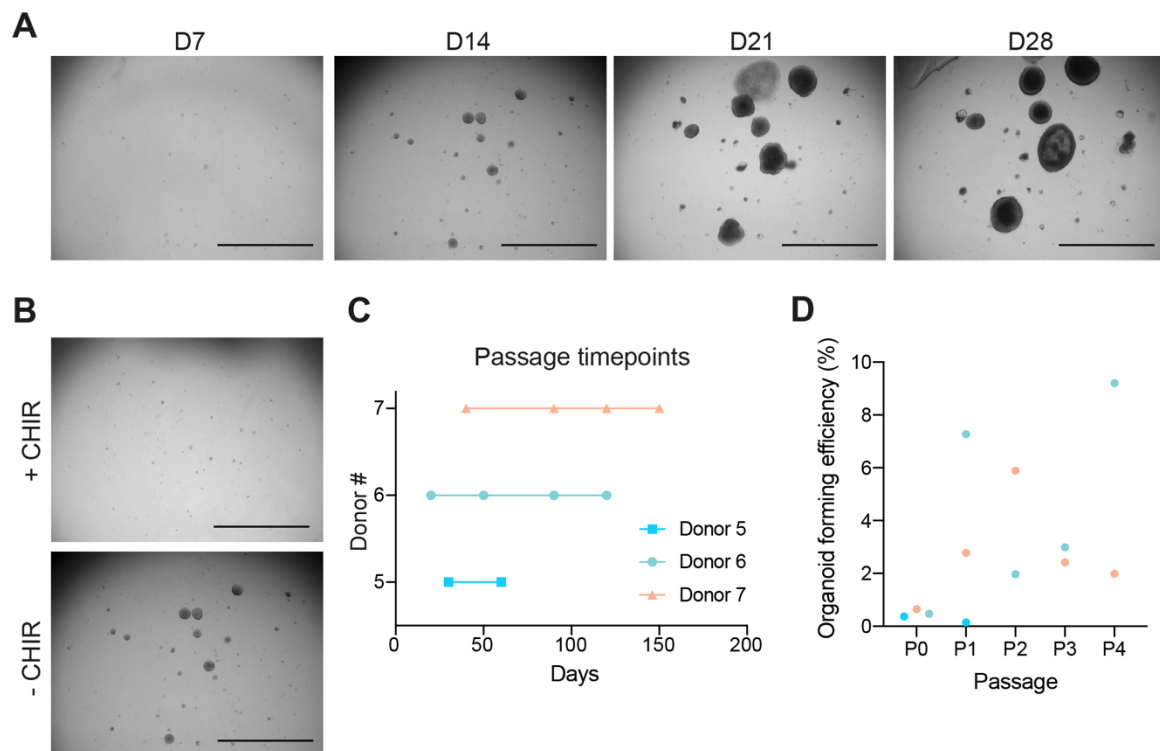


Figure 3.7. HTII-280⁻ cells form airway organoids in low Wnt conditions (figure legend on next page).

Figure 3.7. HTII-280⁻ cells form airway organoids in low Wnt conditions.

A. Representative brightfield images of organoids derived from HTII-280⁻ cells and cultured in -CHIR99021 (-CHIR) medium. Scale bar, 2000 μm. **B.** Representative brightfield images of primary HTII-280⁻ cells grown with or without CHIR (D14). D = day post-plating. Scale bar, 2000 μm. **C.** Organoid cultures from different patients were passaged at different timepoints depending on growth. Each point represents a single passage. **D.** Organoid forming efficiencies over multiple passages for HTII-280⁻ cells grown in -CHIR medium for 3 individual donors. A single point represents the mean of 3 technical replicates (separate wells) for each individual donor. P0 to P1, 3 biological replicates; P2 to P4, 2 biological replicates.

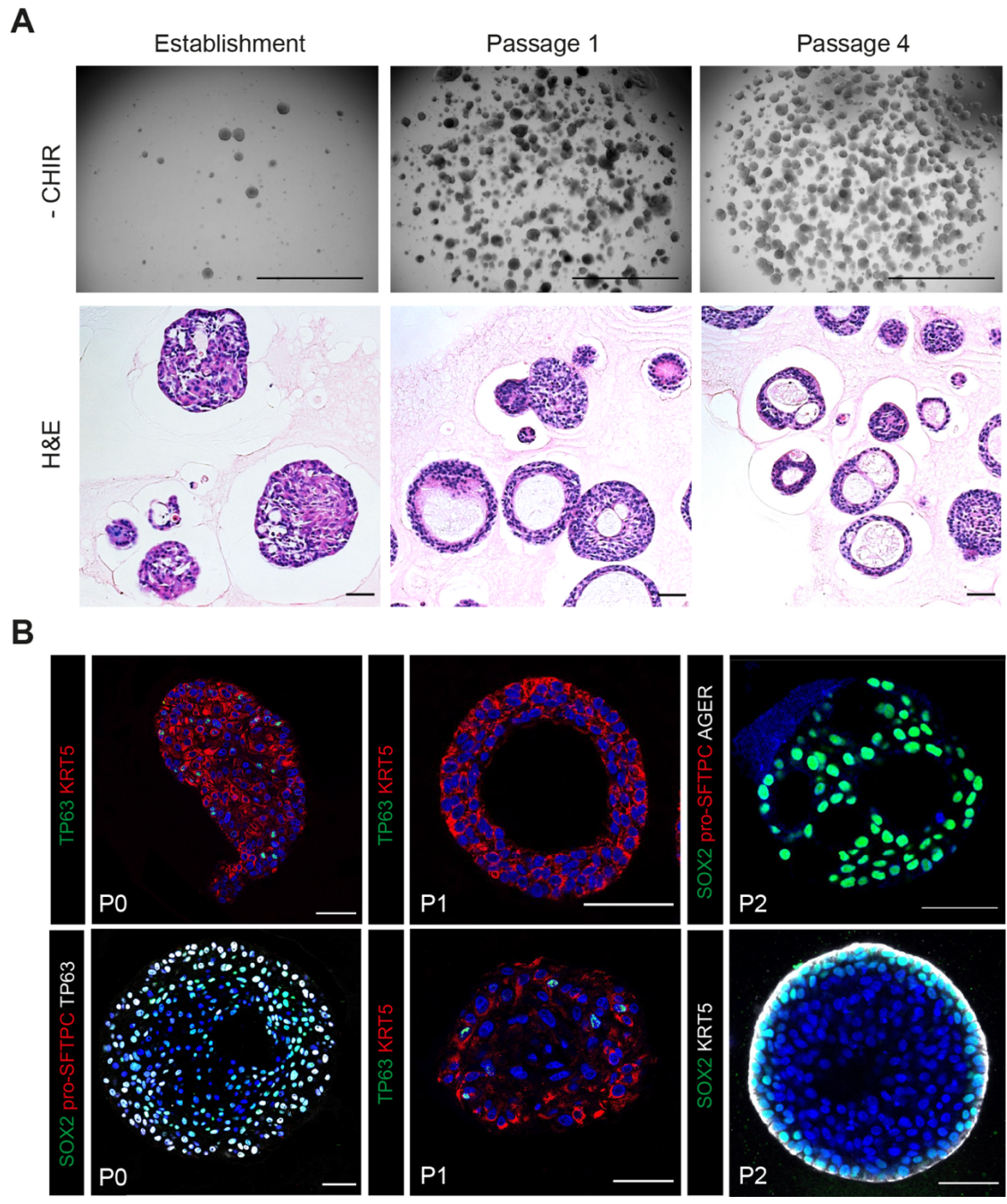


Figure 3.8. Passage of HTII-280⁻ cell-derived organoids (figure legend on next page).

Figure 3.8. Passage of HTII-280⁻ cell-derived organoids.

A. Representative brightfield and H&E images of HTII-280⁻ cells grown without CHIR (D14) across multiple passages. Scale bar, 2000 μm (brightfield); 50 μm (H&E). **B.** IF images of HTII-280⁻ derived organoids across passages; TP63 (green, white), SOX2 (green), and KRT5 (red, white), pro-SFTPC (red) and AGER (white). DAPI, cell nuclei (blue). Scale bar, 50 μm .

While I had successfully established airway organoids derived from HTII-280⁻ cells, Hans Clevers' group has since reported culture conditions to grow human airway organoids in slightly different conditions (Sachs et al., 2019). Therefore, I compared the culture conditions and characterised these two organoid systems in parallel. Their media conditions were similar to my -CHIR medium except for two main factors; EGF was not added, and the p38 Map-kinase (MAPK) inhibitor SB202190 (SB2) was included (Table 3.1). In order to simplify conditions and make appropriate comparisons between cultures, all other factors were included at the same concentrations as I had used previously. Additionally, I observed that removal of EGF had no apparent effects on organoid establishment or cellular composition within the organoids, therefore I included EGF in the culture (Figure 3.9A). I therefore referred to the published airway medium as '-CHIR/+SB2 medium'.

Primary HTII-280⁻ cells cultured in -CHIR/+SB2 medium formed mainly large, cystic organoids with a single lumen, although rare smaller filled structures were also observed, as found in a separate study (Figure 3.9A, Zhou et al., 2018). Upon passaging by enzymatic dissociation and re-plating as single cells, organoids remained stable for more than 150 days in culture, with passaging possible every 2-3 weeks (Figure 3.9B). Primary organoid forming efficiency was low, likely due to the low number of starting organoid-forming cells present within the HTII-280⁻ mixture of cells from parenchymal lung tissue, which was expected to include a number of cell types including ciliated, secretory and hAT1 cells (Figure 3.6B). However, organoid forming efficiency greatly increased upon the first passage. This was likely in part due to the enrichment of basal cells, with organoid forming efficiency remaining between 10% and 15% for multiple passages, generally higher than those of cells cultured in -CHIR medium (Figure 3.9C; Figure 3.7D). Organoid morphologies varied, with some cystic organoids with an inner lumen or rounded structures with no lumen, although interestingly the majority of primary organoids comprised a single, large lumen (Figure 3.9D). The formation of HTII-280⁻ organoids with a large lumen in -CHIR/+SB2 medium was in stark contrast to organoids formed from primary HTII-280⁻

cells cultured in -CHIR medium, which resulted almost exclusively in the establishment of large, filled organoids with no visible lumen. Although not assessed during the present study, Sachs et al. also reported the presence of functional ciliated cells lining the luminal surfaces of their airway organoids, a cell type not observed in my -CHIR medium (Sachs et al., 2019). Therefore, the formation of an organoid lumen from primary HTII-280⁻ cells, and possibly the differentiation of ciliated cells, was likely due to p38 MAPK inhibition through SB2 addition, although the precise mechanism for this is currently unknown. To test this hypothesis, I cultured airway organoids continually in -CHIR medium for 4 months, then switched to -CHIR/+SB2 conditions (Figure 3.10A). Interestingly, only the -CHIR/+SB2 cultured organoids formed a lumen, again suggesting that p38 MAPK inhibition leads to lumen formation of airway organoids *in vitro*.

IF analysis of primary organoids in -CHIR/+SB2 medium revealed that cystic organoids consisted of a well-organised, layered epithelium consisting of KRT5⁺ TP63⁺ basal cells within the outermost layers, which also co-expressed PDPN, another basal cell marker (Figure 3.9D). The airway-lineage marker SOX2 was observed in the majority of cells, and the secretory club cell marker SCGB1A1 was expressed in cells on the luminal side of the organoids, with positive staining also present within the lumen. Meanwhile, the hAT2 markers pro-SFTPC and HTII-280 were not present (Figure 3.9D). These organoids persisted throughout multiple passages, maintaining stable expression of KRT5 and possessing some TP63⁺ cells. Secretory club cells were also observed, with SCGB1A1 staining again present on the luminal surface. No expression of hAT2 markers was present even during later culture, indicating that there was no aberrant trans-differentiation of airway cells to alveolar lineages in this culture condition (Figure 3.9D).

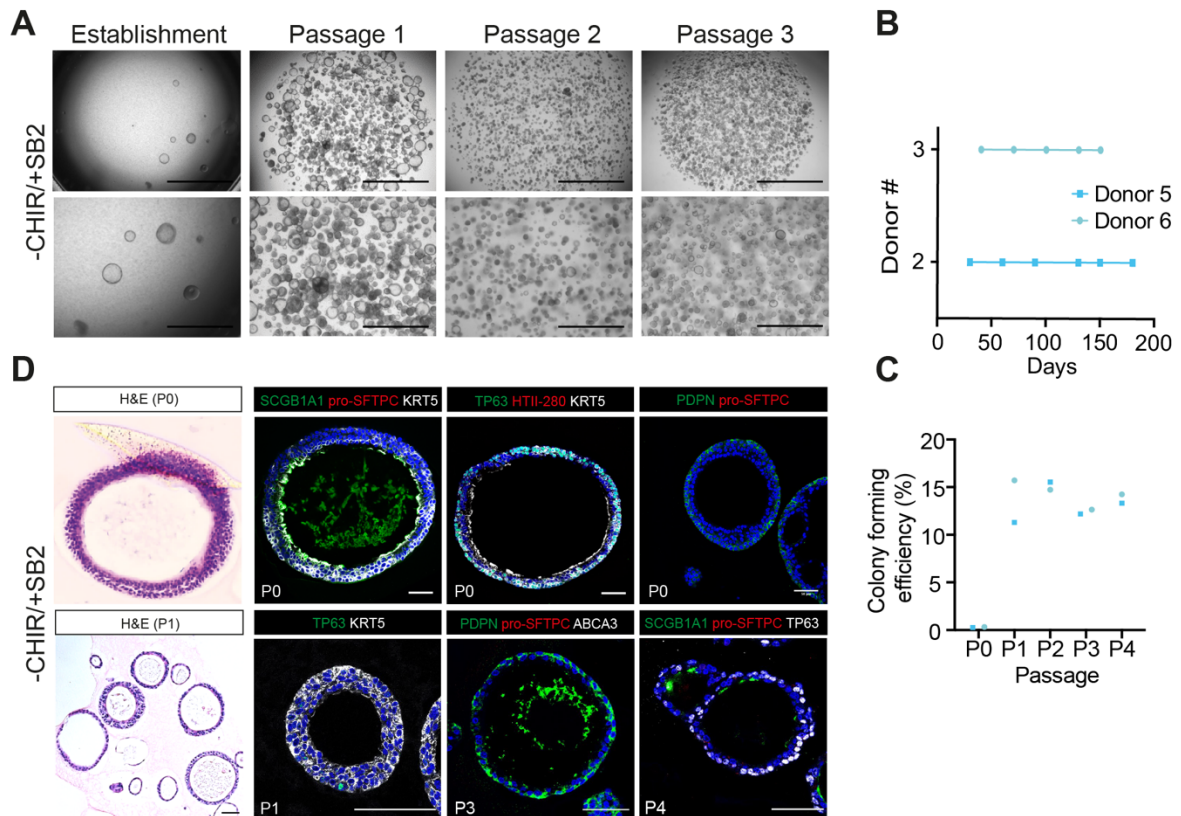


Figure 3.9. Culture of primary HTII-280⁻ in Sachs et al. 2019 human airway organoid conditions.

A. Representative brightfield images of HTII-280⁻ cells grown without CHIR and with addition of SB2 (D14) across multiple passages. Scale bar, 2000 μm (top panel); 1000 μm (bottom panel). **B.** Organoid cultures from 2 separate patients were passaged at different timepoints depending on growth. Each point represents a single passage. **C.** Organoid forming efficiencies over multiple passages for HTII-280⁻ cells cultured in -CHIR/+SB2 medium for 2 individual donors. A single point represents the mean of 3 technical replicates (separate wells) for each individual donor. **D.** Representative H&E and IF images of HTII-280⁻ cells cultured in +SB2 medium at both primary culture and following passage. KRT5 (white), TP63 (green, white), SCGB1A1 (green), PDPN (green), pro-SFTPC (red), HTII-280 (red) and ABCA3 (white). Images were obtained at D21. Scale bars, 50 μm .

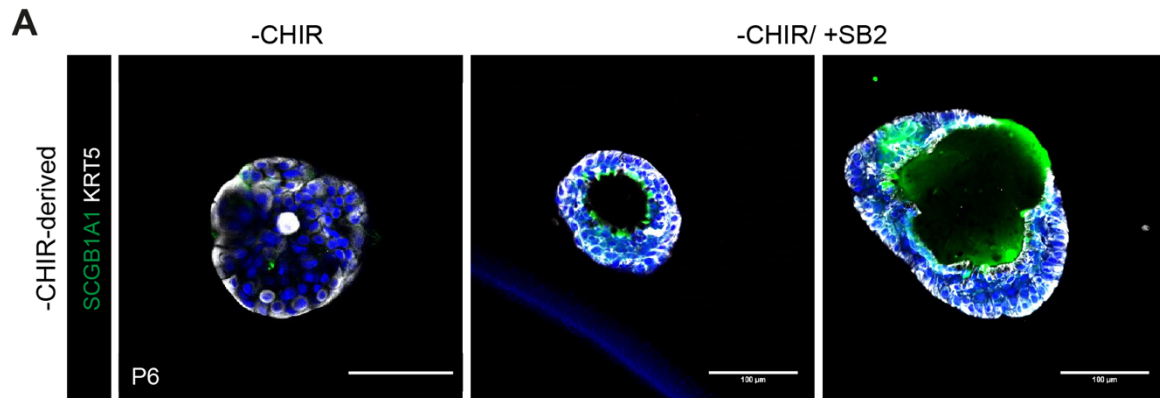


Figure 3.10. Switching airway organoids to media containing SB2 leads to lumen formation.

A. IF images of airway organoids at passage 6 that were switched from -CHIR medium to -CHIR/+SB2 medium. SCGB1A1 (green), KRT5 (white), DAPI (cell nuclei, blue). Scale bar, 100 μ m.

3.4. Conclusions

In conclusion, isolation of EpCAM⁺ cells derived from healthy adult human lung parenchymal tissues and subsequent 3D-culture in medium comprising FGF7 and Wnt signalling resulted in formation of organoids comprising either alveolar or airway lineages. Promisingly, the culture conditions were able to support epithelial cells from multiple donor lungs. TGF β inhibition allowed for long-term maintenance of EpCAM⁺ organoids, although the culture composition changed over time, with airway lineage organoids becoming more abundant compared to their alveolar counterparts during early culture. This was followed by loss of alveolar lineages following 3 to 6 months, leading to the outgrowth of organoids with ‘undetermined’ identities. Investigation of individual cell lineage growth through the isolation and culture of single HTII-280⁺ cells in low Wnt conditions resulted in the formation of airway organoids mainly comprising basal and secretory club cells. Primary organoids established in -CHIR medium formed large, filled structures, while additional supplementation with the p38 MAPK inhibitor SB2 resulted in the production of organoids that almost exclusively possessed a single, inner lumen. SB2-treated organoids possessed improved passage ability and organoid forming efficiency versus cells cultured in -CHIR medium alone. My data suggest that p38 Map kinase inhibition resulted in more stable, long-term maintenance of human airway cell types as 3D-organoids, and may have contributed to lumen production and ciliated cell differentiation in primary organoids through a currently unknown mechanism.

CHAPTER 4

Results II: Establishment and characterisation of a chemically-defined *in vitro* human alveolar organoid system from adult lung stem cells

4.1. Introduction

The gas-exchanging alveolar region of the lung is vital for proper lung function, and dysregulation or damage to this region leads to a host of chronic lung diseases, including Bronchopulmonary dysplasia (BPD) and Idiopathic pulmonary fibrosis (IPF). Such diseases are characterised by destruction of the alveolar epithelial unit, resulting in inefficient gas-exchange and severe breathing difficulties. To better understand and treat such diseases, a system to study human epithelial alveolar cell types, particularly resident alveolar type 2 (hAT2) stem cells is required. However, lack of knowledge about the molecular mechanisms underlying hAT2 regulation and differentiation has made this challenging. Efforts have been made to establish *in vitro* culture systems that support functional hAT2 cells. However, many of these *in vitro* culture conditions are short-term cultures and still utilise supporting cells such as mesenchymal cells (Barkauskas et al., 2013; Glisinski et al., 2020; Zacharias et al., 2018). These approaches do not fully support cell self-renewal and differentiation, and make it difficult to assess regulatory signalling pathways on an individual cell type. Identifying essential factors would allow for the identification of precise regulatory signals that are required for hAT2 cell maintenance, differentiation and self-renewal and may highlight key disease mechanisms. In this chapter, I will investigate the molecular requirements for self-renewal and differentiation of primary

donor-derived, FACS-purified hAT2 cells. Using this knowledge, I will then establish and characterise an *in vitro* 3D-organoid system for the propagation and maintenance of purified hAT2 cells in chemically-defined conditions. Much of the work within this chapter has recently been published (Youk et al., 2020).

4.2. Aims

- Identify the molecular requirements for supporting the growth of primary adult hAT2 cells from healthy background lungs in 3D-culture.
- Establish chemically-defined conditions for the long-term culture of human alveolar organoids (hAOs) from FACS-purified HTII-280⁺ hAT2 cells.
- Characterise hAT2-derived organoids during long-term culture and assess their functional maturity and requirements for differentiation to hAT1 cells.
- Assess the utility of adult-derived hAOs in downstream applications such as gene editing and viral infection studies.

4.3. Results

4.3.1. *Establishment of alveolar organoids from primary hAT2 cells*

I aimed to establish and characterise *in vitro* alveolar organoids derived from human adult primary hAT2 cells. HTII-280⁺ and HTII-280⁻ cells were isolated with FACS as before (Chapter 3) and 5000 HTII-280⁺ cells were placed into organoid culture with complete medium (Figure 4.1A and 4.1B; Table 3.1). As a non-hAT2 control, HTII-280⁻ cells were cultured in –CHIR medium as in Section 3.3.4. To confirm hAT2 identity in HTII-280⁺ cells, transcript levels for the key hAT2 marker *SFTPC* were assessed, revealing higher levels in HTII-280⁺ cells versus HTII-280⁻ cells, in accordance with IF analysis of tissue specimens (Figure 4.1C; Figure 3.1B). Additionally, the hAT1 marker *AGER* was expressed at higher levels in HTII-280⁻ cells. Culture of HTII-280⁺ cells in complete medium resulted in the emergence of heterogenous organoids that differed in both their size and morphology (Figure 4.1D). By day 7 of culture, HTII-280⁺-derived organoids were small and rounded, but became larger and more folded by day 15, although some organoids

established a cystic appearance (Figure 4.1D). Organoids continued to exhibit growth capacity for up to 4 weeks prior to passaging (Figure 4.1D). In addition to complete medium, organoid establishment and growth was assessed in -CHIR medium. By comparing the HTII-280⁺ cultures to their HTII-280⁻ counterparts, I observed that exogenous Wnt signalling was vital for the outgrowth of organoids from primary HTII-280⁺ cells, with limited organoid formation observed in -CHIR medium (Figure 4.1E). In contrast, HTII-280⁻ cells only formed organoids in the absence of CHIR (Figure 3.7B). This suggested the different molecular requirements for self-renewal of hAT2 cells and airway cells derived from human lung parenchyma. Organoid morphology also differed between the two populations, as was observed previously in EpCAM⁺ cultures (Figure 3.5A).

IF analysis revealed that primary HTII-280⁺ organoids strongly expressed cytoplasmic pro-SFTPC in all cells, as well as ABCA3, identifying the cells as hAT2 cells (Figure 4.1F). Therefore, throughout the remainder of this study, I will refer to these structures as human alveolar organoids (hAOs). Transmission electron microscopy (TEM) analysis of hAOs at passage (P)2 (day 21 post-re-plating) revealed the presence of lamellar bodies and microvilli on the apical cell surface (Figure 4.2A, 4.2B and 4.2C). TEM analysis was kindly performed by Yongsuk Her (Biomedical Research Centre, KAIST), Taewoo Kim (KAIST) and Ho Min Kim (KAIST). The presence of these microstructures, coupled with surfactant production and ABCA3 presence, highlighted that hAT2 cells within hAOs cultured in complete medium were functionally mature. As described above, two different organoid morphologies existed in primary hAO cultures; folded and cystic, with folded organoids making up a higher proportion of observed organoids in primary cultures (Figure 4.2D, 4.2E and 4.2 F). The hAT2 cell surface marker HTII-280 was strongly expressed in primary cultures, although the location of expression differed between individual organoids, displaying inner, outer or dual localisation (Figure 4.1F and 4.2D). Interestingly, cystic organoids almost exclusively expressed HTII-280 on the inner surface of the organoids, while folded organoids displayed more variation in HTII-280 localisation (Figure 4.2F). *In vivo*, HTII-280 is localised to the apical cell surface (Gonzalez et al., 2010; Figure 3.1B). I therefore questioned whether the position of HTII-280 staining in hAOs correlated with cellular polarity. IF analysis of F-actin and Scribble (SCRIB) revealed apical localisation of F-actin and basolateral distribution of SCRIB, in accordance with previous studies (El-Hashash and Warburton, 2011; Rodriguez-Boulan and Macara, 2014). Although CRB3 has

previously been identified as marking the apical domain of epithelial cells, including proximal airway epithelium during lung development (Pocha and Knust, 2013; Szymaniak et al., 2015), it was found to be expressed more broadly within cultured hAT2 cells (Figure 4.2G). Staining and imaging of F-actin and CRB3 were performed by Taewoo Kim (KAIST). The above findings indicated that hAT2 cells within hAOs maintain correct polarity, irrespective of HTII-280 cellular location. Therefore, HTII-280 localisation does not accurately correspond with hAT2 cell polarity *in vitro*.

Following enzymatic dissociation into single cells, HTII-280⁺ cells were again able to form organoids in culture, with similar folded or sometimes cystic morphologies to those observed in primary culture (Figure 4.3A). Further passaging appeared to result in the eventual loss of the large, folded structures observed during primary cultures. Instead, organoids became more homogenous, presenting themselves in small, spherical arrangements with a small inner lumen (Figure 4.3A). To assess whether hAT2 cells maintained genetic stability following long-term *in vitro* culture, 6-month-old organoids were dissociated and subjected to karyotype analysis, as kindly performed by Seon Young Kim (Chungnam National University College of Medicine; Figure 4.3B). Cultured hAT2 cells presented with normal karyotype numbers, suggesting the absence of genetic aberrations and maintenance of chromosomal-level genomic stability even following long-term culture (Figure 4.3B). This finding suggested that my culture system maintained healthy primary hAT2 cells and prevented any aberrant cell transformations. Like human lung cultures from other cell populations, passage ability varied between individual donors, with some cultures growing at faster rates than others, although hAOs were generally passaged every 3-4 weeks for up to 11 months (Figure 4.3C and 4.3D). Organoid forming efficiency also increased up until P3, after which it began to slowly decline, along with average hAO size (Figure 4.3C, 4.3D and 4.3E). On the level of cumulative population doublings, cell doublings continued to occur until at least P6, although some donor samples exhibited a decrease, suggesting population reduction (Figure 4.3G). However, samples for which population doubling decreased also tended to exhibit lower primary organoid forming efficiency and reduced passage ability, and often correlated with smoking-status of the donor or poorer sample quality (*also see Chapter 2 – Methods*).

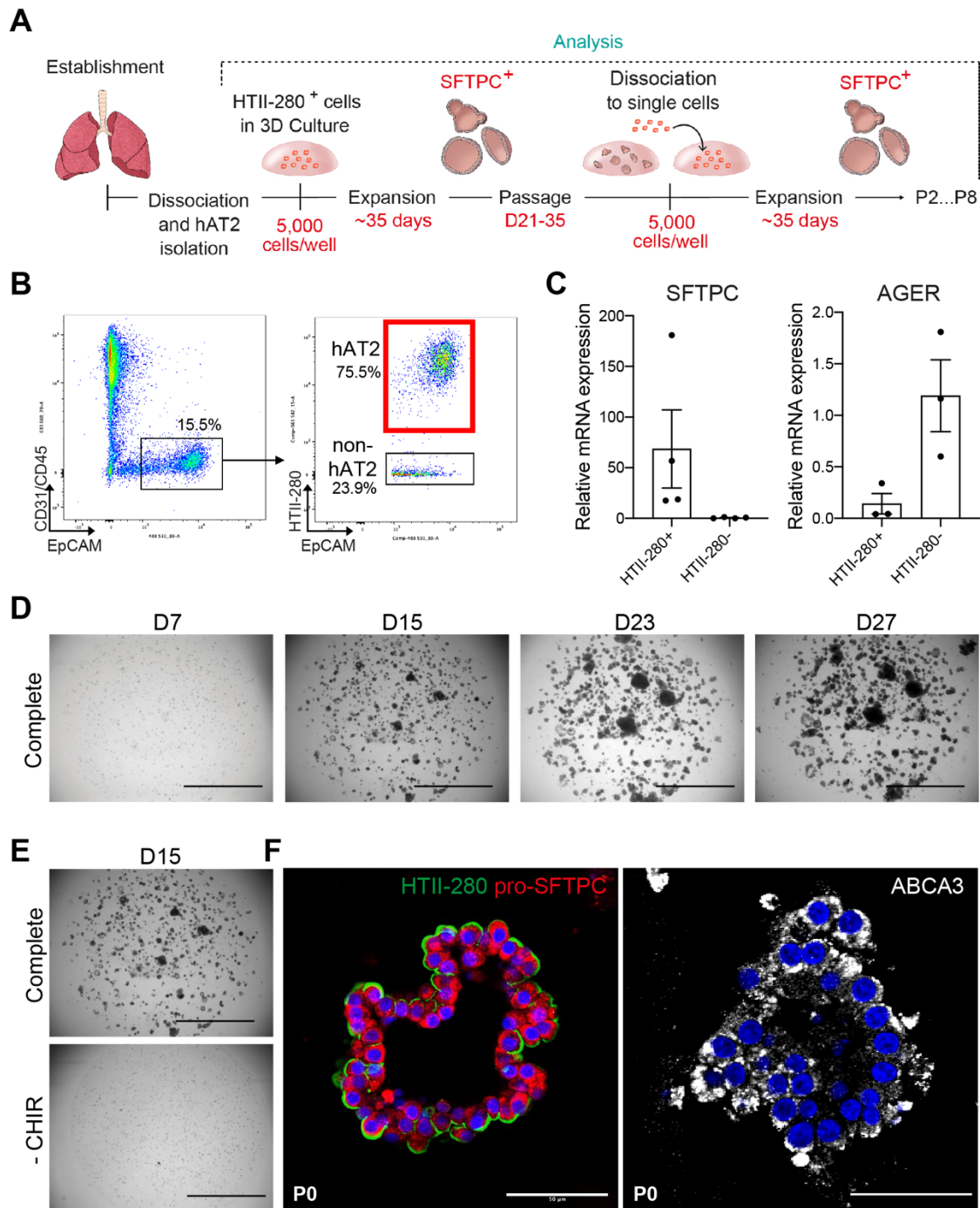


Figure 4.1. Primary HTII-280⁺ cells cultured in high Wnt conditions form hAOs comprising hAT2 cells (figure legend continued on next page).

A. Schematic outlining the process for isolation and culture of hAT2 cells. Adapted from Youk *et al.* 2020. **B.** FACS gating strategy for the isolation of CD31⁻/CD45⁻/EpCAM⁺/HTII-280⁺ hAT2 cells from healthy donor lungs (FACS plot was also utilised in Figure 3.6A). **C.** Relative mRNA expression of *SFTPC* and *AGER* in primary HTII-280⁺ and HTII-280⁻ cells. Data are mean \pm SEM for 3 individual donor samples and values are expressed relative to the housekeeping gene *GAPDH*. **D.** Representative brightfield images of primary HTII-280⁺ cells cultured in complete medium. Scale bar, 2000 μ m. **E.** HTII-280⁺ cells cultured in complete or -CHIR medium. Scale bar, 2000 μ m. **F.** IF images of primary (P0) HTII-280⁺ derived hAOs

grown in complete medium for 21 days. pro-SFTPC (red), ABCA3 (white), HTII-280 (green) and DAPI (blue). Scale bar, 50 μm .

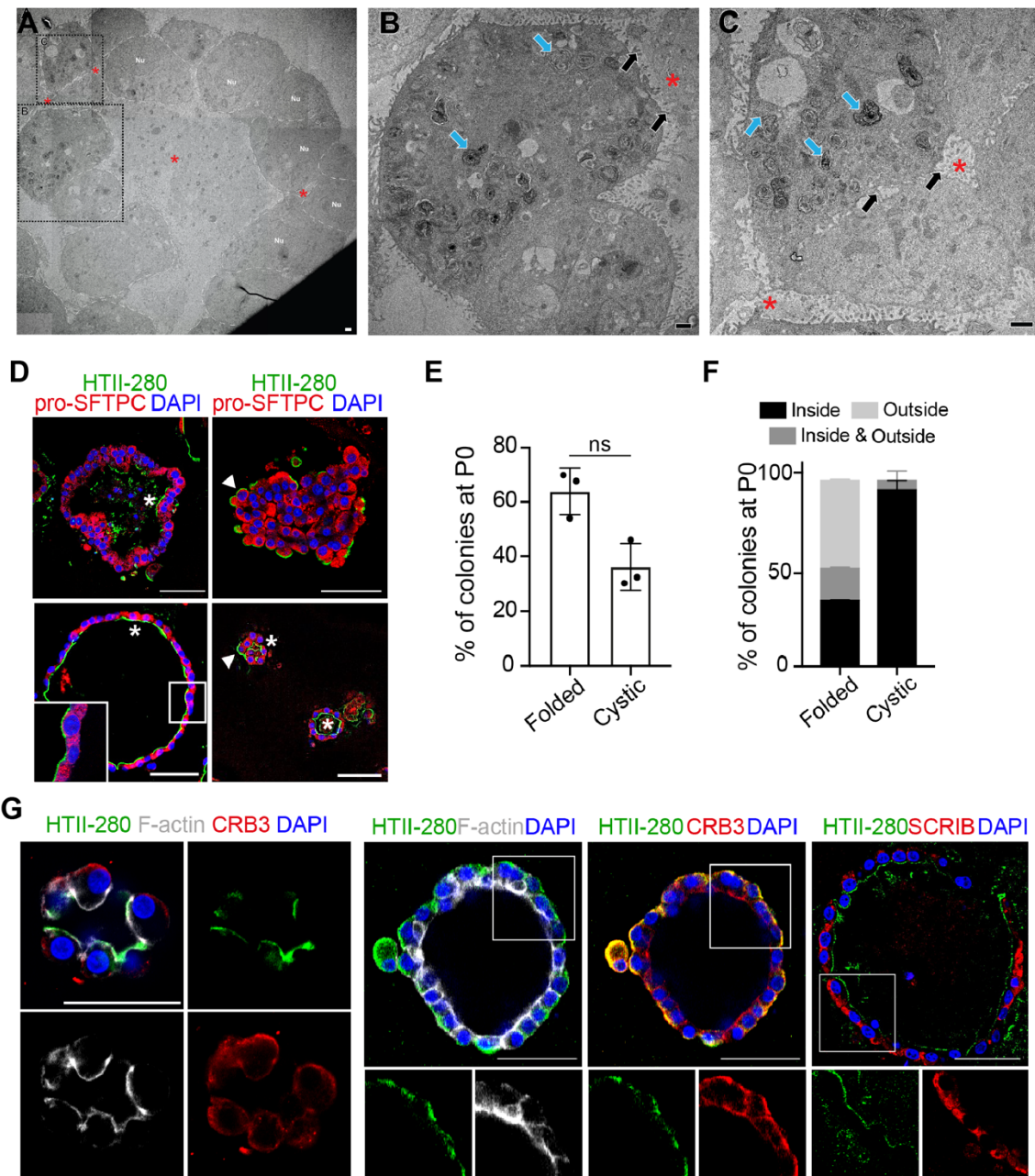


Figure 4.2. Cultured hAT2 cells from alveolar organoids are functionally mature and display correct polarity (figure legend continued on next page).

A. TEM image of a representative alveolar organoid comprising multiple hAT2 cells. Individual hAT2 cell membranes are delineated with white dashed lines. Red asterisk, alveolar space; Nu, nucleus. Image is representative of 10 individual hAOs derived from 1 donor at passage 2 (P2). **B and C.** Two individual hAT2 cells (boxed regions from A) comprising lamellar bodies (blue arrows) and microvilli (black arrows). n=10 individual alveolar organoids at P2 comprised from 1 donor. A-C scale bars, 1 μm . Images were obtained by Yongsuk Her (Biomedical Research Centre, KAIST), Taewoo Kim (KAIST), and Ho Min Kim (KAIST), and have previously been published (Youk *et al.* 2020). **D.** IF images of folded (with or without a small

lumen) and cystic (round with a large lumen) hAOs. HTII-280 (green), pro-SFTPC (red) and DAPI (cell nuclei, blue). Asterisk, luminal HTII-280 expression; arrowhead, basal HTII-280 expression. Scale bar, 50 μm . **E.** Quantification of primary hAO morphology, expressed as a percentage of total organoids at P0. Data are mean \pm SEM for 3 individual donor samples ($n = 67$ for donor 1, $n = 50$ for donor 2 and $n = 50$ for donor 3; $n =$ total number of organoids scored per donor). Statistical significance was tested using the non-parametric Mann-Whitney U test; ns = non-significant. **F.** Quantification of HTII-280 staining location for folded or cystic primary alveolar organoids analysed in E. **G.** IF images of representative primary alveolar organoids expressing HTII-280 (green), F-actin (white), CRB3 (red), SCRIB (red) and DAPI (blue). Scale bar, 50 μm . Images for F-actin and CRB3 obtained by Taewoo Kim (KAIST).

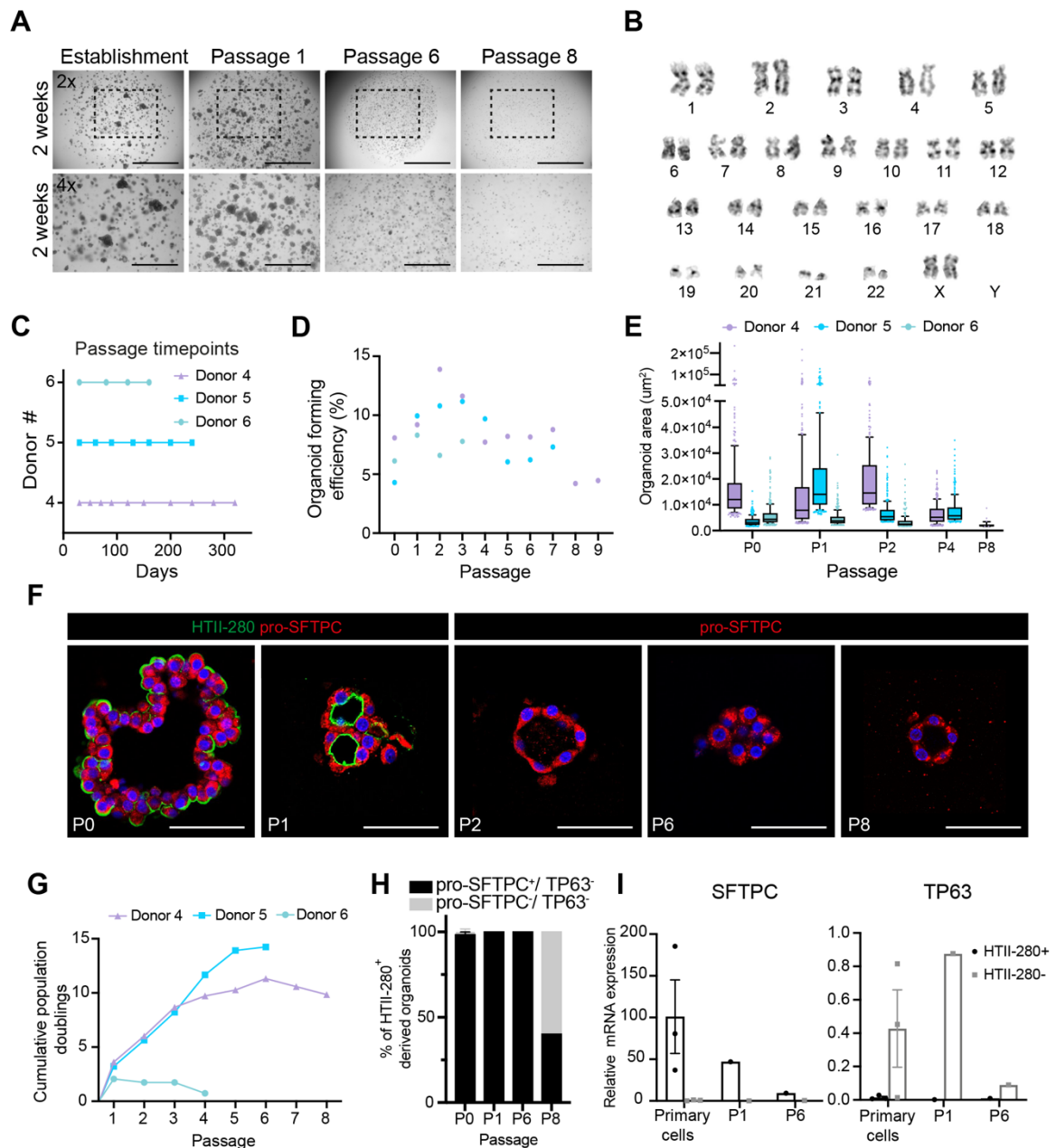


Figure 4.3. Human alveolar organoids can be stably maintained for up to 11 months in culture and exhibit no chromosomal aberrations (figure legend on next page).

Figure 4.3. Human alveolar organoids can be stably maintained for up to 11 months in culture and exhibit no chromosomal aberrations

A. Brightfield images of HTII-280⁺-derived hAOs across multiple passages. Scale bars; brightfield, 2000 μm (top row) and 1000 μm (bottom row). **B.** Representative karyotype of hAO-derived hAT2 cells following 6 months of culture (P5). N = 1 donor, n = 6 hAT2 cells, all arrested in G2/M phase. Karyotyping performed by Seon Young Kim. **C.** Organoid cultures derived from HTII-280⁺ cells from different donors were passaged at various timepoints depending on growth. Each point represents a single passage. **D.** Organoid forming efficiencies over multiple passages for HTII-280⁺ cells grown in complete medium. A single point represents the mean of 3 technical replicates (separate wells) for each individual donor. N=3 individual donor samples (P0 to P3), 2 donor samples (P4 to P7), and 1 donor sample (P8 and P9). **E.** Quantification of alveolar organoid surface area for 3 donor samples over long-term culture. Areas are presented as mean (10-90 percentile), with each dot representing an individual organoid (n= 300 organoids per donor at each passage, except P2 donor 3, where n= 228 and P8 where n = 37). **F.** IF analysis of HTII-280⁺-derived alveolar organoids up to P8 (9 months in culture). HTII-280 (green), pro-SFTPC (red), DAPI (nuclei, blue). Scale bars, 50 μm . **G.** Cumulative population doublings for hAT2 organoids derived from 3 separate donors. Calculation for population doublings can be found in *Methods*. **H.** Quantification of organoid identity from HTII-280⁺-derived cultures based on pro-SFTPC and TP63 IF staining. Data are presented as mean \pm SEM of 2 biological replicates (P0 and P1) and 1 biological replicate (P6 and P8). n = 131 for P0, n = 55 for P1, n = 50 for P6 and n = 25 for P8, where n denotes the total number of organoids quantified. **I.** Relative mRNA expression of the hAT2 marker *SFTPC* and the basal cell marker *TP63* in HTII-280⁺ and HTII-280⁻ derived organoids at multiple passages. Primary cells, 3 biological replicates; P1 and P6, 1 biological replicate.

During primary culture, almost 100% of organoids were classed as hAOs consisting entirely of pro-SFTPC⁺ hAT2 cells, with only a single organoid from one of the three analysed donors not staining for any tested lung lineage (Figure 4.3H). hAT2 cell identity was still maintained at P6 (following 6 months of culture), although following this point the number of pro-SFTPC⁺ hAOs began to reduce (Figure 4.3H). No TP63⁺ cells were observed in hAOs at any stage of culture, indicating that no aberrant differentiation to basal-like cells was occurring (negative staining data not shown). Despite the gradual loss of pro-SFTPC expression, 40% of organoids still expressed pro-SFTPC following 8 to 9 months of culture, the longest amount of time adult-derived hAT2 cells have been successfully maintained *in vitro* (Table 4.1). This finding differs to hAOs derived from EpCAM⁺ cells, which were greatly reduced in number by P3 (Figure 3.5B). This may have been due to preferential selection of airway and undetermined cell types in EpCAM⁺ cultures. This suggested that specifically isolating hAT2 cells using HTII-280 resulted in more stable culture and propagation of hAOs and increased retention of hAT2 cell markers

compared to culturing EpCAM⁺ epithelial cells. Promisingly, no hAOs throughout any of the passages displayed airway cell phenotypes (negative staining data not shown). This indicated both that the sorting strategy for hAT2 cells resulted in little to no contamination with airway cell types, and that hAO-containing hAT2 cells do not aberrantly transdifferentiate to airway cell types in my culture system (Figure 4.3H). Analysis of alveolar and airway transcripts in primary HTII-280⁺ cells and HTII-280⁺-derived hAOs at early and late passage revealed that *SFTPC* expression persisted during culture, even up to P6, albeit at lower levels than primary cells (Figure 4.3I). However, the expression of the basal cell marker *TP63* was not observed in any hAO cultures, confirming the IF findings (Figure 4.3H and 4.3I; negative TP63 staining data not shown).

Table 4.1. Comparison of hAOs in chemically-defined conditions versus co-culture

Isolation strategy	Culture method	Cell types present (primary)	hAO culture capacity and primary forming efficiency	Reference
FACS enrichment from primary distal lung tissue (EpCAM ⁺ HTII-280 ⁺)	Chemically-defined	Pro-SFTPC ⁺ hAT2 cells	> 10 months (11 passages) ~5-9%	Youk et al., 2020 (current study)
FACS enrichment of adherent overnight cells from primary lung tissue (EpCAM ⁺ HTII-280 ⁺)	Co-culture with MRC5 fibroblasts and ALI-medium (Randell et al., 2011)	Some SFTPC ⁺ hAT2 cells	~ 3 passages 4.2% ± 0.8%	Barkauskas et al., 2013
MACS enrichment from primary distal lung tissue (EpCAM ⁺ HTII-280 ⁺ TM4SF1 ⁺)	Co-culture with MRC5 fibroblasts and SAGM (Lonza)	SFTPC ⁺ hAT2 cells and AQP5 ⁺ cells	Not disclosed ~4-5%	Zacharias et al., 2018

4.3.2. Investigation of molecular pathways involved in hAT2-to-hAT1 differentiation

Now that I had established that hAT2 cells could maintain their identity and stable expansion *in vitro* for at least 6 months, I next wanted to assess whether they also maintained their ability to differentiate into hAT1 cells. Co-culture systems involving mouse-derived AT2 cells and fibroblasts exhibit differentiation of AT2 cells to morphologically-distinct AT1 cells that are co-maintained within the same organoid (Barkauskas et al., 2013). However, differentiation of hAT2 cells has traditionally involved 2D-culture in un-defined conditions such as serum addition, although co-maintenance of hAT2 and hAT1 cells in the same culture has not been achieved (Dobbs et al., 1988; Jacob et al., 2017; Katsura et al., 2020). Therefore, it was important to first ascertain whether hAT2 cells cultured in my culture system maintained their differentiation capacity *in vitro*. A number of primary hAOs cultured in the presence of CHIR (complete medium) strongly co-expressed the hAT1 marker HOPX with pro-SFTPC, although as mentioned previously this observation has already been made in hAT2 cells of the adult lung *in vivo* (Figure 4.4A; Figure 3.1B; Travaglini et al., 2020). Additionally, co-expression of SFTPC with the hAT1 marker PDPN was also observed in some cells, although AGER presence was not present in any hAOs (Figure 4.4A). Additionally, cells morphologically resembling hAT1 cells were not observed. Therefore, these findings confirmed that culture of hAT2 cells in complete medium resulted in formation of organoids entirely comprised of hAT2 cells. However, upon removing P2 hAOs from complete medium at D10 of 3D culture, and transferring to 2D culture with 10% human serum addition, hAT2 cells began to elongate and lose their columnar shape (Figure 4.4B). The change in cell shape was accompanied by a loss of pro-SFTPC expression, and a gain of AT1 marker expression including AQP5 and AGER, indicating that cultured hAO-derived hAT2 cells maintained their ability to differentiate *in vitro* (Figure 4.4B). 2D culture and characterisation was performed by Taewoo Kim (Ju lab, KAIST) with my help.

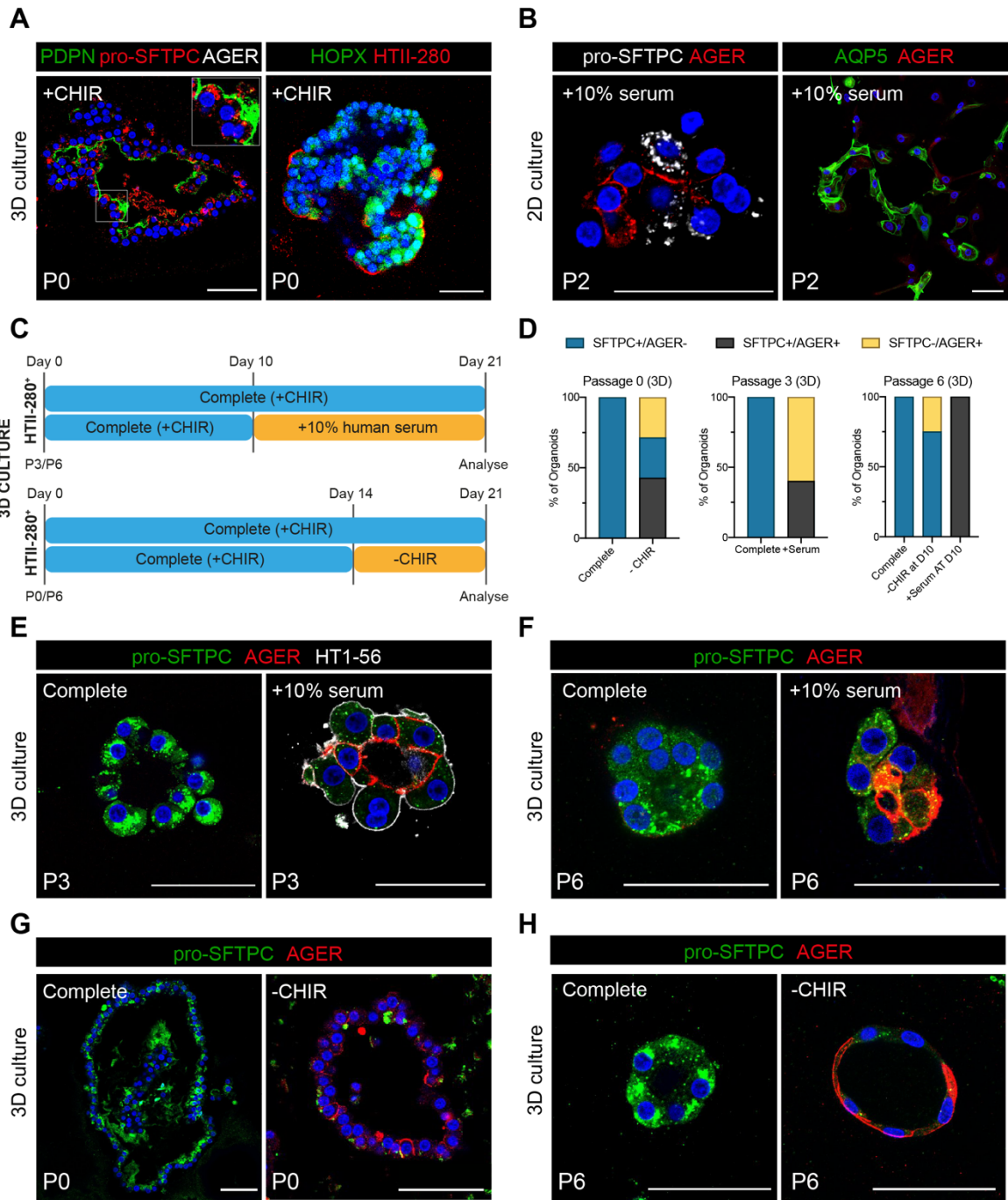


Figure 4.4. Organoid-derived hAT2 cells maintain their ability to differentiate into hAT1 cells following long-term culture (figure legend continued on next page).

A. IF analysis of primary hAT2-derived organoids cultured continuously in complete medium. pro-SFTPC (red), HTII-280 (red), PDPN (green), HOPX (green), AGER (white) and DAPI (blue). **B.** IF analysis of P2 hAT2 cells cultured in 2D with 10% human serum. AGER (red), AQP5 (green), pro-SFTPC (white) and DAPI (blue). 2D culture was performed by Taewoo Kim (Ju lab, KAIST). **C.** Schematic of experimental set-up for culture of hAOs following addition of 10% human serum, or withdrawal of CHIR. **D.** Quantification of organoid identities at passage 0, 3 and 6 when cultured in 3D with the treatments outlined in C. **E to H.** Representative immunofluorescent images of hAT2 cell-derived organoids following 3D culture in 10%

human serum at P3 and P6 (E and F) or following withdrawal of CHIR at D14 in P0 or P6 cultures (G and H). pro-SFTPC (green), AGER (red), HTI-56 (white), DAPI (blue). Images obtained at D21. Scale bars, 50 μm .

Despite effective differentiation of hAT2 cells into hAT1 cell fate in 2D culture, it was unclear whether hAT1 differentiation was occurring because of undefined factors within the serum, or due to direct contact with the plate plastic, as mechanical cues have already been demonstrated as important contributors for AT2-to-AT1 differentiation (Li et al., 2018a). Therefore, I next investigated whether addition of serum to hAOs within 3D culture also resulted in differentiation to hAT1 cells (Dobbs et al., 1988; Jacob et al., 2017). hAOs at P3 and P6 were cultured normally in complete medium for 10 days, after which the conditions were switched to basic medium containing 10% human serum (Figure 4.4C). Upon analysis at D21 (11 days post-serum addition), hAOs exhibited a clear loss of pro-SFTPC expression, and gain of the AT1 markers HTI-56 and AGER (Figure 4.4D, 4.4E and 4.4F). However, unlike 2D culture, serum addition to 3D cultures did not result in the clear morphological change in cells. This potentially suggested that undefined components within the serum resulted in loss of hAT2 identity and induction of AT1 marker expression, while a stiff surface such as a tissue culture plastic may influence changes in cell morphology.

As human serum is undefined, and consists of many complex components, study of precise regulatory signals and mechanisms for hAT2-to-hAT1 differentiation is difficult to assess. Therefore, I investigated potential molecular mechanisms that regulate the differentiation of hAT2 cells into hAT1 cell fate. Previous work in the mouse has suggested that Wnt activation is important for maintenance of AT2 identity, while loss of localised Wnt signalling can lead to AT1 differentiation (Frank et al., 2016). In order to assess the effect of Wnt activity on adult hAT2 differentiation, primary (P0) and late culture (P6) hAOs were initially cultured in 3D in complete medium for 14 days, followed by withdrawal of CHIR for a further 7 days (Figure 4.4C). This allowed hAT2 cells to initially form hAOs, as immediate culture in –CHIR medium led to failure of organoid formation (Figure 4.1E). Following removal of CHIR from the culture system at D14, primary hAOs exhibited clear loss of pro-SFTPC expression upon analysis at D21, and gain of AGER expression, although no change in cell morphology was achieved (Figure 4.4G). P6 organoids also

exhibited gain of AGER expression following CHIR withdrawal, again confirming that cultured hAT2 cells maintained their differentiation ability even following long-term culture (Figure 4.4H). Interestingly, a number of organoids in P6 cultures displayed cell elongation, with resulting cells more closely resembling the morphological characteristics of hAT1 cells. Notably, throughout all differentiation experiments, no hAOs were observed that comprised both hAT2 and fully-differentiated hAT1 cells within the individual organoid at the analysed timepoint. No airway markers were observed (negative data not shown). These results suggest that Wnt activation, mediated by CHIR, is required for maintaining hAT2 identity and loss of Wnt activation leads to hAT1 differentiation in the culture condition, as previously reported in mouse AT2 cells.

Due to the lack of retention of hAT2 cells in hAOs in my –CHIR differentiation medium, I reasoned to test whether low Wnt activation allowed me to retain hAT2 and hAT1 cells within the individual hAOs, providing a better platform to assess their transitioning process. Therefore, I used WNT3A-conditioned medium as an alternative source of Wnt activity, which seems to reveal lower Wnt activity compared to CHIR. To do this, I first cultured primary hAT2 cells in media containing WNT3A-conditioned medium from D0, and analysed organoid growth and cellular composition. As a control, hAOs cultured in complete medium (+CHIR) were used. Brightfield images of organoids at D21 revealed that hAT2 cells cultured in complete medium formed mostly folded organoids as normal, and IF analysis revealed that all hAOs expressed pro-SFTPC and no AGER (Figure 4.5A). In contrast, although many hAOs formed in WNT3A conditions were folded, a few structures arose that were cystic, more than were observed in controls. As hAOs can occasionally form cystic structures, IF analysis was performed to determine the identity of cystic organoids in WNT3A conditions. Unlike cystic hAOs formed in complete medium, cystic organoids arising from WNT3A conditions expressed AGER, with virtually no pro-SFTPC expression present within these organoids upon analysis at D21, highlighting hAT1 differentiation (Figure 4.5A). However, as was observed in serum-treated and CHIR-withdrawal 3D-cultures, no hAOs in WNT3A conditions retained both hAT2 and fully-differentiated hAT1 cells within the same structure. Following passage without sorting, organoid forming efficiency for WNT3A-cultured hAT2 cells decreased in comparison to controls, likely due to the increased presence of hAT1 cells, that were not thought to possess self-renewal capacity (Figure 4.5B). Due to the difficulty in maintaining WNT3A cultures overtime, I was unable to assess the effect of WNT3A on mid- or late-

passage hAOs. Therefore, I instead assessed WNT3A addition in P3 and P6 organoids that had previously been cultured in CHIR-containing complete medium (Figure 4.5C). Addition of WNT3A-conditioned medium as the Wnt source to P3 and P6 hAOs again resulted in induction of hAT1 cell markers and loss of pro-SFTPC by D21, with some P3 and P6 hAOs even consisting of cell markers from both lineages (Figure 4.5D and 4.5E). However, AGER⁺ cells within these mixed organoids did not morphologically resemble fully-differentiated hAT1 cells (Figure 4.5D). Furthermore, occasional cells existed that co-expressed pro-SFTPC and AGER, perhaps representing differentiating cells. Interestingly, as was observed in CHIR-withdrawal P6 hAOs, P6 WNT3A cultures consisted of a number of organoids comprised entirely of elongated hAT1 cells, again suggesting that later passage hAT2 cells could more readily differentiate (Figure 4.5D). However, WNT3A-conditioned medium did not support co-retention of hAT2 and fully-differentiated hAT1 cells within the same organoid, as has been observed for the mouse (Barkauskas et al., 2013). Therefore, conditions will need to be optimised further in order to support both cell types within the same culture system to investigate hAT2-hAT1 interactions.

4.3.3. Investigation of purification strategies to specifically isolate hAT2 cells following sub-culture

All experiments performed in this project involved the initial isolation of HTII-280⁺ cells as hAT2 cells from human lung specimens, followed by serial single-cell passage of hAOs without further sorting. This allowed for propagation of hAOs in complete medium, as organoids consisted entirely of hAT2 cells. However, in conditions where induction of hAT1 cells was achieved, it would be helpful to establish a better quantitative assessment, such as flow cytometry analysis with surface markers, to assess the number of hAT2 cells and achieve their isolation from hAOs. To confirm that HTII-280 was still expressed on all viable hAT2 cells, I dissociated primary non-differentiated hAOs cultured in complete medium at day 21 and re-sorted with FACS based on their HTII-280 expression. Although the majority of cells still expressed HTII-280, approximately ~20% of cells were found to be HTII-280⁻ (Figure 4.6A). However, analysis of mRNA transcript levels found that hAO-derived HTII-280⁻ cells still expressed *SFTPC* at a higher level than airway organoids, although levels were reduced compared with HTII-280⁺ cells (Figure 4.6B). Despite the

reduction in *SFTPC* levels, culture of both cell types in complete medium resulted in organoid establishment (Figure 4.6C and 4.6D). These data indicated that HTII-280 may not be a useful marker for detecting hAT2 cells in culture, due to the transient loss of HTII-280 expression from a proportion of viable hAT2 cells.

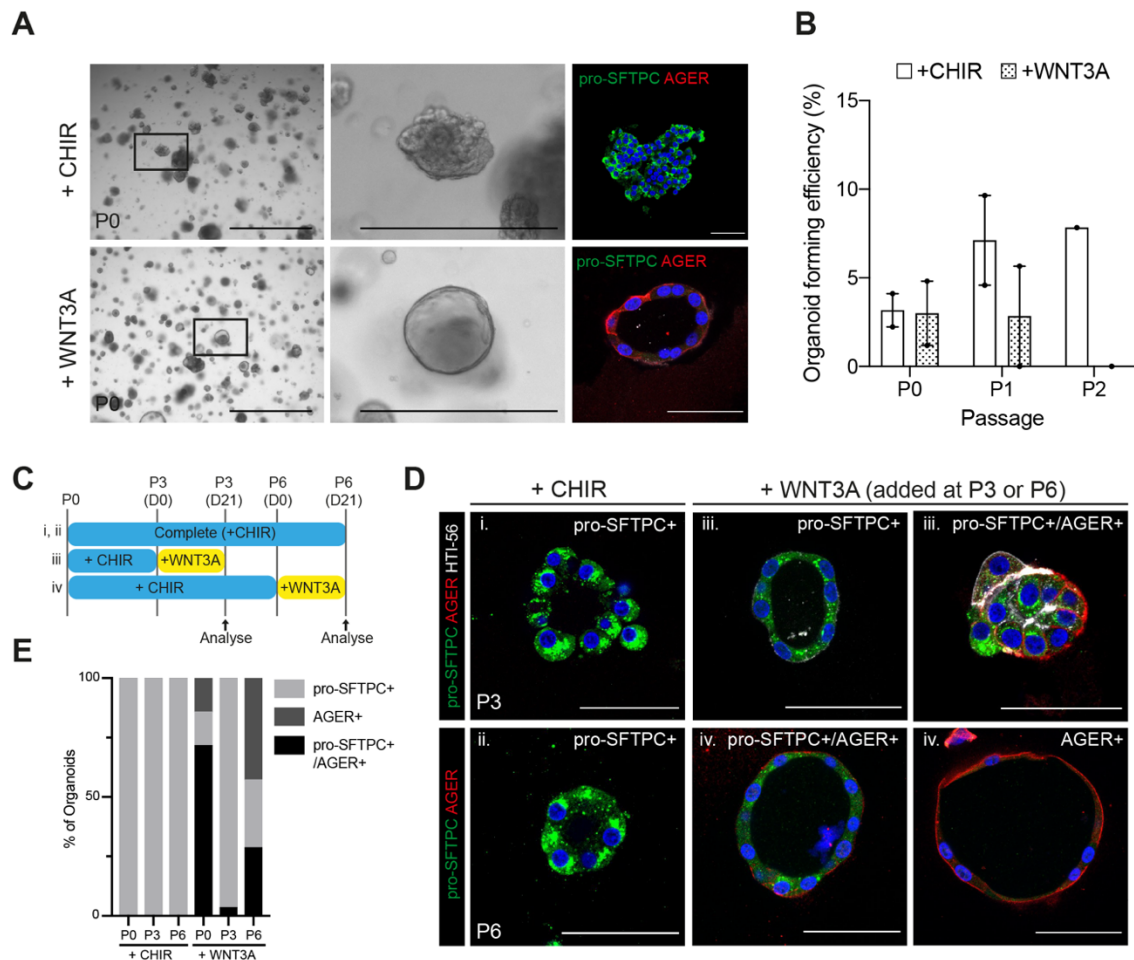


Figure 4.5. WNT3A-conditioned medium results in hAT1 marker induction in hAOs.

A. Brightfield and IF images of primary human HTII-280⁺ epithelial cells cultured in either CHIR (complete) or media containing WNT3A-conditioned medium. pro-SFTPC (green), AGER (red) and DAPI (blue). Scale bars; 2000 μ m (left panels), 400 μ m (middle panels) and 50 μ m (right panels). **B.** Organoid forming efficiency of HTII-280⁺ cells cultured with CHIR or WNT3A from primary culture. Data are presented as mean \pm SEM for 2 individual donors (P0 and P1) and 1 donor (P2). **C.** Experimental design for addition of WNT3A-conditioned medium to hAOs at P3 or P6. Organoids were cultured continuously in complete (+CHIR) medium up until switch to WNT3A-medium. **D.** IF images of HTII-280⁺ derived alveolar organoids cultured continuously with CHIR or supplemented with WNT3A-conditioned medium at P3 or P6. pro-SFTPC (green), AGER (red), HTI-56 (white). Scale bars; 50 μ m. **E.** Quantification of organoid staining from ‘A’ and ‘C’. Data are presented as the mean from 1 biological replicate.

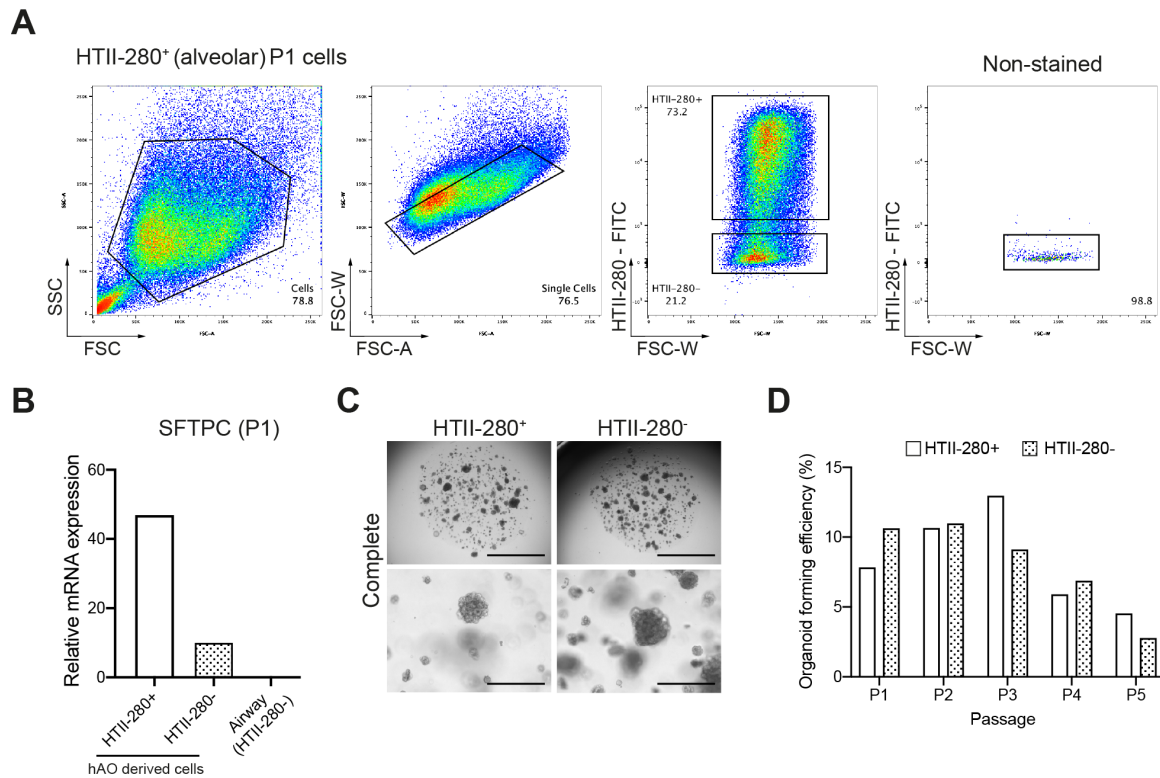


Figure 4.6. HTII-280 does not reliably correspond with hAT2 identity during continuous in vitro culture.

A. Representative FACS plot of gating strategy used to isolate P1 cells (HTII-280⁺ at primary establishment) using HTII-280. **B.** Relative mRNA expression levels of *SFTPC* in P1 HTII-280⁺ and HTII-280⁻ cells derived from hAOs. Data are presented as the mean of 2 technical replicates (1 biological replicate) and are expressed relative to the housekeeping gene *GAPDH*. **C.** Brightfield images of hAO-derived P1 HTII-280⁺ and HTII-280⁻ cells cultured in complete medium. Scale bar; 2000 μm (top), 1000 μm (bottom). **D.** Quantification of organoid forming efficiency for hAO-derived HTII-280⁺ and HTII-280⁻ cells (P1). Data are presented as the mean of 3 technical replicates (1 biological replicate).

Therefore, I sought to investigate whether additional strategies could be used as an alternative isolation approach. LysoTracker is a fluorescent dye that labels acidic components of organelles within live cells and has been recently shown to label the lamellar bodies of hPSC-derived hAT2 cells, as well as hAT2 cells in precision cut lung slices (Korogi et al., 2019; Yamamoto et al., 2017). Hence, I first investigated whether LysoTracker could also be used to isolate adult hAT2 cells from primary lung tissue. Following gating for EpCAM⁺ epithelial cells, FACS analysis demonstrated that the majority of HTII-280⁺ cells also retained high levels of LysoTracker (LysoTracker^{hi}), while the remaining cells retained low levels (LysoTracker^{low}; Figure 4.7A). The presence of a

small proportion (~ 1%) of HTII-280⁺ Lysotracker^{low} cells may indicate the presence of an immature population of hAT2 cells, as Lysotracker is accumulated into functional lamellar bodies. Upon culturing in complete medium, HTII-280⁺ Lysotracker^{hi} cells successfully formed organoids by day 14 of culture, with 100% able to accumulate Lysotracker dye (Figure 4.7B). The majority of these cells also expressed pro-SFTPC (data not shown). In comparison, although HTII-280⁺ Lysotracker^{low} cells also formed organoids, albeit at a lower efficiency, these could not be passaged due to lack of growth, although this could have been due to insufficient starting number of cells (Figure 4.7B and 4.7C). This indicated that Lysotracker could be used to isolate adult hAT2 cells from primary tissue. Upon comparison of Lysotracker-derived hAO cultures with HTII-280⁺-derived hAOs, it was thought that Lysotracker had no adverse effects on hAT2 cell viability or proliferation (Figure 4.3D and 4.7C). In contrast to HTII-280⁺ cells, HTII-280⁻ cells formed airway organoids in -CHIR medium as usual, regardless of Lysotracker staining status. As non-hAT2 cell types such as basal cells are not thought to possess acidic organelles that can accumulate Lysotracker dye, it is likely that the positive staining observed in primary HTII-280⁻ cells was due to the presence of residual dye. It is also important to note that even in the HTII-280⁻Lysotracker^{hi} primary population, the staining intensity did not match that of the HTII-280⁺ Lysotracker^{hi} hAT2 cells, and they do not represent a substantial population (Figure 4.7A).

Following from this, I then determined whether Lysotracker could also be used as an improved method for isolating hAT2 cells following 3D *in vitro* culture. Taking hAOs at P6, HTII-280 and Lysotracker expression were assessed by FACS, leading to the observation of four separate populations (Figure 4.7D). The largest population was made up of HTII-280⁺ Lysotracker^{hi} cells, which were postulated to be hAT2 cells, while a population of HTII-280⁻Lysotracker^{hi} cells was also present. Upon plating these populations, I found that the HTII-280⁺Lysotracker^{hi} population most readily formed hAOs in complete medium, displaying the highest level of organoid forming efficiency (Figure 4.7E). However, both HTII-280⁻Lysotracker^{hi} and HTII-280⁻Lysotracker^{low} cells were also able to re-form hAOs, albeit with a lower efficiency (Figure 4.7E). When P6 HTII-280⁺ cells were compared with primary HTII-280⁺ cells, it was promising to observe that over 90% of the population retained high expression of Lysotracker dye, indicating the maintenance of functional lamellar bodies (Figure 4.7F). One possible issue with the use of Lysotracker was that positive staining also existed in some primary HTII-280⁻ cells. This

meant that without an additional marker such as HTII-280, separating hAT2 cells from other epithelial cell types could prove challenging.

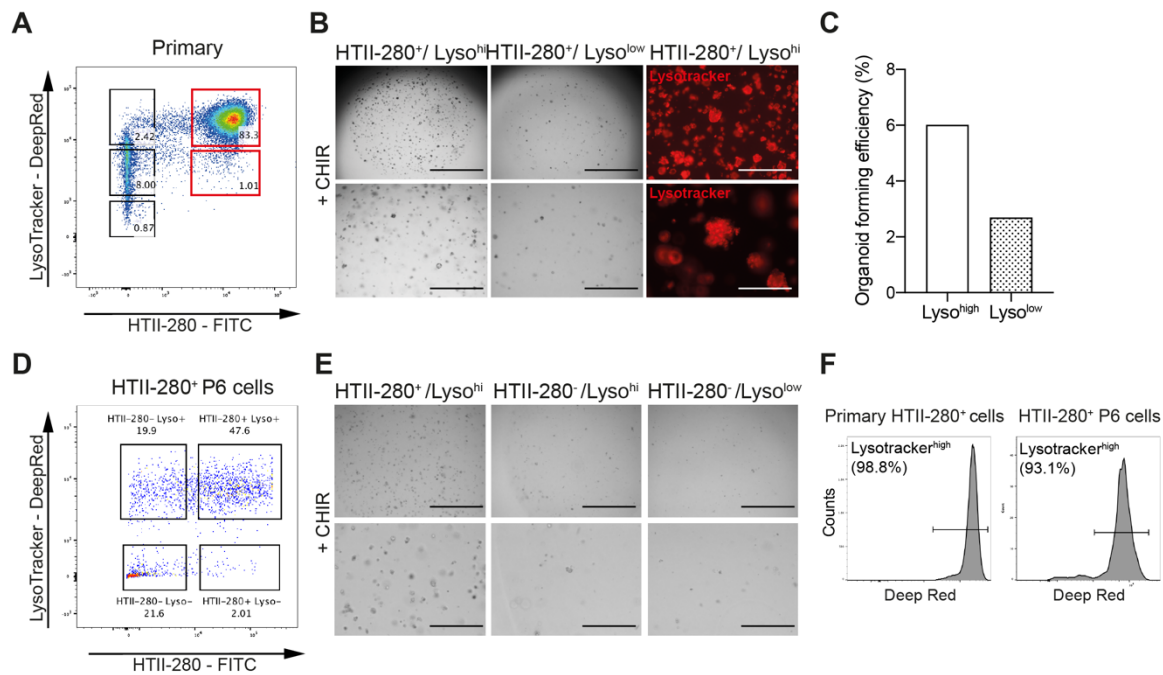


Figure 4.7. Investigation of the use of LysoTracker for improved sub-culturing of organoid-derived hAT2 cells.

A. Representative FACS plot of primary epithelial cells (EpCAM⁺) gated on the basis of their HTII-280 and LysoTracker-DeepRed staining. **B.** Representative brightfield and IF images of HTII-280⁺/LysoTracker^{hi} and HTII-280⁺/LysoTracker^{low} cells cultured in complete medium for 14 days. Scale bar (left and middle panels); 2000µm (top), 1000 µm (bottom); right panel 1000 µm (top), 400 µm (bottom). **C.** Organoid forming efficiency of primary HTII-280⁺/LysoTracker^{hi} and HTII-280⁺/LysoTracker^{low} cells cultured in complete medium. Data are presented as mean of 3 technical replicates (Lyso^{high}) and 2 technical replicates (Lyso^{low}) from 1 donor. **D.** FACS plot of passage 6 cells gated for HTII-280 and LysoTracker. **E.** Representative brightfield images of P6 hAO-derived cells following HTII-280/LysoTracker FACS isolation. Scale bar; 2000µm (top), 1000 µm (bottom). **F.** FACS histogram of LysoTracker-Deep Red staining in primary and P6 HTII-280⁺ cells.

I also investigated other surface markers that could potentially be used to isolate and propagate adult hAT2 cells. MHCII class antigens have been successfully used to isolate AT2 cells from mouse lungs in my laboratory and others (Choi et al., 2020; Hasegawa et al., 2017). Notably, in a previous study, the analysis of immunohistochemistry for MHCII class antigens, HLA-DR and HLA-DP, revealed their expression on the surface of hAT2 cells (Cunningham et al., 1994). As studies have shown that HLA-DR is expressed at higher

levels on the surface of hAT2 cells than HLA-DP, I chose this antigen to proceed with further analysis. I first confirmed that HLA-DR is expressed in hAT2 cells in lung tissues (Figure 4.8A). Utilising freshly isolated cells from normal human lungs, CD31⁻CD45⁻EpCAM⁺ cells were gated based on their HTII-280 and HLA-DR expression. From this, it was observed that all HTII-280⁺ cells were also positive for HLA-DR, while the majority of HTII-280⁻ cells were negative for HLA-DR (Figure 4.8B and 4.8C). Upon culture, HTII-280⁺ HLA-DR⁺ and HTII-280⁻ HLA-DR⁻ formed organoids in complete and -CHIR medium, respectively (Figure 4.8D). A small proportion of cells were HTII-280⁻HLA-DR⁺, although only represented a minor population, and single cells from this population failed to form organoids in subsequent culture. This suggested that at least in primary culture, HLA-DR was expressed mainly in HTII-280⁺ hAT2 cells. Next, to assess whether HLA-DR could also be used to isolate hAT2 cells from organoid culture, P6 cells obtained from HTII-280⁺ derived hAOs were analysed and sorted using the same strategy as above. I found that the three populations that existed in primary tissue were present again, with HTII-280⁺ HLA-DR⁺ cells comprising the largest population (Figure 4.8E). However, the HTII-280⁻ HLA-DR⁻ cell population was much more substantial than in primary cells. When placed into culture with complete medium, all three populations formed organoids, although HTII-280⁺ HLA-DR⁺ cells produced the largest hAOs with the highest forming efficiency (Figure 4.8F). Therefore, it is likely that the use of additional markers such as LysoTracker or HLA-DR will enable us to purify hAT2 cells that have the better capacity to form organoids during subculture of adult hAOs. Due to LysoTracker requiring successful incorporation into live hAT2 cells, HLA-DR may prove to be a more useful additional hAT2 marker, depending on the downstream application.

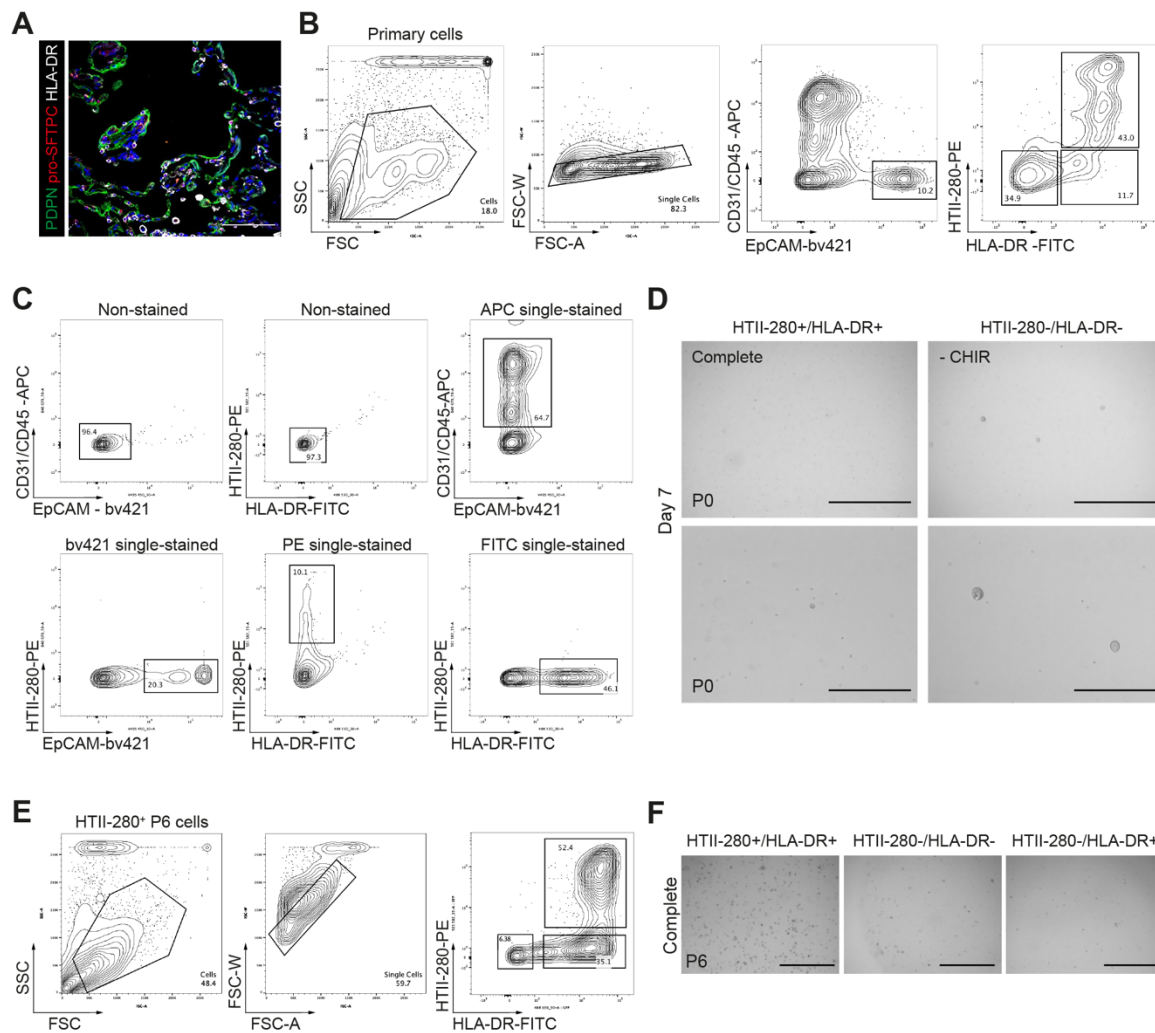


Figure 4.8. HLA-DR as a novel marker to isolate adult hAT2 cells from primary human lungs and cultured hAOs.

A. Representative IF staining of healthy human lung alveoli. PDPN (green), pro-SFTPC (red), HLA-DR (white) and DAPI (blue). Scale bar, 50 μ m. B. FACS gating strategy for isolation of hAT2 cells from primary adult human lung tissue based on their CD31⁻/CD45⁻/EpCAM⁺/HTII-280⁺/HLA-DR⁺ expression profile. C. Non-stained and single-stained controls for markers used in B. D. Brightfield images of organoids formed from two of the cell populations isolated in B. Images were obtained at D7 of culture and grown in complete or -CHIR medium. Scale bars, 1000 μ m (top panel), 400 μ m (bottom panel). E. HLA-DR/HTII-280 gating strategy for isolation of cells from P6 HTII-280⁺ derived cultures. F. Brightfield images of cells isolated in E. Cells were grown in complete medium, and images obtained at day 14 of culture. Scale bars, 1000 μ m.

Finally, the use of fluorescent-reporters for marking hAT2 cells would be extremely useful not only for detecting and isolating hAT2 cells, but also for tracing their differentiation behaviours. For this, primary HTII-280⁺ hAT2 cells were cultured as hAOs as normal for

21 days. At day 21, hAOs were dissociated to single cells, and transduced with Lenti-EF1a-tagRFP-SFTPC-eGFP (hereafter SFTPC-eGFP; Lim et al., 2020) plasmid DNA using lentiviral transduction (Figure 4.9A). The plasmid and lentivirus was kindly provided by Dr Kyungtae Lim in the laboratory of Dr Emma Rawlins. At 48-hours post-transduction, I observed RFP⁺ and GFP⁺ cells, which became abundant by day 14 (Figure 4.9B). IF analysis revealed that all RFP⁺GFP⁺ cells formed organoids that also expressed pro-SFTPC. Quantification of the number of transduced cells confirmed that 100% of transduced (RFP⁺) cells also expressed the SFTPC-eGFP reporter, with a transduction efficiency of around 17%, highlighting the exclusive presence of SFTPC-expressing hAT2 cells (Figure 4.9C and 4.9D). Reporter hAO lines could successfully re-form organoids following dissociation to single cells and FACS enrichment of the RFP⁺GFP⁺ fraction, although cell expansion proved difficult (Figure 4.9E and 4.9F). This may be due to toxicity of the lentiviral system to fragile hAT2 cells, although cell death was not specifically assessed. Therefore, gene-editing of hAOs will require further optimisation. However, these data demonstrated that hAT2 cells propagated as hAOs could undergo gene-editing strategies. This, when combined with other fluorescent reporters, would prove useful in applications such as studying cell differentiation upon chemical modulation.

4.3.4. Downstream applications of hAOs

The ability to freeze-thaw lines of hAOs would increase flexibility for experimental design and would allow researchers to more easily collaborate and share specific hAO lines. To assess freeze-thaw ability, I enzymatically dissociated P3 organoids from HTII-280⁺ cultures and froze down at least 100,000 single cells/ mL in a solution of FBS/10% DMSO. Upon rapid thawing and plating, HTII-280⁺-derived cells re-formed organoids that retained pro-SFTPC expression, although there was a decrease in initial organoid forming efficiency when compared with non-frozen P3 controls (Figure 4.10A to 4.10C). Use of serum-free commercial freezing medium (Bambanker) also yielded similar results (data not shown). Further culture and passage of these cells usually resulted in an improvement in organoid forming efficiency over initial efficiency (data not shown). These data suggest that hAOs could be frozen for long-term storage, and re-plated to form hAOs, although with an initial reduction in cell viability.

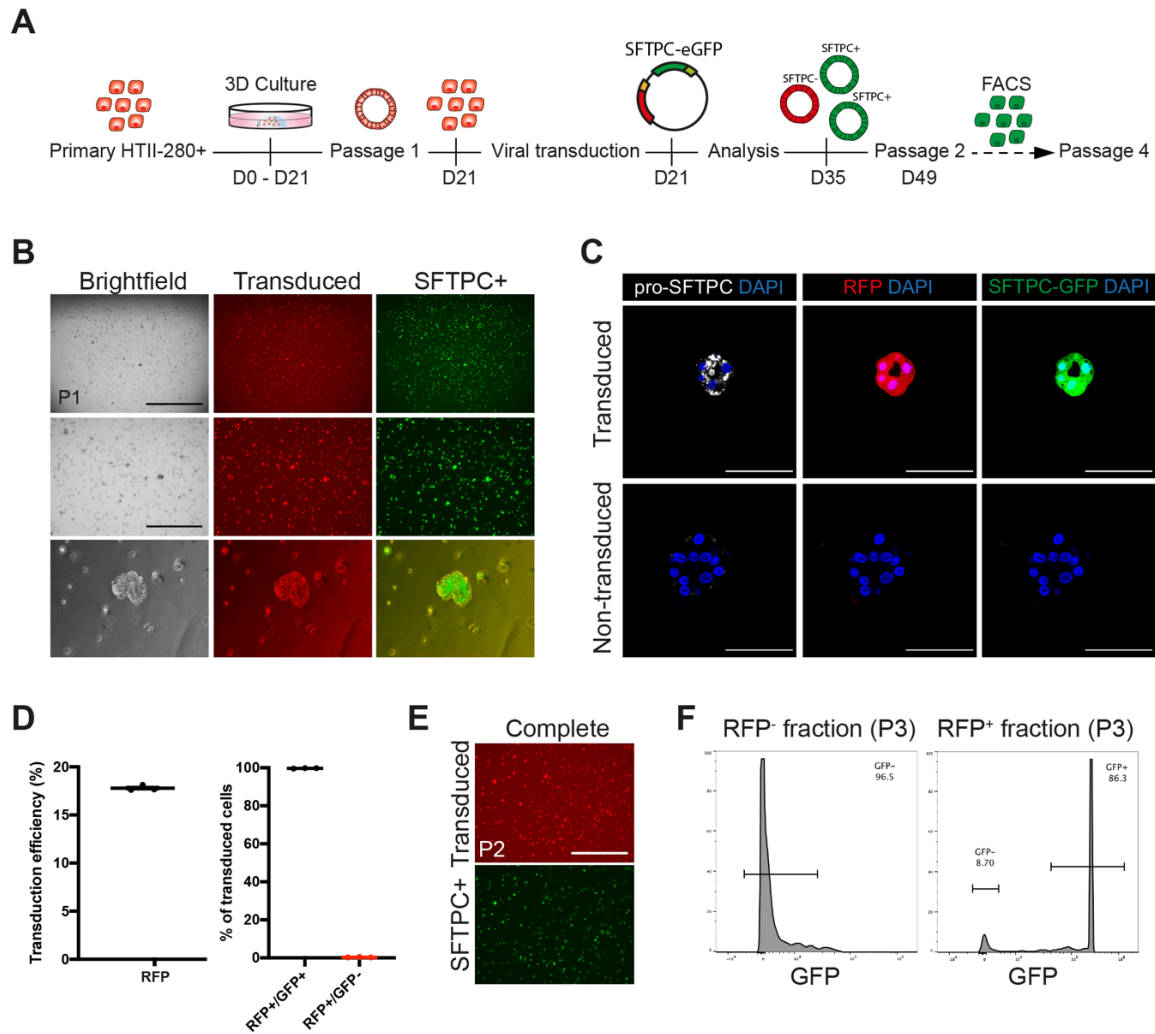


Figure 4.9. *hAT2*-derived alveolar organoids can undergo successful lentiviral transduction but exhibit limited expansion.

A. Schematic outlining the process for generating SFTPC-eGFP reporter lines in primary hAT2 cells using lentiviral transduction. **B.** Brightfield and fluorescent images of hAOs following lentiviral transduction at P1. RFP⁺ = successful transduction, GFP⁺ = SFTPC-expressing. Scale bars; 2000 μ m (top row) and 1000 μ m (middle row). **C.** IF images of transduced and non-transduced organoids. pro-SFTPC (white), successful transduction (RFP), SFTPC⁺ reporter (GFP), DAPI (blue). Scale bar, 50 μ m. **D.** Transduction efficiency and percentage of RFP⁺/GFP⁺ and RFP⁺/GFP⁻ cells achieved for 3 technical replicates (P1). Line represents the mean of the technical replicates. For transduction of P1 hAT2 cells, 100% of transduced cells expressed GFP (SFTPC). **E.** Representative IF images of SFTPC-eGFP reporter hAOs following passage (P2). Scale bar, 1000 μ m. **F.** FACS histogram of GFP expression in RFP⁻ and RFP⁺ hAO fractions at P3.

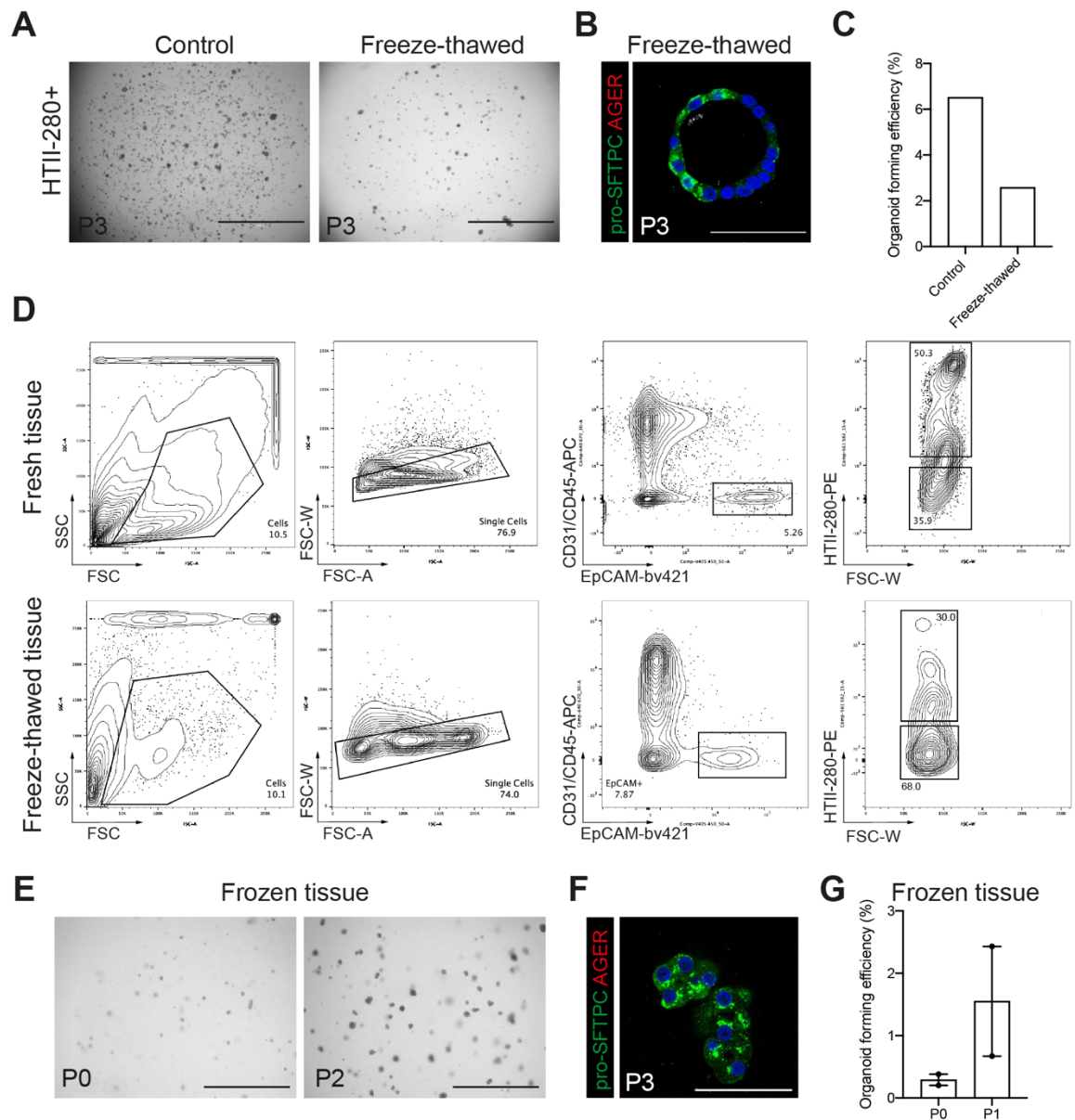


Figure 4.10. Alveolar organoids can be freeze-thawed for long-term storage and culture (figure legend continued on next page).

A. Brightfield images of HTII-280⁺ human distal lung cells following freeze-thawing in DMSO-containing freezing medium at P3, or continuous culture of the same primary cell line without freezing. Images were obtained at day 14 of culture. Scale bar, 2000 μ m. **B.** IF image of a HTII-280⁺ derived alveolar organoid following one round of freeze-thawing. pro-SFTPC (green), AGER (red), DAPI (blue). Scale bar, 50 μ m. **C.** Organoid forming efficiency of HTII-280⁺ cells following one round of freeze-thawing versus non-frozen control. Data are presented as mean for 2 technical replicates (control) and 3 technical replicates (freeze-thawed), for 1 biological sample. **D.** FACS gating strategy for the isolation of HTII-280⁺ and HTII-280⁻ cells from frozen human clinical lung specimens versus fresh tissue control. It is important to note that the featured clinical specimen was derived from a more proximal lung region, which is reflected in the lower proportion of hAT2 (HTII-280⁺) cells versus distally obtained samples. **E.** Brightfield images of HTII-280⁺ derived

organoids from frozen human lung tissue at P0 and P2. Scale bar, 1000 μm . F. IF image of a HTII-280⁺ alveolar organoid derived from frozen human lung tissue. Scale bar, 50 μm . G. Organoid forming efficiency of HTII-280⁺ cells derived from frozen human lung tissue versus non-frozen control. Data are presented as mean \pm SEM for 2 biological replicates (3 technical replicates each).

Another important aspect is whether viable hAT2 cells could be obtained from frozen human lung tissue. This would greatly improve experimental design, as procurement of fresh human lung specimens can often be challenging or sporadic. The ability to isolate viable hAT2 cells from frozen tissue would make the culture of primary hAT2 cells more accessible, allowing for reduced wastage of valuable tissue, shipment of frozen tissue, or storage of frozen samples until they are required. In order to assess viability of cells from frozen lung tissue, clinical lung specimens were divided in half upon arrival, with one half being mechanically minced and resuspended in freezing medium (FBS/10% DMSO) for freezing, while the other half was processed immediately for FACS. Cell isolation from frozen tissue was performed one week after fresh tissue. FACS analysis revealed that HTII-280⁺ cells made up the largest proportion of cells from gated CD31⁻CD45⁻EpCAM⁺ cells, as previously observed (Figure 4.10D). It is important to note that the featured clinical specimen was derived from a more proximal lung region, which was reflected in the lower proportion of hAT2 (HTII-280⁺) cells versus distally obtained samples (50% versus more than 75% in distally acquired samples). In contrast, FACS analysis of cells derived from freeze-thawed lung tissue of the same region revealed a reduction in the number of HTII-280⁺ cells, possibly suggesting reduced survivability of the hAT2 cell fraction (Figure 4.10D). Upon plating the frozen tissue-derived HTII-280⁺ cells, the ability to form hAOs was maintained, although overall organoid forming efficiency was reduced in comparison with controls (Figure 4.10E, 4.10F and 4.10G; Figure 4.3D). However, upon passaging, organoid growth was partially rescued (Figure 4.10G). hAOs derived from hAT2 cells of frozen lung tissue still maintained their ability to produce surfactant, as evidenced by the expression of pro-SFTPC (Figure 4.10F).

Finally, the utility of organoid systems as models for understanding human disease is an attractive alternative or supplement to *in vivo* animal studies, owing to their ability to more closely mimic human physiology. To this end, the ability of adult-derived hAOs to model viral infection was assessed. Covid-19, the disease caused by the virus SARS-CoV-2, can

result in respiratory distress and pneumonia, with one of the main targets of the virus being the alveoli and hAT2 cells (Carcatterra and Caruso, 2021). In collaboration with researchers from the Korea Advanced Institute of Science and Technology and the Korea Centers for Disease Control and Prevention (see also *Contributions*), adult hAOs established using my culture system were shown to express the SARS-CoV-2 viral entry factors ACE2 and TMPRSS2. Adult hAOs also demonstrated viral permissiveness, activation of endogenous immune responses, and loss of hAT2 identity, highlighting their utility in modelling human viral infection response (Youk et al., 2020).

4.4. Conclusions

Throughout this chapter, I have demonstrated how I developed and characterised a novel *in vitro* 3D-organoid platform in chemically-defined conditions from adult lung-derived, FACS-enriched HTII-280⁺ hAT2 cells. Resulting hAOs could be clonally expanded, were functionally mature and exhibited differentiation ability to hAT1 cells upon modulation of Wnt signalling or serum addition. HLA-DR was identified as an alternative marker for the isolation of hAT2 cells from both primary human lungs and established hAOs, while the possibility of generating fluorescent reporter lines through gene-editing was also assessed. Furthermore, hAOs were able to be freeze-thawed and derived from frozen primary tissue, increasing their accessibility and allowing long-term storage. Finally, assessment of hAO use in downstream applications indicated their permissiveness to viral infection. As previously mentioned, my established hAO system has been used to study SARS-CoV-2 infection (Youk et al., 2020). In conclusion, these data suggest the usefulness of adult-derived hAO cultures in assessing the effects of molecular pathways and disease on hAT2 stem cell maintenance and differentiation.

CHAPTER 5A

Results IIIA: Establishment and characterisation of epithelial lung organoids from patients with Idiopathic pulmonary fibrosis (IPF)

5A.1. Introduction

Idiopathic pulmonary fibrosis (IPF) is a devastating disease that causes irreversible damage to the gas-exchanging alveoli. Characteristic hallmarks of IPF include the presence of usual interstitial pneumonia (UIP), increased deposition of collagen and extracellular matrix (ECM), architectural remodelling and clusters of fibroblasts and myofibroblasts arranged in fibroblastic foci (Barratt et al., 2018). Currently, only two approved treatments exist for treating IPF, and neither are effective in halting or reversing disease progression (Lancaster et al., 2019; Margaritopoulos et al., 2016; Ryerson et al., 2019). Recent studies have suggested that the disease may arise through dysregulation of the alveolar type 2 (hAT2) population (Lawson et al., 2004; Nureki et al., 2018; Parimon et al., 2020). However, there are currently no suitable human-specific IPF lung models and fibrotic mouse models fail to fully recapitulate all aspects of the disease (Tashiro et al., 2017). A lack of relevant models has hindered attempts in furthering the understanding of IPF initiation and progression, making development of new therapeutic drugs challenging. Therefore, establishment of a human-specific IPF disease model would be advantageous. In this chapter, I will assess differences in the characteristics, molecular requirements and growth ability of epithelial cells from IPF patient lungs and compare these with healthy alveolar

and airway controls. In order to achieve this, I will employ my organoid system established in Chapter 3 and Chapter 4.

5A.2. Aims

- Characterise epithelial cell composition of distal lung parenchyma from human IPF patients.
- Establish and characterise distal epithelial lung organoids from IPF patient lungs.
- Compare IPF-derived lung organoids with airway organoids and hAOs from healthy donor lungs in terms of cellular composition, self-renewal and long-term maintenance.

5A.3. Results

5A.3.1. *Characterisation of the distal lung of adult IPF patients*

I first aimed to examine how the lung architecture of human IPF lungs differed to the lungs of healthy donors. Concentrating on the distal lung region, analysis of H&E staining derived from multiple human IPF lungs suggested the inter- and intra-heterogeneity of the pathologic phenotypes in the lungs. An assortment of micro-architectures were present, including relatively unaffected distal airways, dysregulated alveoli with thickened interstitium, regions of immune infiltrates, fibroblastic foci and epithelial honeycombing (Table 5.1, Figure 5.1A). IF analysis of alveolar structures revealed the presence of hAT2 cells expressing pro-SFTPC (Figure 5.1B). Expression of the hAT1 marker PDPN was limited, indicating that these cell types were likely already damaged or lost from the alveolar epithelium (Figure 5.1B). This was in stark contrast to healthy background lungs, which stained extensively for PDPN (Figure 3.1B). Many alveolar regions of IPF lungs displayed extensive HTII-280 staining along the epithelium, an observation that has previously been made in damaged human lungs (Figure 5.1B; Figure 3.1B; Gonzalez et al., 2010). Some of these HTII-280⁺ cells expressed pro-SFTPC, but many did not (Figure 5.1B and 5.1C). In contrast to alveoli, IPF distal airways appeared relatively unaffected, with TP63⁺ basal cells still localised to the base of the pseudostratified airway epithelium. SOX2⁺ cells were also present throughout the airway epithelium, although some regions appeared to possess higher quantities of the secretory club cell protein SCGB1A1, an

observation that has been made previously (Xu et al., 2016). Importantly, no alveolar markers, including HOPX and ABCA3, were present in distal IPF airways (Figure 5.1B).

A hallmark feature of human IPF lungs is the presence of epithelial ‘honeycombing’ as a result of active tissue remodelling (Barratt et al., 2018). These epithelial honeycombs were present throughout all IPF lungs analysed. Therefore, I next aimed to identify the cell types within these regions. IF staining revealed that the cellular architecture of these honeycomb regions was diverse, with a host of lung lineage markers expressed throughout the structures (Figure 5.1C). Due to the distal location, a number of cells expressed pro-SFTPC. However, a number of TP63⁺ cells were observed within close proximity to hAT2 marker-expressing cells, a phenomenon that does not occur within healthy lungs (Figure 5.1C.i and Figure 5.1C.i’; Figure 3.1B and 3.1D). Interestingly, some epithelial cells within honeycomb regions co-expressed markers of both hAT2 and airway lineages, as evidenced by co-expression of pro-SFTPC and HTII-280 with the airway-related transcription factor SOX2 (Figure 5.1C.ii, Figure 5.1C.ii’, Figure 5.1C.iii and Figure 5.1C.iii’). HTII-280 marked the apical epithelial layer of honeycomb regions and was often co-expressed with KRT17, another marker that has been shown to be expressed in airway basal cells of healthy human lungs (Figure 5.1C.iv and Figure 5.1C.iv’; Figure 3.1D). Apart from epithelial honeycombs, smaller hAT2-containing cysts were also observed; these expressed pro-SFTPC, HTII-280, ABCA3 and occasionally TP63, but not SOX2 (Figure 5.1C.v, Figure 5.1C.vi and Figure 5.1C.vii). Additional cysts were also found and expressed SOX2 and HTII-280, but not ABCA3 (Figure 5.1C.viii). As previously reported, these data showed the aberrant epithelial cells or states in lung tissues of IPF patients. Some of these epithelial cells co-expressed both alveolar and airway-related markers within disease-associated ‘honeycomb’ regions, indicating aberrant differentiation. In contrast, no aberrant cell types were observed in the lungs of healthy controls (Figure 3.1).

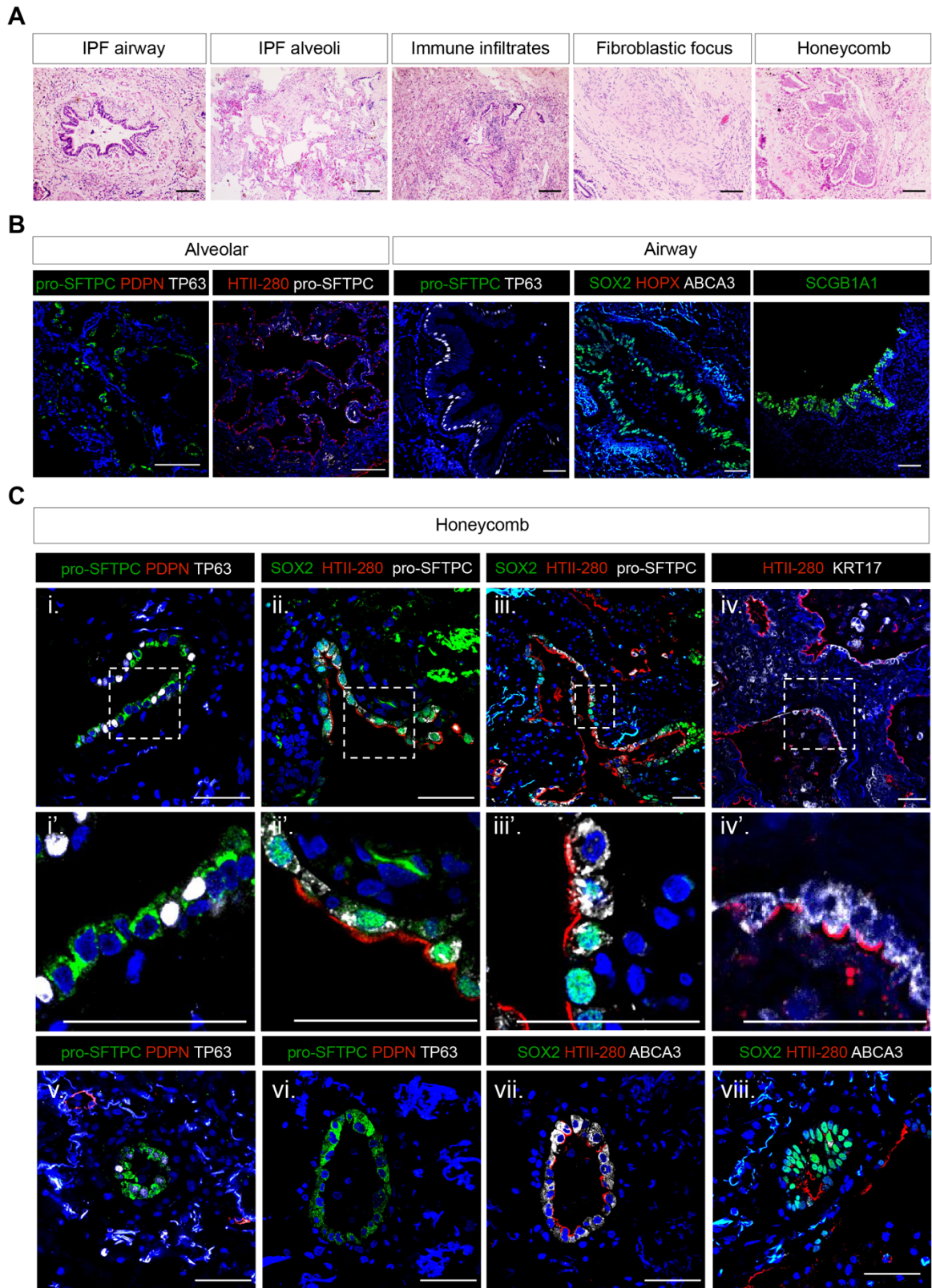


Figure 5.1. Human IPF lungs are characterised by honeycomb structures containing abnormal airway-like cells in the distal region of the lung (figure legend on next page).

Figure 5.1. Human IPF lungs are characterised by honeycomb structures containing abnormal airway-like cells in the distal region of the lung.

A. Representative H&E images of regions and microstructures observed in human end-stage IPF lungs. Scale bars, 100 μ m. B. IF staining of alveolar and airway regions of IPF lungs, showing markers for the following cell types (from left to right); hAT2 (pro-SFTPC, green), hAT1 (PDPN, red), basal (TP63, white); hAT2 (HTII-280, red), pro-SFTPC (white); hAT2 (pro-SFTPC, green), basal (TP63, white); airway (SOX2, green), hAT1 (HOPX, red), hAT2 (ABCA3, white); secretory club (SCGB1A1, green). Scale bar; 100 μ m. C. IF staining of honeycomb lesions. i and i', hAT2 (pro-SFTPC, green), hAT1 (PDPN, red), basal (TP63, white); ii, ii', iii and iii', airway (SOX2, green), hAT2 (HTII-280, red), hAT2 (pro-SFTPC, white); iv and iv', hAT2 (HTII-280, red), basal (KRT17, white). Middle row images (i', ii', iii' and iv') are increased magnifications of boxed regions of panels in the top row. Bottom row (v, vi, vii and viii); cysts containing hyperplastic hAT2 cells. v and vi, hAT2 (pro-SFTPC, green), AT1 (PDPN, red), basal (TP63, white); vii and viii, airway (SOX2, green), AT2 (HTII-280, red), hAT2 (ABCA3, white). Scale bars; 100 μ m (top and bottom panels), 50 μ m (middle panels). All featured images are representative of 5 individual patient lungs.

Table 5.1. Patient samples utilised for characterisation of IPF tissue and organoids.

Patient number	Age	Sex	Procedure and diagnosis	Background lung disease	Smoking history
IPF 1	68	M	Single right lung transplant	IPF	No
IPF 2	57	M	Single left lung transplant	IPF	Yes (past)
IPF 3	67	M	Lung transplant	IPF and emphysema	Yes (past)
IPF 4	66	M	Single left lung transplant	IPF	Yes (past)
IPF 5	56	M	Single left lung transplant	IPF	No
IPF 6	64	M	Lung transplant	IPF	Yes (past)

5A.3.2. Characterisation of isolated EpCAM⁺ IPF-derived lung cells

Following characterisation of the cellular composition of distal IPF lungs, I next sought to analyse cellular behaviours of epithelial cells isolated from IPF lung tissues. hAOs and airway organoids derived from healthy adult lungs were used as controls. IPF tissues obtained from distal lung regions of patients undergoing lung transplant were mechanically and enzymatically dissociated to single cells, as performed previously for healthy tissue (Figure 5.2A to 5.2E). Of note, IPF tissue was generally stiffer and much more fibrous than healthy donor tissue, as was expected due to the fibrotic nature of IPF (Figure 5.2A and

5.2B; Figure 3.2A). As a result of the increased fibrosis, one-hour enzymatic digestion was not sufficient to properly dissociate the tissue, and some fibrotic tissue was still present even following 2-hours of digestion (Figure 5.2C to 5.2E). After 2-hour digestion, cells were subjected to FACS-isolation, and epithelial cells selected based on their CD31⁻CD45⁻EpCAM⁺ profile (Figure 5.3A). The proportion of EpCAM⁺ cells in processed IPF lungs was increased versus healthy lungs (30% versus 15%), likely due to the reduced efficiency of tissue digestion resulting in fewer stromal cell populations present upon FACS analysis (Figure 5.3A; Figure 3.6A). As with healthy control lungs, EpCAM⁺ IPF cells were then isolated based on their HTII-280 expression (Figure 5.3A). I found that the number of EpCAM⁺HTII-280⁺ cells were dramatically reduced in IPF lungs, a finding that was consistent across all IPF lung samples analysed (N=6) and has also been observed in other studies (Figure 5.3A; Figure 4.6A; Xu et al., 2016). This result was likely due to the overall reduction in hAT2 cells in IPF lungs, and the increase in cells of other lineages. Due to the observation that HTII-280-expression in IPF lungs did not exclusively mark hAT2 cells, but instead could also be found on aberrant epithelial cells that co-express both alveolar and airway lineages, the question arose as to whether isolated cells reflected this finding. Therefore, I performed qPCR analysis on both IPF and healthy HTII-280⁺ and HTII-280⁻ epithelial cells to assess the expressions of lung lineage markers. As shown previously, healthy HTII-280⁺ cells were enriched for hAT2 cells, expressing markers such as *SFTPC* and *ABCA3*. In contrast, primary HTII-280⁻ cells from healthy lungs expressed a heterogeneous mix of cell-lineage markers, including airway markers such as *SOX2* and *TP63* (Figure 5.3B; Figure 3.6B). Similar to healthy controls, IPF-derived HTII-280⁺ cells maintained expression of the hAT2 markers *SFTPC* and *ABCA3*, with comparable levels to control samples. However, as was observed in the tissue, HTII-280⁺ IPF cells expressed increased levels of both *SOX2* and *TP63* versus healthy controls. Interestingly, *HOPX* was also increased in IPF-derived HTII-280⁺ cells in comparison with controls. In contrast, transcriptional levels of multiple lung lineage genes in HTII-280⁻ cells were similar between IPF and healthy lungs. Unexpectedly, *TP63* levels were higher in IPF-derived HTII-280⁺ cells than HTII-280⁻ cells of both IPF and donor lungs (Figure 5.3B). This may be due to increased levels of heterogeneity in the HTII-280⁻ population of both healthy and IPF lungs, which are thought to contain multiple cell types including basal, secretory and hAT1 cells (Figure 3.6B). Together, these data suggest that IPF distal lungs retain diverse epithelial cells or states compared to the healthy donor lungs, with IPF-derived HTII-280⁺ epithelial cells in particular comprising increased variation in their cell types or states.

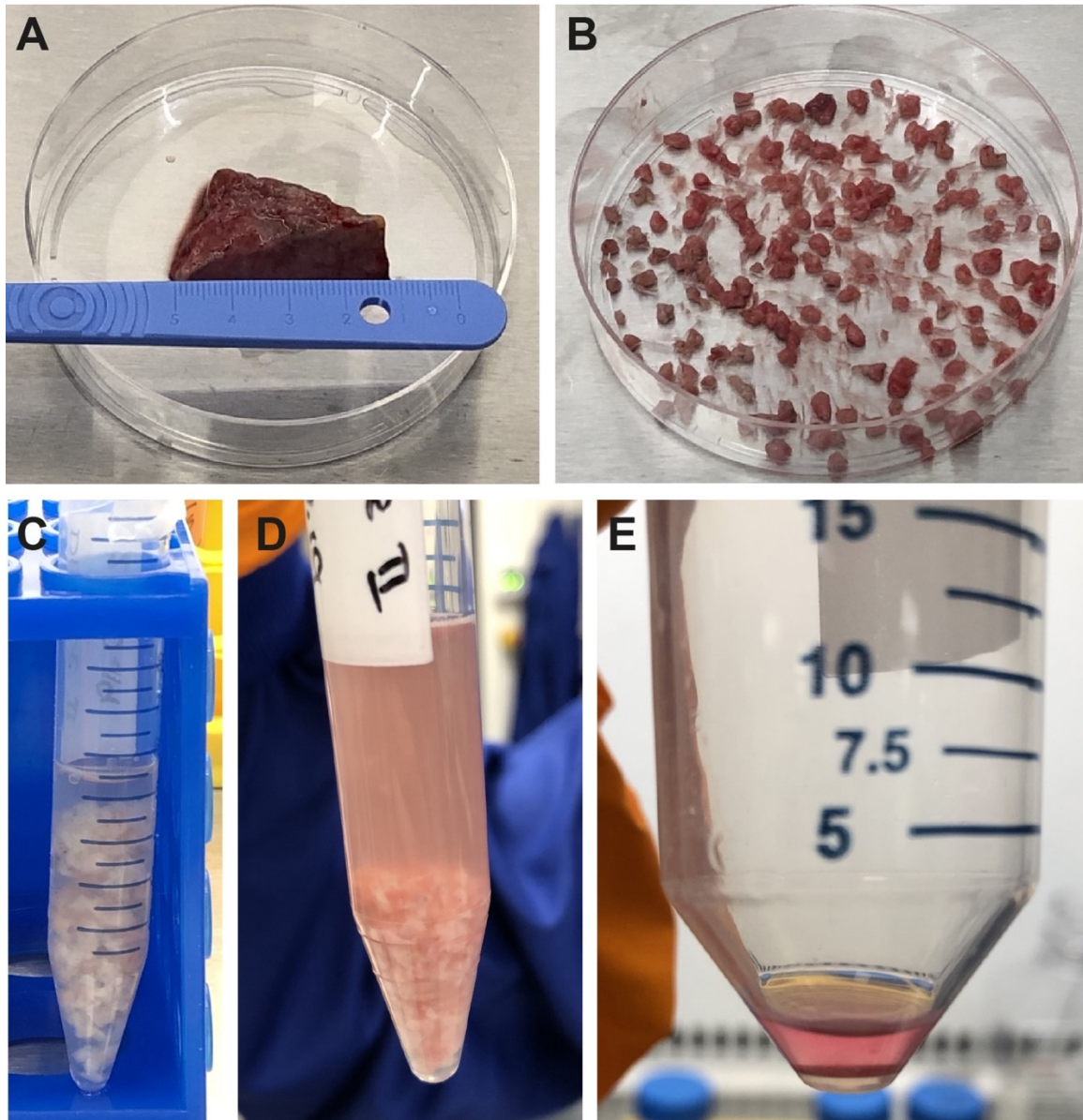


Figure 5.2. Tissue dissociation method for deriving cells from human IPF distal lung samples.

A. Representative image of clinical lung specimen derived from human IPF lung. **B.** Representative image of tissue pieces following mechanical dissociation with a scalpel. **C.** Tissue debris following 1-hour enzymatic digestion. Note the increased fibrous nature of IPF lung tissue versus healthy lung tissue **D.** Digested cellular supernatant following 2-hour enzymatic digestion. Some indigestible tissue still remained. **E.** Cell pellet following filtration of digested tissue through a 100 μm cell strainer and centrifugation.

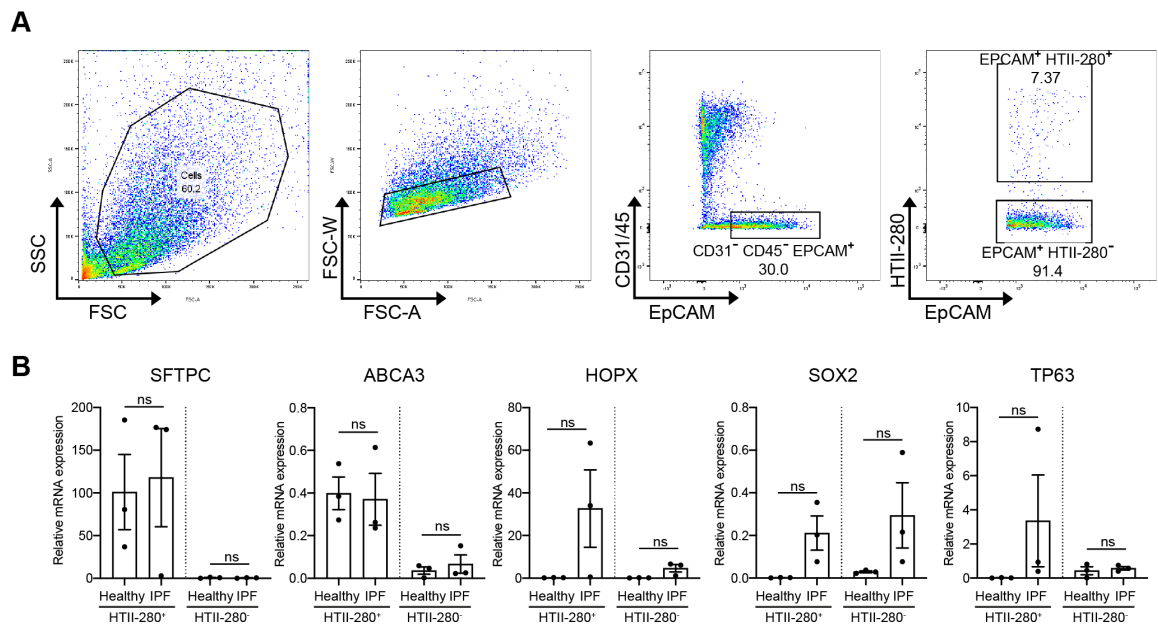


Figure 5.3. The number of HTII-280⁺ cells is dramatically reduced in IPF lungs.

A. Representative FACS plot for the isolation of CD31⁻ CD45⁻ EpCAM⁺ HTII-280⁺ and CD31⁻ CD45⁻ EpCAM⁺ HTII-280⁻ cells derived from human IPF lung tissue. FACS plots are representative of 3 individual patient samples. **B.** Analysis of mRNA expression levels for the genes *SFTPC*, *ABCA3*, *HOPX*, *SOX2* and *TP63* in healthy and IPF-derived HTII-280⁺ and HTII-280⁻ cells. Data are the mean ± SEM of 3 biological replicates, and are expressed as relative mRNA expression versus the housekeeping gene *GAPDH*. Statistical significance was tested using the non-parametric Mann-Whitney U test; ns = non-significant.

5A.3.3. Establishment and characterisation of epithelial organoids derived from human IPF lungs

I next aimed to place these cells into 3D-culture in order to assess their growth capacity and differentiation potential versus healthy control organoids. To make appropriate comparisons between individual cultures, and due to the presence of diverse cell types/states in IPF HTII-280⁺ cells, I tested three separate media conditions that could support either the growth of hAOs or airway organoids; complete medium, -CHIR medium and -CHIR/+SB2 medium (Table 3.1). Primary FACS-isolated HTII-280⁺ and HTII-280⁻ cells from IPF lungs were plated at a density of 5000 cells per well, and cultured in Matrigel for 14 days in one of the three media conditions. Analysis of cultured HTII-280⁺ cells revealed the formation of organoids in all three tested conditions, although the organoid forming efficiency varied between patient samples, particularly for complete medium,

which failed to produce organoids from some patient samples (Figure 5.4A and 5.4B; Table 2.2). This was likely due to the high disease heterogeneity present between IPF patients. However, a consistent finding was that the largest and most numerous organoids were established in -CHIR medium, an observation that is also made upon culture of healthy airway cells (Figure 5.4A). This was in stark contrast to healthy HTII-280⁺ cultures, which consistently formed organoids only in the presence of CHIR (complete medium) owing to the enrichment of Wnt-dependent hAT2 cells (Figure 5.4B). Despite successful organoid formation from HTII-280⁺ IPF cells, the overall organoid forming efficiency was generally low, perhaps reflecting a reduction in IPF cell self-renewal capacity or viability. Culture of IPF-derived HTII-280⁻ cells yielded a similar observation to HTII-280⁺ IPF cells, where organoids again formed under all three tested conditions, and the largest and most numerous structures arose in -CHIR medium (Figure 5.4C and 5.4D). In contrast to IPF HTII-280⁻ cells, healthy HTII-280⁻ cells consistently did not yield organoids in complete medium (Figure 5.4D; Figure 3.7B). Representative H&E images from both HTII-280⁺ and HTII-280⁻ IPF cells suggested the unusual organoid morphologies that arose from both cell populations (Figure 5.4E). The majority of IPF-derived organoids throughout all tested conditions displayed structures more similar to healthy airway organoids, either being large and filled or cystic with a single lumen (Figure 5.4E). However, a number of organoids existed in both complete and -CHIR conditions that possessed multiple lumen (Figure 5.4E). Very few organoids were observed as having the folded morphology I have described previously for healthy hAOs (Figure 5.4E).

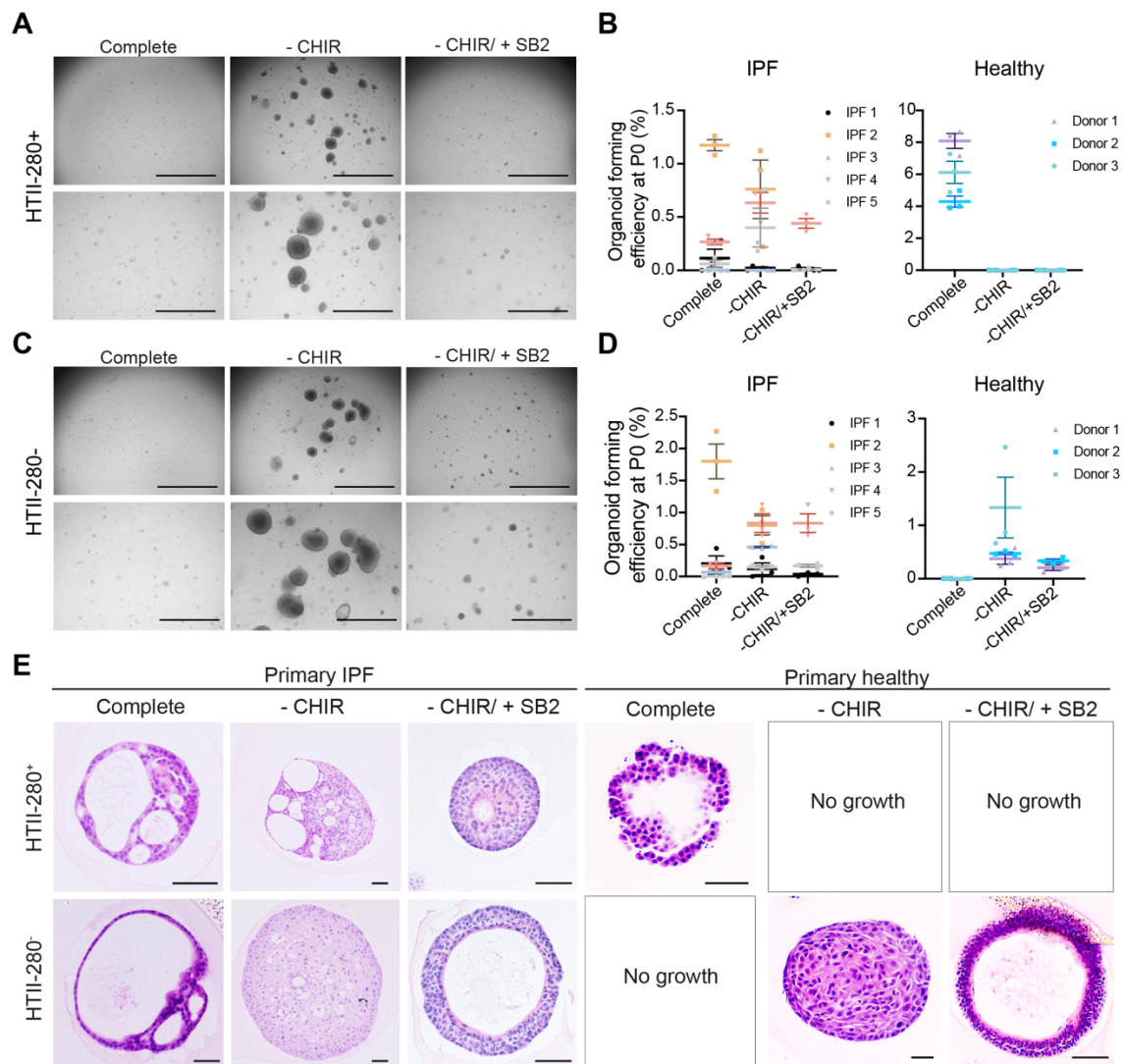


Figure 5.4. IPF-derived epithelial cells exhibit growth in low Wnt conditions and form organoids with unusual morphologies.

A. Brightfield images of primary IPF-derived HTII-280⁺ cells grown under 3 conditions; complete, -CHIR and -CHIR/+SB2. Scale bars; 2000 μ m (top row), 1000 μ m (bottom row). Images obtained at day (D)14. **B.** Organoid forming efficiency at passage 0 (P0, D14) for IPF and healthy donor-derived HTII-280⁺ cells cultured in 3 separate conditions. A single line represents the mean of 3 technical replicates for each individual donor. Data are presented as mean \pm SEM of 3 technical replicates for 5 separate biological replicates (IPF) or 3 biological replicates (healthy). **C.** Brightfield images of primary IPF-derived HTII-280⁻ cells grown under 3 separate conditions. Scale bars; 2000 μ m (top row), 1000 μ m (bottom row). Images obtained at D14. **D.** Organoid forming efficiency at P0 (D14) for IPF and healthy donor-derived HTII-280⁻ cells cultured in three separate conditions. A single line represents the mean of 3 technical replicates for each individual donor. Data are presented as mean \pm SEM of 3 technical replicates for 5 separate biological replicates (IPF) or 3 biological replicates (healthy). **E.** Representative H&E images of primary HTII-280⁺ and HTII-280⁻ organoids derived from IPF or healthy lungs (Chapter 3) and cultured under 3 separate conditions. Images were obtained following formaldehyde-fixation at D21 of primary culture. Scale bars, 50 μ m.

I next assessed the cellular composition of IPF organoids cultured under the three tested conditions. IF analysis of primary IPF organoids at D21 suggested that the majority of organoids throughout all conditions comprised cells expressing airway markers, including TP63, KRT5, SOX2 and SCGB1A1 (Figure 5.5A). Unlike healthy controls, where primary airway organoids only formed from HTII-280⁻ cells, airway organoids were present in cultures derived from both HTII-280⁺ and HTII-280⁻ populations obtained from IPF lungs (Figure 5.5A; Chapter 3). Out of five patient-derived organoid lines, hAOs were only observed in one line, and were present upon culture of both HTII-280⁺ or HTII-280⁻ cells in complete medium (Figure 5.5A). However, their frequency was dramatically low, with the majority of organoids possessing airway identity. These data suggest that in the majority of IPF lung tissues derived from patients with end-stage disease, the number of viable hAT2 cells that retain their ability for self-renewal *in vitro* is low. Furthermore, HTII-280 marks epithelial IPF cells with airway phenotypes that can be expanded as airway organoids *in vitro*, a finding that recapitulates observations in patient-derived IPF tissue.

Analysis of qPCR data for alveolar and airway related genes in primary IPF organoids from HTII-280⁺ cells confirmed the high levels of *TP63* versus controls, again demonstrating enrichment for basal-like cells (Figure 5.5B). HTII-280⁻ IPF-derived organoids expressed low levels of *SFTPC*, which was also observed in healthy HTII-280⁻ derived organoids. In contrast, the levels of *SFTPC* transcription in IPF-derived HTII-280⁺ organoids cultured in complete medium were comparable to healthy controls, highlighting an apparent discrepancy between transcriptional and protein levels, as very few pro-SFTPC-containing organoids were observed in culture (Figure 5.5A, 5.5B and 5.5C). IPF-derived HTII-280⁺ cells cultured in -CHIR and -CHIR/+SB2 medium also expressed higher transcriptional levels of *SFTPC* than HTII-280⁻ IPF and healthy control cells. This finding was not observed during IF analysis. Thus, these data suggested the possibility that a proportion of HTII-280⁺ cells from IPF lungs maintained the capacity for transcription of surfactant-related proteins such as SFTPC, but there may be an issue with downstream processing which resulted in a reduction or loss of protein. Upon passage to single cells without further sorting, IPF organoids from both HTII-280 lineages were able to reform organoids in all three media conditions. Passaged organoids contained cells of airway lineages, which persisted throughout subsequent culture (Figure 5.5D, 5.5E and 5.5F). No hAOs or alveolar cell types were observed within any patient-derived cultures from P1 onwards.

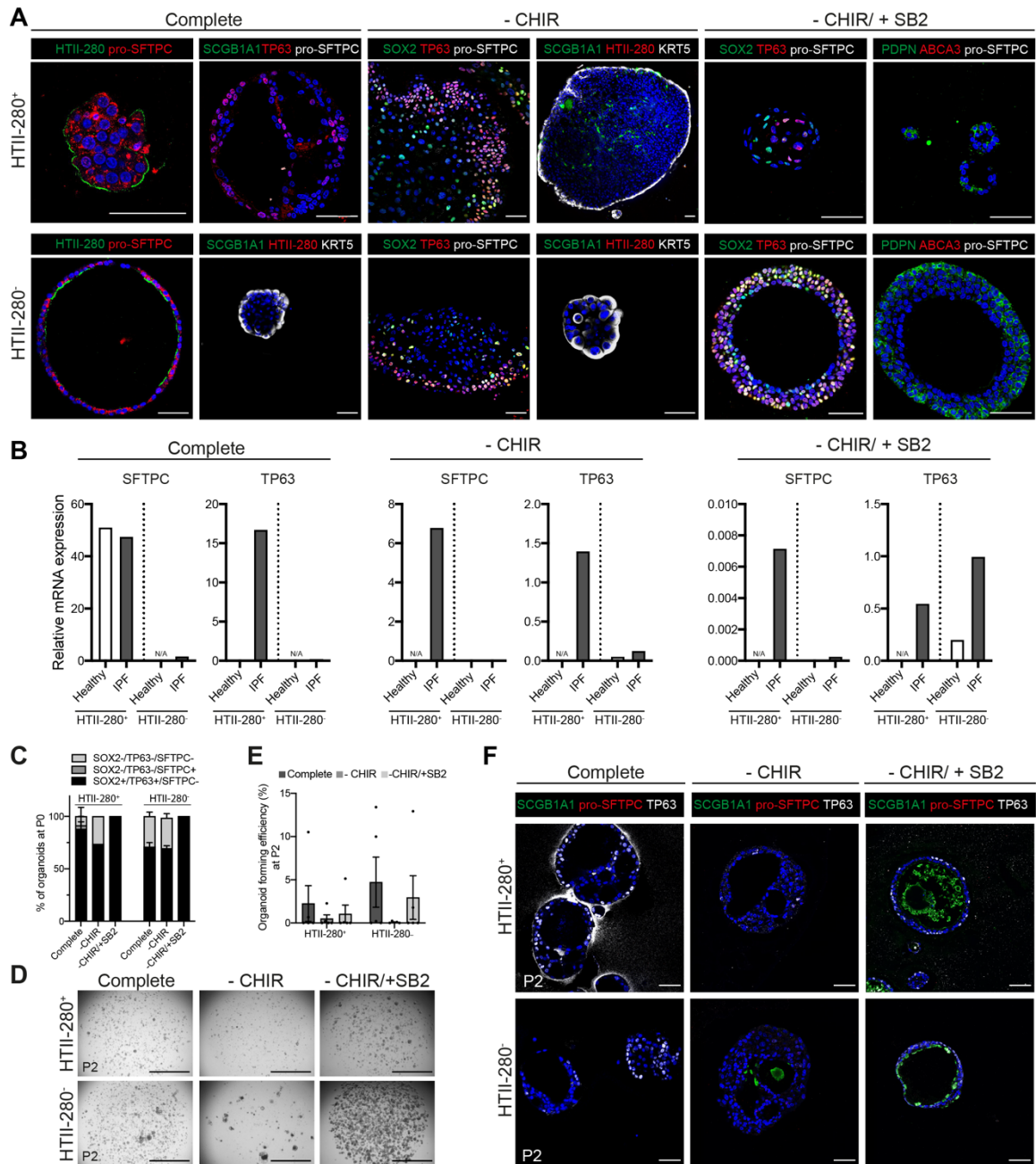


Figure 5.5. IPF-derived HTII-280⁺ and HTII-280⁻ cells form organoids comprising airway cell types which persist upon passage (figure legend continued on next page).

A. IF images of primary (P0) organoids derived from HTII-280⁺ and HTII-280⁻ IPF cells under 3 separate culture conditions; complete, -CHIR and -CHIR/+SB2. HTII-280 (green), pro-SFTPC (red), SCGB1A1 (green), TP63 (red), pro-SFTPC (white), KRT5 (white), SOX2 (green), PDPN (green), ABCA3 (red), DAPI (blue). Scale bars, 50 μ m. **B.** Analysis of mRNA expression levels for the genes *SFTPC* and *TP63* in primary healthy and IPF HTII-280⁺ and HTII-280⁻-derived organoids relative to the housekeeping gene *RPL13A*. Data are the mean of 2 technical replicates for 1 biological replicate, and are expressed as relative mRNA expression versus the housekeeping gene *GAPDH*. N/A = organoids could not be assessed in highlighted medium due to lack of growth. **C.** Quantification of IF data from primary IPF-derived organoids. Data are

presented as mean \pm SEM of 2 biological replicates, except for HTII-280⁺ (-CHIR and -CHIR/+SB2) and HTII-280⁻ (-CHIR/+SB2), which are derived from 1 biological replicate. **D.** Brightfield images of IPF-derived HTII-280⁺ and HTII-280⁻ cell-derived organoids at P2. Images were obtained at D14. Scale bars, 2000 μ m. **E.** Organoid forming efficiency of HTII-280⁺ and HTII-280⁻ derived IPF organoids at P2. Data are presented as mean \pm SEM of 5 biological replicates. **F.** IF images of HTII-280⁺ and HTII-280⁻ derived IPF organoids at P2. SCGB1A1 (green), pro-SFTPC (red), TP63 (white), DAPI (blue). Scale bars; 50 μ m.

To further assess SFTPC-levels in IPF-derived organoids, I inserted a SFTPC-eGFP reporter plasmid into P1 HTII-280⁺ IPF organoids following lentiviral transduction (Figure 5.6A; Lim et al., 2020). Patient-derived IPF organoids could undergo gene-editing, as evidenced by RFP-expression in organoids at 14-days post-transduction. However, overall transduction efficiency was reduced versus healthy HTII-280⁺ cells, and the number of transduced cells expressing *SFTPC-eGFP* was also reduced (Figure 5.6A to 5.6C; Figure 4.10). The majority of RFP⁺ transduced cells were SFTPC⁻, confirming the low number of *SFTPC*-expressing cells present in IPF HTII-280⁺ cells (Figure 5.6B and 5.6C). IF and FACS analysis further confirmed the lack of *SFTPC*-expressing cells (Figure 5.6D and 5.6E).

5A.4. Conclusions

In this chapter, I investigated differences in the cellular architecture of human IPF patient lungs versus healthy donor lungs, and established organoids derived from IPF patient tissues. IF analysis showed that, in contrast to healthy lungs, distal human IPF lung tissue comprised a diverse array of tissue microarchitectures as a result of active tissue remodelling. These observations included dysregulated alveoli with thickened alveolar interstitial walls, mass inflammation, accumulation of fibroblast populations arranged in ‘fibroblast foci’ and epithelial honeycombing. Analysis of epithelial populations, particularly within epithelial honeycombs, revealed the presence of cells that possessed aberrant differentiation by expressing both alveolar- and airway-related markers, including pro-SFTPC, HTII-280 and SOX2. FACS-enrichment of epithelial populations from IPF lungs revealed a substantial reduction in the total number of HTII-280⁺ epithelial cells. IPF-derived HTII-280⁺ cells expressed both alveolar and airway markers, including *SFTPC*, *ABCA3*, *TP63* and *SOX2*, confirming *in vivo* observations of protein presence. Culture of

IPF-derived cells under conditions that were previously shown to support the growth of alveolar or airway cells from healthy lungs revealed an absence of alveolar cell types and an abundance of airway organoids.

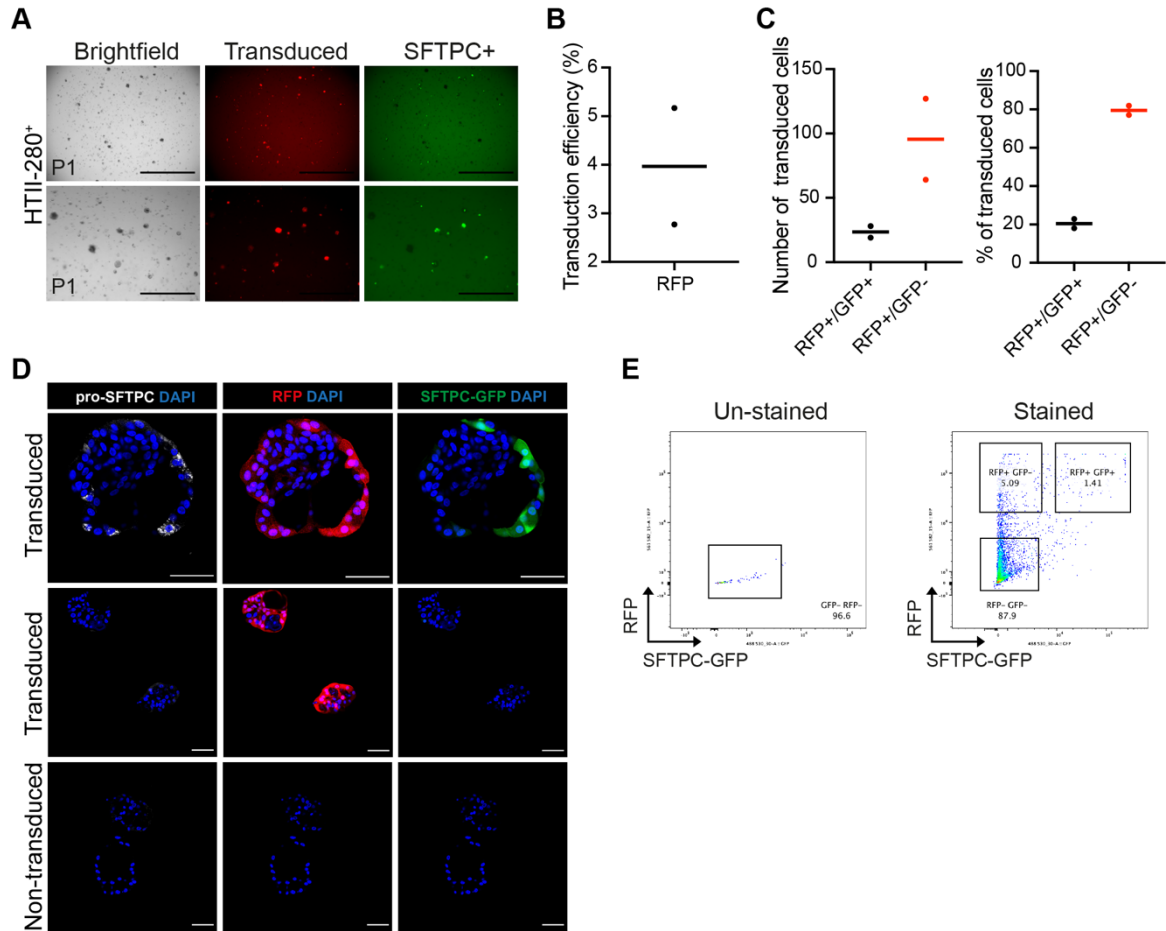


Figure 5.6. Lentiviral transduction of IPF-derived HTII-280⁺ cells with SFTPC-GFP reporter highlights low number of SFTPC-expressing hAT2 cells in culture.

A. Brightfield and fluorescent images of IPF-derived HTII-280⁺ organoids following lentiviral transduction with a SFTPC-eGFP reporter at passage 1 (P1). Scale bars; 2000 μ m (top row), 1000 μ m (bottom row). **B.** Transduction efficiency of HTII-280⁺ IPF organoids. Data are presented as mean (line) of 2 technical replicates (dots), expressed as a percentage. **C.** Total number and total percentage of RFP⁺/GFP⁺ and RFP⁺/GFP⁻ following lentiviral transduction. **D.** IF images of transduced and non-transduced organoids. pro-SFTPC (white), successful transduction (RFP), SFTPC⁺ reporter (GFP), DAPI (blue). Images obtained following formaldehyde fixation at D21 (P1). Scale bar, 50 μ m. **E.** FACS analysis of transduced IPF HTII-280⁺ cells at P2.

CHAPTER 5B

Results IIIB: Investigating the role of hypoxia in the appearance of aberrant epithelial cells in human Idiopathic pulmonary fibrosis (IPF)

5B.1. Introduction

I found aberrant epithelial cells that co-express both alveolar and airway lineage markers in the lung tissues of IPF patients, similar to what has been reported previously (Adams et al., 2020; Habermann et al., 2020; Xu et al., 2016). However, little is known in regard to how they arise within distal IPF lungs. It has been suggested that HIF1 α -mediated hypoxia is involved in both the development and progression of IPF, although studies have mainly involved the investigation of hypoxia effects on fibroblast populations and not on epithelial cell types such as hAT2 cells (Aquino-Gálvez et al., 2019; Senavirathna et al., 2018). Recently, we identified the distinct population of damage-associated transient progenitors (DATPs) that derive from AT2 cells and emerge during regeneration after alveolar injury in mouse lungs (Choi et al., 2020). A HIF1 α -mediated pathway was found to regulate DATP behaviours during this differentiation process. Importantly, we discovered aberrant accumulation of DATP-like cells in IPF patient tissues, suggesting their implication in IPF progression. Given the similar gene expression signatures in our DATPs and basaloid cell populations in IPF lungs (Adams et al., 2020; Choi et al., 2020; Habermann et al., 2020; Kobayashi et al., 2020), I hypothesise that HIF1 α -mediated hypoxia may be involved in the appearance of aberrant IPF epithelial cell populations in the distal lung parenchyma that

express airway-related transcripts. In this chapter, I will investigate the effect of IPF-related hypoxia conditions on hAT2 cells from healthy donor lungs in order to assess their possible role as an origin cell for aberrant IPF epithelial cells *in vitro*.

5B.2. Aims

- Investigate the effect of HIF1 α -mediated hypoxia on hAT2 cells derived from healthy tissue, as increased hypoxia is common in late-stage IPF lungs.
- Assess potential downstream signalling pathway responsible for findings in hAT2 cells under hypoxic conditions.
- Elucidate potential mechanism and cellular origin for the appearance of aberrant epithelial cell types in IPF lungs.

5B.3. Results

5B.3.1. *Up-regulation of hypoxia-related genes in human IPF lungs*

To investigate the possible effect of hypoxia on the hAT2 cell population, I first examined the level of hypoxia in human IPF lungs. qPCR analysis revealed increased levels of the HIF1 α -regulated gene *SLC2A1* (Glucose Transporter 1; GLUT1) in IPF-derived HTII-280⁺ cells compared to controls (Figure 5.7A). Furthermore, analysis of published data from the IPF cell atlas showed an increase in *HIF1 α* levels in IPF lungs versus donor lungs across many cell types, including hAT2 cells and aberrant basaloid cells (Adams et al., 2020; Habermann et al., 2020; Neumark et al., 2020). These data led me to first ask how increased hypoxia signalling, through the stabilisation and accumulation of HIF1 α , affects the hAT2 cell population.

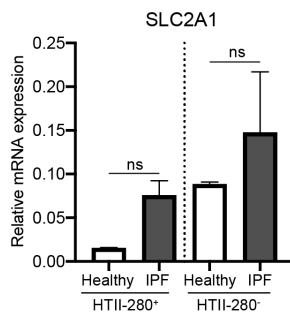
A

Figure 5.7. Levels of hypoxia are increased in IPF epithelial cells versus healthy controls.

A. Relative mRNA expression levels of the downstream hypoxia gene *SLC2A1* in primary tissue-derived HTII-280⁺ and HTII-280⁻ cells from IPF lungs or healthy controls. Data are presented as the mean \pm SEM of 3 biological replicates, and are expressed as the relative mRNA expression versus the housekeeping gene *GAPDH*. Statistical significance was tested

using the non-parametric Mann-Whitney U test; ns = non-significant.

5B.3.2. Chemical induction of HIF1 α -mediated hypoxia results in SOX2 expression in hAT2-derived organoids

To assess the effect of hypoxia on the cellular behaviours and identity of hAT2 cells *in vitro*, I first aimed to modulate the oxygen levels in the culture environment. To optimise the culture system, I utilised primary HTII-280⁻ cells isolated from a normal lung background donor. I placed these cells in culture in -CHIR medium as usual, and allowed them to form airway organoids over 7 days. On day 7, I removed one plate of organoids and placed these in an incubator that had been pre-set to 5% oxygen, and cultured these for a further 8 days. At day 15, brightfield images revealed no major differences between organoid morphology or growth capacity between cells cultured in atmospheric oxygen or 5% oxygen (Figure 5.8A). Furthermore, quantification of gene expression levels for the downstream hypoxia gene *SLC2A1* indicated no increase in expression levels in cells cultured in 5% oxygen versus control cells (~21% oxygen; Figure 5.8B). These data suggested that culturing cells in a regular incubator set to 5% oxygen was not sufficient in activating hypoxia *in vitro* in this study. This could be due to a number of reasons, including rapid influx of atmospheric oxygen upon opening the tissue culture incubator and presence of normal oxygen levels upon media changes. Both of these scenarios would potentially lead to improper maintenance of 5% oxygen levels. Therefore, I next aimed to investigate an alternative approach to induce hypoxia *in vitro*.

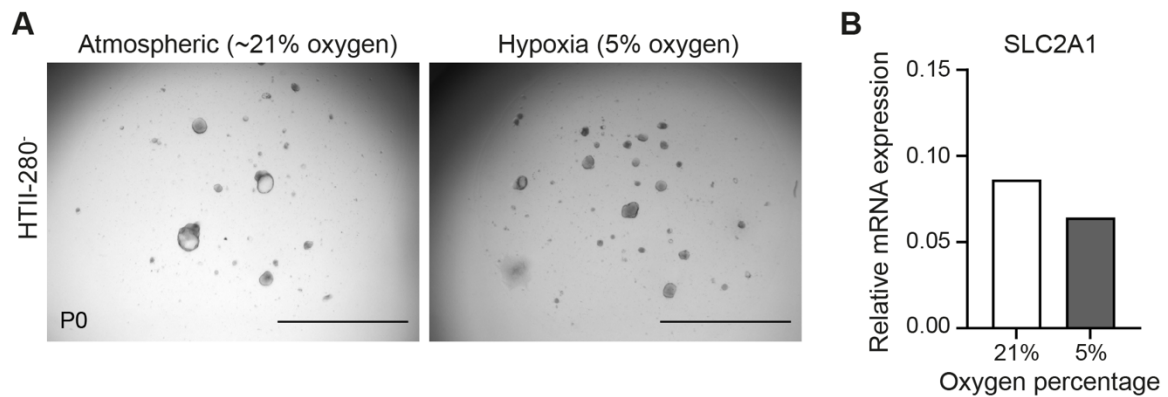


Figure 5.8. Culture of airway organoids in 5% oxygen did not lead to upregulation of the downstream hypoxia-related gene *SLC2A1*.

A. Representative brightfield images of primary HTII-280⁺ cells cultured in atmospheric (~21% oxygen) or hypoxic (5% oxygen) culture conditions. Hypoxia organoids were cultured for 7 days under normal atmospheric oxygen conditions before being switched to 5% oxygen on day 7. All cells were cultured in -CHIR medium. Images were taken at day 15 of culture. Scale bar; 2000 μ M. **B.** Relative mRNA expression levels of the downstream hypoxia gene *SLC2A1* in HTII-280⁺ cells from A. Data are presented as the mean of 2 technical replicates (individual wells) for both 21% and 5% oxygen (1 biological replicate). mRNA expression is presented relative to the housekeeping gene *GAPDH*.

Cobalt chloride (CoCl_2) and deferoxamine (DFO) are chemical inducers of hypoxia that act to stabilise HIF1 α by inhibiting the function of prolyl-hydroxylases (PHDs) which normally act to degrade HIF1 α (Guo et al., 2006). Multiple studies have utilised these chemicals to induce hypoxia-like processes under normal atmospheric oxygen conditions (Guo et al., 2006; Triantafyllou et al., 2006; Wu and Yotnda, 2011). Primary HTII-280⁺ hAT2 cells derived from healthy donor lungs were cultured as normal for 14 days in order to form hAOs, after which either CoCl_2 or DFO were supplemented to the cell media for a further 7 days (Figure 5.9A). To assess the potential effects of hypoxia on long-term cultured hAT2 cells, P6 hAOs were also utilised. There were no discernible changes both in morphologies and organoid forming efficiency of primary hAT2 cells treated with COCl_2 or DFO at a concentration of either 50 μ M or 100 μ M (Figure 5.9B and 5.9C). Due to the similarity between CoCl_2 and DFO-treated organoids, I used DFO for subsequent experiments. qPCR analysis confirmed the induction of the hypoxia-related genes *SLC2A1* and *VEGFA* in DFO-treated organoids compared to control, indicating DFO successfully induced hypoxia in hAO cultures (Figure 5.9D). Interestingly, the expression of *SFTPC* was reduced in DFO-treated cultures (Figure 5.9D).

To assess whether hypoxia resulted in a loss of hAT2 identity in hAOs, I performed immunofluorescence (IF) analysis. As found previously, control hAOs cultured in complete medium exclusively contained cells expressing pro-SFTPC (Figure 5.9E and 5.9F). However, following 7-day DFO treatment, no AGER⁺ cells were identified, indicating that loss of *SFTPC* was not due to differentiation to hAT1 cells. Instead, three separate organoid types arose from DFO-treated hAO cultures: 1) pro-SFTPC⁺/SOX2⁻ organoids that were indistinguishable from control hAOs; 2) pro-SFTPC⁺/SOX2⁺ (mixed) organoids that consisted of a mixture of cells expressing both markers; and 3) pro-SFTPC⁻/SOX2⁺ organoids that had lost their pro-SFTPC expression and exclusively expressed SOX2 (Figure 5.9E and 5.9F). A similar observation was made when P6 organoids were treated with DFO, although the number of pro-SFTPC⁻/SOX2⁺ organoids was increased versus DFO-treatment in primary cells, perhaps suggesting increased cellular plasticity. Interestingly, mixed organoids not only comprised pro-SFTPC⁺ and SOX2⁺ cells, but also single cells that expressed both markers. To avoid confusion, the use of the term ‘mixed’ organoid will encompass all organoids that comprise a mixture of pro-SFTPC⁻ single positive, SOX2⁻ single positive and pro-SFTPC⁺/SOX2⁺ dual-expressing cells. Cells within mixed organoids were reminiscent of the aberrant cell types observed in epithelial honeycomb regions of human IPF lungs, suggesting that trans-differentiation of IPF lung epithelial cells may result from inappropriate regulation in resident hAT2 cells (Figure 5.1C). This led me to further investigate how HIF1 α -mediated signalling pathway controls the induction of SOX2⁺ cells in IPF hAT2 cells, and what biological significance of such cells are in the initiation and progression of IPF.

5B.3.3. Aberrant SOX2⁺ epithelial cells localise to IPF honeycomb cysts and exhibit increased Notch signalling

As shown previously, SOX2⁺ cells existed within epithelial honeycomb cysts of distal IPF lungs, where they often co-expressed the hAT2 markers pro-SFTPC and HTII-280, or resided within close-proximity of pro-SFTPC-expressing hAT2 cells (Figure 5.1C). Notch signalling has been implicated in IPF progression and has been demonstrated to exist downstream of HIF1 α -mediated hypoxia signalling in multiple tissues (Gustafsson et al., 2005; Li et al., 2018b; Mukherjee et al., 2011; Wasnick et al., 2019; Zong et al., 2016). I therefore asked whether Notch signalling is upregulated in IPF lungs, and specifically

within aberrant SOX2⁺ epithelial cells. qPCR analysis for the Notch target gene *HES1* demonstrated an increase in expression level for both HTII-280⁺ and HTII-280⁻ IPF cells versus control cells (Figure 5.10A). IF staining data confirmed an increase in nuclear HES1 expression within IPF lungs, particularly in SOX2-expressing epithelial honeycombs (Figure 5.10B). HES1⁺ SOX2⁺ cells also expressed pro-SFTPC and HTII-280, confirming their identity as aberrant IPF cells (Figure 5.10B). These data suggested that Notch signalling was increased in cells of human IPF lungs, including aberrant SOX2⁺ distal epithelial cells.

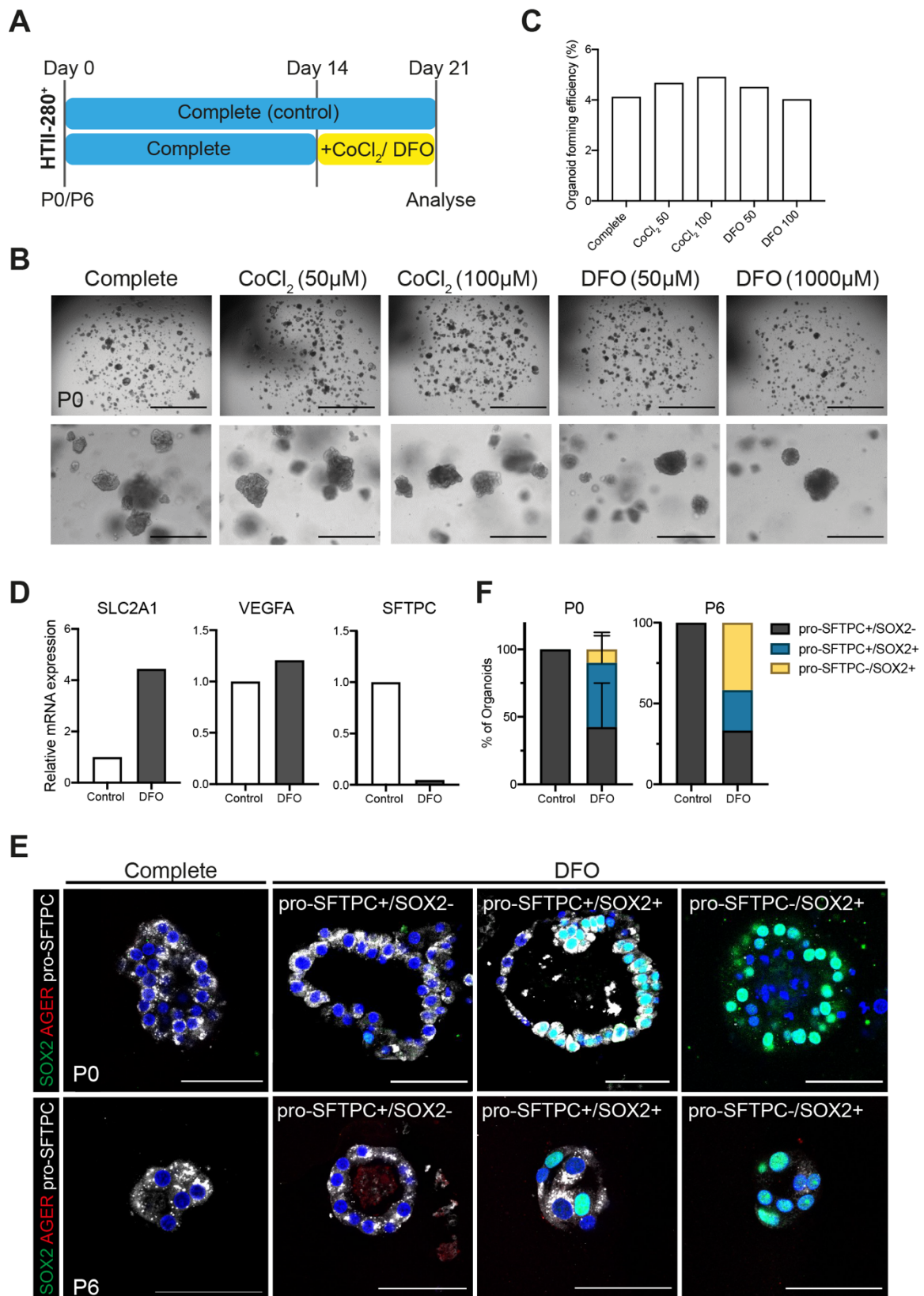


Figure 5.9. DFO treatment leads to SOX2 induction in SFTPC⁺ hAT2 cells (figure legend on next page).

Figure 5.9. DFO treatment leads to SOX2 induction in SFTPC⁺ hAT2 cells.

A. Schematic outlining the experimental design of culturing control HTII-280⁺ hAT2 cells under chemically-induced hypoxic conditions using supplementation of control (complete) medium with Cobalt Chloride (CoCl₂) or Deferoxamine (DFO) at D14 of culture. **B.** Brightfield images of HTII-280⁺ hAOs cultured in complete medium (control) or hypoxia-induced conditions at two different concentrations (50 μM and 100 μM). Scale bars; 2000 μm (top row), 400 μm (bottom row). **C.** Organoid forming efficiency of cultures in B. **D.** Relative mRNA expression levels of the downstream hypoxia genes *SLC2A1* and *VEGFA*, and the hAT2 gene *SFTPC* in control versus DFO-treated organoids. Data are presented as the mean of 2 technical replicates (1 biological replicate), and are expressed as the relative mRNA expression versus control hAT2 organoids. **E.** IF images of control and DFO-treated hAOs (treated at either P0 or P6). SOX2 (green), AGER (red), pro-SFTPC (white), DAPI (blue). **F.** Quantification of immunofluorescent data obtained in E. Data are presented as the mean ±SEM (where relevant). For control, n = 35 organoids for P0 pooled from 2 donor samples, n = 27 organoids for P6 from 1 donor sample. For DFO, n = 20 organoids for P0 pooled from 2 donor samples, n = 12 for P6 from 1 donor sample.

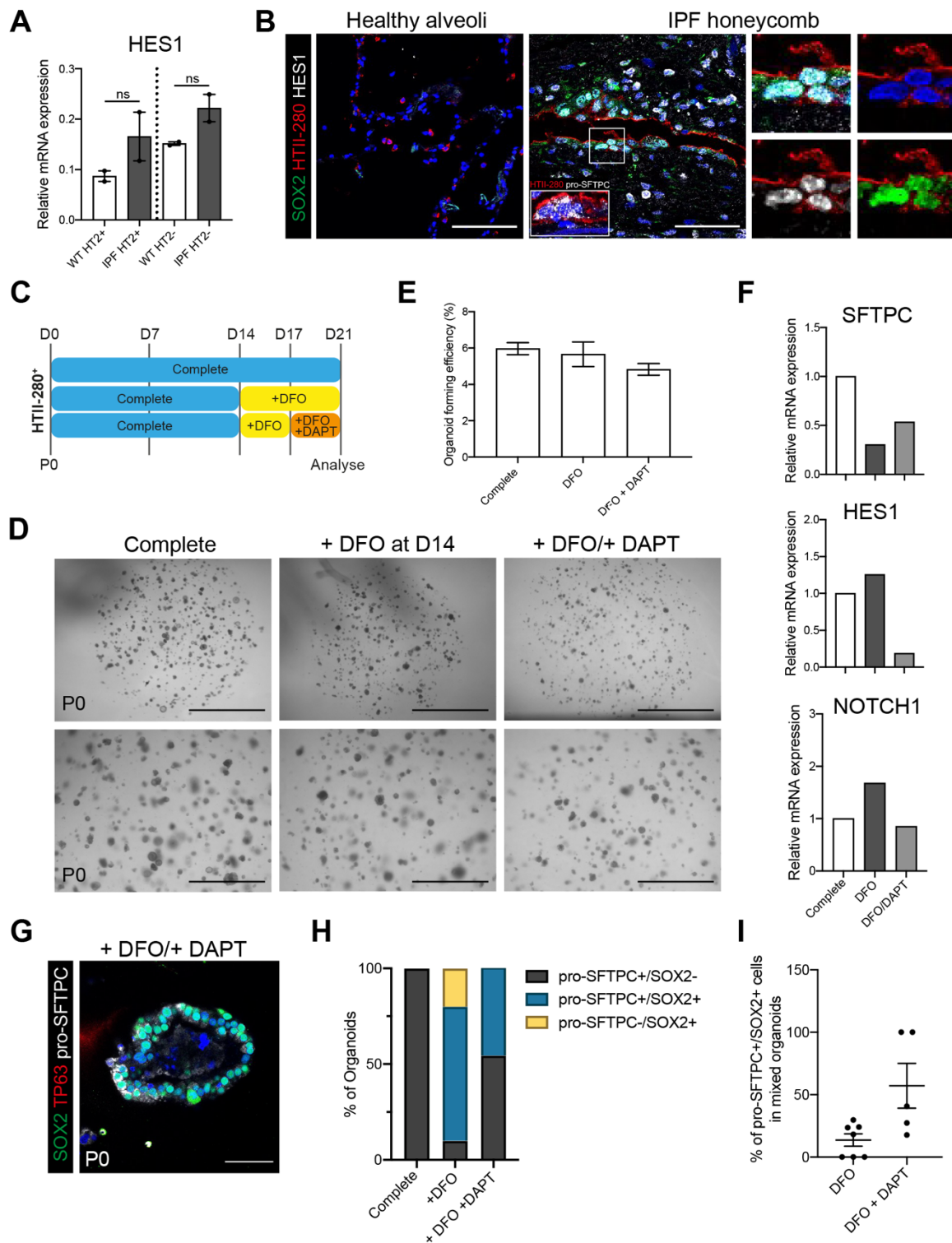


Figure 5.10. Notch signaling is increased in IPF honeycomb lesions and may function downstream of hypoxia (figure legend continued on next page).

A. Relative mRNA expression levels of the Notch target gene *HES1* in primary tissue-derived HTII-280⁺ and HTII-280⁻ cells from IPF lungs or healthy (WT) controls. Data are presented as the mean \pm SEM of 3 biological replicates, and are expressed as the relative mRNA expression versus the housekeeping gene *GAPDH*. Statistical significance was tested using the non-parametric Mann-Whitney U test; ns = non-significant. **B.** Staining data for Notch signalling components in healthy and IPF human lung tissue. SOX2

(green), HTII-280 (red), HES1 (white) and DAPI (blue). Inset, HTII-280 (red), pro-SFTPC (white). Scale bars, 50 μm . **C.** Schematic outlining the experimental design of culturing control HTII-280⁺ AT2 cells with DFO, or with additional supplementation of the Notch inhibitor DAPT. **D.** Brightfield images of primary HTII-280⁺ healthy lung tissue-derived hAT2 cells cultured in control (complete) medium, +DFO and additional supplementation with DAPT. Scale bars; 2000 μm (top panel), 1000 μm (bottom panel). Images obtained at day 21 of primary culture. **E.** Organoid forming efficiency of healthy-derived HTII-280⁺ hAOs cultured in control, +DFO and +DFO/+DAPT conditions. Data are presented as the mean \pm SEM for 2 biological replicates. **F.** Relative mRNA expression levels of *SFTPC*, *HES1* and *NOTCH1* in control and DFO-treated organoids. Data are presented as the mean of 2 technical replicates (1 biological sample), and are expressed as the relative mRNA expression versus control hAOs. **G.** Representative IF image of mixed organoid formed arising in +DFO/+DAPT treatment. SOX2 (green), TP63 (red), pro-SFTPC (white) and DAPI (blue). **H.** Quantification of pro-SFTPC and SOX2 staining in organoids derived from D. **I.** Quantification of pro-SFTPC⁺/SOX2⁺ cells in mixed (pro-SFTPC⁺/SOX2⁺) organoids of DFO-treated and DFO/DAPT-treated organoids, expressed as a percentage of the total number of DAPI⁺ cell nuclei. Each dot represents a single (mixed phenotype) organoid. The number of pro-SFTPC⁺/SOX2⁺ cells and total DAPI⁺ cells were quantified for a single plane per organoid. Data are presented as the mean \pm SEM; n = 7 (DFO) and n = 5 (DFO + DAPT), where n denotes the total number of mixed organoids assessed for 1 donor sample.

To next assess whether Notch signalling is also implicated in the induction of SOX2 expression in hypoxia-treated hAT2 cells, I employed the use of the γ -secretase inhibitor DAPT. Under normal circumstances, Notch ligand binding to a Notch receptor leads to cleavage of the Notch intracellular domain (NICD) by γ -secretase, allowing the NICD to translocate to the nucleus and activate target gene transcription by acting as a co-activator. Therefore, DAPT inhibits this Notch-enabled gene transcription by inhibiting NICD cleavage. Primary HTII-280⁺ cells were isolated from healthy donor lungs as before, and cultured in complete medium for 21 days (Figure 5.10C). For DFO-treatment, cell medium was supplemented with DFO from D14 to D21, while DAPT-treated cells were cultured with DFO for 3 days (D14 to D17) followed by additional DAPT-treatment for a further 4 days (D17 to D21). Organoids were successfully formed under all 3 conditions (Figure 5.10D and 5.10E). Analysis of gene expression levels of *HES1* and *NOTCH1* showed increased expression in DFO-treated organoid versus controls (Figure 5.10F). DAPT-treatment resulted in a decrease in expression of both genes, with a reduction in *HES1* levels versus DFO-treated hAOs, confirming successful inhibition of Notch signalling (Figure 5.10F). *SFTPC* expression was slightly rescued in DAPT-treated hAOs versus DFO-treated hAOs at the transcriptional level (Figure 5.10F). IF staining indicated

that DAPT-treated hAT2 cells still formed mixed organoids, likely owing to the initial 3-day culture in DFO prior to DAPT addition, although the overall number of these organoids was decreased in comparison with DFO-treatment (Figure 5.10G and 5.10H). However, there was an increase in pro-SFTPC⁺/SOX2⁻ hAOs (Figure 5.10H). No pro-SFTPC⁻/SOX2⁺ organoids were observed in DAPT-treated hAO cultures. Interestingly, quantification of the number of individual pro-SFTPC⁺/SOX2⁺ cells within mixed organoids showed an increase in the number of these cells versus DFO-treatment alone, suggesting that Notch inhibition stalls the aberrant differentiation of hAT2 cells to SOX2⁺ airway-like cells (Figure 5.10G and 5.10I). These findings suggested that Notch signalling, a pathway already implicated in IPF progression, may function downstream of chemically-induced HIF1 α stabilisation, where it acts to induce the aberrant expression of SOX2 in hAT2 cells. This ultimately implicated hAT2 cells as a potential cell-of-origin for this transdifferentiated aberrant epithelial cell populations observed in human IPF lungs.

5B.3.4. *ITGB4* as a potential marker for aberrant SOX2⁺ IPF cells

Analysis of the IPF cell atlas revealed that aberrant IPF basaloid cells shared a similar transcriptional signature to our DATPs (Adams et al., 2020; Choi et al., 2020; Habermann et al., 2020; Neumark et al., 2020; IPF Cell Atlas). I therefore tested whether pro-SFTPC⁺/SOX2⁺ cells, identified in this study, can be detected by a marker for DATPs. I especially sought to identify surface markers enabling the isolation of these cells for *in vitro* organoid cultures. Among DATP markers, the expression of ITGB4 has been known in basal cells, but also reported at increased levels in IPF lung tissues (IPF Cell Atlas; Adams et al., 2020; Habermann et al., 2020; Neumark et al., 2020). I therefore wanted to assess whether ITGB4 could be utilised in specifically isolating aberrant SOX2⁺ cells from both IPF lungs and DFO-treated organoid cultures. IF analysis of ITGB4 in healthy human alveoli revealed a complete absence of ITGB4⁺ cells, while ITGB4⁺ cells are observed at the base of SOX2⁺ airways, identifying them as basal cells, as expected (Figure 5.11A). In contrast, while unaffected airways of IPF lungs also displayed ITGB4-positivity in the basal cell layer (data not shown), IPF parenchymal alveolar regions demonstrated distinct ITGB4⁺ cells within epithelial honeycomb cysts (Figure 5.11A). These ITGB4⁺ cells co-expressed SOX2 and HTII-280, as well as pro-SFTPC, indicating that ITGB4 could potentially be applied in selecting these cells. Assessment of control and DFO-treated

hAT2-derived organoids revealed positive ITGB4-expression in DFO-treated, SOX2⁺ organoids (Figure 5.11B and 5.11C). Similarly, analysis of primary IPF-derived HTII-280⁺ and HTII-280⁻ organoids cultured in both complete or -CHIR conditions also suggested ITGB4 presence, with cells often co-expressing HTII-280, as was observed *in vivo* (Figure 5.11B, 5.11C and 5.11D). These findings suggested that IPF-derived organoids resemble aberrant airway cell types found in the epithelium of distal IPF lung parenchyma.

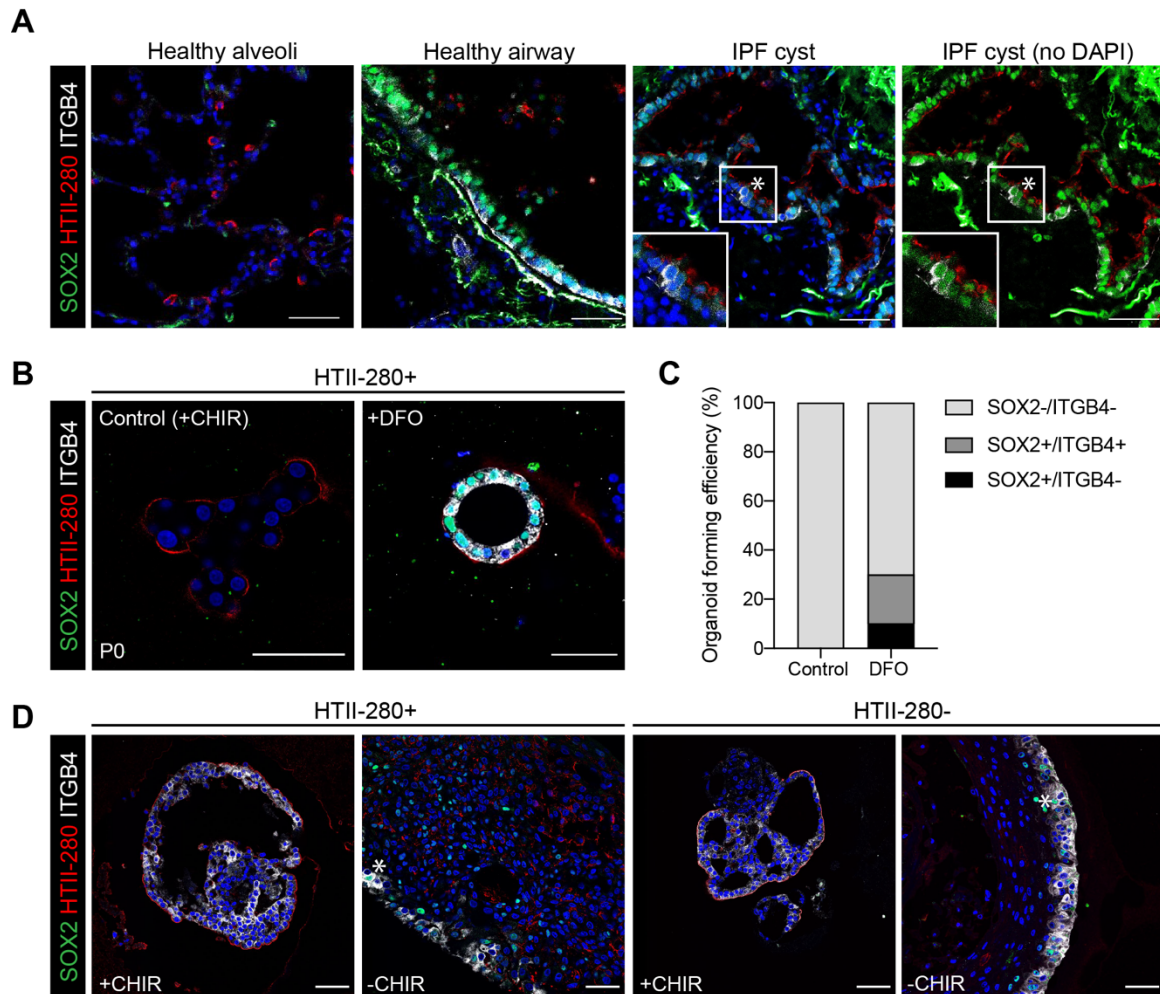


Figure 5.11. ITGB4 is expressed in epithelial cells of IPF honeycomb cysts.

A. IF images of healthy human distal lungs (alveoli and airways) and IPF honeycomb cysts. SOX2 (green), HTII-280 (red), ITGB4 (white) and DAPI (blue). Scale bars; 50 μ m. **B.** IF images of control and DFO-treated AT2 organoids. SOX2 (green), HTII-280 (red), ITGB4 (white), DAPI (blue). Images were obtained at day 21 of culture. Scale bars; 50 μ m. **C.** Quantification of the number of ITGB4⁺ organoids in control and DFO-treated AT2-derived organoids from IF data obtained in B. n = 10 organoids quantified **D.** IF images of patient-derived HTII-280⁺ and HTII-280⁻ primary organoids from IPF lungs. Cells were cultured either in complete medium (+CHIR) or – CHIR medium. SOX2 (green), HTII-280 (red), ITGB4 (white), DAPI (blue). Images were obtained at day 21 of culture. Scale bars; 50 μ m.

I next attempted to specifically isolate these cells for culture in order to assess their cellular behaviours *in vitro*. Due to the observation that aberrant hAT2-derived SOX2⁺ cells often co-express HTII-280 both *in vivo* and *in vitro*, I combined the expression of HTII-280 and ITGB4 to exclude basal cells but obtain aberrant airway-like SOX2⁺ honeycomb epithelial cells for FACS (Figure 5.12A and 5.12B). This led to the observation of four separate populations; HTII-280⁺ITGB4⁻ cells (likely hAT2 cells) which made up 5% of total epithelial cells, a small population of HTII-280⁺ITGB4⁺ cells which were expected to consist of aberrant SOX2⁺ cells, and two large populations of HTII-280⁻ITGB4⁺ (basal) cells and HTII-280⁻ITGB4⁻ cells. This was in contrast to epithelial cells derived from control donor lungs, where the largest population of cells was the HTII-280⁺ITGB4⁻ fraction, while ITGB4 expression was practically non-existent due to the lack of basal cells (Figure 5.12C). qPCR analysis for multiple genes revealed that the hypoxia-induced gene *SLC2A1* was expressed at higher levels in three of the IPF-derived populations (HTII-280⁻ITGB4⁺, HTII-280⁺ITGB4⁺ and HTII-280⁻ITGB4⁻) versus healthy controls (Figure 5.12D). In addition, a number of the IPF populations also expressed higher levels of *HES1* and *SOX2*, while *SFTPC* levels were reduced (Figure 5.12D). Upon 3D-culture of the resulting cell populations, control cells cultured in complete medium (HTII-280⁺ITGB4⁻) and -CHIR medium (HTII-280⁻ITGB4⁺) formed hAOs and airway organoids, respectively (Figure 5.12E). In contrast, IPF-derived cells formed organoids mainly from the HTII-280⁻ITGB4⁺ population, although a small number of organoids also arose from the additional 3 populations, albeit with low organoid forming efficiency (Figure 5.12E and 5.12F). Due to low cell number, it was difficult to assess their cellular composition, although their morphology indicated that they were airway organoids (Figure 5.12E). While control organoids successfully re-formed following passage and re-plating of single cells, only HTII-280⁻ITGB4⁺ cells from IPF lungs could be passaged (data not shown). These data suggested that the HTII-280⁺ITGB4⁺ IPF population displayed decreased clonogenic capacity. The HTII-280⁻ITGB4⁺ population resulted in the highest self-renewal capacity *in vitro*. However, it was difficult to assess whether ITGB4⁺ IPF cells arose from epithelial honeycombs or less-damaged airways.

Utilising the same FACS isolation strategy as for primary IPF tissue, I next assessed HTII-280 and ITGB4 marker expression in passaged control and DFO-treated hAT2-derived organoids. This led to the observation that DFO-treatment resulted in an increase in both HTII-280⁺ITGB4⁺ and HTII-280⁻ITGB4⁺ cells, confirming what I had

demonstrated previously with IF analysis (Figure 5.13A and 5.13B; Figure 5.11B). However, upon plating of single cells, only control cells were able to re-form organoids, with DFO-treated cells of all populations failing to form organoids, despite being re-cultured in complete medium upon plating (Figure 5.13C and 5.13D).

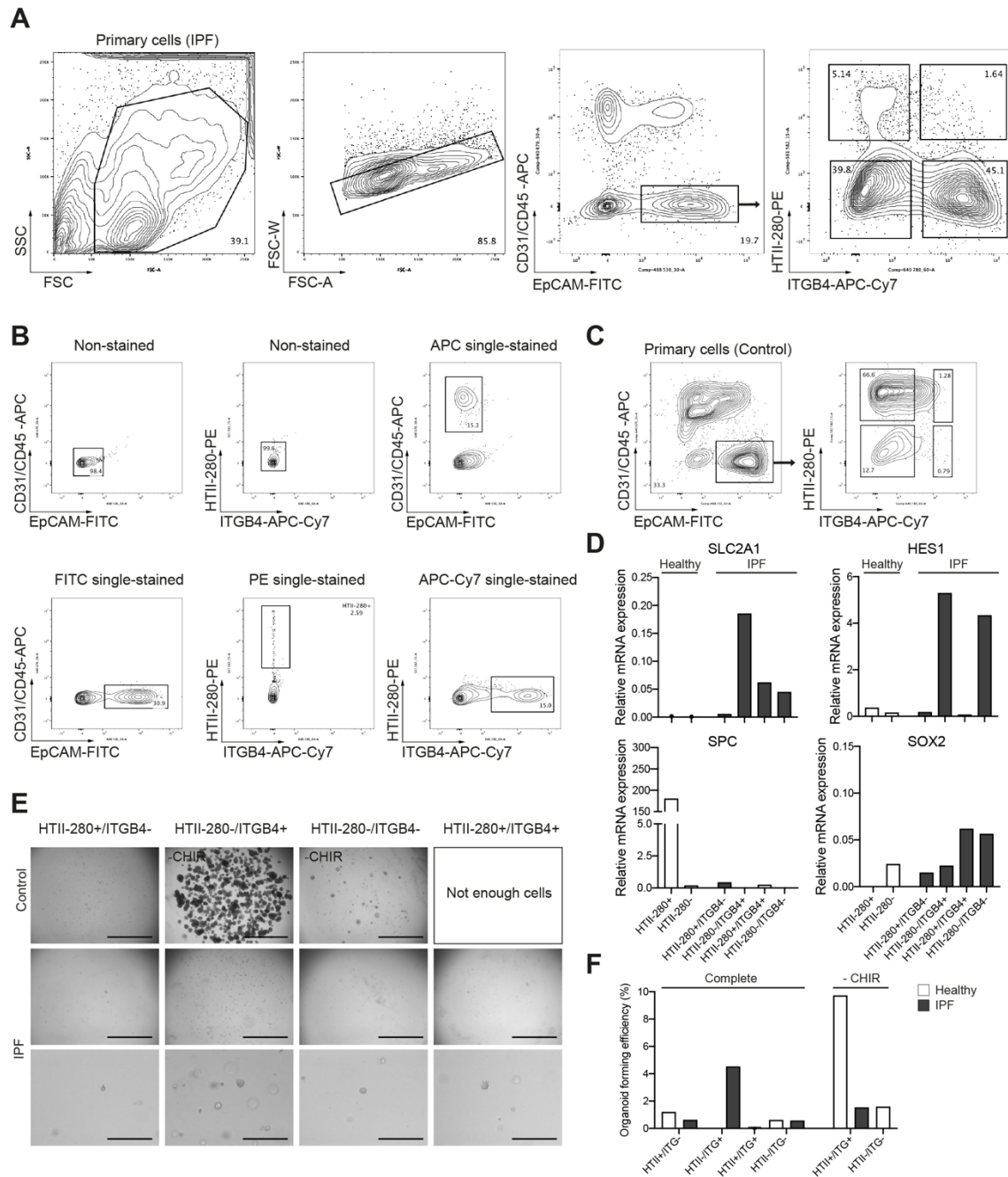


Figure 5.12. The number of *ITGB4*⁺ cells is drastically increased in IPF distal lungs (figure legend continued on next page).

A. FACS gating strategy for isolation of epithelial cells from primary human IPF lung tissue based on their CD31⁺/CD45⁺/EpCAM⁺ expression profile, which were then further gated using HTII-280 and ITGB4. **B.** Non-stained and single-stained controls for markers used in A. **C.** FACS gating strategy for isolation of HTII-

280 and ITGB4 epithelial cells from healthy background lungs, using the same markers as in A. **D.** Relative mRNA expression of lung lineage markers in the four populations identified in A. Data are presented as the mean of two technical replicates for 1 donor per disease state. **E.** Representative brightfield images of the 3 populations of cells isolated in A. Cells were cultured in complete (+CHIR) conditions, unless otherwise stated, and imaged at D14. Scale bars; 2000 μm (top panels), 1000 μm (bottom panels). **F.** Quantification of organoid forming efficiency from cultures in E. Data are presented as the mean of two technical replicates (1 biological replicate).

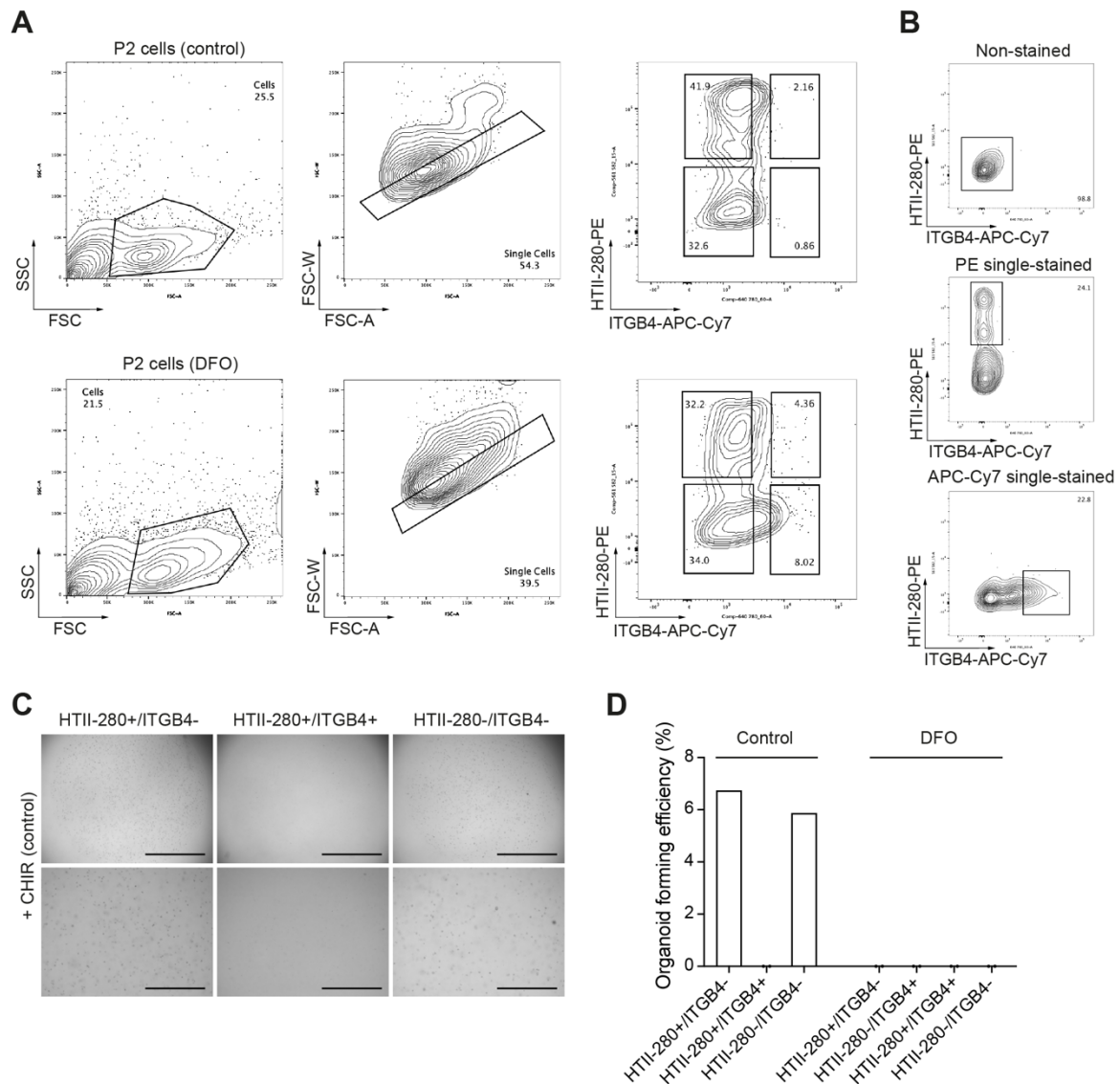


Figure 5.13. Treatment of hAT2 organoids with DFO leads to an increase in ITGB4+ cells (figure legend continued on next page).

A. FACS gating strategy for isolation of epithelial cells from cultured hAOs based on their CD31⁻/CD45⁻/EpCAM⁺ expression profile, which were then further gated using HTII-280 and ITGB4. Control cells and DFO-treated cells were analysed. **B.** Non-stained and single-stained controls for markers used in A. **C.** Representative brightfield images of the 3 populations of cells isolated in A. Cells were cultured in complete (+CHIR) conditions and imaged at D14. Scale bars; 2000 μm (top panels), 1000 μm (bottom panels). **D.**

Quantification of organoid forming efficiency from cultures in C. Data are presented as the mean of two technical replicates (1 biological replicate).

5B.3.5. SOX2⁺ cells in both hAOs and IPF lung tissue display increased levels of proliferation

Given the observation of SOX2⁺ airway-like cells in DFO-treated hAOs, IPF-derived organoids and IPF lung tissues, I asked what the biological significance of these cells are in the progression of IPF. Due to repeated epithelial damage, hAT2 cells are thought to become irreversibly damaged, where they can no longer self-renew or differentiate into hAT1 cells (Parimon et al., 2020). However, one of the defining features of IPF is hyperplasia of hAT2 cells that are often found in the honeycomb regions and/or around the fibroblastic foci (Barratt et al., 2018), suggesting the emergence of “hyperproliferative hAT2” cells during IPF progression. I therefore investigated the proliferative capacity of SOX2⁺ cells in DFO-treated hAOs and the honeycomb regions of IPF lung tissues.

Control (complete medium) hAOs at D21 of primary culture exhibited no proliferative cells, as confirmed by the absence of the proliferation marker KI67 (Figure 5.14A and 5.14B). In contrast, DFO-treated hAOs exhibited a significant increase in the number of KI67⁺ cells per organoid (Figure 5.14B; number of KI67⁺ cells quantified as a percentage of the total number of DAPI⁺ nuclei). Importantly, KI67⁺ cells were observed only within SOX2⁺ or mixed organoids, whereas SFTPC⁺/SOX2⁻ organoids contained no KI67⁺ cells (Figure 5.14A and 5.14B). Within mixed organoids, proliferation occurred exclusively in SOX2-expressing cells. Proliferation could also be observed within individual pro-SFTPC⁺/SOX2⁺ cells within mixed organoids (Figure 5.14A, asterisk). This recapitulated *in vivo* findings, where IF analysis revealed KI67⁺ expression in some SOX2⁺ cells that co-expressed ITGB4, a marker for basal cells or aberrant basaloid cells in IPF lung tissues, while there are no hAT2 cells expressing KI67 in the alveoli (Figure 5.14C; IPF Cell Atlas). I should note that, due to the lengthy duration between surgery and collection of clinical lung specimens for processing, observed proliferation in the tissue may not be fully reflective of true proliferation levels *in vivo*. Hence, this may explain the relatively low overall numbers of KI67⁺ cells.

I then further assessed the clonogenic capacity of these cells by performing single-cell passage. Due to the increased presence of SOX2⁺ cells, and the prior observation that low Wnt conditions allowed for expansion of human airway cells, I used both complete and -CHIR medium (Figure 5.14D, Table 3.1). Control and DFO-treated hAOs were dissociated into single cells, and replated as organoids. Unexpectedly, however, cells from DFO-hAOs failed to re-form organoids under either condition (Figure 5.11E and 5.11F). Meanwhile, control cells re-formed organoids as usual (Figure 5.14E and 5.14F). Although SOX2⁺ cells in DFO-treated cultures are initially proliferative, it is likely that prolonged culture (> 7 days) under chemically-stimulated hypoxic conditions may infer a decrease in cell viability or self-renewal capacity which becomes apparent upon passage. It would be important to further elucidate the underlying mechanisms that modulate their behaviours and contribution to IPF progression in the future study. Together, my results suggest that HIF1 α -mediated hypoxia induces the trans-differentiation of hAT2 cells into aberrant airway-like cells expressing SOX2, which are possibly similar to DATPs or basaloid cells within IPF lungs. In my system, these cells retain proliferative potency and likely contribute to development of the honeycomb cysts in IPF lung tissues.

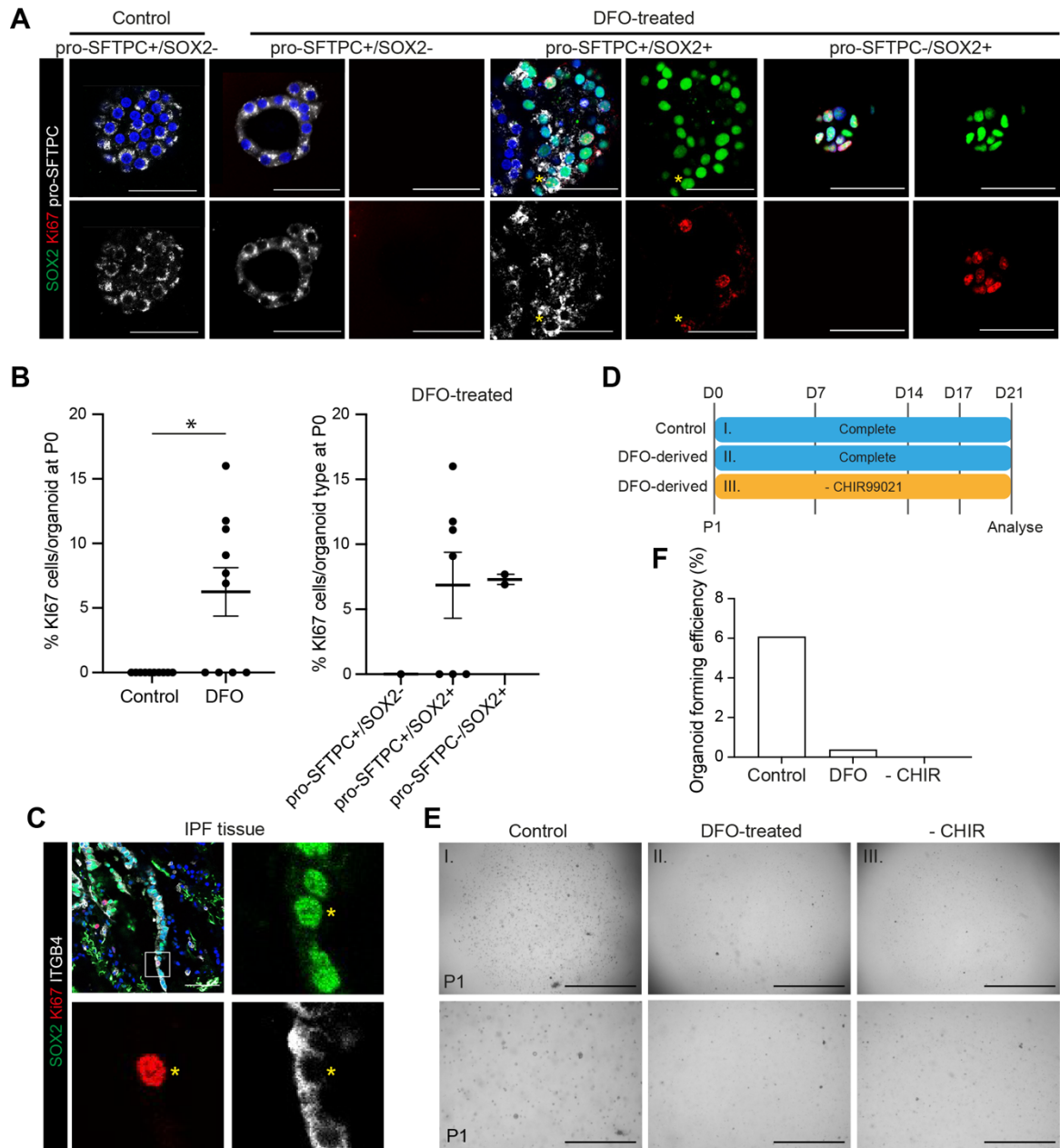


Figure 5.14. *hAT2*-derived *SOX2*⁺ cells display increased proliferation versus *SOX2*⁻ *hAT2* cells (figure legend continued on next page).

A. IF images of *hAT2*-derived organoids cultured in control (complete medium) or following 7-day treatment of DFO (treated at day 14, imaged at day 21). *SOX2* (green), *KI67* (red), *pro-SFTPC* (white), *DAPI* (blue). Asterisk denotes proliferative *SFTPC*⁺/*SOX2*⁺ cell expressing *KI67*. Scale bars; 50 μ m. **B.** Left; quantification of the number of *KI67*⁺ cells per total number of *DAPI*⁺ cell nuclei identified in DFO-treated and control hAOs at day 21. Each individual dot represents one organoid and data are presented as the mean \pm SEM (n=20 organoids pooled from two donors). Statistical significance was tested using the non-parametric Mann-Whitney U test; * = p < 0.05. Right; quantification of the number of *KI67*⁺ cells per total number of *DAPI*⁺ cell nuclei identified in the three separate types of DFO-treated hAOs. Number of cells were quantified for each organoid on a single plane. Asterisk denotes proliferative *KI67*⁺ *pro-SFTPC*⁺ *SOX2*⁺ cell within mixed organoid. **C.** IF image of distal honeycomb in IPF patient lung epithelium. *SOX2* (green), *KI67* (red),

ITGB4 (white) and DAPI (blue). Asterisk denotes proliferative ITGB4⁺/SOX2⁺ cell expressing KI67. Scale bar, 50 μ m. **D** Schematic for culture strategy of control and DFO-treated organoids following passage. **E**. Brightfield images of control, DFO-treated (complete medium) and DFO-treated (-CHIR) following passage. Scale bars; 2000 μ m (top panels), 1000 μ m (bottom panels). **F**. Quantification of organoid forming efficiency of cultures in E. Data are presented as the mean of 2 technical replicates (individual wells) for each condition for 1 donor sample.

5B.4. Conclusions

In this chapter, I aimed to assess the effect of chemically-induced hypoxia on healthy donor-derived hAT2 cells *in vitro* and to identify a potential mechanism for the appearance of airway-like cells within distal IPF lungs. Chemical induction of hypoxia using DFO from day 14 to 21 of culture resulted in an overall reduction in the number of pro-SFTPC-expressing hAOs. In contrast, there was an increase in the number of organoids expressing the airway transcription factor SOX2, a finding not observed in control hAOs. Interestingly, a proportion of organoids arose in DFO-treated hAO cultures that co-expressed pro-SFTPC and SOX2 within the same organoid, as well as within individual cells, a finding that was reminiscent of the aberrant pro-SFTPC⁺/SOX2⁺ cells observed in the lungs of IPF patients. This may reflect a potential heterogeneity in hAT2 cell response to hypoxia. These data suggest that trans-differentiation into airway-like cells of the distal IPF lung may result from inappropriate signalling cascades in resident hAT2 cells. These findings fit in with previous work from the mouse (Choi et al., 2020; Kobayashi et al., 2020; Strunz et al., 2020). Upon damage to the alveoli, DATPs emerge from AT2 cells to assist with regeneration of the alveolar epithelium, with transition to the DATP state found to be essential for differentiation to AT1 cells. However, chronic inflammation and injury resulted in aberrant accumulation of DATPs, with high HIF1 α implicated in the stall of DATP differentiation to AT1 cells. Importantly, aberrant accumulation of DATP-like cells has been observed in IPF patient tissues, suggesting their implication in IPF progression. DATP-like cells express similar molecular signatures to the previously identified basaloid cells of IPF lungs, making it possible that they represent the same or similar population. Furthermore, as found during the present work, DATPs also express SOX2.

In addition to SOX2 expression, DFO-treated hAOs exhibited higher levels of proliferation, with proliferative cells exclusively occurring within SOX2⁺ and mixed organoids, a finding

that was also confirmed in IPF lung tissue. Importantly, in mixed organoids, KI67 was exclusively expressed in SOX2⁺ and pro-SFTPC⁺ SOX2⁺ cells, indicating that the presence of SOX2 inferred a proliferative effect. As hAT2 cells are considered to be relatively quiescent, it is possible that upon injury, activation of SOX2 and an airway-like molecular programme allows for increased proliferation in an attempt to rapidly repair the damaged epithelium. Notch pathway components were increased in IPF lungs and DFO-treated hAOs, and blocking Notch signalling resulted in a partial rescue of hAT2 identity in DFO-treated hAOs, suggesting that DFO-induced hypoxia may function through downstream Notch signalling. ITGB4 was identified as a potential marker for aberrant pro-SFTPC⁺/SOX2⁺ and SOX2⁺ cells, and was found to be massively increased in IPF lungs and DFO-treated hAOs. Together, these data highlight that hAT2 cells possess the capacity to differentiate to airway-like cells under IPF disease-associated processes such as hypoxia, identifying hAT2 cells as a potential cell-of-origin for the appearance of airway cell types in distal IPF lungs.

CHAPTER 5C

Results IIIC: Investigating the effect of inflammatory cytokines on hAT2 cell identity

5C.1. Introduction

Idiopathic pulmonary fibrosis (IPF) is a disease of heterogenous nature and unknown etiology, making it unlikely that a single signalling pathway is responsible for all disease observations. Rather, it is feasible that a whole host of mechanisms and signalling pathways interact in a complex crosstalk leading to IPF initiation and progression. In addition to increased fibrosis and reduced tissue oxygenation, inflammation through the release of inflammatory cytokines has been considered to play a role in IPF pathogenesis (Barratt et al., 2018). In particular, cytokines including IL-1 β and TNF- α are specific contenders, due to the observation of high cytokine levels in bronchoalveolar lavage fluid (BALF) obtained from IPF patient lungs (Schruf et al., 2020). Recently, we uncovered that pro-inflammatory cytokines, including IL-1 α , IL-1 β , and IL-17A, are integral to regenerate the alveoli after bleomycin-induced lung injury via induction of damage associated transient progenitor (DATP) states (Choi et al., 2020; Katsura et al., 2019). Importantly, persistent IL-1 β signalling resulted in abnormal accumulation of DATPs, which was also observed in IPF lungs. These results led me to hypothesise that pro-inflammatory cytokines induce aberrant SOX2⁺ airway-like cells derived from hAT2 cells in IPF lung tissues. To prove my hypothesis, I will assess whether treatment of hAT2 cell-derived hAOs from healthy donor

lungs with the cytokines IL-1 β and TNF- α could have a similar effect on hAT2 cell identity as chemical induction of hypoxia.

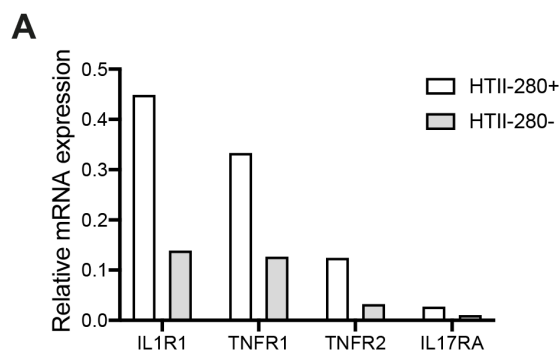
5C.2. Aims

- Investigate the effect of inflammatory cytokines on the cellular behaviours of hAT2 cells (IL-1 β and TNF- α).
- Characterise cytokine-treated hAOs in terms of cell identity and self-renewal capacity.

5C.3. Results

5C.3.1. Increased inflammatory cytokine presence in human IPF lungs

In addition to our recent study, both IL-1 β and TNF- α have been previously implicated in IPF progression due to their up-regulation in patient-derived BALF (Reyfman et al., 2019; Schruf et al., 2020). I first examined the expression levels of functional receptors for these cytokines in freshly isolated HTII-280⁺ and HTII-280⁻ cells from healthy donors. qPCR analysis showed higher levels of IL1R1, TNFR1 and TNFR2 expression in the HTII-280⁺ (hAT2) cells compared to those in HTII-280⁻ cells (Figure 5.15A). In contrast, the IL-17 receptor IL17RA was expressed at relatively low levels for both populations of cells. These data indicate that hAT2 cells can be responsive to IL-1 β and TNF- α signalling, as previously shown in other studies (Choi et al., 2020; Reyfman et al., 2019).



housekeeping gene *GAPDH*.

Figure 5.15. IL-1 β and TNF- α receptors are up-regulated in hAT2 cells.

A. Relative mRNA expression levels of the cytokine receptors IL1R1, TNFR1, TNFR2 and IL17RA in primary donor lung-derived HTII-280⁺ and HTII-280⁻ epithelial cells. Data are presented as the mean of 2 technical replicates (1 biological replicate) and are expressed as the relative mRNA expression versus the

5C.3.2. IL-1 β and TNF- α signalling in hAT2 cells leads to aberrant differentiation to KRT5-expressing airway-like cells in vitro

To investigate the effect of exogenous cytokines on hAOs, primary hAT2 cells from healthy donors were isolated as before (CD31⁻CD45⁻EpCAM⁺HTII-280⁺) and placed in 3D-culture as single cells in either complete medium (control) or with addition of 100 ng/mL human recombinant IL-1 β (+IL-1 β) or 100 ng/mL human recombinant TNF- α (+TNF- α). Cytokines were supplemented to complete medium every other day up to 28 days of the culture period. At D14, brightfield images showed the formation of small, folded structures throughout all 3 conditions, with their morphology suggesting their identity as hAOs (Figure 5.16A). Organoid forming efficiency was similar between all 3 conditions, although TNF- α -treated organoids showed a slight decrease in the total number of organoids for some donors (Figure 5.16B). However, by D28, organoid morphology had dramatically changed. While control hAOs still possessed a small and folded structure, IL-1 β -treated and TNF- α -treated cultures became more heterogeneous, with a number of large cystic or folded organoids (Figure 5.16A). These large structures closely resembled the airway organoids that arose normally from HTII-280⁻ cultures. To rule out the possibility of cytokine treatment causing outgrowth of potential contaminating airway cells within the cultures, primary HTII-280⁺ cells were also cultured in -CHIR medium, which does not support hAO formation but does allow airway organoid growth (Chapter 3 and Chapter 4). However, few organoids formed under this condition, confirming that HTII-280⁺ hAT2 cells formed the large organoids mediated by IL-1 β and TNF- α . Additionally, culture of HTII-280⁻ airway organoids with IL-1 β and TNF- α failed to exhibit an expansion (data not shown). Therefore, I could confirm that the large structures arising following IL-1 β - or TNF- α -treatment were arising from the hAT2 cell population.

In order to assess the cellular identity of IL-1 β - and TNF- α -treated organoids, I employed immunofluorescence (IF) analysis. Control hAOs cultured in complete medium consisted of cells expressing pro-SFTPC, as previously described (Figure 5.16D; Chapter 4). In contrast, the majority of cells in IL-1 β -treated organoids completely lost pro-SFTPC expression, and strongly expressed the basal cell marker KRT5 (Figure 5.15D). However, despite the KRT5 expression, no airway markers, including TP63 and SOX2, were observed in these cells (Figure 5.16D and 5.16E). Loss of *SFTPC* expression was also observed at the transcriptional level, along with an increase in *TP63* (Figure 5.16F). In

contrast, TNF- α -treated organoids contained airway cells expressing SOX2⁺, TP63⁺ and KRT5⁺ cells, with a complete loss of pro-SFTPC (Figure 5.16D and 5.16E). Loss of *SFTPC* expression from TNF- α -treated organoids was also observed at the transcriptional level, in addition to an increase in *TP63*, as observed for IL-1 β (Figure 5.16F). Together, these results indicated that hAT2 cells possessed the capacity for differentiation into aberrant airway-like cells when subjected to IPF processes, including increased IL-1 β and TNF- α signalling or hypoxia (Figure 5.16; Chapter 5B).

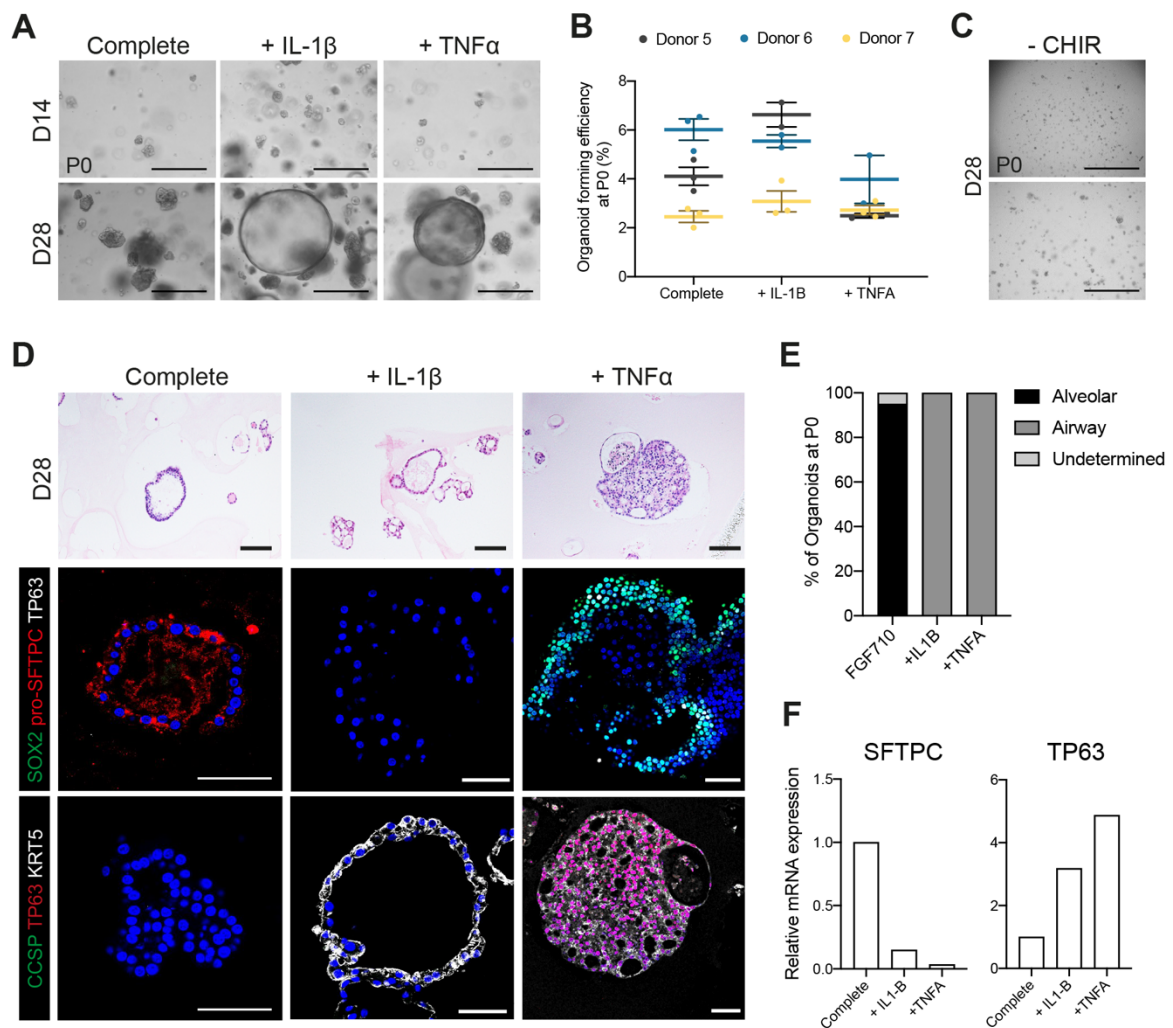


Figure 5.16. IL-1 β and TNF- α treatment induce airway-like phenotypes in hAT2 cell-derived hAOs (figure legend continued on next page).

A. Representative brightfield images of primary hAT2-derived organoids from healthy human lungs following continuous culture in complete medium, or treatment with the cytokines IL-1 β and TNF- α . Images were obtained at day (D) 14 and D28 of culture. Scale bars, 400 μ m. P0 = passage 0. B. Organoid forming efficiency of cultures established in A. The number of organoids were quantified at D14 of culture. C. Brightfield images of primary hAT2-derived organoids at day 28 of culture following continuous culture in medium lacking CHIR99021. D. Representative H&E and IF images of hAOs at D28 of culture following

continuous culture in complete medium, or with the cytokines IL-1 β and TNF- α . SOX2 (green), pro-SFTPC (red), TP63 (white, red), CCSP (green), KRT5 (white) and DAPI (blue). Scale bars, 50 μ m. E. Quantification of IF staining of organoids in D. F. Relative mRNA expression levels of *SFTPC* in complete, IL-1 β , and TNF- α cultures. Data are presented as the mean of 2 technical replicates, and are expressed as the relative mRNA expression versus the housekeeping gene *GAPDH*.

5C.4. Conclusions

In this chapter I demonstrated that IL-1 β and TNF- α , both inflammatory cytokines that exhibit marked increases in the lungs of IPF patients, led to the formation of airway-like organoids when applied to donor hAT2-derived hAOs *in vitro*. Organoid morphology in IL-1 β - and TNF- α -treated hAOs greatly changed between D14 and D28 of culture, with the appearance of large, cystic organoids. This was in stark contrast to control hAOs, which maintained a folded appearance and exclusively expressed hAT2 markers such as pro-SFTPC. Such findings were also confirmed at the transcriptional level, with a reduction in *SFTPC* expression and an increase in *TP63* expression in IL-1 β - and TNF- α -treated hAOs. Interestingly, induction of airway cell fate in hAT2 cells was also achieved upon DFO treatment. These findings fit in with recent mouse studies from my lab (Choi et al., 2020). Upon injury with bleomycin, IL-1 β is secreted by interstitial macrophages, which primes IL1R1⁺ AT2 cells prior to their differentiation to DATPs and AT1 cells *in vivo* (Choi et al., 2020). Under normal reparative processes, transition through the DATP state was essential for AT1 formation. However, chronic inflammation through sustained IL-1 β treatment of adult mouse AT2 organoids resulted in an accumulation of DATPs and stalled AT1 differentiation. DATPs were found to be enriched for expression of Hif1 α , and deletion of Hif1 α from mouse AT2 cells during injury prevented the formation of DATPs *in vivo*. Furthermore, blocking Hif1 α with digoxin prevented DATP formation from IL-1 β -treated AT2 cells *in vitro*. Therefore, in the context of chronic injury and inflammation within the human lung, it is possible that an accumulation of DATPs or DATP-like cells is a result of persistent IL-1 β , which can enhance Hif1 α levels leading to the induction of metabolic changes in AT2 cells. Together, these data, combined with my previous findings in regard to hypoxia, highlight that hAT2 cells possess the ability to differentiate to airway cell types under conditions of increased cytokine presence. Thus, I propose that aberrant

epithelial cell types present within distal IPF lungs may arise as a result of dysregulated signalling acting upon the hAT2 population.

CHAPTER 6

Discussion

In the human lung, epithelial alveolar type 2 (hAT2) cells are suspected to maintain the alveolar epithelium, while their dysregulation has been implicated in Idiopathic pulmonary fibrosis (IPF; Lawson et al., 2004; Nureki et al., 2018; Parimon et al., 2020; Sisson et al., 2010). During my PhD programme, I aimed to understand cellular behaviours of hAT2 cells in healthy and diseased lungs by developing alveolar organoids derived from primary hAT2 cells. I determined the molecular mechanisms underpinning aberrant trans-differentiation of hAT2 cells mediated by hypoxia, which is implicated in IPF. The model of human primary *in vitro* organoids from healthy background lungs showed the long-term maintenance of functionally mature hAT2 cells in chemically-defined conditions (Chapter 3 and Chapter 4). Human alveolar organoids (hAOs) required Wnt signalling for their self-renewal capacity and maintenance of hAT2 identity *in vitro*, in contrast to airway cell types, while reduced Wnt signalling promoted hAT2-to-alveolar type 1 (hAT1) differentiation. Isolation of epithelial (EpCAM⁺) cells from IPF patient lungs revealed a substantial decrease in hAT2 viability and organoid-forming ability, with organoid cultures instead being enriched with airway cell types (Chapter 5A). Importantly, culture of healthy donor-derived hAT2 cells with a chemical-inducer of hypoxia resulted in the aberrant expression of SOX2, which was found to often be co-expressed with pro-SFTPC (Chapter 5B). These cells exhibited higher proliferative capacity than non-SOX2-expressing hAT2 cells, and were also observed within IPF patient lungs. Inhibition of Notch signalling reduced the number of SOX2⁺ hAT2 cell-derived organoids, suggesting that hypoxia may function through the Notch pathway. Finally, *in vitro* culture of healthy hAOs with exogenous IL-1 β and TNF- α , two cytokines that are increased in human IPF lungs, resulted in aberrant

differentiation of hAT2 cells to KRT5-expressing, basal-like airway cells (Chapter 5C). Together, these results suggest that aberrant activation of signalling pathways implicated in IPF may function in causing hAT2 cell differentiation to airway-like cells and loss of alveolar stem cell maintenance.

6.1. Alveolar and airway organoids from normal background human adult lungs

6.1.1. *Fgf* and *Wnt* signalling are essential for *in vitro* self-renewal of distal *EpCAM*⁺ and *hAT2* primary human lung cells

Throughout lung development, and during repair following lung injury, a number of signalling pathways are activated or modulated to achieve appropriate tissue patterning, cell specification, differentiation and proliferation. During Chapter 3 and Chapter 4, I found that *EpCAM*⁺ distal human lung cells require FGF7 and Wnt signalling for primary self-renewal capacity. This finding draws parallels with what is currently known from a number of *in vivo* studies in the mouse, in addition to work utilising human embryonic lungs and human pluripotent and induced-pluripotent cells (hPSCs and iPSCs). Several *Fgf* ligands are expressed during lung development, including *Fgf7* and *Fgf10* (Volckaert and De Langhe, 2015). During development, *Fgf10* signalling is vital for lung branching morphogenesis in the mouse (Volckaert and De Langhe, 2015). Conversely, although not vital for lung morphogenesis, *Fgf7* stimulates rat AT2 cells to proliferate (Portnoy et al., 2004; Zhang et al., 2004). Furthermore, an *Axin2*⁺/*Pdgfra*⁺ alveolar mesenchymal lineage was found to promote mouse AT2 self-renewal via *Il-6* and *Fgf7* signalling (Zepp et al., 2017). In the human, FGF7 and FGF10 also appear to play key roles in lung development. Culture of human embryonic distal lung epithelial tips in the presence of factors including FGF7, FGF10 and Wnt activation was sufficient to promote organoid formation and growth (Miller et al., 2018; Nikolić et al., 2017). In hPSCs, differentiation of ventralised anterior foregut endoderm (VAFE) to *NKX2.1*⁺ lung progenitors was achieved through FGF7 and FGF10 presence, in addition to Notch and GSK3 inhibition (Gotoh et al., 2014; Yamamoto et al., 2017). Removal of FGF7 completely abolished primary *EpCAM*⁺ organoid formation in the current study, as has been reported recently for organoids derived from mouse secretory club and AT2 cells (Choi et al., 2021). FGF7 was also previously found to be

required for initial expansion of human epithelial lung tip progenitor cells from pseudoglandular lungs (Miller et al., 2018). On the other hand, removal of FGF10 from EpCAM⁺ cultures in the present study was found to not have any obvious effects on organoid formation or identity, a discovery that has also been noted in the culture of mouse epithelial lung organoids (Figure 3.2; Choi et al., 2021). However, it is important to note that the inclusion of CHIR99021 (CHIR, a GSK3 β inhibitor) could possibly compensate for FGF10 removal, as FGF10 is known to be a major activator of β -catenin signalling (Danopoulos et al., 2019a). The same may not apply to FGF7, as it has been reported that FGF7 and FGF10 function in different ways (Danopoulos et al., 2019a). Together, these studies highlight the importance of Fgf signalling in the maintenance of epithelial lung progenitor populations *in vitro*.

My finding that human-derived epithelial lung organoids could only be passaged long-term in the presence of TGF β inhibition, regardless of specific lineage, is similar to observations made in multiple human organoid systems (Broutier et al., 2017; Huch and Koo, 2015; Huch et al., 2015; Nikolić et al., 2017; Sachs et al., 2019). This is unlike epithelial organoids derived from multiple mouse tissues, including the lung, where TGF β inhibition is usually not required (Choi et al., 2021; Huch and Koo, 2015; Nikolić et al., 2017). Despite this clear species difference, no studies have yet addressed the reason behind this finding. Therefore, the precise mechanism for TGF β inhibition and its role in long-term self-renewal capacity of human epithelial cells *in vitro* warrants further study.

Despite the observation for the importance of exogenous Wnt presence, there was a clear difference in Wnt-dependence between primary FACS-purified hAT2 cells and airway cell lineages, with hAT2 cells requiring high exogenous Wnt signalling in the form of CHIR addition. The observation that differing levels of Wnt signalling dictates either alveolar or airway lineage is supported by a number of studies. Lineage tracing in the mouse has identified a subset of Wnt-responsive *Axin2*⁺ AT2 cells that have an increased capacity for regeneration of the alveolar epithelium (Frank et al., 2016; Nabhan et al., 2018). A similar population has also been proposed for the human lung (Zacharias et al., 2018). High Wnt signalling was also found to promote alveolar differentiation in hPSC-derived VAFE cells, while low Wnt encouraged airway lineages (McCauley et al., 2017). Furthermore, removal and then subsequent add-back of CHIR to hPSC-derived hAT2 organoids resulted in their expansion and maturation (Jacob et al., 2017). Therefore, Wnt activation is important in

promoting self-renewal and long-term maintenance of lung epithelial progenitor populations, particularly the hAT2 cell population, both *in vitro* and *in vivo*.

One apparent discrepancy that arose from this study was the observation that during primary culture, EpCAM⁺ lung cells were able to form both alveolar and airway organoids under high Wnt (CHIR) conditions. In contrast, when hAT2 cells were removed from the primary cell suspension during FACS enrichment using HTII-280, HTII-280⁻ cells failed to form organoids in high Wnt cultures. Instead, low Wnt signalling in the form of CHIR removal was required for primary airway organoid establishment, as has been previously reported (Sachs et al., 2019). HTII-280⁻-derived organoids established in -CHIR medium were identical to the airway organoids formed from EpCAM⁺-derived cells in complete medium; large, filled organoids comprising basal/parabasal and secretory cells. Interestingly, airway organoids were also able to form from primary EpCAM⁺ cells in the presence of WNT3A-conditioned medium, while hAOs remained small, likely due to the lower levels of Wnt signalling versus CHIR-treated cultures. The only difference between EpCAM⁺ and HTII-280⁻ cultures was the absence of hAT2 cells from the HTII-280⁻ culture system. It is possible that the presence of hAT2 cells allows for the growth of airway cell types in high Wnt conditions, either through physical cell-to-cell contact, or secretion of ligands and signalling molecules, some of which could have diluted Wnt activation. Similar scenarios have been demonstrated previously. For example, secretory cell de-differentiation to basal cells was inhibited upon co-culture of mouse basal and secretory cells, but not when secretory club cells were cultured alone (Tata et al., 2013). Furthermore, another study recently published by the Sato group also found that they could co-culture human organoids of alveolar and airway lineage in WNT3A-conditioned medium (Ebisudani et al., 2021). However, they did not investigate whether airway organoids displayed the same growth ability in the absence of hAT2 cells. The cell secretome is often an understudied but nonetheless important area of future research. It would therefore be interesting to study the secretome of cultured *in vitro* human epithelial cells of multiple lung lineages, and assess which factors may play a part in the interaction between cell lineages of alveolar and airway fate. Identification of such factors may lead to further improvements in culture conditions for human epithelial lung cells.

6.1.2. p38 MAP-Kinase inhibition and its potential role in lumen establishment in primary airway organoids

Culture of non-sorted adult human lung cells in low Wnt (-CHIR) conditions along with p38 MAP-kinase (MAPK) inhibition resulted in the formation of airway organoids (Sachs et al., 2019). Organoids were well-organised, and displayed a large, single-lumen during primary culture. Similarly, when I utilised the same culture conditions in FACS-isolated HTII-280⁺ cells, the formation of airway organoids with a large inner lumen was also achieved. However, this was in stark contrast to the large, filled spheres that arose from culture in -CHIR medium (without p38 MAPK inhibition). Similar to my own findings, another study also achieved the formation of filled airway organoids in the absence of p38 MAPK inhibition (Salahudeen et al., 2020). Furthermore, I found that upon switching late passage airway organoids from my media (-CHIR) to -CHIR/+SB2 conditions, organoids formed a lumen (Figure 3.10). This suggests that inhibition of p38 MAPK plays a role in lumen formation within airway organoids. The question therefore arises as to how p38 MAPK inhibition may be involved in lumen formation in human primary airway organoids. In epithelial cells, p38 MAPK inhibition can decrease ligand-driven degradation of the EGF receptor, allowing for increased cell proliferation, and can also act in reducing cellular senescence (Frey et al., 2006). Furthermore, p38 MAPK signalling has been implicated in the regulation of Wnt/ β -catenin signalling in embryonic mouse cells (Bikkavilli et al., 2008). However, neither of these described roles explain the formation of a lumen. The difference in organoid structure may relate to differences in cellular polarity. For example, human enteroids grown in BME form an inner lumen with appropriate apical-basal polarity, while suspension culture resulted in the loss of a lumen and correct polarity (Co et al., 2019). However, not much is currently known about the possible role of p38 MAPK inhibition in establishing cellular polarity. Additionally, I did not observe ciliated cells in airway organoids cultured in -CHIR medium, while they were present in -CHIR/+SB2 medium, perhaps suggesting another role in ciliated cell differentiation (Sachs et al., 2019).

6.1.3. Modulation of Wnt signalling allows hAT2-hAT1 differentiation *in vitro*

The molecular requirements for the full differentiation of hAT2-to-hAT1 cells have remained elusive, owing to the complex nature of the human alveolar epithelium. In chapter 4, I demonstrated that cultured hAT2 cells exhibited differentiation potential to hAT1 cells, even following 6 months of *in vitro* propagation as hAOs (Figure 4.4). Both 2D and 3D

culture of early passage (P; P2 and P3) hAOs in 10% human serum was sufficient to drive partial differentiation to hAT1 cells. This was evident by the observed loss of pro-SFTPC expression and gain of hAT1 markers such as AGER. However, only 2D-cultured, serum-supplemented early passage hAOs differentiated into elongated hAT1 cells similar to those found *in vivo*, which has been previously found following culture of freshly-isolated rat AT2 cells (Dobbs et al., 1988) and hAT2 cells derived from hPSCs (Jacob et al., 2017). This finding may reflect the *in vivo* environment of the lung alveoli, where breathing movements continuously cause stretch and relaxation of the alveolar epithelium (Li et al., 2018a). As the chemical composition of human serum is undefined, it is difficult to postulate which factors are responsible for induction of hAT2-to-hAT1 differentiation. In the mouse, an *Axin2*⁺ AT2 subset has been identified that plays a critical role during alveologenesis (Frank et al., 2016; Nabhan et al., 2018). It was found that Wnt signalling promoted *Axin2*⁺ AT2 cell growth while inhibiting their differentiation into the AT1 lineage, indicating that Wnt signalling was important for maintenance of AT2 identity. Therefore, in addition to serum-supplementation, I found that removal of exogenous Wnt activation was also sufficient to drive hAT2-to-hAT1 differentiation in 3D hAO culture. Wnt ligands have been previously reported to function as local signals, with a range of approximately one to two cells (Farin et al., 2016). In the mouse, *Axin2*⁺ AT2 cells have been found to reside in a niche consisting of single *Pdgfra*⁺ fibroblasts (Nabhan et al., 2018). These *Pdgfra*⁺ fibroblasts express *Wnt5a* and other *Wnt* genes, and maintain AT2 identity. Upon AT2 cell-division, resulting daughter cells leave the Wnt-niche, leading to loss of *Axin2* expression and differentiation to AT1 cells. Furthermore, treatment of adult hAT2 cells with XAV-939, a potent inhibitor of Wnt/ β -catenin-mediated transcription, increased the number of AQP5⁺ cells at the expense of SFTPC expression (Zacharias et al., 2018). However, resulting AQP5⁺ cells remained cuboidal in shape, indicating incomplete hAT1 differentiation. Furthermore, cells were co-cultured with MRC5 fibroblasts in commercial media, so it is not known whether the inhibition of Wnt-mediated transcription occurred directly on the hAT2 population, or indirectly through the supporting cells. Nevertheless, these studies highlight the importance of Wnt signalling in maintaining hAT2 cell identity, while a reduction in Wnt exposure caused hAT1 differentiation.

Interestingly, I observed that removal of CHIR from 6-month-old (P6) hAOs led to an increase in the number of organoids consisting of elongated AGER⁺ cells (Figure 4.4 F and 4.4 G). The same was also observed in P6 hAOs supplemented with WNT3A, but not in

serum-cultured P6 hAOs or primary hAOs (Figure 4.4). These data suggest that hAT2 cells within later-passage hAOs may be able to more readily differentiate to fully-elongated hAT1 cells, either through increased cellular plasticity or enrichment of hAT2 cells that possess increased differentiation capacity.

6.1.4. Culture of adult-derived hAOs versus recently published systems

I found that culture of FACS-purified adult hAT2 cells in chemically-defined conditions displayed a number of advantages over previously reported co-culture systems. Firstly, the utilisation of chemically-defined conditions allows for in-depth study of regulatory mechanisms for cell maintenance and differentiation. Secondly, my culture system exhibits long-term maintenance of hAT2 cell identity, with pro-SFTPC expression still observed following 6-months of culture. In contrast, culture of adult hAT2 cells with MRC5 fibroblasts exhibited limited culture capacity, low organoid forming efficiency and loss of SFTPC expression, even in multiple cells of primary culture (Barkauskas et al., 2013). This is likely due to MRC5 fibroblasts not being able to fully support hAT2 cell identity. Additionally, digested whole cell pellets were cultured overnight prior to FACS-enrichment for HTII-280⁺ cells, which may have created a cell bias. Similarly, a separate study utilising a population of 'Wnt-responsive' hAT2 cells cultured with MRC5 fibroblasts and SAGM (Small Airway Epithelial Growth Medium, Lonza) displayed similar limited long-term culture capacity (Zacharias et al., 2018).

Recently, a number of studies involving the establishment of adult-derived hAOs were published, including the publication of my own organoid system (Youk et al., 2020). An overview of the findings from each of these studies can be found in Table 6.1. Each of these published studies achieved similar maintenance of hAT2 cell identity in culture over time, but some of the findings differ to what I found during the present work. For the culture of primary tissue-derived hAT2 cells, I found that culture in cell medium containing FGF7, FGF10, EGF, NOGGIN, CHIR99021 and SB431542 was sufficient to drive hAT2 self-renewal and maintenance *in vitro* (also discussed in section 6.1). Similarly, a report by Katsura et al. utilised a comparable culture strategy, resulting in the production of folded hAOs that expressed SFTPC and HTII-280, although the p38 inhibitor BIRB796 and heparin were also included (Katsura et al., 2020). Another study by Ebisudani et al. also succeeded in establishing SFTPC-expressing folded hAOs from enriched adult hAT2 cells,

although overall organoid forming efficiency was low in comparison with other studies (0.03-0.1% in primary culture; Ebisudani et al., 2021; Table 6.1). It was also shown that cultured hAT2 cells (passage 7) exhibited some autocrine/paracrine secretion of Wnt signalling when cultured with RSPO1, although exhibited increased growth ability when WNT3A was also included (Ebisudani et al., 2021).

However, an alternative study by Salahudeen et al. developed a hAO culture system utilising a dramatically simplified media composition (Salahudeen et al., 2020). Most notably, their culture system excluded all Fgf and Wnt signalling. This was surprising, as my study and others found that Fgf and Wnt signalling were essential for primary hAT2 growth *in vitro* (Ebisudani et al., 2021; Katsura et al., 2020; Youk et al., 2020). However, the findings of Salahudeen et al. may be due to differences in initial culture composition and preparation. While my study and others utilised FACS-purified populations of HTII-280⁺ hAT2 cells, Salahudeen et al. plated entire cell suspensions of un-sorted lung tissue in droplets of BME II (a collagen/laminin mixture). These cell suspensions would include non-epithelial cell lineages, including cells of the stroma. Therefore, it is possible that the presence of multiple cell types could have provided additional supporting signals, allowing for initial organoid growth in simplified media conditions. This culture system was found to support both alveolar and airway organoids, but the authors did not report the ratio of the two organoid types. Purified hAOs were later established from EpCAM⁺Lysotracker⁺ hAT2 cells derived from mixed cultures, and formed organoids for up to 4 months. However, unlike the folded hAO structures that have been reported previously, many of the resulting hAOs were solid spheres, with unusual distribution of HTII-280 staining, although there is no suggestion as to whether this may be due to improper cell polarity. Addition of Wnt signalling in the form of WNT3A and RSPO1 was found to increase the growth capacity of hAOs from purified cultures, in accordance with previous work and the present study (Ebisudani et al., 2021; Katsura et al., 2020; Youk et al., 2020).

Throughout all of these studies, it is evident that culture with growth factors and signalling molecules associated with lung development or alveolar regeneration can lead to proliferation and maintenance of hAT2 cells as *in vitro* 3D-organoids. However, differences in starting cell populations or culture composition can cause variations in organoid forming efficiency, long-term maintenance and hAO cell composition.

Table 6.1. Comparison of culture methods for adult hAO production in chemically-defined conditions.

Isolation strategy	3D-culture matrix	Media composition (main factors)	Primary organoid forming efficiency	hAO culture capacity	Reference
FACS enrichment from primary distal lung tissue (EpCAM ⁺ HTII-280 ⁺)	Matrigel (5000 cells/ 20 μ L in 48-well plate)	CHIR99021, FGF7, FGF10, NOGGIN, EGF, SB431542	~5-9%	> 10 months	(Youk et al., 2020,current study)
FACS enrichment from primary distal lung tissue (EpCAM ⁺ HTII-280 ⁺)	Matrigel (1000 to 3000 cells/ 50 μ L)	CHIR99021, FGF10, NOGGIN, EGF, SB431542, BIRB796*, heparin	~11-13%	At least 6 months	(Katsura et al., 2020)
1) Direct plating of whole-tissue-derived cell suspension. 2) EpCAM ⁺ MACS enrichment. 3) EpCAM ⁺ Lysotracker ⁺ FACS-enrichment from established organoids.	BME II (10 volumes to whole cell pellet, or 1000 cells/5 μ L for EpCAM ⁺)	NOGGIN, EGF, A83-01** (also tested WNT3A, RSPO1, WNT-C59***)	Not disclosed	~ 4 months	(Salahudeen et al., 2020)
FACS enrichment from primary distal lung tissue (EpCAM ⁺ HTII-280 ⁺)	Matrigel (30,000 cells/well in 48-well plate)	Afamin-WNT3A, EGF, NOGGIN, RSPO1, A83-01, IGF1, FGF2, FGF7, FGF10, NRG1	0.03–0.1% (10-30 organoids per well)	> 8 months (only in presence of NRG1)	(Ebisudani et al., 2021)

*BIRB796 is a p38 MAPK inhibitor, **A83-01 is a TGF β inhibitor, *** WNT-C59 is a serum-containing fibroblast-conditioned medium.

6.1.5. Loss of pro-SFTPC expression in hAOs following 6 months of culture

During the continuous culture of bulk EpCAM⁺ adult lung cells, I observed that a proportion of organoids began to arise that did not stain for any tested markers following IF analysis. Due to the marked decrease in the number of hAOs (pro-SFTPC⁺) coinciding with an increase in the number of “undetermined” organoids, it is possible that the undetermined cell population was arising directly from the hAT2 population. A similar loss of hAT2 marker expression was also observed in FACS-enriched hAOs during later culture. Although my culture system supported the maintenance of FACS-enriched adult hAT2 cells for at least 6 months (and up to 10 months) of continuous culture, longer than any previously reported *in vitro* system (Barkauskas et al., 2013; Ebisudani et al., 2021; Katsura et al., 2020; Salahudeen et al., 2020; Zacharias et al., 2018), I observed that the number of pro-SFTPC⁺ hAOs decreased over time. Cells within these hAOs often still expressed HTII-280, but due to the lack of surfactant production or other standardised hAT2 markers they could no longer be considered as hAT2 cells. Additionally, differential expression of HTII-280 on the surface of hAT2 cells both *in vitro* and *in vivo*, in combination with its still unknown role makes it unreliable as a hAT2 marker *in vitro* (Gonzalez et al., 2010; Korogi et al., 2019). Furthermore, hAO forming efficiency slowly decreased over time. Although loss of SFTPC expression was not carefully assessed in alternative hAO systems during long-term culture, some did report an overall reduction in forming efficiency over time (Ebisudani et al., 2021). One possible reason for the observed loss of hAT2 identity and self-renewal capacity over time may be that the current culture conditions do not fully support the hAT2 cell population for long-term maintenance. Studies of human alveolar epithelial cells are still in their infancy, therefore a number of molecular mechanisms involved in their maintenance may await discovery. However, there are a number of alternative reasons that could explain the loss of surfactant production or hAT2 identity over time.

Firstly, the telomere length in isolated adult hAT2 cells may limit their expansion ability *in vitro*. It is well reported that telomere shortening is associated with age-related cellular senescence (Childs et al., 2015; Victorelli and Passos, 2017). Additionally, environmental factors such as smoking or pollution exposure can lead to accelerated telomere shortening in lung tissues (Astuti et al., 2017). In the lung epithelium, the hAT2 population in particular has been shown to exhibit pronounced telomere shortening in smokers and in

patients suffering with diseases such as IPF (Alder et al., 2008; Alder et al., 2015; Courtwright and El-Chemaly, 2019; Kropski et al., 2015). Furthermore, telomere-associated mutations have been linked to some forms of IPF (Courtwright and El-Chemaly, 2019). Telomere length or cellular senescence were not assessed during the present study, therefore their role in the loss of hAT2 cell identity following 6-month culture is currently unknown, but should be addressed in future. Secondly, the age of the donor from which hAT2 cells were derived may influence surfactant production and culture maintenance. Analyses of aged human lungs (age >60 years) versus young lungs (age <40 years) have revealed a reduction in the number of hAT2 cells with age, as confirmed through analysis of pro-SFTPC staining (Lee et al., 2021). However, it is not clear whether additional hAT2 markers were assessed, and the authors did not address the possibility that the lack of pro-SFTPC could have been due to a reduction in surfactant processing or secretion as opposed to a complete loss of the hAT2 population. One of the difficulties of working with human adult lungs is the variable range of ages and lung statuses of individual donors, which are difficult to control. Due to the lung being directly linked to the environment, even a relatively healthy individual may have been exposed to environmental factors such as high air pollution or passive smoking, even if they were not a smoker themselves. The effect of such factors on hAT2 and other lung cell populations are not well known. All donors featured in the present study were aged between 52 and 74 (median age 57), with 4 out of 9 being classed as current smokers (Chapter 2, Table 2.2). Organoid forming efficiency and passage ability varied between all samples, as would be expected due to the diverse tissue backgrounds (Chapter 3 and 4). It is therefore possible that hAO culture capacity could correlate with patient age or smoking-status, although hAOs from a wider range of patients would need to be investigated before this could be confirmed.

Genetic lineage tracing studies in mouse models have indicated that AT2 cells have the potential to be a stem cell population, although it is debated as to whether all AT2 cells possess the same capacity for self-renewal and differentiation (Nabhan et al., 2018; Zacharias et al., 2018). Compared with stem cell populations of other tissues such as the intestines, AT2 cells are considered to be generally quiescent, with turnover estimated as once every 4 months in a rare subpopulation of *Axin2*⁺ mouse AT2 cells (Nabhan et al., 2018). However, there is currently little evidence to suggest that hAT2 cells in adult human lungs (and indeed the mouse lung) are true stem cells i.e., possess the capacity for self-renewal and differentiation *indefinitely*. Therefore, they may instead represent a long-lived,

epithelial progenitor population as opposed to a bona fide stem cell. It could be that when hAT2 cells are taken from aged human lungs and placed into culture, the resulting expansion and proliferation that is observed during primary and early culture occurs at a much faster rate than would transpire *in vivo*. This could potentially lead to accelerated telomere shortening and cellular senescence, or eventual loss of *SFTPC* expression and surfactant secretion in already aged hAT2 cells. Accelerated cellular ageing could also explain the observed reduction in hAO forming efficiency over time. For example, in a recent study utilising paediatric and adult lung samples, it was found that paediatric airway epithelial cells exhibited higher colony forming ability, increased proliferation and improved *in vitro* growth than their adult counterparts (Maughan et al., 2020).

Therefore, as opposed to an omission of a specific signalling factor, the loss of hAT2 identity *in vitro* after long-term culture may be a result of the intrinsic biology of hAT2 cells derived from already aged or smoke-damaged lungs. For my study, I unfortunately did not receive samples from a large enough range of ages or smoking statuses to address whether patient age or smoking status could influence *in vitro* growth capacity of hAT2 cells. Therefore, in future it would be interesting to compare culture capacity and maintenance of hAT2 cells from young and old lungs, and from age-matched lungs of smokers versus non-smokers. Furthermore, analysis of telomere length and cellular senescence in early and late passage hAOs from a range of donor backgrounds warrants additional study. This would allow for a better understanding of the effect of age or environmental factors on hAT2 cell maintenance and surfactant production *in vitro*.

6.2. Aberrant epithelial cell types co-expressing alveolar and airway transcripts are present within human IPF lungs

I found that the distal lungs of IPF patients comprised a number of aberrant cell types not observed in healthy lungs, including an epithelial population of SOX2⁺ pro-SFTPC⁺ cells localised to honeycomb cysts. This finding is consistent with recent studies employing single cell RNA sequencing (scRNA-seq; Adams et al., 2020; Habermann et al., 2020; Xu et al., 2016). scRNA-seq studies have aimed to elucidate the diverse transcriptional signatures present within epithelial populations of human distal IPF lungs. In 2016, Xu et al. first reported the presence of “indeterminate” cell types within the EpCAM⁺ population

of human IPF lungs, which were named and characterised based on their mixed alveolar (hAT2 and hAT1) and airway transcriptional signature (Xu et al., 2016). Two further cell clusters were also identified in distal IPF lungs; secretory club/goblet cells and basal cells. Furthermore, both SOX2 and TP63 were predicted to be upstream regulators of “indeterminate cells”. SOX2 expression was also observed in some cells expressing RNAs normally restricted to hAT2 cells, and was frequently co-expressed with SOX9, highlighting potential disruption in proximal-distal patterning. Meanwhile, “normal” hAT2 cells were only observed in healthy lungs, with no cells co-expressing alveolar and airway transcripts, as I also found during the present study (Travaglini et al., 2020; Xu et al., 2016). This work by Xu et al. highlights the abundance of cells expressing airway-related transcripts present within EpCAM⁺ cell populations of human IPF lungs. More recent studies have further probed the presence of airway-like cells in distal IPF lungs. Both Adams et al. and Habermann et al. identified a population of KRT5⁺KRT17⁺ cells in IPF peripheral lung tissue, with the former referring to these cells as “basaloid” cells (Adams et al., 2020; Habermann et al., 2020). It is difficult to determine whether the aberrant cell types observed in the Xu et al. study are the same as basaloid cells, or whether they represent slightly different cell lineages or states. Therefore, further work is required to assess the physiological relevance and phenotypic characteristics of these cell types. However, it is clear that IPF disease processes result in the appearance of aberrant epithelial cell types of unknown lineage.

6.2.1. Origin of aberrant epithelial cell types in human IPF lungs

The origin of airway-like cells in distal IPF lungs has been widely debated. One suggestion is the possibility that upon damage, airway cells migrate down from the distal airways into the alveoli in order to help with regeneration, as has been observed for the mouse (Kumar et al., 2011; Vaughan et al., 2015; Zuo et al., 2015). A number of reports have suggested a population of Sox2-derived Krt5⁺ airway cells that can migrate to distal alveolar regions upon damage in order to repair the epithelial barrier in mouse lungs (Kumar et al., 2011; Ray et al., 2016; Vaughan et al., 2015; Xi et al., 2017; Zuo et al., 2015). Furthermore, it was reported that a rare population of human SOX9⁺ basal cells were able to give rise to alveolar and bronchiolar epithelium when transplanted into injured mouse lungs (Ma et al., 2018). These studies highlight the ability for resident Krt5⁺ airway cell populations to not only migrate to distal alveolar regions, but also potentially give rise to alveolar lineages.

Additionally, Flk1/KDR⁺ secretory club cells have also been shown to exhibit differentiation plasticity to AT2 cells in both mouse and human lungs, respectively (Choi et al., 2021). Such findings again suggest the possibility of AT2 cells arising from airway lineages under certain conditions.

However, another possible origin for the bronchiolisation of human IPF lungs, and the mechanism I suggest based off my current findings, could be the resident hAT2 cell population itself. Upon alveolar injury, the mouse lung has demonstrated a remarkable regenerative capacity, with AT2 cell populations rapidly proliferating and differentiating to AT1 cells to successfully repair the damage (Barkauskas et al., 2013). However, chronic injury or inefficient repair can disrupt this regenerative process, leading to tissue dysfunction and disease. A number of recent studies have reported the presence of an AT2-AT1 intermediate cell state that emerges during injury repair in murine lungs (Choi et al., 2020; Kobayashi et al., 2020; Strunz et al., 2020). Choi et al. demonstrated that injury-induced Il-1 β promoted AT2-AT1 differentiation via a primed cell state and transient progenitor (termed “damage-associated transient progenitor; DATP). Meanwhile, chronic inflammation impaired full maturation to AT1 cells, resulting in an accumulation of Krt8⁺/Cldn4⁺ DATP cells via a Hif1 α -mediated glycolysis pathway. In the normal lung, Krt8 is a marker of luminal cell types (Rock et al., 2011). Similar populations of cells have also been observed in the distal lungs of IPF patients (Choi et al., 2020; Kobayashi et al., 2020). I found that hypoxic culture through chemical-stabilisation of HIF1 α led to induction of SOX2 expression in hAT2 cells. Interestingly, glycolysis is known to maintain pluripotency in iPSCs, and activates a number of factors including SOX2 (Spyrou et al., 2019). Therefore, Hif1 α -mediated glycolysis may be key in triggering increased hAT2 plasticity upon injury, and should be studied in more detail.

A similar airway-like signature was also achieved in hAT2 cells upon treatment with the inflammatory cytokines IL-1 β and TNF- α *in vitro*. Resulting cells share similar signatures to DATPs, which express multiple airway related markers including Krt8, Krt17 and Itgb4 (Choi et al., 2020; Kobayashi et al., 2020). Similarly, Il-13 was recently found to induce a Krt5 airway gene signature in murine AT2 cells *in vitro* (Glisinski et al., 2020). IL-13-treatment in hAT2 cells exhibited a loss of SFTPC expression, but KRT5 expression was not observed. However, this could be due to the culture system, which employed co-culture with MRC5 fibroblasts as opposed to chemically-defined conditions.

It is therefore unknown whether IL-13 was having a direct effect on the hAT2 cells, or indirectly through the fibroblasts. Likewise, an air-liquid interface (ALI) culture system using iPSC-derived hAT2 cells led to induction of airway-related gene signatures upon culture in a multi-cytokine culture cocktail (Schruf et al., 2020). Additionally, a recent pre-print from the Peng and Chapman labs identified that hAT2 cells undergo trans-differentiation into metaplastic KRT5⁺ cells when cultured with adult human lung mesenchyme (AHLM; Kathiriya et al., 2020). A hAT2-basal cell intermediate was observed prior to full-differentiation, which may be similar to the SOX2⁺ pro-SFTPC⁺ cells I discovered *in vitro* following 7-days of hypoxic culture. Although it was not addressed why AHLM from healthy human lungs had this effect on hAT2 cells *in vitro*, it is clear that hAT2 cells possess the ability to differentiate into airway-like or basal-like cells under certain conditions. Interestingly, the authors also demonstrated that transplantation of hAT2 cells into fibrotic mouse lungs resulted in the same trans-differentiation to KRT5⁺ cells as was observed *in vitro*. The proportion of hAT2 cells undergoing trans-differentiation was increased upon co-transplantation with AHLM. These studies mark hAT2 cells as a key potential origin for the appearance of airway-like cells in the distal lungs of IPF patients.

6.2.2. Hypoxia-induced Notch signalling and SOX2 expression in hAT2 cells

Previous studies of hypoxia in IPF have mainly focussed on fibroblast populations, with limited data available on its effect on lung epithelial cells, such as hAT2 cells. However, with the current consensus suggesting that hAT2 cells are a major cell type involved in IPF initiation and progression, it was important to assess IPF-related hypoxia on hAT2 cells (Lawson et al., 2004; Nureki et al., 2018; Parimon et al., 2020; Sisson et al., 2010). Additionally, a hypoxic subpopulation of hAT2 cells have been identified in human IPF lungs (Xi et al., 2017). In this study, I have demonstrated that upon chemical-induction of HIF1 α -mediated hypoxia, hAT2 cells undergo aberrant differentiation to SOX2-expressing airway-like cells. These resulting cells exhibited increased proliferation compared with SOX2⁻ hAT2 cells, and closely resembled some of the aberrant pro-SFTPC⁺SOX2⁺ epithelial cells observed in distal IPF lungs. Similar SOX2-induced proliferation has been observed in a number of human cancers, which are often also associated with hypoxia (Chen et al., 2008; Chou et al., 2013; Liu et al., 2018; Maurizi et al., 2018; Takeda et al., 2018). SOX2 expression is associated with poor prognosis in lung cancer patients, where

it promotes excess proliferation (Chou et al., 2013). Furthermore, HIF-dependent demethylation of SOX2 mRNA has been found to induce an endometrial cancer stem-like cell phenotype *in vitro* (Chen et al., 2020). This finding was observed under both low oxygen (2%) and chemical-stabilisation of HIF1 α with cobalt chloride (CoCl₂). Meanwhile, in gastric cancer, SOX2 was found to enhance HIF1 α promoter activity in order to regulate glucose metabolism in human cell lines (Gan et al., 2018). As I have described previously, glycolysis is known to maintain pluripotency in iPSCs, and activates a number of factors including SOX2 (Spyrou et al., 2019). Interestingly, DATPs that occur as a result of lung regeneration in the mouse also express SOX2, and transcriptionally resemble cells that are not only observed in human IPF lung tissue, but also in patients with lung adenocarcinoma (Choi et al., 2020). Therefore, while induction of the DATP state is essential for alveolar regeneration following injury, chronic damage can potentially lead to hypoxia and SOX2 expression, which can work co-operatively in promoting cellular proliferation and plasticity. Disease processes in IPF initiation and progression may therefore employ similar processes to lung cancer.

I found that inhibition of Notch signalling reduced the number of SOX2⁺ hAT2-derived cells in chemically-stimulated hypoxia cultures. Notch signalling has been found to be increased in human IPF lungs and experimental models of lung fibrosis (Aoyagi-Ikeda et al., 2011; Hu and Phan, 2016; Kiyokawa and Morimoto, 2020; Wasnick et al., 2019). IF analysis revealed an increase in nuclear HES1 staining in IPF hAT2 cells, both in the present study and elsewhere (Wasnick et al., 2019). Furthermore, inhibition of *NOTCH1* in human IPF precision-cut lung slices (PCLS) improved surfactant processing (Wasnick et al., 2019). Furthermore, SOX2-induction has previously been implicated downstream of Notch and hypoxia in certain cancers (Batchuluun et al., 2017; Li et al., 2018b; Seo et al., 2016; Wu et al., 2019). For example, a hypoxia-Notch-SOX2 signaling axis was observed in cancer stem cells of ovarian cancer (Seo et al., 2016). Following influenza infection in the mouse, Hif1 α has been found to drive Notch signalling and expansion of Krt5⁺ basal-like cells. A host of other studies have also implicated increased Notch signalling in the induction of SOX2 in multiple systems (Gustafsson et al., 2005; Seo et al., 2016). Finally, in the human, single-cell transcriptional profiling of hAT2s from fibrotic lungs highlighted a hypoxic subpopulation exhibiting activated Notch signalling, reduced SFTPC and trans-differentiation to a KRT5⁺ basal cell-like state (Xi et al., 2017). The authors isolated hAT2 cells based on their HTII-280⁺ status, although as I have shown in the current study,

HTII-280 in fibrotic IPF-lungs marks a number of cell types or states (Figure 5.1B and 5.1C). Although SOX2 expression was not assessed, its presence was likely based on the presence of other airway and basal cell markers.

Blocking Notch signalling using the γ -secretase inhibitor DAPT reduced the overall number of SOX2⁺ hAOs. hAT2 cells and mouse AT2 cells have been shown to express Notch receptors on their cell surface, although they are not known to express Notch ligands (Choi et al., 2021). As hAOs in complete medium consist entirely of hAT2 cells, the question arises as to what the source of the Notch ligands could be. In *Drosophila melanogaster*, it has been found that a blood cell type termed a crystal cell expresses elevated levels of a Hif α ortholog under conditions of normal oxygen. This Hif α ortholog can activate full-length Notch receptor signalling via a noncanonical, ligand-independent mechanism. This same mechanism was also observed under hypoxic stress, in which the Hif α ortholog directly binds to the Notch receptor. Although this same mechanism has not yet been proven in mammals, the observation of up-regulation of Hif α protein in well-oxygenated environments indicates that it could be conserved in mammals (Mukherjee et al., 2011).

Hypoxia is a complex process that can involve multiple signalling pathways and interactions (Lee et al., 2019). Although I have demonstrated that Notch signalling may play a part in eliciting the downstream effects of HIF1 α stabilisation in the aberrant differentiation of hAT2 cells to SOX2⁺ airway-like cells, the possibility of other mechanism involvement cannot be overlooked. For example, it is well reported that hypoxia can lead to the nuclear translocation of YAP, another signalling pathway found to be increased in hAT2 cells of IPF lungs (Gokey et al., 2018). In IPF, YAP acts to increase cell proliferation and migration, and may contribute to the pathogenesis of IPF by inhibiting epithelial differentiation (Gokey et al., 2018). Additionally, YAP has previously been found as an important regulator of AT2 to AT1 differentiation, with YAP activation leading to increased AT1 marker expression and total number of AT1 cells (Gokey et al., 2021; Liu et al., 2016). Hypoxia is known to activate NF κ B activity, a major signalling pathway involved with inflammation (van Uden et al., 2008). Hypoxia has also been known to activate Wnt signalling in cancers of multiple tissues, including the lung and liver (Hong et al., 2017; Xu et al., 2017; Zhang et al., 2013). However, of particular interest is the glycolysis pathway, due to its role in inducing cellular plasticity and pluripotency. The

molecular mechanisms underlying IPF initiation and progression are therefore complex, and it is likely that multiple signalling pathways interact across various cell compartments in order to achieve the mass fibrosis and epithelial remodelling that is observed.

A chemical inducer of hypoxia (deferrioxamine, DFO) was utilised in establishing a hypoxic *in vitro* environment. DFO acts as an iron chelator, which prevents degradation of HIF1 α by sequestering iron from prolyl hydroxylases (PHDs) under an oxygen rich environment (Guo et al., 2006; Triantafyllou et al., 2006). This is clearly different to the process that occurs under low oxygen conditions, and creates an artificial system. Although chemical inducers such as DFO and cobalt chloride are commonly used and well-established as hypoxia mimics *in vitro*, it will be important to also establish whether the same effects observed during the present study also occur under low oxygen conditions. In particular, I observed that DFO-treated hAOs lost their self-renewal capacity upon passage to single cells, even when re-plated in growth factor-enriched complete medium. It is possible that 7-day culture with DFO could cause a decrease in cell viability or culture capacity, and may not be directly linked to hypoxia itself. The question therefore arises as to whether the same effect on cell viability would have been observed if the hAOs were cultured under low oxygen conditions. For example, iron plays a critical role in proliferation, and iron deficiency results in G1/S cell cycle arrest and apoptosis, a factor that could have played a part in the observed failure for DFO-treated cells to re-form organoids (Fu and Richardson, 2007). Unfortunately, due to time constraints, I was unable to investigate apoptosis on DFO-treated hAOs, or the effect of low oxygen on hAT2 cell identity and self-renewal capacity. However, the effects of low oxygen versus chemical-inducers of hypoxia on viability and SOX2-induction in hAT2 cells needs to be addressed.

6.2.3. *IL-1 β and TNF- α -mediated induction of airway cell fate in hAT2-derived hAOs*

Multiple reports have suggested that various inflammatory cytokines are present at increased levels in the bronchoalveolar lavage fluid (BALF) and sputum of IPF patients, including IL-1 β and TNF- α (Kolb et al., 2001; Oikonomou et al., 2006; Piguet et al., 1993; Schruf et al., 2020). Furthermore, IL-1 β is responsible for priming *IL1R1*⁺ AT2 cells towards differentiation to AT1 cells upon lung injury in the mouse, with chronic inflammation linked to an accumulation of intermediate DATPs and a stall in AT1

differentiation (Choi et al., 2020). Interestingly, DATPs share similar molecular signatures to aberrant basaloid cells in IPF lungs (Choi et al., 2020; Kobayashi et al., 2020). Therefore, I aimed to investigate the effect of pro-inflammatory cytokines on the cellular behaviours of hAT2 cells. Upon culture of primary hAT2 cells in complete medium supplemented with either IL-1 β or TNF- α , organoids arose that no longer expressed hAT2 markers such as pro-SFTPC, but instead expressed airway cell markers (Chapter 5C). This finding is in accordance with a number of recent studies. As stated above, DATPs possess similar molecular signatures to IPF basaloid cells, with expression of a number of airway-related markers including *KRT8*, *KRT17* and *ITGB4* (Adams et al., 2020; Choi et al., 2020; Habermann et al., 2020; Kobayashi et al., 2020). Additionally, I observed a number of cells within IPF parenchymal honeycombs that displayed heterogenous marker presence, including airway-like cells expressing TP63 and SOX2 but no pro-SFTPC (Figure 5.1).

As described in Section 6.2.1, IL-13 was found to reduce SFTPC expression in adult-derived hAT2 organoids when co-cultured with MRC5 fibroblasts (Glisinski et al., 2020). Furthermore, culture of iPSC-derived hAT2 cells in ALI culture with a cytokine cocktail containing nine separate cytokines, including IL-1 β and TNF- α , resulted in a reduction in alveolar marker expression and an increase in airway-related genes such as *SOX2*, *TP63* and *KRT5* (Schruf et al., 2020). The authors proposed that their cytokine cocktail mimicked IPF conditions due to the ability of the cocktail to induce collagen I formation in primary human lung fibroblasts. Although the authors found that removal of IL-1 β or TNF- α alone was not sufficient to reduce the induction of airway transcripts, this could be due to synergistic interactions between the remaining cytokines. However, another study that utilised IL-1 β in the culture of primary adult hAT2 cells as hAOs did not report an induction of airway transcripts, although this could be due to the relatively short culture time compared with previous studies (IL-1 β added from day 0 to day 7; Katsura et al., 2020).

It was interesting to observe that TNF- α cultures comprised organoids co-expressing markers such as KRT5, SOX2 and TP63, while IL-1 β -treated hAT2-derived organoids only expressed KRT5. This raises the possibility that IL-1 β -treated culture may be preferentially supporting outgrowth of parabasal-like cells, which are known to express KRT5 but not TP63 (Hynds and Janes, 2017). Expression of KRT8 was not assessed. It is not known why these organoids do not also exhibit SOX2 expression. Additionally, no SCGB1A1⁺ secretory club cells were observed throughout any of the IL-1 β or TNF- α -treated cultures.

Unlike hypoxia-cultured hAOs, IL-1 β and TNF- α -treated hAOs did not comprise cells that co-expressed alveolar and airway-related markers. However, this could be due to the difference in treatment timing between hypoxia and cytokine cultures. While hypoxia-cultured hAOs were treated with DFO for only 7 days (D; D14-D21), cytokine-treated hAOs were cultured with IL-1 β or TNF- α continuously until analysis (D0-D21/28). This long-term, continuous culture with inflammatory cytokines likely mimics chronic inflammation. It is therefore possible that the longer culture time in the presence of high cytokine concentrations could have driven hAT2 cells to full-differentiation to an airway-like fate. Hence analysis at an earlier time-point would be required to assess whether cytokine-treated hAOs go through a hAT2-airway cell intermediate. Furthermore, the heterogenous nature of the organoids may reflect an underlying heterogeneity in hAT2 response to cytokines or HIF1 α -stabilisation. For example, only a subset of mouse AT2 cells express IL1R1 (Choi et al., 2020). However, this would have to be carefully assessed.

6.2.4. Lack of hAT2 cells and abundance of airway cell types in IPF-derived patient organoids

Culture of FACS-enriched HTII-280⁺ and HTII-280⁻ cells from epithelial cells of IPF patients resulted in the formation of very few hAOs, with hAOs established from only one of the five patient samples analysed. The lack of hAOs from IPF patient lungs likely corresponds with the severity of the disease. All IPF patients featured in this study were already in the final stages of the disease, where lung transplantation was the final option after all other treatment options had been exhausted. The end-stage nature of the disease, coupled with heavy smoking in some patients, may have accounted for the poor survivability of hAT2 cells in culture. For example, while hAT2 cells generally displayed viability of 80-90% when derived from healthy donor tissue, this number was dramatically reduced to around 30% for IPF patients (viability was assessed by Trypan Blue exclusion in cells). The inability of IPF-derived hAT2 cells to form hAOs, even within a growth factor-enriched environment, highlights that the cells have already been intrinsically damaged.

Another potential reason for the lack of hAT2 cells in patient-derived IPF epithelial organoids is due to the presence of aberrant cell types expressing airway transcripts. Instead of the formation of hAOs, IPF-derived HTII-280⁺ cells form airway organoids in 3D-

culture. However, no organoids were observed in culture that co-expressed airway and alveolar markers. From IF staining of IPF lung tissue, it was clear that populations of aberrant alveolar/airway cell types were present, with many of these cells also staining for HTII-280 on their surface. Therefore, it is highly likely that these cells were responsible for the formation of airway organoids in HTII-280⁺ cultures. However, organoids expressing both alveolar and airway markers at the protein level were not observed, but this may be due to organoid analysis not occurring until 21 days after plating. It is therefore likely that any cells expressing both alveolar and airway markers differentiated fully to airway cell types during culture, as was observed in a proportion of organoids from hypoxia-treated hAO cultures. Interestingly, analysis of freshly isolated HTII-280⁺ IPF cells prior to culture revealed that *SFTPC* expression was maintained at the gene level, a finding which was also observed in cultured (P1) cells. Despite this observation, pro-SFTPC was not observed at the protein level. The question therefore arises as to why there is a discrepancy in SFTPC expression between the gene and protein level. Although I could not address this during the present study, the lack of pro-SFTPC could be due to a block in proper processing/secretion of the protein. In future, it would be interesting to establish and characterise organoids from early-stage IPF patient lungs, and compare these to mid- and late-stage disease. This could potentially lead to the identification of biomarkers that could be used to diagnose IPF at an earlier stage, in addition to a better understanding of hAT2 dysregulation during disease progression.

6.3. Limitations and Future work

6.3.1. *Lack of sequencing for IPF-derived tissue and organoids*

One of the attractive benefits of utilising organoids derived from patient tissues is the possibility of capturing the disease-specific and patient-specific gene expression and genomic landscape. Multiple studies of various tissues have also demonstrated that organoids have the capacity to recapitulate disease-related processes *in vitro* (Broutier et al., 2017; Lancaster and Huch, 2019). In this work, I established organoids from the lungs of patients with severe cases of IPF. Although these organoids led to a number of findings, including loss of hAT2 cells and increase in airway cell types, one of the major limitations of this work is the lack of transcriptional phenotyping of the IPF-derived organoids and

tissue. Without such profiling, it is difficult to make conclusions on whether particular findings are truly due to disease processes. As IPF material was limited, I was unfortunately unable to perform bulk or single-cell transcriptional profiling on IPF-derived lung tissue or organoids. In future, it will be important to carefully phenotype IPF lung tissue samples and their resulting organoids, allowing comparisons to be made and similarities to be identified. This will allow us to determine whether patient-derived IPF organoids can maintain epigenetic disease signatures. Furthermore, transcriptional profiling of IPF lung tissue and organoids could enable improved *in vitro* disease culture conditions, as IPF-related pathways could be modulated accordingly to better mimic the *in vivo* disease environment. For example, while the TGF β inhibitor SB431542 was used for long-term maintenance of both healthy and IPF organoids, TGF β is active in IPF *in vivo* (Meng et al., 2016; Yue et al., 2010).

6.3.2. Use of DFO as a hypoxia mimetic

During this study, I utilised DFO as a chemical inducer of hypoxia *in vitro*. While the use of hypoxia-mimetic agents such as CoCl₂ and DFO for the induction of hypoxia and HIF1 α stabilisation *in vitro* has been well reported, there are a number of potential issues with their use (Guo et al., 2006; Pavlacky and Polak, 2020; Triantafyllou et al., 2006; Wu and Yotnda, 2011). For example, DFO functions as an iron chelator, which can bind free iron in a stable complex, resulting in the prevention of the iron subsequently entering chemical reactions. As iron plays a critical role in many cellular processes, the use of iron-chelators such as DFO could create undesired interference in a number of various pathways. Furthermore, while hypoxia resulting from low oxygen concentrations increases reactive oxygen species (ROS), DFO can be used to reduce ROS levels. This highlights that the mechanism and outcome of DFO treatment may differ to true, low oxygen-induced hypoxia and HIF1 α stabilisation. Therefore, it is difficult to ascertain whether the findings obtained from DFO treatment of hAT2 cells, such as SOX2 activation, are truly due to hypoxia and HIF1 α stabilisation, or whether they are the result of an alternative mechanism. It will be vital that future work addresses this uncertainty by culturing hAT2 cells under low oxygen conditions. Although I have shown that culture of human lung airway cells in a regular incubator set to 5% oxygen was not sufficient to up-regulate downstream hypoxia genes versus controls, this may be due to improper maintenance of the correct oxygen concentration. As an alternative, a hypoxia chamber could be used which can more

accurately control low oxygen concentrations (Wu and Yotnda, 2011). Furthermore, cell culture medium should be de-gassed prior to use, which reduces oxygen concentration in the medium, and plates should undergo limited handling so that low oxygen concentrations can be maintained (Wu and Yotnda, 2011). Such measures will be important in determining the effect of low oxygen concentration and HIF1 α stabilisation on hAT2 identity.

6.3.3. Current drawbacks to adult hAT2-derived hAO system

Although I successfully established a chemically-defined *in vitro* organoid system for the culture and maintenance of adult hAT2 cells, there are still a number of issues that need to be addressed in the future. Firstly, adult hAOs do not produce the full-spectrum of alveolar epithelium (i.e., hAT2 and hAT1 cells), likely due to differences in signalling requirements such as described previously (Section 6.1.3). This has so far made it difficult to assess hAT2 and hAT1 interactions. However, this finding is not restricted to adult hAOs, with hAT2 cells from both hPSCs/iPSCs and embryonic lungs failing to maintain morphologically distinct hAT2 and hAT1 cells within the same organoid/culture system (Barkauskas et al., 2013; Ebisudani et al., 2021; Jacob et al., 2017; Katsura et al., 2020; Nikolić et al., 2017; Salahudeen et al., 2020; Yamamoto et al., 2017; Youk et al., 2020; Zacharias et al., 2018). This is in stark contrast to mouse alveolar organoids that possess both AT2 cells and morphologically distinct AT1 cells, although this is only observed in co-culture systems with stromal cell populations (Barkauskas et al., 2013; Choi et al., 2021). Such a finding is likely due to differences in molecular requirements of AT2 cells between the mouse and human.

Secondly, current hAO systems, including my own, lack complete cellular interactions. This is a particularly important consideration when modelling complex diseases such as IPF, which likely exhibit cell-cell interactions between multiple cell types, including cells of the epithelium, stroma and immune system. Future work could involve developing optimised conditions that allow hAT2 cells to be co-cultured with multiple cell types, including immune cell populations and cells of the stroma. However, this may prove challenging, owing to potential differences in culture requirements. Despite this, there are already a few studies that have demonstrated successful assessment of interactions between epithelial and immune cells in organoid culture, particularly for the intestine (Cattaneo et al., 2020; Chakrabarti et al., 2018; Holokai et al., 2019; Schreurs et al., 2021). Additionally,

hAOs lack the tissue architecture observed *in vivo*. Future advances in engineering strategies such as “lung-on-a-chip” technology may be able to address this issue, possibly even allowing the co-retention of alveolar and airway cell types in distinct epithelial compartments. Finally, long-term maintenance of SFTPC expression in hAT2 cells *in vitro* appears to be a common problem across many hAO systems. However, further study is required to assess the effects of age and environmental factors on surfactant production and long-term maintenance of cultured, adult-derived hAT2 cells.

Regardless of these challenges, it is an exciting time for the field of human lung biology.

CONCLUSIONS

1. Primary adult hAT2 cells can be propagated and maintained as self-renewing alveolar organoids from both EpCAM⁺ and EpCAM⁺ HTII-280⁺ cells upon the activation of FGF7 and Wnt signalling, and the inhibition of TGFβ.
2. In contrast to hAOs, airway organoids derived from EpCAM⁺ HTII-280⁻ human distal lung epithelial cells did not require exogenous Wnt signalling for their self-renewal.
3. Cultured hAT2 cells can be maintained for at least 6 months in culture, are functionally mature and exhibit differentiation capacity to hAT1 cells upon modulation of Wnt signalling, even during late culture.
4. hAOs could be used for a number of downstream applications including gene-editing and viral infection studies.
5. IPF lungs comprise a number of aberrant cell types expressing both alveolar and airway transcripts, and EpCAM⁺ cells derived from IPF lungs mainly form airway organoids *in vitro*, with very few hAOs present, likely reflecting aspects of the *in vivo* environment.
6. Hypoxia signalling is increased within HTII-280⁺ fraction of IPF lungs, and DFO-stimulated chemical induction of hypoxia in hAOs results in the reduction of pro-SFTPC-expressing cells and induction of the airway fate transcription factor SOX2. Some cells co-expressed pro-SFTPC and SOX2, resembling aberrant cell types *in vivo*.
7. Notch signalling may function downstream of hypoxia, as blocking the Notch pathway in DFO-treated hAOs reduced the number of SOX2-expressing cells.
8. Treatment of hAOs with continuous, high levels of IL-1β and TNF-α to mimic chronic inflammation leads to induction of airway-associated markers.
9. Aberrant epithelial cell types observed within human IPF lungs, such as basaloid cells or DATPs, may arise through dysregulated signalling processes in the resident hAT2 cell population.

REFERENCES

- Adams, T. S., Schupp, J. C., Poli, S., Ayaub, E. A., Neumark, N., Ahangari, F., Chu, S. G., Raby, B. A., DeIuliis, G., Januszyk, M., et al. (2020). Single-cell RNA-seq reveals ectopic and aberrant lung-resident cell populations in idiopathic pulmonary fibrosis. *Sci. Adv.* **6**, 1–17.
- Adamson, I. Y. and Bowden, D. H. (1975). Derivation of type 1 epithelium from type 2 cells in the developing rat lung. *Lab. Invest.* **32**,.
- Al Alam, D., El Agha, E., Sakurai, R., Kheirollahi, V., Moiseenko, A., Danopoulos, S., Shrestha, A., Schmoldt, C., Quantius, J., Herold, S., et al. (2015). Evidence for the involvement of fibroblast growth factor 10 in lipofibroblast formation during embryonic lung development. *Development* **142**,.
- Alder, J. K., Chen, J. J.-L., Lancaster, L., Danoff, S., Su, S. -c., Cogan, J. D., Vulto, I., Xie, M., Qi, X., Tudor, R. M., et al. (2008). Short telomeres are a risk factor for idiopathic pulmonary fibrosis. *Proc. Natl. Acad. Sci.* **105**,.
- Alder, J. K., Barkauskas, C. E., Limjunyawong, N., Stanley, S. E., Kembou, F., Tudor, R. M., Hogan, B. L. M., Mitzner, W. and Armanios, M. (2015). Telomere dysfunction causes alveolar stem cell failure. *Proc. Natl. Acad. Sci. U. S. A.* **112**,.
- Alysandratos, K.-D., Russo, S. J., Petcherski, A., Taddeo, E. P., Acín-Pérez, R., Villacorta-Martin, C., Jean, J. C., Mulugeta, S., Rodriguez, L. R., Blum, B. C., et al. (2021). Patient-specific iPSCs carrying an SFTPC mutation reveal the intrinsic alveolar epithelial dysfunction at the inception of interstitial lung disease. *Cell Rep.* **36**,.
- Aoyagi-Ikeda, K., Maeno, T., Matsui, H., Ueno, M., Hara, K., Aoki, Y., Aoki, F., Shimizu, T., Doi, H., Kawai-Kowase, K., et al. (2011). Notch induces myofibroblast differentiation of alveolar epithelial cells via transforming growth factor- β -Smad3 pathway. *Am. J. Respir. Cell Mol. Biol.* **45**,.
- Aquino-Gálvez, A., González-Ávila, G., Jiménez-Sánchez, L. L., Maldonado-Martínez, H. A., Cisneros, J., Toscano-Marquez, F., Castillejos-López, M., Torres-Espíndola, L. M., Velázquez-Cruz, R., Rodríguez, V. H. O., et al. (2019). Dysregulated expression of hypoxia-inducible factors augments myofibroblasts differentiation in idiopathic pulmonary fibrosis. *Respir. Res.* **20**,.
- Arman, E., Haffner-Krausz, R., Gorivodsky, M. and Lonai, P. (1999). Fgfr2 is

required for limb outgrowth and lung-branching morphogenesis. *Proc. Natl. Acad. Sci. U. S. A.* **96**,.

- Ask, K., Bonniaud, P., Maass, K., Eickelberg, O., Margetts, P. J., Warburton, D., Groffen, J., Gauldie, J. and Kolb, M.** (2008). Progressive pulmonary fibrosis is mediated by TGF-beta isoform 1 but not TGF-beta3. *Int. J. Biochem. Cell Biol.* **40**, 484–95.
- Astuti, Y., Wardhana, A., Watkins, J., Wulaningsih, W. and PILAR Research Network** (2017). Cigarette smoking and telomere length: A systematic review of 84 studies and meta-analysis. *Environ. Res.* **158**,.
- Balhara, J. and Gounni, A. S.** (2012). The alveolar macrophages in asthma: A double-edged sword. *Mucosal Immunol.* **5**, 605–609.
- Barkauskas, C. E., Cronce, M. J., Rackley, C. R., Bowie, E. J., Keene, D. R., Stripp, B. R., Randell, S. H., Noble, P. W. and Hogan, B. L. M. M.** (2013). Type 2 alveolar cells are stem cells in adult lung. *J. Clin. Invest.* **123**, 3025–3036.
- Barkauskas, C. E., Chung, M. I., Fioret, B., Gao, X., Katsura, H. and Hogan, B. L. M.** (2017). Lung organoids: Current uses and future promise. *Dev.* **144**, 986–997.
- Barker, N., van Es, J. H., Kuipers, J., Kujala, P., van den Born, M., Cozijnsen, M., Haegebarth, A., Korving, J., Begthel, H., Peters, P. J., et al.** (2007). Identification of stem cells in small intestine and colon by marker gene *Lgr5*. *Nature* **449**,.
- Barratt, S., Creamer, A., Hayton, C. and Chaudhuri, N.** (2018). Idiopathic Pulmonary Fibrosis (IPF): An Overview. *J. Clin. Med.* **7**, 201.
- Batchuluun, K., Azuma, M., Fujiwara, K., Yashiro, T. and Kikuchi, M.** (2017). Notch Signaling and Maintenance of SOX2 Expression in Rat Anterior Pituitary Cells. *Acta Histochem. Cytochem.* **50**,.
- Beers, M. F. and Moodley, Y.** (2017). When Is an alveolar type 2 cell an alveolar type 2 cell?: A conundrum for lung stem cell biology and regenerative medicine. *Am. J. Respir. Cell Mol. Biol.* **57**, 18–27.
- Bellusci, S., Henderson, R., Winnier, G., Oikawa, T. and Hogan, B. L.** (1996). Evidence from normal expression and targeted misexpression that bone morphogenetic protein (Bmp-4) plays a role in mouse embryonic lung morphogenesis. *Development* **122**,.
- Bikkavilli, R. K., Feigin, M. E. and Malbon, C. C.** (2008). p38 mitogen-activated protein kinase regulates canonical Wnt- β -catenin signaling by inactivation of GSK3 β . *J. Cell Sci.* **121**,.

- Bitterman, P. B., Wewers, M. D., Rennard, S. I., Adelberg, S. and Crystal, R. G.** (1986). Modulation of alveolar macrophage-driven fibroblast proliferation by alternative macrophage mediators. *J. Clin. Invest.* **77**,.
- Bourbon, J., Boucherat, O., Chailley-Heu, B. and Delacourt, C.** (2005). Control Mechanisms of Lung Alveolar Development and Their Disorders in Bronchopulmonary Dysplasia. *Pediatr. Res.* **57**, 38R-46R.
- Bray, S. J.** (2006). Notch signalling: a simple pathway becomes complex. *Nat. Rev. Mol. Cell Biol.* **7**,.
- Bray, S. J.** (2016). Notch signalling in context. *Nat. Rev. Mol. Cell Biol.* **17**,.
- Broutier, L., Mastrogiovanni, G., Verstegen, M. M. A., Francies, H. E., Gavarró, L. M., Bradshaw, C. R., Allen, G. E., Arnes-Benito, R., Sidorova, O., Gaspersz, M. P., et al.** (2017). Human primary liver cancer-derived organoid cultures for disease modeling and drug screening. *Nat. Med.* **23**, 1424–1435.
- Carcattera, M. and Caruso, C.** (2021). Alveolar epithelial cell type II as main target of SARS-CoV-2 virus and COVID-19 development via NF-Kb pathway deregulation: A physio-pathological theory. *Med. Hypotheses* **146**,.
- Cardoso, W. V. and Lü, J.** (2006). Regulation of early lung morphogenesis: Questions, facts and controversies. *Development* **133**, 1611–1624.
- Cattaneo, C. M., Dijkstra, K. K., Fanchi, L. F., Kelderman, S., Kaing, S., van Rooij, N., van den Brink, S., Schumacher, T. N. and Voest, E. E.** (2020). Tumor organoid-T-cell coculture systems. *Nat. Protoc.* **15**,.
- Chakrabarti, J., Holokai, L., Syu, L., Steele, N., Chang, J., Dlugosz, A. and Zavros, Y.** (2018). Mouse-Derived Gastric Organoid and Immune Cell Co-culture for the Study of the Tumor Microenvironment.
- Chen, Y., Shi, L., Zhang, L., Li, R., Liang, J., Yu, W., Sun, L., Yang, X., Wang, Y., Zhang, Y., et al.** (2008). The Molecular Mechanism Governing the Oncogenic Potential of SOX2 in Breast Cancer. *J. Biol. Chem.* **283**,.
- Chen, Y. W., Huang, S. X., De Carvalho, A. L. R. T., Ho, S. H., Islam, M. N., Volpi, S., Notarangelo, L. D., Ciancanelli, M., Casanova, J. L., Bhattacharya, J., et al.** (2017). A three-dimensional model of human lung development and disease from pluripotent stem cells. *Nat. Cell Biol.* **19**, 542–549.
- Chen, G., Liu, B., Yin, S., Li, S., Guo, Y., Wang, M., Wang, K. and Wan, X.** (2020). Hypoxia induces an endometrial cancer stem-like cell phenotype via HIF-dependent demethylation of SOX2 mRNA. *Oncogenesis* **9**,.

- Childs, B. G., Durik, M., Baker, D. J. and van Deursen, J. M.** (2015). Cellular senescence in aging and age-related disease: from mechanisms to therapy. *Nat. Med.* **21**,.
- Chilosi, M., Poletti, V., Zamò, A., Lestani, M., Montagna, L., Piccoli, P., Pedron, S., Bertaso, M., Scarpa, A., Murer, B., et al.** (2003). Aberrant Wnt/ β -catenin pathway activation in idiopathic pulmonary fibrosis. *Am. J. Pathol.* **162**, 1495–1502.
- Choi, J., Park, J. E., Tsagkogeorga, G., Yanagita, M., Koo, B. K., Han, N. and Lee, J. H.** (2020). Inflammatory Signals Induce AT2 Cell-Derived Damage-Associated Transient Progenitors that Mediate Alveolar Regeneration. *Cell Stem Cell* **27**, 366-382.e7.
- Choi, J., Jang, Y. J., Dabrowska, C., Iich, E., Evans, K. V., Hall, H., Janes, S. M., Simons, B. D., Koo, B.-K., Kim, J., et al.** (2021). Release of Notch activity coordinated by IL-1 β signalling confers differentiation plasticity of airway progenitors via Fosl2 during alveolar regeneration. *Nat. Cell Biol.* **23**,.
- Chou, Y.-T., Lee, C.-C., Hsiao, S.-H., Lin, S.-E., Lin, S.-C., Chung, C.-H., Chung, C.-H., Kao, Y.-R., Wang, Y.-H., Chen, C.-T., et al.** (2013). The emerging role of SOX2 in cell proliferation and survival and its crosstalk with oncogenic signaling in lung cancer. *Stem Cells* **31**,.
- Chung, M.-I., Bujnis, M., Barkauskas, C. E., Kobayashi, Y. and Hogan, B. L. M.** (2018). Niche-mediated BMP/SMAD signaling regulates lung alveolar stem cell proliferation and differentiation. *Development* **145**,.
- Clevers, H., Loh, K. M. and Nusse, R.** (2014a). An integral program for tissue renewal and regeneration: Wnt signaling and stem cell control. *Science (80-.).* **346**,.
- Clevers, H., Loh, K. M. and Nusse, R.** (2014b). Stem cell signaling. An integral program for tissue renewal and regeneration: Wnt signaling and stem cell control. *Science* **346**,.
- Co, J. Y., Margalef-Català, M., Li, X., Mah, A. T., Kuo, C. J., Monack, D. M. and Amieva, M. R.** (2019). Controlling Epithelial Polarity: A Human Enteroid Model for Host-Pathogen Interactions. *Cell Rep.* **26**,.
- Courtwright, A. M. and El-Chemaly, S.** (2019). Telomeres in Interstitial Lung Disease: The Short and the Long of It. *Ann. Am. Thorac. Soc.* **16**,.
- Crapo, J. D., Barry, B. E., Gehr, P., Bachofen, M. and Weibel, E. R.** (1982). Cell number and cell characteristics of the normal human lung. *Am. Rev. Respir. Dis.* **126**, 332–337.

- Cunningham, A. C., Milne, D. S., Wilkes, J., Dark, J. H., Tetley, T. D. and Kirby, J. A.** (1994). Constitutive expression of MHC and adhesion molecules by alveolar epithelial cells (type II pneumocytes) isolated from human lung and comparison with immunocytochemical findings. *J. Cell Sci.* **107**, 443–449.
- Danopoulos, S., Alonso, I., Thornton, M. E., Grubbs, B. H., Bellusci, S., Warburton, D. and Al Alam, D.** (2018). Human lung branching morphogenesis is orchestrated by the spatiotemporal distribution of ACTA2, SOX2, and SOX9. *Am. J. Physiol. Lung Cell. Mol. Physiol.* **314**,.
- Danopoulos, S., Shiosaki, J. and Al Alam, D.** (2019a). FGF Signaling in Lung Development and Disease: Human Versus Mouse. *Front. Genet.* **10**,.
- Danopoulos, S., Thornton, M. E., Grubbs, B. H., Frey, M. R., Warburton, D., Bellusci, S. and Al Alam, D.** (2019b). Discordant roles for FGF ligands in lung branching morphogenesis between human and mouse. *J. Pathol.* **247**,.
- Davidson, L. and Berkelhamer, S.** (2017). Bronchopulmonary Dysplasia: Chronic Lung Disease of Infancy and Long-Term Pulmonary Outcomes. *J. Clin. Med.* **6**, 1–20.
- Davis, J. D. and Wypych, T. P.** (2021). Cellular and functional heterogeneity of the airway epithelium. *Mucosal Immunol.* **14**,.
- de Carvalho, A. L. R. T., Strikoudis, A., Liu, H.-Y. Y., Chen, Y.-W. W., Dantas, T. J., Vallee, R. B., Correia-Pinto, J. and Snoeck, H.-W. W.** (2019). Glycogen synthase kinase 3 induces multilineage maturation of human pluripotent stem cell-derived lung progenitors in 3D culture. *Dev.* **146**, 1–16.
- De Moerlooze, L., Spencer-Dene, B., Revest, J. M., Hajihosseini, M., Rosewell, I. and Dickson, C.** (2000). An important role for the IIIb isoform of fibroblast growth factor receptor 2 (FGFR2) in mesenchymal-epithelial signalling during mouse organogenesis. *Development* **127**,.
- Degryse, A. L., Tanjore, H., Xu, X. C., Polosukhin, V. V, Jones, B. R., McMahon, F. B., Gleaves, L. A., Blackwell, T. S. and Lawson, W. E.** (2010). Repetitive intratracheal bleomycin models several features of idiopathic pulmonary fibrosis. *Am. J. Physiol. Lung Cell. Mol. Physiol.* **299**,.
- Desai, T. J., Brownfield, D. G. and Krasnow, M. A.** (2014). Alveolar progenitor and stem cells in lung development, renewal and cancer. *Nature* **507**, 190–194.
- Desai, O., Winkler, J., Minasyan, M. and Herzog, E. L.** (2018). The Role of Immune and Inflammatory Cells in Idiopathic Pulmonary Fibrosis. *Front. Med.* **5**,.
- Dickens, J. A., Rutherford, E. N., Abreu, S., Chambers, J. E., Ellis, M. O., van**

- Schadewijk, A., Hiemstra, P. S. and Marciniak, S. J.** (2021). Novel insights into surfactant protein C trafficking revealed through the study of a pathogenic mutant. *Eur. Respir. J.*
- Dinarello, C. A.** (2018). Overview of the IL-1 family in innate inflammation and acquired immunity. *Immunol. Rev.* **281**,.
- Dobbs, L. G., Williams, M. C. and Gonzalez, R.** (1988). Monoclonal antibodies specific to apical surfaces of rat alveolar type I cells bind to surfaces of cultured, but not freshly isolated, type II cells. *Biochim. Biophys. Acta* **970**,.
- Dost, A. F. M., Moye, A. L., Vedaie, M., Tran, L. M., Fung, E., Heinze, D., Villacorta-Martin, C., Huang, J., Hekman, R., Kwan, J. H., et al.** (2020). Organoids Model Transcriptional Hallmarks of Oncogenic KRAS Activation in Lung Epithelial Progenitor Cells. *Cell Stem Cell* **27**, 663-678.e8.
- Dutta, D., Heo, I. and Clevers, H.** (2017). Disease Modeling in Stem Cell-Derived 3D Organoid Systems. *Trends Mol. Med.* **23**, 393–410.
- Dye, B. R., Hill, D. R., Ferguson, M. A., Tsai, Y. H., Nagy, M. S., Dyal, R., Wells, J. M., Mayhew, C. N., Nattiv, R., Klein, O. D., et al.** (2015). In vitro generation of human pluripotent stem cell derived lung organoids. *Elife* **2015**, 1–25.
- Dye, B. R., Dedhia, P. H., Miller, A. J., Nagy, M. S., White, E. S., Shea, L. D. and Spence, J. R.** (2016). A bioengineered niche promotes in vivo engraftment and maturation of pluripotent stem cell derived human lung organoids. *Elife* **5**, 1–18.
- Ebisudani, T., Sugimoto, S., Haga, K., Mitsuishi, A., Takai-Todaka, R., Fujii, M., Toshimitsu, K., Hamamoto, J., Sugihara, K., Hishida, T., et al.** (2021). Direct derivation of human alveolospheres for SARS-CoV-2 infection modeling and drug screening. *Cell Rep.* **35**,.
- El-Hashash, A. H. and Warburton, D.** (2011). Cell polarity and spindle orientation in the distal epithelium of embryonic lung. *Dev. Dyn.* **240**, 441–445.
- Evans, K. V. and Lee, J.** (2020). Alveolar wars: The rise of in vitro models to understand human lung alveolar maintenance, regeneration, and disease. *Stem Cells Transl. Med.* **9**,.
- Evans, M. J., Cabral, L. J., Stephens, R. J. and Freeman, G.** (1973). Renewal of alveolar epithelium in the rat following exposure to NO₂. *Clin. Res.*
- Farin, H. F., Jordens, I., Mosa, M. H., Basak, O., Korving, J., Tauriello, D. V. F., de Punder, K., Angers, S., Peters, P. J., Maurice, M. M., et al.** (2016). Visualization of a short-range Wnt gradient in the intestinal stem-cell niche. *Nature* **530**,.

- Fernandez, I. E. and Eickelberg, O.** (2012). New cellular and molecular mechanisms of lung injury and fibrosis in idiopathic pulmonary fibrosis. *Lancet* **380**, 680–688.
- Finn, J., Sottoriva, K., Pajcini, K. V., Kitajewski, J. K., Chen, C., Zhang, W., Malik, A. B. and Liu, Y.** (2019). Dlk1-Mediated Temporal Regulation of Notch Signaling Is Required for Differentiation of Alveolar Type II to Type I Cells during Repair. *Cell Rep.* **26**, 2942-2954.e5.
- Foster, K. A., Oster, C. G., Mayer, M. M., Avery, M. L. and Audus, K. L.** (1998). Characterization of the A549 Cell Line as a Type II Pulmonary Epithelial Cell Model for Drug Metabolism. *Exp. Cell Res.* **243**,.
- Frank, D. B., Peng, T., Zepp, J. A., Snitow, M., Vincent, T. L., Penkala, I. J., Cui, Z., Herriges, M. J., Morley, M. P., Zhou, S., et al.** (2016). Emergence of a Wave of Wnt Signaling that Regulates Lung Alveologenesis by Controlling Epithelial Self-Renewal and Differentiation. *Cell Rep.* **17**, 2312–2325.
- Frank, D. B., Penkala, I. J., Zepp, J. A., Sivakumar, A., Linares-Saldana, R., Zacharias, W. J., Stolz, K. G., Pankin, J., Lu, M., Wang, Q., et al.** (2019). Early lineage specification defines alveolar epithelial ontogeny in the murine lung. *Proc. Natl. Acad. Sci.* **116**,.
- Frey, M. R., Dise, R. S., Edelblum, K. L. and Polk, D. B.** (2006). p38 kinase regulates epidermal growth factor receptor downregulation and cellular migration. *EMBO J.* **25**,.
- Fu, D. and Richardson, D. R.** (2007). Iron chelation and regulation of the cell cycle: 2 mechanisms of posttranscriptional regulation of the universal cyclin-dependent kinase inhibitor p21CIP1/WAF1 by iron depletion. *Blood* **110**,.
- Fuchs, S., Hollins, A. J., Laue, M., Schaefer, U. F., Roemer, K., Gumbleton, M. and Lehr, C. M.** (2003). Differentiation of human alveolar epithelial cells in primary culture: Morphological characterization and synthesis of caveolin-1 and surfactant protein-C. *Cell Tissue Res.* **311**, 31–45.
- Fujita, M., Shannon, J. M., Morikawa, O., Gauldie, J., Hara, N. and Mason, R. J.** (2003). Overexpression of tumor necrosis factor-alpha diminishes pulmonary fibrosis induced by bleomycin or transforming growth factor-beta. *Am. J. Respir. Cell Mol. Biol.* **29**,.
- Gan, L., Meng, J., Xu, M., Liu, M., Qi, Y., Tan, C., Wang, Y., Zhang, P., Weng, W., Sheng, W., et al.** (2018). Extracellular matrix protein 1 promotes cell metastasis and glucose metabolism by inducing integrin β 4/FAK/SOX2/HIF-1 α signaling pathway

- in gastric cancer. *Oncogene* **37**,.
- Glisinski, K. M., Schlobohm, A. J., Paramore, S. V., Birukova, A., Moseley, M. A., Foster, M. W. and Barkauskas, C. E.** (2020). Interleukin-13 disrupts type 2 pneumocyte stem cell activity. *JCI Insight* **5**, e131232.
- Gokey, J. J., Green, J., Carraro, G., Perl, A.-K. T., Xu, Y., Stripp, B. R., Whitsett, J. A. and Sridharan, A.** (2018). Active epithelial Hippo signaling in idiopathic pulmonary fibrosis. *JCI Insight* **3**,.
- Gokey, J. J., Snowball, J., Sridharan, A., Sudha, P., Kitzmiller, J. A., Xu, Y. and Whitsett, J. A.** (2021). YAP regulates alveolar epithelial cell differentiation and AGER via NFIB/KLF5/NKX2-1. *iScience* **24**,.
- Gonzalez, R. F., Allen, L. and Dobbs, L. G.** (2009). Rat alveolar type I cells proliferate, express OCT-4, and exhibit phenotypic plasticity in vitro. *Am. J. Physiol. Cell. Mol. Physiol.* **297**,.
- Gonzalez, R. F., Allen, L., Gonzales, L., Ballard, P. L. and Dobbs, L. G.** (2010). HTII-280 , a Biomarker Specific to the Apical Plasma Membrane of Human Lung Alveolar Type II Cells The Journal of Histochemistry & Cytochemistry. **58**, 891–901.
- Goss, A. M., Tian, Y., Tsukiyama, T., Cohen, E. D., Zhou, D., Lu, M. M., Yamaguchi, T. P. and Morrisey, E. E.** (2009). Wnt2/2b and β -Catenin Signaling Are Necessary and Sufficient to Specify Lung Progenitors in the Foregut. *Dev. Cell* **17**,.
- Gotoh, S., Ito, I., Nagasaki, T., Yamamoto, Y., Konishi, S., Korogi, Y., Matsumoto, H., Muro, S., Hirai, T., Funato, M., et al.** (2014). Generation of Alveolar Epithelial Spheroids via Isolated Progenitor Cells from Human Pluripotent Stem Cells. **3**, 394–403.
- Guilliams, M., De Kler, I., Henri, S., Post, S., Vanhoutte, L., De Prijck, S., Deswarte, K., Malissen, B., Hammad, H. and Lambrecht, B. N.** (2013). Alveolar macrophages develop from fetal monocytes that differentiate into long-lived cells in the first week of life via GM-CSF. *J. Exp. Med.* **210**, 1977–1992.
- Guo, L., Degenstein, L. and Fuchs, E.** (1996). Keratinocyte growth factor is required for hair development but not for wound healing. *Genes Dev.* **10**,.
- Guo, M., Song, L.-P., Jiang, Y., Liu, W., Yu, Y. and Chen, G.-Q.** (2006). Hypoxia-mimetic agents desferrioxamine and cobalt chloride induce leukemic cell apoptosis through different hypoxia-inducible factor-1 α independent mechanisms.

Apoptosis **11**,.

- Gustafsson, M. V., Zheng, X., Pereira, T., Gradin, K., Jin, S., Lundkvist, J., Ruas, J. L., Poellinger, L., Lendahl, U. and Bondesson, M.** (2005). Hypoxia Requires Notch Signaling to Maintain the Undifferentiated Cell State. *Dev. Cell* **9**,.
- Habermann, A. C., Gutierrez, A. J., Bui, L. T., Yahn, S. L., Winters, N. I., Calvi, C. L., Peter, L., Chung, M. I., Taylor, C. J., Jetter, C., et al.** (2020). Single-cell RNA sequencing reveals profibrotic roles of distinct epithelial and mesenchymal lineages in pulmonary fibrosis. *Sci. Adv.* **6**,.
- Haies, D. M., Gil, J. and Weibel, E. R.** (1981). Morphometric study of rat lung cells. I. Numerical and dimensional characteristics of parenchymal cell population. *Am. Rev. Respir. Dis.* **123**,.
- Hasegawa, K., Sato, A., Tanimura, K., Uemasu, K., Hamakawa, Y., Fuseya, Y., Sato, S., Muro, S. and Hirai, T.** (2017). Fraction of MHCII and EpCAM expression characterizes distal lung epithelial cells for alveolar type 2 cell isolation. *Respir. Res.* **18**, 1–13.
- Herring, M. J., Putney, L. F., Wyatt, G., Finkbeiner, W. E. and Hyde, D. M.** (2014). Growth of alveoli during postnatal development in humans based on stereological estimation. *Am. J. Physiol. Lung Cell. Mol. Physiol.* **307**,.
- Hogan, B. L. M., Barkauskas, C. E., Chapman, H. A., Epstein, J. A., Jain, R., Hsia, C. C. W., Niklason, L., Calle, E., Le, A., Randell, S. H., et al.** (2014). Repair and regeneration of the respiratory system: Complexity, plasticity, and mechanisms of lung stem cell function. *Cell Stem Cell* **15**, 123–138.
- Holokai, L. L., Chakrabarti, J., Lundy, J., Croagh, D., Woodson, C., Steele, N., Magliano, M. P., Frankel, T., Jenkins, B., Wang, J., et al.** (2019). An Organoid/Immune Cell Co-Culture as a Predictive Model for the Treatment of Pancreatic Cancer. *FASEB J.* **33**,.
- Hong, K. U., Reynolds, S. D., Giangreco, A., Hurley, C. M. and Stripp, B. R.** (2001). Clara cell secretory protein-expressing cells of the airway neuroepithelial body microenvironment include a label-retaining subset and are critical for epithelial renewal after progenitor cell depletion. *Am. J. Respir. Cell Mol. Biol.* **24**, 671–681.
- Hong, K. U., Reynolds, S. D., Watkins, S., Fuchs, E. and Stripp, B. R.** (2004). In vivo differentiation potential of tracheal basal cells: evidence for multipotent and unipotent subpopulations. *Am. J. Physiol. Cell. Mol. Physiol.* **286**,.
- Hong, C.-F., Chen, W.-Y. and Wu, C.-W.** (2017). Upregulation of Wnt signaling under

- hypoxia promotes lung cancer progression. *Oncol. Rep.* **38**,.
- Hu, B. and Phan, S. H.** (2016). Notch in fibrosis and as a target of anti-fibrotic therapy. *Pharmacol. Res.* **108**,.
- Huch, M. and Koo, B.-K.** (2015). Modeling mouse and human development using organoid cultures. *Development* **142**,.
- Huch, M., Gehart, H., Boxtel, R. Van, Hamer, K., Blokzijl, F., Versteegen, M. M. A., Ellis, E., Wenum, M. Van, Fuchs, S. A., Ligt, J. De, et al.** (2015). Article Long-Term Culture of Genome-Stable Bipotent Stem Cells from Adult Human Liver. *Cell* **160**, 299–312.
- Hynds, R. E. and Janes, S. M.** (2017). Airway basal cell heterogeneity and lung squamous cell carcinoma. *Cancer Prev. Res.* **10**, 491–493.
- Hynds, R. E., Butler, C. R., Janes, S. M. and Giangreco, A.** (2016). Expansion of Human Airway Basal Stem Cells and Their Differentiation as 3D Tracheospheres.
- Jackson, E. L.** (2001). Analysis of lung tumor initiation and progression using conditional expression of oncogenic K-ras. *Genes Dev.* **15**,.
- Jacob, A., Morley, M., Hawkins, F., McCauley, K. B., Jean, J. C., Heins, H., Na, C. L., Weaver, T. E., Vedaie, M., Hurley, K., et al.** (2017). Differentiation of Human Pluripotent Stem Cells into Functional Lung Alveolar Epithelial Cells. *Cell Stem Cell* **21**, 472-488.e10.
- Jacob, A., Vedaie, M., Roberts, D. A., Thomas, D. C., Villacorta-Martin, C., Alysandratos, K.-D., Hawkins, F. and Kotton, D. N.** (2019). Derivation of self-renewing lung alveolar epithelial type II cells from human pluripotent stem cells. *Nat. Protoc.* **14**, 1–41.
- Jain, R., Barkauskas, C. E., Takeda, N., Bowie, E. J., Aghajanian, H., Wang, Q., Padmanabhan, A., Manderfield, L. J., Gupta, M., Li, D., et al.** (2015). Plasticity of Hopx⁺ type I alveolar cells to regenerate type II cells in the lung. *Nat. Commun.* **6**,.
- Jobe, A. H. and Ikegami, M.** (1998). Mechanisms initiating lung injury in the preterm. *Early Hum. Dev.* **53**, 81–94.
- Jobe, A. H., Hillman, N., Polglase, G., Kramer, B. W., Kallapur, S. and Pillow, J.** (2008). Injury and inflammation from resuscitation of the preterm infant. *Neonatology* **94**, 190–196.
- John, A. E., Graves, R. H., Pun, K. T., Vitulli, G., Forty, E. J., Mercer, P. F., Morrell, J. L., Barrett, J. W., Rogers, R. F., Hafeji, M., et al.** (2020).

Translational pharmacology of an inhaled small molecule $\alpha\text{v}\beta\text{6}$ integrin inhibitor for idiopathic pulmonary fibrosis. *Nat. Commun.* **11**, 1–14.

- Kathiriya, J. J., Wang, C., Brumwell, A., Cassandras, M., Le Saux, C., Wolters, P., Matthay, M., Chapman, H. A. and Peng, T.** (2020). Human alveolar Type 2 epithelium transdifferentiates into metaplastic KRT5+ basal cells during alveolar repair. *bioRxiv*.
- Katsura, H., Kobayashi, Y., Tata, P. R. and Hogan, B. L. M.** (2019). IL-1 and TNF α Contribute to the Inflammatory Niche to Enhance Alveolar Regeneration. *Stem cell reports* **12**,.
- Katsura, H., Sontake, V., Tata, A., Kobayashi, Y., Edwards, C. E., Heaton, B. E., Konkimalla, A., Asakura, T., Mikami, Y., Fritch, E. J., et al.** (2020). Human Lung Stem Cell-Based Alveolospheres Provide Insights into SARS-CoV-2-Mediated Interferon Responses and Pneumocyte Dysfunction. *Cell Stem Cell*.
- Katzen, J., Wagner, B. D., Venosa, A., Kopp, M., Tomer, Y., Russo, S. J., Headen, A. C., Basil, M. C., Stark, J. M., Mulugeta, S., et al.** (2019). A SFTPC BRICHOS mutant links epithelial ER stress and spontaneous lung fibrosis. *JCI Insight* **4**, 1–19.
- Khalil, N., O'Connor, R. N., Flanders, K. C. and Unruh, H.** (1996). TGF-beta 1, but not TGF-beta 2 or TGF-beta 3, is differentially present in epithelial cells of advanced pulmonary fibrosis: an immunohistochemical study. *Am. J. Respir. Cell Mol. Biol.* **14**, 131–8.
- Kim, C. F., Jackson, E. L., Woolfenden, A. E., Lawrence, S., Babar, I., Vogel, S., Crowley, D., Bronson, R. T. and Jacks, T.** (2005). Identification of bronchioalveolar stem cells in normal lung and lung cancer. *Cell* **121**, 823–835.
- King, T. E., Albera, C., Bradford, W. Z., Costabel, U., Hormel, P., Lancaster, L., Noble, P. W., Sahn, S. A., Szwarcberg, J., Thomeer, M., et al.** (2009). Effect of interferon gamma-1b on survival in patients with idiopathic pulmonary fibrosis (INSPIRE): a multicentre, randomised, placebo-controlled trial. *Lancet* **374**,.
- Kiyokawa, H. and Morimoto, M.** (2020). Notch signaling in the mammalian respiratory system, specifically the trachea and lungs, in development, homeostasis, regeneration, and disease. *Dev. Growth Differ.* **62**,.
- Knudsen, L. and Ochs, M.** (2018). The micromechanics of lung alveoli: structure and function of surfactant and tissue components. *Histochem. Cell Biol.* **150**,.
- Kobayashi, Y., Tata, A., Konkimalla, A., Katsura, H., Lee, R. F., Ou, J., Banovich, N. E., Kropski, J. A. and Tata, P. R.** (2020). Persistence of a regeneration-

associated, transitional alveolar epithelial cell state in pulmonary fibrosis. *Nat. Cell Biol.* **22**, 934–946.

Kolb, M., Margetts, P. J., Anthony, D. C., Pitossi, F. and Gauldie, J. (2001). Transient expression of IL-1 β induces acute lung injury and chronic repair leading to pulmonary fibrosis. *J. Clin. Invest.* **107**,.

Königshoff, M., Balsara, N., Pfaff, E. M., Kramer, M., Chrobak, I., Seeger, W. and Eickelberg, O. (2008). Functional Wnt signaling is increased in idiopathic pulmonary fibrosis. *PLoS One* **3**, 1–12.

Korogi, Y., Gotoh, S., Ikeo, S., Yamamoto, Y., Sone, N., Tamai, K., Konishi, S., Nagasaki, T., Matsumoto, H., Ito, I., et al. (2019). In Vitro Disease Modeling of Hermansky-Pudlak Syndrome Type 2 Using Human Induced Pluripotent Stem Cell-Derived Alveolar Organoids. *Stem Cell Reports* **12**, 431–440.

Kropski, J. A. and Blackwell, T. S. (2018). Endoplasmic reticulum stress in the pathogenesis of fibrotic disease. *J. Clin. Invest.* **128**,.

Kropski, J. A., Pritchett, J. M., Zoz, D. F., Crossno, P. F., Markin, C., Garnett, E. T., Degryse, A. L., Mitchell, D. B., Polosukhin, V. V, Rickman, O. B., et al. (2015). Extensive phenotyping of individuals at risk for familial interstitial pneumonia reveals clues to the pathogenesis of interstitial lung disease. *Am. J. Respir. Crit. Care Med.* **191**,.

Kumar, P. A., Hu, Y., Yamamoto, Y., Hoe, N. B., Wei, T. S., Mu, D., Sun, Y., Joo, L. S., Dagher, R., Zielonka, E. M., et al. (2011). Distal airway stem cells yield alveoli in vitro and during lung regeneration following H1N1 influenza infection. *Cell* **147**, 525–538.

Lamers, M. M., Vaart, J., Knoop, K., Riesebosch, S., Breugem, T. I., Mykytyn, A. Z., Beumer, J., Schipper, D., Bezstarosti, K., Koopman, C. D., et al. (2021). An organoid-derived bronchioalveolar model for SARS-CoV-2 infection of human alveolar type II-like cells. *EMBO J.* **40**,.

Lancaster, M. A. and Huch, M. (2019). Disease modelling in human organoids. *Dis. Model. Mech.* **12**,.

Lancaster, L., Crestani, B., Hernandez, P., Inoue, Y., Wachtlin, D., Loaiza, L., Quaresma, M., Stowasser, S. and Richeldi, L. (2019). Safety and survival data in patients with idiopathic pulmonary fibrosis treated with nintedanib: Pooled data from six clinical trials. *BMJ Open Respir. Res.* **6**, 1–7.

Laresgoiti, U., Nikolić, M. Z., Rao, C., Brady, J. L., Richardson, R. V., Batchen, E.

- J., Chapman, K. E. and Rawlins, E. L.** (2016). Lung epithelial tip progenitors integrate Glucocorticoid and STAT3-mediated signals to control progeny fate. *Development*.
- Lawson, W. E., Grant, S. W., Ambrosini, V., Womble, K. E., Dawson, E. P., Lane, K. B., Markin, C., Renzoni, E., Lympany, P., Thomas, A. Q., et al.** (2004). Genetic mutations in surfactant protein C are a rare cause of sporadic cases of IPF. *Thorax* **59**, 977–980.
- Lee, C. G., Cho, S. J., Kang, M. J., Chapoval, S. P., Lee, P. J., Noble, P. W., Yehualaeshet, T., Lu, B., Flavell, R. A., Milbrandt, J., et al.** (2004). Early growth response gene 1-mediated apoptosis is essential for transforming growth factor beta1-induced pulmonary fibrosis. *J. Exp. Med.* **200**,.
- Lee, J. H., Kim, J., Gludish, D., Roach, R. R., Saunders, A. H., Barrios, J., Woo, A. J., Chen, H., Conner, D. A., Fujiwara, Y., et al.** (2013). Surfactant protein-C chromatin-bound green fluorescence protein reporter mice reveal heterogeneity of surfactant protein C-expressing lung cells. *Am. J. Respir. Cell Mol. Biol.* **48**, 288–298.
- Lee, J.-H., Bhang, D. H., Beede, A., Huang, T. L., Stripp, B. R., Bloch, K. D., Wagers, A. J., Tseng, Y.-H., Ryeom, S. and Kim, C. F.** (2014). Lung Stem Cell Differentiation in Mice Directed by Endothelial Cells via a BMP4-NFATc1-Thrombospondin-1 Axis. *Cell* **156**, 440–55.
- Lee, J. H., Tammela, T., Hofree, M., Choi, J., Marjanovic, N. D., Han, S., Canner, D., Wu, K., Paschini, M., Bhang, D. H., et al.** (2017). Anatomically and Functionally Distinct Lung Mesenchymal Populations Marked by Lgr5 and Lgr6. *Cell* **170**, 1149-1163.e12.
- Lee, J. W., Ko, J., Ju, C. and Eltzschig, H. K.** (2019). Hypoxia signaling in human diseases and therapeutic targets. *Exp. Mol. Med.* **51**,.
- Lee, J., Islam, M. N., Boostanpour, K., Aran, D., Christenson, S., Matthay, M. A., Eckalbar, W., DePianto, D. J., Arron, J. R., Magee, L., et al.** (2021). Molecular programs of fibrotic change in aging human lung. *bioRxiv* 2021.01.18.427195.
- Leeman, K. T., Pessina, P., Lee, J. H. and Kim, C. F.** (2019). Mesenchymal Stem Cells Increase Alveolar Differentiation in Lung Progenitor Organoid Cultures. *Sci. Rep.* **9**, 1–10.
- Li, R., Herriges, J. C., Chen, L., Mecham, R. P. and Sun, X.** (2017). FGF receptors control alveolar elastogenesis. *Development* **144**,.

- Li, J., Wang, Z., Chu, Q., Jiang, K., Li, J. and Tang, N.** (2018a). The Strength of Mechanical Forces Determines the Differentiation of Alveolar Epithelial Cells. *Dev. Cell* **44**, 297-312.e5.
- Li, Y., Wu, L., Yu, M., Yang, F., Wu, B., Lu, S., Tu, M. and Xu, H.** (2018b). HIF-1 α is Critical for the Activation of Notch Signaling in Neurogenesis During Acute Epilepsy. *Neuroscience* **394**,.
- Lim, K., Tang, W., Sun, D., He, P., Teichmann, S. A., Marioni, J. C., Meyer, K. B. and Rawlins, E. L.** (2020). Acquisition of alveolar fate and differentiation competence by human fetal lung epithelial progenitor cells. *bioRxiv*.
- Liu, Z., Wu, H., Jiang, K., Wang, Y., Zhang, W., Chu, Q., Li, J., Huang, H., Cai, T., Ji, H., et al.** (2016). MAPK-Mediated YAP Activation Controls Mechanical-Tension-Induced Pulmonary Alveolar Regeneration. *Cell Rep.* **16**, 1810–1819.
- Liu, P., Tang, H., Song, C., Wang, J., Chen, B., Huang, X., Pei, X. and Liu, L.** (2018). SOX2 Promotes Cell Proliferation and Metastasis in Triple Negative Breast Cancer. *Front. Pharmacol.* **9**,.
- Liu, Q., Liu, K., Cui, G., Huang, X., Yao, S., Guo, W., Qin, Z., Li, Y., Yang, R., Pu, W., et al.** (2019). Lung regeneration by multipotent stem cells residing at the bronchioalveolar-duct junction. *Nat. Genet.* **51**, 728–738.
- Ma, Q., Ma, Y., Dai, X., Ren, T., Fu, Y., Liu, W., Han, Y., Wu, Y., Cheng, Y., Zhang, T., et al.** (2018). Regeneration of functional alveoli by adult human SOX9⁺airway basal cell transplantation. *Protein Cell* **9**, 267–282.
- MacDonald, B. T., Tamai, K. and He, X.** (2009). Wnt/beta-catenin signaling: components, mechanisms, and diseases. *Dev. Cell* **17**,.
- Maguire, J. A., Mulugeta, S. and Beers, M. F.** (2011). Endoplasmic reticulum stress induced by surfactant protein C BRICHOS mutants promotes proinflammatory signaling by epithelial cells. *Am. J. Respir. Cell Mol. Biol.* **44**, 404–414.
- Margaritopoulos, G. A., Vasarmidi, E. and Antoniou, K. M.** (2016). Pirfenidone in the treatment of idiopathic pulmonary fibrosis: An evidence-based review of its place in therapy. *Core Evid.* **11**, 11–22.
- Margaritopoulos, G. A., Trachalaki, A., Wells, A. U., Vasarmidi, E., Bibaki, E., Papastratigakis, G., Detorakis, S., Tzanakis, N. and Antoniou, K. M.** (2018). Pirfenidone improves survival in IPF: Results from a real-life study. *BMC Pulm. Med.* **18**, 1–7.
- Mason, R. J. and Williams, M. C.** (1977). Type II alveolar cell. Defender of the

- alveolus. *Am. Rev. Respir. Dis.* **115**, 81–91.
- Maughan, E. F., Nigro, E., Pennycuick, A., Gowers, K. H. C., Denais, C., Gómez-López, S., Lazarus, K. A., Butler, C. R., Lee, D. D. H., Orr, J. C., et al.** (2020). Cell-intrinsic differences between human airway epithelial cells from children and adults. *bioRxiv*.
- Maurizi, G., Verma, N., Gadi, A., Mansukhani, A. and Basilico, C.** (2018). Sox2 is required for tumor development and cancer cell proliferation in osteosarcoma. *Oncogene* **37**,.
- McCauley, K. B., Hawkins, F., Serra, M., Thomas, D. C., Jacob, A. and Kotton, D. N.** (2017). Efficient Derivation of Functional Human Airway Epithelium from Pluripotent Stem Cells via Temporal Regulation of Wnt Signaling. *Cell Stem Cell* **20**, 844-857.e6.
- Meng, X. M., Nikolic-Paterson, D. J. and Lan, H. Y.** (2016). TGF- β : The master regulator of fibrosis. *Nat. Rev. Nephrol.* **12**, 325–338.
- Mercer, R. R., Russell, M. L., Roggli, V. L. and Crapo, J. D.** (1994). Cell number and distribution in human and rat airways. *Am. J. Respir. Cell Mol. Biol.* **10**,.
- Miettinen, P. J., Berger, J. E., Meneses, J., Phung, Y., Pedersen, R. A., Werb, Z. and Derynck, R.** (1995). Epithelial immaturity and multiorgan failure in mice lacking epidermal growth factor receptor. *Nature* **376**,.
- Miettinen, P. J., Warburton, D., Bu, D., Zhao, J.-S., Berger, J. E., Minoo, P., Koivisto, T., Allen, L., Dobbs, L., Werb, Z., et al.** (1997). Impaired Lung Branching Morphogenesis in the Absence of Functional EGF Receptor. *Dev. Biol.* **186**,.
- Miller, A. J., Hill, D. R., Nagy, M. S., Aoki, Y., Dye, B. R., Chin, A. M., Huang, S., Zhu, F., White, E. S., Lama, V., et al.** (2018). In Vitro Induction and In Vivo Engraftment of Lung Bud Tip Progenitor Cells Derived from Human Pluripotent Stem Cells. *Stem Cell Reports* **10**, 101–119.
- Miller, A. J., Dye, B. R., Ferrer-Torres, D., Hill, D. R., Overeem, A. W., Shea, L. D. and Spence, J. R.** (2019). Generation of lung organoids from human pluripotent stem cells in vitro. *Nat. Protoc.* **14**,.
- Minoo, P., Hamdan, H., Bu, D., Warburton, D., Stepanik, P. and Delemos, R.** (1995). TTF-1 regulates lung epithelial morphogenesis. *Dev. Biol.* **172**, 694–698.
- Montoro, D. T., Haber, A. L., Biton, M., Vinarsky, V., Lin, B., Birket, S. E., Yuan, F., Chen, S., Leung, H. M., Villoria, J., et al.** (2018). A revised airway epithelial

- hierarchy includes CFTR-expressing ionocytes. *Nature* **560**,.
- Morrissey, E. E. and Hogan, B. L. M.** (2010). Preparing for the First Breath: Genetic and Cellular Mechanisms in Lung Development. *Dev. Cell* **18**, 8–23.
- Mukherjee, T., Kim, W. S., Mandal, L. and Banerjee, U.** (2011). Interaction Between Notch and Hif- α in Development and Survival of *Drosophila* Blood Cells. *Science (80-.)*. **332**,.
- Nabhan, A. N., Brownfield, D. G., Harbury, P. B., Krasnow, M. A. and Desai, T. J.** (2018). Single-cell Wnt signaling niches maintain stemness of alveolar type 2 cells. *Science (80-.)*. **359**, 1118–1123.
- Narayanan, M., Owers-Bradley, J., Beardsmore, C. S., Mada, M., Ball, I., Garipov, R., Panesar, K. S., Kuehni, C. E., Spycher, B. D., Williams, S. E., et al.** (2012). Alveolarization continues during childhood and adolescence: new evidence from helium-3 magnetic resonance. *Am. J. Respir. Crit. Care Med.* **185**,.
- Neuhaus, V., Schaudien, D., Golovina, T., Temann, U. A., Thompson, C., Lippmann, T., Bersch, C., Pfennig, O., Jonigk, D., Braubach, P., et al.** (2017). Assessment of long-term cultivated human precision-cut lung slices as an ex vivo system for evaluation of chronic cytotoxicity and functionality. *J. Occup. Med. Toxicol.* **12**, 1–8.
- Neumark, N., Cosme, C., Rose, K.-A. and Kaminski, N.** (2020). The Idiopathic Pulmonary Fibrosis Cell Atlas. *Am. J. Physiol. Cell. Mol. Physiol.* **319**,.
- Nikolić, M. Z. and Rawlins, E. L.** (2017). Lung Organoids and Their Use To Study Cell-Cell Interaction. *Curr. Pathobiol. Rep.* **5**, 223–231.
- Nikolić, M. Z., Caritg, O., Jeng, Q., Johnson, J. A., Sun, D., Howell, K. J., Brady, J. L., Laresgoiti, U., Allen, G., Butler, R., et al.** (2017). Human embryonic lung epithelial tips are multipotent progenitors that can be expanded in vitro as long-term self-renewing organoids. *Elife* **6**, 1–33.
- Nikolić, M. Z., Sun, D. and Rawlins, E. L.** (2018). Human lung development: Recent progress and new challenges. *Dev.* **145**,.
- Nureki, S. I., Tomer, Y., Venosa, A., Katzen, J., Russo, S. J., Jamil, S., Barrett, M., Nguyen, V., Kopp, M., Mulugeta, S., et al.** (2018). Expression of mutant Sftpc in murine alveolar epithelia drives spontaneous lung fibrosis. *J. Clin. Invest.* **128**, 4008–4024.
- Ochs, M., Nyengaard, J. R., Jung, A., Knudsen, L., Voigt, M., Wahlers, T., Richter, J. and Gundersen, H. J. G.** (2004). The Number of Alveoli in the Human Lung.

Am. J. Respir. Crit. Care Med. **169**, 120–124.

- Oikonomou, N., Harokopos, V., Zalevsky, J., Valavanis, C., Kotanidou, A., Szymkowski, D. E., Kollias, G. and Aidinis, V.** (2006). Soluble TNF mediates the transition from pulmonary inflammation to fibrosis. *PLoS One* **1**,.
- Parimon, T., Yao, C., Stripp, B. R., Noble, P. W. and Chen, P.** (2020). Alveolar Epithelial Type II Cells as Drivers of Lung Fibrosis in Idiopathic Pulmonary Fibrosis. *Int. J. Mol. Sci.* **21**,.
- Parrish, A. R., Gandolfi, A. J. and Brendel, K.** (1995). Precision-cut tissue slices: Applications in pharmacology and toxicology. *Life Sci.* **57**, 1887–1901.
- Pavlacky, J. and Polak, J.** (2020). Technical Feasibility and Physiological Relevance of Hypoxic Cell Culture Models. *Front. Endocrinol. (Lausanne)*. **11**,.
- Peng, R., Sridhar, S., Tyagi, G., Phillips, J. E., Garrido, R., Harris, P., Burns, L., Renteria, L., Woods, J., Chen, L., et al.** (2013). Bleomycin induces molecular changes directly relevant to idiopathic pulmonary fibrosis: a model for ‘active’ disease. *PLoS One* **8**,.
- Penkala, I. J., Liberti, D. C., Pankin, J., Sivakumar, A., Kremp, M. M., Jayachandran, S., Katzen, J., Leach, J. P., Windmueller, R., Stolz, K., et al.** (2021). Age-dependent alveolar epithelial plasticity orchestrates lung homeostasis and regeneration. *Cell Stem Cell* **28**, 1775-1789.e5.
- Piguet, P. F., Ribaux, C., Karpuz, V., Grau, G. E. and Kapanci, Y.** (1993). Expression and localization of tumor necrosis factor-alpha and its mRNA in idiopathic pulmonary fibrosis. *Am. J. Pathol.* **143**,.
- Placke, M. E. and Fisher, G. L.** (1987). Adult peripheral lung organ culture-A model for respiratory tract toxicology. *Toxicol. Appl. Pharmacol.* **90**, 284–298.
- Plasschaert, L. W., Žilionis, R., Choo-Wing, R., Savova, V., Knehr, J., Roma, G., Klein, A. M. and Jaffe, A. B.** (2018). A single-cell atlas of the airway epithelium reveals the CFTR-rich pulmonary ionocyte. *Nature* **560**,.
- Pocha, S. M. and Knust, E.** (2013). Complexities of Crumbs function and regulation in tissue morphogenesis. *Curr. Biol.* **23**,.
- Portnoy, J., Curran-Everett, D. and Mason, R. J.** (2004). Keratinocyte Growth Factor Stimulates Alveolar Type II Cell Proliferation through the Extracellular Signal-Regulated Kinase and Phosphatidylinositol 3-OH Kinase Pathways. *Am. J. Respir. Cell Mol. Biol.* **30**,.
- Powell, P. P., Wang, C. C., Horinouchi, H., Shepherd, K., Jacobson, M., Lipson, M.**

- and Jones, R.** (1998). Differential expression of fibroblast growth factor receptors 1 to 4 and ligand genes in late fetal and early postnatal rat lung. *Am. J. Respir. Cell Mol. Biol.* **19**,.
- Raghu, G., Brown, K. K., Costabel, U., Cottin, V., du Bois, R. M., Lasky, J. A., Thomeer, M., Utz, J. P., Khandker, R. K., McDermott, L., et al.** (2008). Treatment of idiopathic pulmonary fibrosis with etanercept: an exploratory, placebo-controlled trial. *Am. J. Respir. Crit. Care Med.* **178**,.
- Rankin, S. A., Han, L., McCracken, K. W., Kenny, A. P., Anglin, C. T., Grigg, E. A., Crawford, C. M., Wells, J. M., Shannon, J. M. and Zorn, A. M.** (2016). A Retinoic Acid-Hedgehog Cascade Coordinates Mesoderm-Inducing Signals and Endoderm Competence during Lung Specification. *Cell Rep.* **16**,.
- Raslan, A. A. and Yoon, J. K.** (2020). WNT Signaling in Lung Repair and Regeneration. *Mol. Cells* **43**,.
- Rawlins, E. L. and Hogan, B. L. M.** (2008). Ciliated epithelial cell lifespan in the mouse trachea and lung. *Am. J. Physiol. Lung Cell. Mol. Physiol.* **295**,.
- Rawlins, E. L., Okubo, T., Xue, Y., Brass, D. M., Auten, R. L., Hasegawa, H., Wang, F. and Hogan, B. L. M.** (2009a). The Role of Scgb1a1+ Clara Cells in the Long-Term Maintenance and Repair of Lung Airway, but Not Alveolar, Epithelium. *Cell Stem Cell* **4**, 525–534.
- Rawlins, E. L., Clark, C. P., Xue, Y. and Hogan, B. L. M.** (2009b). The Id2+ distal tip lung epithelium contains individual multipotent embryonic progenitor cells. *Development* **136**, 3741–3745.
- Ray, S., Chiba, N., Yao, C., Guan, X., McConnell, A. M., Brockway, B., Que, L., McQualter, J. L. and Stripp, B. R.** (2016). Rare SOX2+ Airway Progenitor Cells Generate KRT5+ Cells that Repopulate Damaged Alveolar Parenchyma following Influenza Virus Infection. *Stem cell reports* **7**,.
- Redente, E. F., Jacobsen, K. M., Solomon, J. J., Lara, A. R., Faubel, S., Keith, R. C., Henson, P. M., Downey, G. P. and Riches, D. W. H.** (2011). Age and sex dimorphisms contribute to the severity of bleomycin-induced lung injury and fibrosis. *Am. J. Physiol. Lung Cell. Mol. Physiol.* **301**,.
- Rehan, V. K., Sugano, S., Wang, Y., Santos, J., Romero, S., Dasgupta, C., Keane, M. P., Stahlman, M. T. and Torday, J. S.** (2006). Evidence for the presence of lipofibroblasts in human lung. *Exp. Lung Res.* **32**, 379–393.
- Ren, H., Birch, N. P. and Suresh, V.** (2016). An Optimised Human Cell Culture Model

- for Alveolar Epithelial Transport. *PLoS One* **11**,.
- Reyfman, P. A., Walter, J. M., Joshi, N., Anekalla, K. R., McQuattie-Pimentel, A. C., Chiu, S., Fernandez, R., Akbarpour, M., Chen, C. I., Ren, Z., et al.** (2019). Single-cell transcriptomic analysis of human lung provides insights into the pathobiology of pulmonary fibrosis. *Am. J. Respir. Crit. Care Med.* **199**, 1517–1536.
- Rock, J. R., Rawlins, E. L., Onaitis, M. W. and Hogan, B. L.** (2009). Basal cells as stem cells of the mouse trachea and human conducting airways. *Dev. Biol.* **106**, 12771–12775.
- Rock, J. R., Gao, X., Xue, Y., Randell, S. H., Kong, Y.-Y. and Hogan, B. L. M.** (2011). Notch-Dependent Differentiation of Adult Airway Basal Stem Cells. *Cell Stem Cell* **8**,.
- Rodriguez-Boulan, E. and Macara, I. G.** (2014). Organization and execution of the epithelial polarity programme. *Nat. Rev. Mol. Cell Biol.* **15**,.
- Rucka, Z., Vanhara, P., Koutna, I., Tesarova, L., Potesilova, M., Stejskal, S., Simara, P., Dolezel, J., Zvonicek, V., Coufal, O., et al.** (2013). Differential effects of insulin and dexamethasone on pulmonary surfactant-associated genes and proteins in A549 and H441 cells and lung tissue. *Int. J. Mol. Med.* **32**,.
- Ryerson, C. J., Kolb, M., Richeldi, L., Lee, J., Wachtlin, D., Stowasser, S. and Poletti, V.** (2019). Effects of nintedanib in patients with idiopathic pulmonary fibrosis by GAP stage. *ERS Monogr.* **5**, 1–9.
- Sachs, N., de Ligt, J., Kopper, O., Gogola, E., Bounova, G., Weeber, F., Balgobind, A. V., Wind, K., Gracanin, A., Begthel, H., et al.** (2018). A Living Biobank of Breast Cancer Organoids Captures Disease Heterogeneity. *Cell* **172**, 373-386.e10.
- Sachs, N., Papaspyropoulos, A., Zomer-van Ommen, D. D., Heo, I., Böttinger, L., Klay, D., Weeber, F., Huelsz-Prince, G., Iakobachvili, N., Amatngalim, G. D., et al.** (2019). Long-term expanding human airway organoids for disease modeling. *EMBO J.* **38**, 1–20.
- Salahudeen, A. A., Choi, S. S., Rustagi, A., Zhu, J., van Unen, V., de la O, S. M., Flynn, R. A., Margalef-Català, M., Santos, A. J. M., Ju, J., et al.** (2020). Progenitor identification and SARS-CoV-2 infection in human distal lung organoids. *Nature* **588**,.
- Salomon, J. J., Muchitsch, V. E., Gausterer, J. C., Schwagerus, E., Huwer, H., Daum, N., Lehr, C.-M. and Ehrhardt, C.** (2014). The Cell Line NCI-H441 Is a Useful *in Vitro* Model for Transport Studies of Human Distal Lung Epithelial

Barrier. *Mol. Pharm.* **11**,.

- Salwig, I., Spitznagel, B., Vazquez-Armendariz, A. I., Khalooghi, K., Guenther, S., Herold, S., Szibor, M. and Braun, T.** (2019). Bronchioalveolar stem cells are a main source for regeneration of distal lung epithelia in vivo. *EMBO J.* **38**, e102099.
- Sato, T., Stange, D. E., Ferrante, M., Vries, R. G. J., Van Es, J. H., Van den Brink, S., Van Houdt, W. J., Pronk, A., Van Gorp, J., Siersema, P. D., et al.** (2011). Long-term expansion of epithelial organoids from human colon, adenoma, adenocarcinoma, and Barrett's epithelium. *Gastroenterology* **141**,.
- Schreurs, R. R. C. E., Baumdick, M. E., Drewniak, A. and Bunders, M. J.** (2021). In vitro co-culture of human intestinal organoids and lamina propria-derived CD4+ T cells. *STAR Protoc.* **2**,.
- Schruf, E., Schroeder, V., Le, H. Q., Schönberger, T., Raedel, D., Stewart, E. L., Fundel-Clemens, K., Bluhmki, T., Weigle, S., Schuler, M., et al.** (2020). Recapitulating idiopathic pulmonary fibrosis related alveolar epithelial dysfunction in a human iPSC-derived air-liquid interface model. *FASEB J.* **34**, 7825–7846.
- Seino, T., Kawasaki, S., Shimokawa, M., Tamagawa, H., Toshimitsu, K., Fujii, M., Ohta, Y., Matano, M., Nanki, K., Kawasaki, K., et al.** (2018). Human Pancreatic Tumor Organoids Reveal Loss of Stem Cell Niche Factor Dependence during Disease Progression. *Cell Stem Cell* **22**, 454-467.e6.
- Sekine, K., Ohuchi, H., Fujiwara, M., Yamasaki, M., Yoshizawa, T., Sato, T., Yagishita, N., Matsui, D., Koga, Y., Itoh, N., et al.** (1999). Fgf10 is essential for limb and lung formation. *Nat. Genet.* **21**,.
- Senavirathna, L. K., Huang, C., Yang, X., Munteanu, M. C., Sathiseelan, R., Xu, D., Henke, C. A. and Liu, L.** (2018). Hypoxia induces pulmonary fibroblast proliferation through NFAT signaling. *Sci. Rep.* **8**,.
- Seo, E. J., Kim, D. K., Jang, I. H., Choi, E. J., Shin, S. H., Lee, S. I., Kwon, S.-M., Kim, K.-H., Suh, D.-S. and Kim, J. H.** (2016). Hypoxia-NOTCH1-SOX2 signaling is important for maintaining cancer stem cells in ovarian cancer. *Oncotarget* **7**,.
- Shiraishi, K., Nakajima, T., Shichino, S., Deshimaru, S., Matsushima, K. and Ueha, S.** (2019a). In vitro expansion of endogenous human alveolar epithelial type II cells in fibroblast-free spheroid culture. *Biochem. Biophys. Res. Commun.* **515**,.
- Shiraishi, K., Shichino, S., Ueha, S., Nakajima, T., Hashimoto, S., Yamazaki, S. and Matsushima, K.** (2019b). Mesenchymal-Epithelial Interactome Analysis Reveals Essential Factors Required for Fibroblast-Free Alveolosphere Formation. *iScience*

11,.

- Sibille, Y. and Reynolds, H. Y.** (1990). Macrophages and polymorphonuclear neutrophils in lung defense and injury. *Am. Rev. Respir. Dis.* **141**, 471–501.
- Singh, G. and Katyal, S. L.** (2006). Clara Cell Proteins. *Ann. N. Y. Acad. Sci.* **923**,.
- Sisson, T. H., Mendez, M., Choi, K., Subbotina, N., Courey, A., Cunningham, A., Dave, A., Engelhardt, J. F., Liu, X., White, E. S., et al.** (2010). Targeted injury of type II alveolar epithelial cells induces pulmonary fibrosis. *Am. J. Respir. Crit. Care Med.* **181**, 254–263.
- Spyrou, J., Gardner, D. K. and Harvey, A. J.** (2019). Metabolism Is a Key Regulator of Induced Pluripotent Stem Cell Reprogramming. *Stem Cells Int.* **2019**,.
- Stegmayr, J., Alsafadi, H. N., Lindstedt, S. and Wagner, D. E.** (2021). Human precision-cut lung slices generated from excess donor lungs as a model for IPF and drug screening. In *12.01 - Idiopathic interstitial pneumonias*, p. European Respiratory Society.
- Strikoudis, A., Cieślak, A., Loffredo, L., Chen, Y. W., Patel, N., Saqi, A., Lederer, D. J. and Snoeck, H. W.** (2019). Modeling of Fibrotic Lung Disease Using 3D Organoids Derived from Human Pluripotent Stem Cells. *Cell Rep.* **27**, 3709-3723.e5.
- Strunz, M., Simon, L. M., Ansari, M., Kathiriya, J. J., Angelidis, I., Mayr, C. H., Tsidiridis, G., Lange, M., Mattner, L. F., Yee, M., et al.** (2020). Alveolar regeneration through a Krt8⁺ transitional stem cell state that persists in human lung fibrosis. *Nat. Commun.* **11**,.
- Sueblinvong, V., Neujahr, D. C., Todd Mills, S., Roser-Page, S., Guidot, D., Rojas, M., Ritzenthaler, J. D. and Roman, J.** (2012). Predisposition for Disrepair in the Aged Lung. *Am. J. Med. Sci.* **344**,.
- Szymaniak, A. D., Mahoney, J. E., Cardoso, W. V. and Varelas, X.** (2015). Crumbs3-Mediated Polarity Directs Airway Epithelial Cell Fate through the Hippo Pathway Effector Yap. *Dev. Cell* **34**,.
- Tahedl, D., Wirkes, A., Tschanz, S. A., Ochs, M. and Mühlfeld, C.** (2014). How common is the lipid body-containing interstitial cell in the mammalian lung? *Am. J. Physiol. - Lung Cell. Mol. Physiol.* **307**, L386–L394.
- Takeda, K., Mizushima, T., Yokoyama, Y., Hirose, H., Wu, X., Qian, Y., Ikehata, K., Miyoshi, N., Takahashi, H., Haraguchi, N., et al.** (2018). Sox2 is associated with cancer stem-like properties in colorectal cancer. *Sci. Rep.* **8**,.
- Tashiro, J., Rubio, G. A., Limper, A. H., Williams, K., Elliot, S. J., Ninou, I., Aidinis,**

- V., Tzouveleakis, A. and Glassberg, M. K. (2017). Exploring animal models that resemble idiopathic pulmonary fibrosis. *Front. Med.* **4**, 1–11.
- Tata, P. R., Mou, H., Pardo-Saganta, A., Zhao, R., Prabhu, M., Law, B. M., Vinarsky, V., Cho, J. L., Breton, S., Sahay, A., et al.** (2013). Dedifferentiation of committed epithelial cells into stem cells in vivo. *Nature* **503**, 218–23.
- Tatler, A. L., Habgood, A., Porte, J., John, A. E., Stavrou, A., Hodge, E., Keramalikoko, C., Violette, S. M., Weinreb, P. H., Knox, A. J., et al.** (2016). Reduced ets domain-containing protein Elk1 promotes pulmonary fibrosis via increased integrin $\alpha\beta6$ expression. *J. Biol. Chem.* **291**, 9540–9553.
- Teixeira, V. H., Nadarajan, P., Graham, T. A., Pipinikas, C. P., Brown, J. M., Falzon, M., Nye, E., Poulson, R., Lawrence, D., Wright, N. A., et al.** (2013). Stochastic homeostasis in human airway epithelium is achieved by neutral competition of basal cell progenitors. *Elife* **2013**, e00966.
- The Idiopathic Pulmonary Fibrosis Clinical Research Network** (2012). Prednisone, Azathioprine, and N-Acetylcysteine for Pulmonary Fibrosis. *N. Engl. J. Med.* **366**.
- Toti, P., Buonocore, G., Tanganelli, P., Catella, A. M., Palmeri, M. L. D., Vatti, R. and Seemayer, T. A.** (1997). Bronchopulmonary dysplasia of the premature baby: An immunohistochemical study. *Pediatr. Pulmonol.* **24**, 22–28.
- Travaglini, K. J., Nabhan, A. N., Penland, L., Sinha, R., Gillich, A., Sit, R. V., Chang, S., Conley, S. D., Mori, Y., Seita, J., et al.** (2020). A molecular cell atlas of the human lung from single-cell RNA sequencing. *Nature* **587**, 619–625.
- Triantafyllou, A., Liakos, P., Tsakalof, A., Georgatsou, E., Simos, G. and Bonanou, S.** (2006). Cobalt induces hypoxia-inducible factor-1alpha (HIF-1alpha) in HeLa cells by an iron-independent, but ROS-, PI-3K- and MAPK-dependent mechanism. *Free Radic. Res.* **40**.
- Uhal, B. D.** (1997). Cell cycle kinetics in the alveolar epithelium. *Am. J. Physiol. - Lung Cell. Mol. Physiol.* **272**, L1031–L1045.
- van Uden, P., Kenneth, N. S. and Rocha, S.** (2008). Regulation of hypoxia-inducible factor-1alpha by NF-kappaB. *Biochem. J.* **412**.
- Vaughan, A. E., Brumwell, A. N., Xi, Y., Gotts, J. E., Brownfield, D. G., Treutlein, B., Tan, K., Tan, V., Liu, F. C., Looney, M. R., et al.** (2015). Lineage-negative progenitors mobilize to regenerate lung epithelium after major injury. *Nature* **517**.
- Victorelli, S. and Passos, J. F.** (2017). Telomeres and Cell Senescence - Size Matters Not. *EBioMedicine* **21**.

- Volckaert, T. and De Langhe, S. P.** (2015). Wnt and FGF mediated epithelial-mesenchymal crosstalk during lung development. *Dev. Dyn.* **244**,.
- Wang, Y., Tang, Z., Huang, H., Li, J., Wang, Z., Yu, Y., Zhang, C., Li, J., Dai, H., Wang, F., et al.** (2018). Pulmonary alveolar type I cell population consists of two distinct subtypes that differ in cell fate. *Proc. Natl. Acad. Sci. U. S. A.* **115**, 2407–2412.
- Wansleben, C., Barkauskas, C. E., Rock, J. R. and Hogan, B. L. M.** (2013). Stem cells of the adult lung: their development and role in homeostasis, regeneration, and disease. *Wiley Interdiscip. Rev. Dev. Biol.* **2**,.
- Wasnick, R., Korfei, M., Piskulak, K., Henneke, I., Wilhelm, J., Mahavadi, P., Beck, D. von der, Koch, M., Shalashova, I., Klymenko, O., et al.** (2019). Restored alveolar epithelial differentiation and reversed human lung fibrosis upon Notch inhibition. *bioRxiv* 580498.
- Watson, J. K., Rulands, S., Wilkinson, A. C., Wuidart, A., Ousset, M., Van Keymeulen, A., Göttgens, B., Blanpain, C., Simons, B. D. and Rawlins, E. L.** (2015). Clonal Dynamics Reveal Two Distinct Populations of Basal Cells in Slow-Turnover Airway Epithelium. *Cell Rep.* **12**, 90–101.
- Wee, P. and Wang, Z.** (2017). Epidermal Growth Factor Receptor Cell Proliferation Signaling Pathways. *Cancers (Basel).* **9**,.
- Weidenfeld, J., Shu, W., Zhang, L., Millar, S. E. and Morrissey, E. E.** (2002). The WNT7b promoter is regulated by TTF-1, GATA6, and Foxa2 in lung epithelium. *J. Biol. Chem.* **277**, 21061–21070.
- Wright, J. R.** (2005). Immunoregulatory functions of surfactant proteins. *Nat. Rev. Immunol.* **5**,.
- Wu, D. and Yotnda, P.** (2011). Induction and testing of hypoxia in cell culture. *J. Vis. Exp.*
- Wu, C. W., Chang, H. C., Chen, T. H., Huang, H. T., Liu, C. J. and Wang, H. C.** (2018). Idiopathic pulmonary fibrosis. *J. Intern. Med. Taiwan* **29**, 283–291.
- Wu, X., Yao, J., Wang, L., Zhang, D., Zhang, L., Reynolds, E. X., Yu, T., Boström, K. I. and Yao, Y.** (2019). Crosstalk between BMP and Notch Induces Sox2 in Cerebral Endothelial Cells. *Cells* **8**,.
- Xi, Y., Kim, T., Brumwell, A. N., Driver, I. H., Wei, Y., Tan, V., Jackson, J. R., Xu, J., Lee, D.-K., Gotts, J. E., et al.** (2017). Local lung hypoxia determines epithelial fate decisions during alveolar regeneration. *Nat. Cell Biol.* **19**,.

- Xu, Y., Mizuno, T., Sridharan, A., Du, Y., Guo, M., Tang, J., Wikenheiser-Brokamp, K. A., Perl, A. T., Funari, V. A., Gokey, J. J., et al.** (2016). Single-cell RNA sequencing identifies diverse roles of epithelial cells in idiopathic pulmonary fibrosis. *JCI Insight* **1**, 1–18.
- Xu, W., Zhou, W., Cheng, M., Wang, J., Liu, Z., He, S., Luo, X., Huang, W., Chen, T., Yan, W., et al.** (2017). Hypoxia activates Wnt/ β -catenin signaling by regulating the expression of BCL9 in human hepatocellular carcinoma. *Sci. Rep.* **7**,.
- Yamamoto, Y., Gotoh, S., Korogi, Y., Seki, M., Konishi, S., Ikeo, S., Sone, N., Nagasaki, T., Matsumoto, H., Muro, S., et al.** (2017). Long-term expansion of alveolar stem cells derived from human iPS cells in organoids. *Nat. Methods* **14**, 1097–1106.
- Youk, J., Kim, T., Evans, K. V., Jeong, Y. Il, Hur, Y., Hong, S. P., Kim, J. H., Yi, K., Kim, S. Y., Na, K. J., et al.** (2020). Three-Dimensional Human Alveolar Stem Cell Culture Models Reveal Infection Response to SARS-CoV-2. *Cell Stem Cell* **27**, 905-919.e10.
- Yue, X., Shan, B. and Lasky, J. A.** (2010). TGF- β : Titan of Lung Fibrogenesis. *Curr. Enzym. Inhib.* **6**,.
- Zacharias, W. J., Frank, D. B., Zepp, J. A., Morley, M. P., Alkhaleel, F. A., Kong, J., Zhou, S., Cantu, E. and Morrisey, E. E.** (2018). Regeneration of the lung alveolus by an evolutionarily conserved epithelial progenitor. *Nature* **555**, 251–255.
- Zepp, J. A., Zacharias, W. J., Frank, D. B., Cavanaugh, C. A., Zhou, S., Morley, M. P. and Morrisey, E. E.** (2017). Distinct Mesenchymal Lineages and Niches Promote Epithelial Self-Renewal and Myofibrogenesis in the Lung. *Cell* **170**,.
- Zhang, F., Nielsen, L. D., Lucas, J. J. and Mason, R. J.** (2004). Transforming Growth Factor- β Antagonizes Alveolar Type II Cell Proliferation Induced by Keratinocyte Growth Factor. *Am. J. Respir. Cell Mol. Biol.* **31**,.
- Zhang, Q., Bai, X., Chen, W., Ma, T., Hu, Q., Liang, C., Xie, S., Chen, C., Hu, L., Xu, S., et al.** (2013). Wnt/ β -catenin signaling enhances hypoxia-induced epithelial–mesenchymal transition in hepatocellular carcinoma via crosstalk with hif-1 α signaling. *Carcinogenesis* **34**,.
- Zhou, Y., Peng, H., Sun, H., Peng, X., Tang, C., Gan, Y., Chen, X., Mathur, A., Hu, B., Slade, M. D., et al.** (2014). Chitinase 3–Like 1 Suppresses Injury and Promotes Fibroproliferative Responses in Mammalian Lung Fibrosis. *Sci. Transl. Med.* **6**,.
- Zhou, J., Li, C., Sachs, N., Chiu, M. C., Wong, B. H. Y., Chu, H., Poon, V. K. M.,**

- Wang, D., Zhao, X., Wen, L., et al.** (2018). Differentiated human airway organoids to assess infectivity of emerging influenza virus. *Proc. Natl. Acad. Sci. U. S. A.* **115**, 6822–6827.
- Zhu, G., Hu, J. and Xi, R.** (2021). The cellular niche for intestinal stem cells: a team effort. *Cell Regen.* **10**,
- Zong, D., Ouyang, R., Li, J., Chen, Y. and Chen, P.** (2016). Notch signaling in lung diseases: focus on Notch1 and Notch3. *Ther. Adv. Respir. Dis.* **10**,
- Zuo, W., Zhang, T., Wu, D. Z. A., Guan, S. P., Liew, A. A., Yamamoto, Y., Wang, X., Lim, S. J., Vincent, M., Lessard, M., et al.** (2015). P63 + Krt5 + distal airway stem cells are essential for lung regeneration. *Nature* **517**, 616–620.